The Scientific Journal of
CosmoIntel
The First Scientific Journal in T-Consciousness Research

April 2022 | No.8

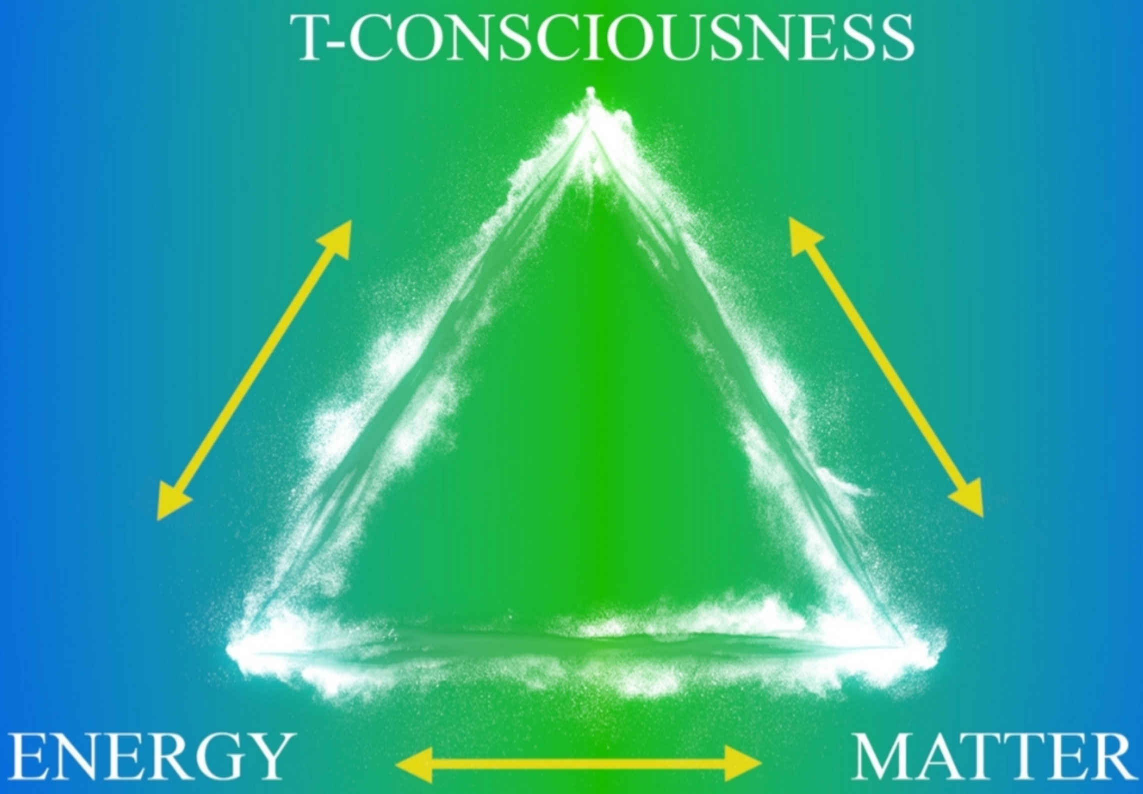

Software Engineering of Molecules: Behavior of Materials and Molecules under the Influence of T-Consciousness Fields

Mohammad Ali Taheri | Founder of T-Consciousness Theory

Interuniversal Press

The Scientific Journal of Cosmointel
Vaughan, Canada

WWW.JOURNALOFCOSMOINTEL.COM

Interuniversal Press

The Scientific Journal of Cosmointel Vaughan, Canada

EDITORIAL

MOHAMMAD ALI TAHERI
Founder of
T-Consciousness Theory

The Journal of Cosmointel was established in 2022. It is an open-access, multidisciplinary journal that focuses on research related to T-Consciousness. The journal is published on a rolling basis to accommodate authors and allow for the flow of the large volume of written research that has been submitted and is becoming available for publication. Journal access is free to all users; registration will be available in the future to ensure receipt of updates on the publication of issues and news. The journal focuses on **Sciencefact** research results and is published by **Cosmointel Inc.**

The Journal of Cosmointel publishes scholarly articles from all fields of science, engineering, medicine, and social sciences that report experiments utilizing Taheri Consciousness Fields (TCFs). Given that Sciencefact focuses on researching the effects of TCFs that are new to the scientific world, the journal is not yet peer-reviewed in the traditional sense at this time (although, the journal articles currently do undergo a rigorous review process by the Cosmointel Committee of Scientific Researchers and Editors). It is our hope that this journal will expand far-reaching interest in the nature and function of TCFs and over time develop a broad base of trained and experienced researchers that will enable a more traditional peer-review process in the future. Cosmointel Inc. is the main monitoring center for **Taheri Consciousness Fields** studies based exclusively on Sciencefact principles. For more information, please visit www.comsointel.com .

Mohammad Ali Taheri is a scholar, visionary thinker, and innovationist known for his numerous theoretical concepts, including *Cosmic Consciousness Network (CCN)* and *Taheri Consciousness Fields (TCFs)* with over 40 years of history. T-Consciousness is introduced and defined as one of the constituent components of the Cosmos in addition to matter and energy, from which TCFs, as non-material/non-energetic fields, are derived. TCFs are unique qualitative fields that are immaterial in nature but have a direct effect on matter and energy, including humans, animals, plants, microorganisms, cells, molecules, and particles. As far as the practical application of T-Consciousness is concerned, two complementary medicines of **Faradarmani** and **Psymentology** have been introduced and put into practice.

In 2020, Mohammad Ali Taheri introduced Sciencefact, that utilizes science as a means to demonstrate and record the effects of TCFs. Although science studies matter and energy alone, Sciencefact and science do share a common ground which is reproducible laboratory experiments that involve matter and energy. What distinguishes Sciencefact from science is the investigation and utilization of CCN through the application of the TCFs.

Established and managed by Mohammad Ali Taheri in 2022, the Journal of Cosmointel is an all-science journal that publishes original research on TCFs. As a scientific journal, all types of scientific research that adhere to ethical guidelines and publishing standards of Cosmointel Journal and T-Consciousness research protocol are eligible for publication. Cosmointel establishes the guidelines for conducting scientific research on TCFs and publishes the results in its journal spanning various disciplines, including biology, *T-Consciousness biology*, physics, engineering, material science, medicine, and neurosciences, psychology, etc.

From Taheri's point of view, T-Consciousness is neither matter nor energy. But, rather, matter and energy both arise from "T-Consciousness" and, when necessary, they are capable of converting back to "T-Consciousness" and vice versa. T-Consciousness operates through TCFs that can alter the *Mind-of-Matter*, which has recently been proven to exist by Sciencefact experiments. The results of these experiments demonstrate that TCFs are capable of rewriting a new *Matter-Memory* [for the *Mind-of-Matter*]. Depending on the different types of TCFs, different types of *Matter-Memory* and different types of programs are formed.

According to these experiments, matter records information in itself through no physical or chemical process. This is the very first time that such a phenomenon is demonstrated in the history of consciousness.

Taheri Consciousness is composed of contrasting subsets that include *T-Consciousness* and *Anti T-Consciousness* which are being introduced for the first time in the history of this subject.

It also consists of categories and functions such as *Constant T-Consciousness* and *Variable T-Consciousness*. It is important to note that the theories of *T-Consciousness Bond, General Connection of Particles, T-Consciousness Charge, Communal-Mind,* and *T-Consciousness Aided Conception*, among many others that have been proposed for the very first time, have been subjected to various field research and laboratory experiments for the past several decades. Within the experience of *Communal-Mind* and *T-Consciousness Aided Conception*, the theory of *T-Consciousness Aided Information Transfer* has also been proposed.

As the above theoretical concepts elucidate, and according to the teachings of the school of **Erfan Keyhani Halqeh**, consciousness in Taheri's view (T-Consciousness) is entirely different from any and all views that, to this day, have been proposed about the concept of consciousness. Hence, it is for the purpose of differentiating between consciousness in Taheri's view and all other views presented throughout history that we call this theory by the specific term of *Taheri's Consciousness Theory (T-Consciousness)*.

All manuscripts must fit into at least one category of the phases outlined below:

The Phase-based Studies of T-Consciousness Fields in Sciencefact.

Sciencefact[1] is taking an unprecedented step by introducing T-Consciousness as a non-material and non-energetic constituent of the universe that can be experienced through the application of TCFs in various areas of science. In the methodology of modern science, laboratory experiments have always been the foundation of research, and their results have served as reliable and firm criteria for accepting or rejecting hypotheses. Sciencefact, as a new field of scientific study, shares a common ground with modern science, in that it too conducts experiments on matter and energy. Therefore, with the aim of investigating and verifying the effect and the mechanism of TCFs, the following process and steps are suggested to achieve scientific findings and to design testing methods in the field of Sciencefact

Phase 0 Studies – Investigating the existence and effects of T-Consciousness Fields:

In this phase, the aim of the study design is to investigate merely the effect (regardless of its application) on the study system in reproducible, standard laboratory experiments. The results of this phase, first and foremost, confirm the existence of TCFs in a standard and limited study. The important factor in the studies of this phase is simplicity; the elimination of multiple and diverse variables with the aim of reaching more direct conclusions and analysis to confirm the existence of TCFs. The proper experimental design with minimal variables, confirmation of reproducibility of the study results, and meticulous presentation of the designed test conditions while detailing the effects of TCFs are among the essential and distinct factors in the studies of this phase.

Phase I Studies – Investigating the varied effects of different T-Consciousness Fields:

After completing phase zero (studying TCFs and designing a standard experiment to confirm their existence) the next step of Sciencefact studies deals with the types of TCFs and the potential variety of responses in the studied system. In this stage, after having confirmed the existence of TCFs (in phase zero), researchers explain the variation in the responses as a result of exposure to TCFs, and describe the results observed in the studied system based on justifiable and repeatable scientific documentation. Stating the standard conditions of study, detailing the effects of TCFs, and providing accurate reports of the effects of various TCFs on the system under study (utilizing approved statistical tests) are among the key factors in this phase (without secondary interpretations of the mechanism of action and by focusing exclusively on what has been observed).

Phase II Studies – Investigating the reason behind the [types of] effects of T-Consciousness Fields:

This phase establishes consistency between the results of the study and the theoretical basis of Taheri's teachings that introduce TCFs and their function. While meeting the objectives of phases zero and I, the researchers present proper and accurate analysis to give an account of corresponding relations between the

1. A term coined by Mohammad Ali Taheri to introduce this new science.

basis of the reported results and the fundamentals of Taheri's teachings with clarity and according to the approved standards of Sciencefact in terms of the special topic of T-Consciousness. For example, in phase II cell studies, after having observed the proliferation of cells in the cell culture medium and presenting data confirming the existence of the TCFs, and after reporting the possible variation of the effects of TCFs, we begin to explain the results based on the principles of T-Consciousness that governs the cell inside the culture medium. Accuracy in establishing a correct and precise correspondence between the obtained results and the Source Texts of Taheri's teachings (without the researcher's personal impression) is crucial and among key factors in this phase.

Phase III Studies - Investigating the mechanism of T-Consciousness Fields' effects:

The most advanced types of experiments designed in the study of TCFs are phase III experiments. In these studies, after completing the previous three stages in the preliminary phases and conducting additional and validating tests by researchers, the mechanism of the TCFs' effects on the studied system is meticulously examined. Among the prerequisites for this phase are rigorous experimental design, sufficient and well-reasoned analysis in accordance with the scientific method, and sufficient command of the principles of Taheri's teachings and the fundamentals of TCFs. In this phase, it will be possible to propose a new scientific theory based on empirical evidence.

Phase IV Studies –

Drawing macro-conclusions pertaining to the mind and memory of matter, etc.

Cosmic Consciousness Network (CCN)
or
Cosmic Internet According to Taheri

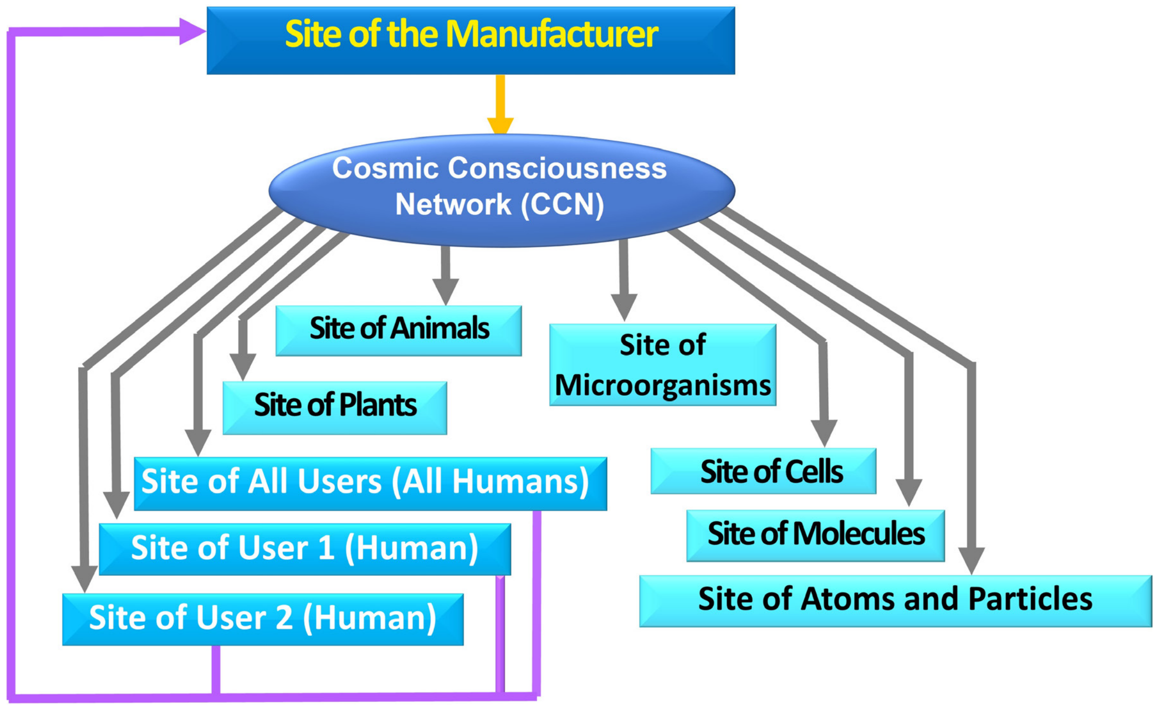

The Scientific Journal of Cosmointel
The First Scientific Journal in T-Consciousness Research

Table of Contents

Mass Changes of Pure Silica in Temperatures up to 1000 °C under the Influence of Consciousness Bond Field: A Study of Taheri Consciousness Theory

Bahareh Kazazi [1*], Mohammad Ali Taheri [2]

1. Civil Engineering, CEO of Hoobe Construction Company, Tehran, Iran.

2. Sciencefact R&D Department, Cosmointel Inc. Research Center, Ontario, Canada.

* Corresponding author:

Bahareh Kazazi
Civil Engineering, CEO of Hoobe Construction Company, Tehran, Iran.

Email: baharkazazi@gmail.com

ABSTRACT

According to Taheri's theory, T-Consciousness can be converted into matter and energy and vice versa. Consciousness Bond Field is one of many Taheri Consciousness Fields (TCFs) founded and introduced by Mohammad Ali Taheri as new Fields. These Fields are neither matter nor energy; therefore, do not possess a quantity, but they have direct effects on both matter and energy. In other words, although TCFs cannot be directly measured, we can investigate their effects indirectly through reproducible experiments. The current study aimed to investigate this hypothesis by measuring the mass change of pure silica through a heating process. Samples made of 95% pure silica powder with a particle size of approximately 1700 nm from one pack and under the same conditions were submitted to the following thermal analyses: DTA (Differential thermal analysis), DSC (Differential scanning calorimetry), and TGA (Thermal gravimetric analysis). The analyses were performed on two sets of experimental samples, one group of samples under the effect of Consciousness Bond Field, and the other group was used as control samples. The 6 mg samples were heated with a growth rate temperature of 10 °C, in the temperature range of 25 to 1000 °C, in Air, under ASTM-E1131. The results demonstrated no changes in the structure of pure silica, such as melting or transformation, glassification, etc. On the other hand, the samples exposed to the T-Consciousness Field lost an average of 7.22% at a temperature of 350 degrees and a total of 14.1% at the final temperature more mass compared to the control samples. Based on the objective observations of the results, it is clear that this significant difference does not have any plausible material explanation, and therefore it indicates the existence of the T-Consciousness Field that was applied. It also provides proof of Taheri's theory of the exchange of T-Consciousness with matter and energy.

Keywords: Silica powder, Taheri Consciousness Fields, Consciousness Bond Field, Thermal analysis

INTRODUCTION

Throughout history, humans have been curious about the world around them. Many efforts have been made in this direction, leading to the discovery of many principles, laws, and fields, such as gravitational field, electromagnetic field, electric field, etc. One of the most fundamental concepts of Taheri's theory of Consciousness is that although T-Consciousness is neither matter nor energy, matter, and energy, as well as physical events, and laws are driven by T-Consciousness. According to Taheri's theory, T-Consciousness can be converted into matter and energy and vice versa [1-2-3]. Many studies have investigated the behavior and properties of materials, including cement mortar under TCFs that began a decade ago [2]. Since then, the research has continued to study cement in various functions, including strength [4] penetration of gamma-neutron radiation [5], penetration of chlorine ions [6], concrete cancer [7], as well as the behavior and intrinsic properties of other materials such as pure aluminum [8-9] or different methods of nanomaterial synthesis [10-11]. Although this study aimed to investigate the function and general behavior of materials, this study revealed many crucial points about T-Consciousness Fields' effects on materials. Among the facts are that despite having less water absorption, the number of cement elements was changed, more specifically the test of cement mass showed that the mass of samples had increased [12]. Also, in another study, the number of crystal defects in aluminum samples increased by around 1000% despite having no energy or force [8] being applied to the material. Another study that evaluated the effect of T-Consciousness Fields was testing the copper density. The results of that study showed that the copper density increased after increasing the length by heat [13] which did not follow the law of conservation of mass & energy.

These findings suggested the possibility of exchange between T-Consciousness, matter, and energy, and therefore the current study aimed to further investigate the possibility of influencing mass balance by applying T-Consciousness Fields.

The nature of consciousness and its place in science has received much attention in the current century. Many philosophical and scientific theories have been proposed in this area. In the1980s, Mohammad Ali Taheri introduced novel fields with a non-material/non-energetic nature named Taheri Consciousness Fields (TCFs). In this perspective, T-Consciousness is one of the three existing elements of the universe apart from matter and energy. According to this theory, there are various TCFs with different functions, which are the subcategories of a networked universal internet called the Cosmic Consciousness Network (CCN). The major difference between the theory of TCFs and other theoretical concepts about consciousness is related to the practical application of the TCFs. TCFs can be applied to all living and non-living creatures, including plants, animals, microorganisms, materials, etc.

Mohammad Ali Taheri, the founder of Erfan Keyhani Halqeh, a school of thought, introduced a new science in 2020 as a branch of this school. He coined the term Sciencefact for this new science because it utilizes scientific investigations to prove the existence of T-Consciousness as an irrefutable phenomenon and a fact. Although science focuses solely on the study of matter and energy and Sciencefact, by contrast, explores the effects of the [non-material/non-energetic] TCFs, Sciencefact has provided a common ground between the two by conducting reproducible laboratory experiments in various scientific fields, and it has used the scientific approach in proving TCFs.

The influence of the TCFs begins with the Connection between CCN as the Whole Taheri Consciousness of the universe and the subjects of study as a part. This Connection called “Ettesal” is established by a certified and trained individual who has been entrusted with the TCFs. The human mind has an intermediary role (Announcer) which plays a part by fleeting attention to the subject of study and then the main achievement obtained as a result of the effects of the TCFs. These Fields cannot be directly measured by science, but it is possible to investigate their effects on various subjects through reproducible laboratory experiments.

The research methodology in the study of T-Consciousness has been founded on the process of Assumption, Argument, and Proof, in which the basic Assumption is: The Cosmos was formed by a third element called T-Consciousness that is different from matter and energy.

The Argument: The existence of TCFs can be demonstrated by its effects on matter and energy (e.g., humans, animals, plants, microorganisms, cells, materials, etc.)

The Proof: is the scientific verification of the effects of TCFs on matter and energy (according to the Argument) through various reproducible scientific experiments.

Accordingly, to investigate and verify the existence, effects, and mechanisms of TCFs, the following five research phases (Phases 0 through 4), and the aims of each phase are outlined below.

Phase-0 studies aim to prove the existence of TCFs by observing their effects. The nature of T-Consciousness and what it is will not be addressed in this phase. Phase-1 explores the varied effects of different TCFs. Phase-2 examines the reason behind the varied effects of these fields. Phase-3 investigates the mechanism of TCFs effects on matter and energy. Finally, Phase-4 draws significant conclusions, particularly with regard to the mind and memory of matter and their relation to the T-Consciousness, etc. [1, 2, 3]

The present research was carried out with the approach of investigating the possibility of changes in the mass of pure silica under the TCF and studying Taheri's theory of T-Consciousness in accordance with Phase-0 of the studies.

Materials and Methods

The Analyses of Pure Silica

First, 95% pure silica powder was selected. XRF (X-ray fluorescence), XRD (X-ray diffraction), and DLS (Dynamic Light Scattering) tests were performed before the experiment to determine the material information. The material was then divided into two groups; one container, for applying TCF, and the other was used as the control sample. Three samples were taken from each container and the following thermal analyses were performed on each of them two times:

DTA (Differential thermal analysis), DSC (Differential scanning calorimetry), TGA (Thermal gravimetric analysis)

The mass value of all samples was 6 mg for all samples, and the growth rate of temperature was 10 ° C in the temperature range of 25 to 1000, in Air, pan Al2O3, following ASTM-E1131-08(2014) by the following two devices:

1- TGA 209 F3Tarsus, Rate 40ml/min
2- SDT Q600 V20.9 Build20-, American TA

Application of Taheri Consciousness Fields

One of the introduced TCFs is called the Consciousness Bond Field and was applied to the samples according to the protocols regulated by the COSMOintel research center (www.COSMOintel.com). A request for Connection to the CCN to utilize TCFs can be placed through the COSMOintel website in the "Assign Announcement" section. This access is available for everyone at no cost. In order to study and experience this Connection, the researchers can register on the website at any time in order to report the experiment to the COSMOintel research center. Certain details of the experiment must be provided to the center; for example, the characteristics or number and name of samples and controls must be specified. This entire experiment was carried out as a double-blind method where lab technicians were completely unaware of the TCFs.

The purity percentage of the sample and material specifications is given below.

1- The XRF (X-ray fluorescence) analysis under the standard ASTM E 1621-21 is shown in the table.

Table 1 . The XRF Analysis Results of Pure Silica Prior to the Experiments

Sample No.	SiO_2 %	Al_2O_3 %	Fe_2O_3 %	CaO %	MgO %	Na_2O %	K_2O %	TiO_2 %	MnO %	P_2O_5 %	LOI %
XRF	94.41	0.091	2.034	0.067	N	0.024	N	0.053	0.029	0.007	2.86

Sample.no	S ppm	Cl ppm	Ba ppm	Co ppm	Cr ppm	Cu ppm
XRF	30	N	100	29	410	25

2- XRD (X-ray diffraction) analysis is shown in Figure 1.

The XRD (X-ray diffraction) Standard: BSIBS En139251-2 and the Generator Settings: 40 mA, 40 kV, Anode Material: Cu, Step Size [°2Th.]: 0.0260.

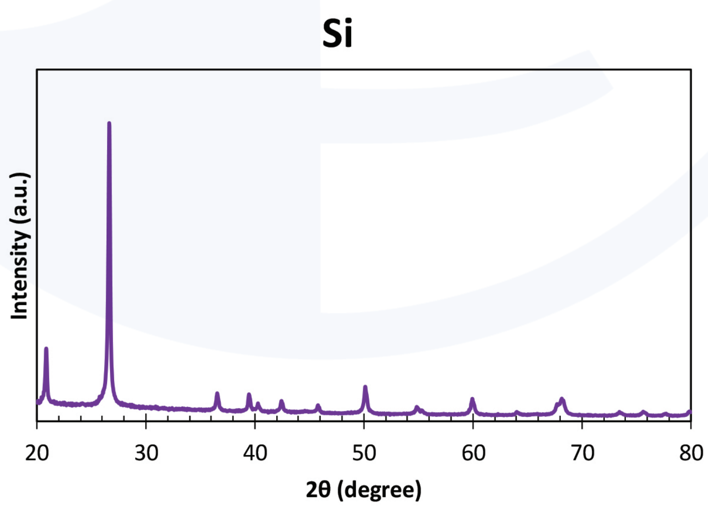

Figure 1. The XRD Analysis Results of Pure Silica Prior to the Experiments

X'Pert Plus HighScore was used to identify the material phase. According to Figure 1, and by matching this diffraction pattern with the reference diffraction patterns, it was determined that the diffraction pattern was related to the quartz phase (SiO2) with the reference code JCPDS No. 01-078-1252.

The Rietveld method using the MAUD software was used to accurately examine the small values obtained from the XRD test related to the samples. Table 2 presents the results:

Table 2 . Quantitative results of X-ray test by the Rietveld method

Sample	a (Angstrom)	c (Angstrom)	Crystallite Size (nm)	Microcirculation
Si	4.918	5.410	69.639	4.10×10^{-7}

3- DLS (Dynamic Light Scattering)

The analysis was performed with the following specifications by HORIBA SZ-100.

Scattering Angle: 90, Temperature of the Holder: 25.2 °C, Dispersion Medium Viscosity: 0.892 mPa·s. Count Rate: 286 kCPS, Dispersant Name: Water

It was found that the average particle size was in the range of 1700 nm.

Results and Discussion

During the first run of experiments following the mentioned specifications, 4 samples were analyzed in device number (1). The result of this analysis is shown in Figure 2.

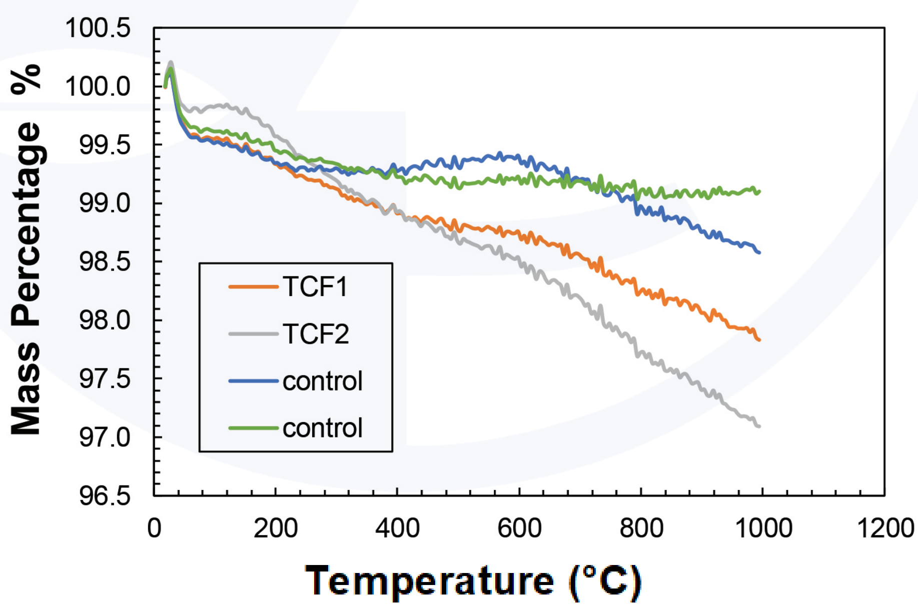

Figure 2. The mass reduction diagram (TGA), for the study and control samples.

Table 3 . Numerical comparison of mass changes

Sample.no	TCF1	TCF2	Control1	Control2
Residual Mass	97.15	97.8	98.6	99.2
Change Mass%	2.97%	2.3%	0%	0%

Silica is reported to have a melting point of around 1700 °C, and it is not expected to change up to a temperature of 1000 °C [14]. The behavior of the control sample of silica is consistent with the known behavior of pure silica, however, the samples under the effect of TCF, shows a loss of mass. Considering the importance of the obtained results and to find out the repeatability of the results, the experiments by repeated by a different device to obtain the DSC/DTA results. The following analyzes were performed on the device number (2).

Figure 3,4 illustrates the thermal properties of the studied samples exposed to TCF (demarked as pk), the control group obtained from the DC and DTA tests:

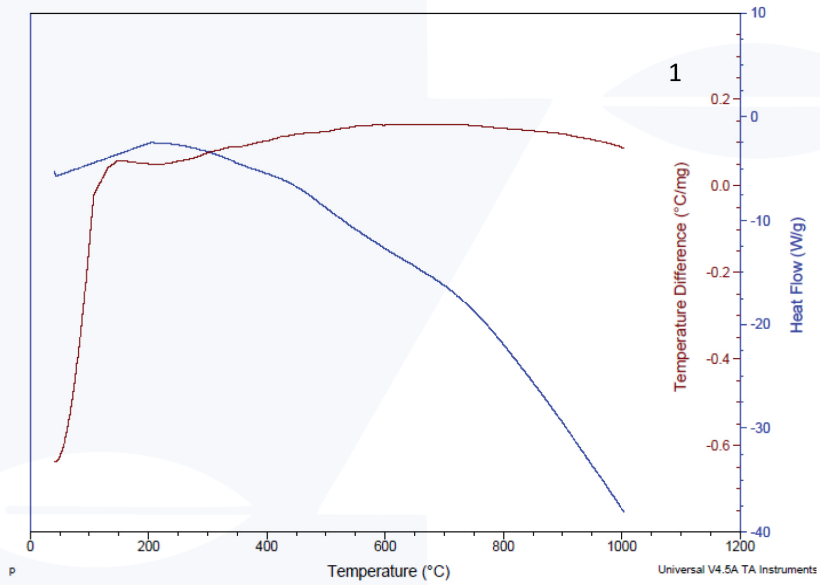

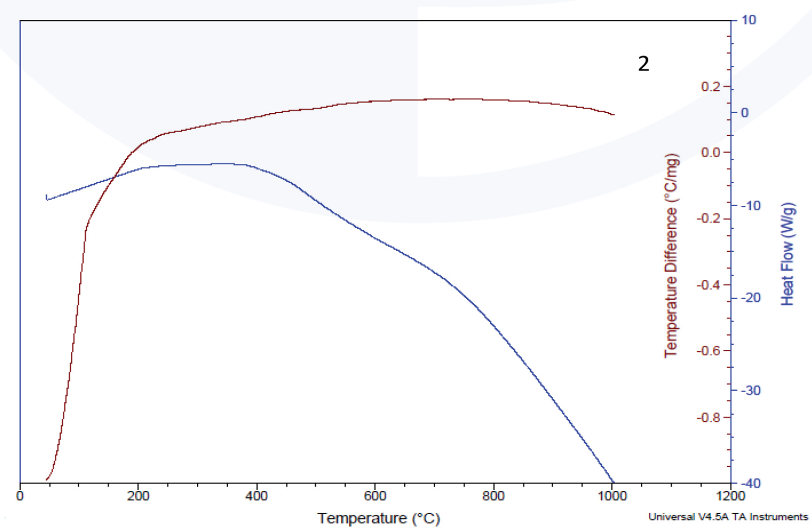

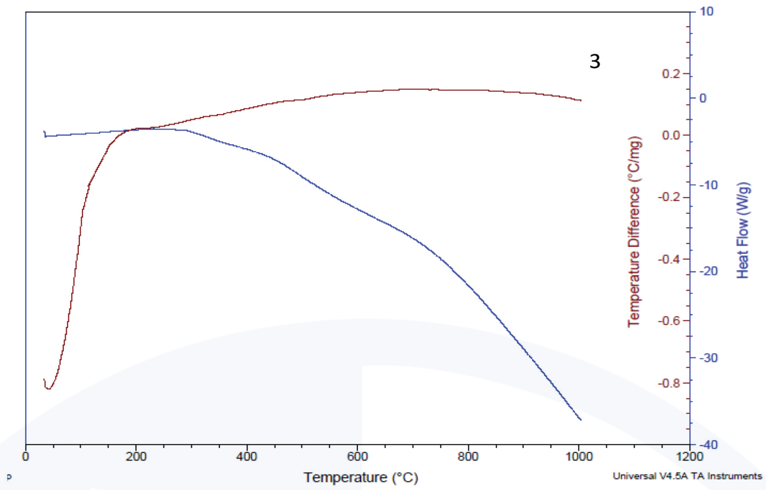

Figure 3. The DTA-DSC analysis graph of the control samples (1,2,3)

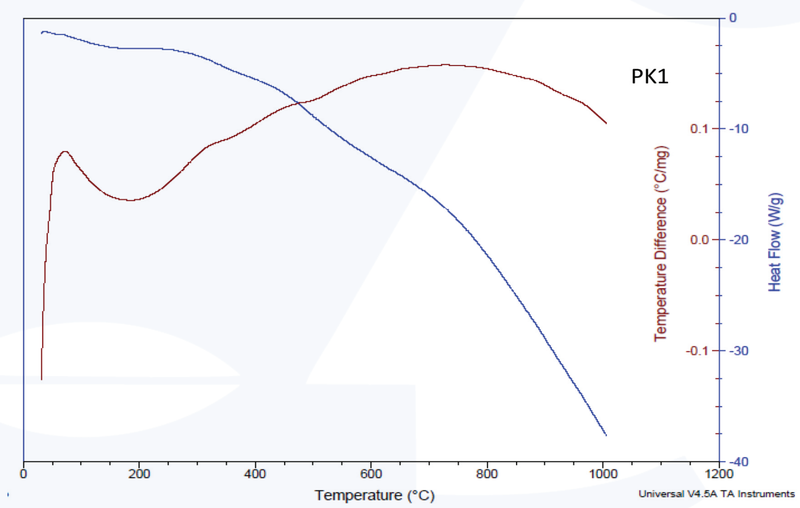

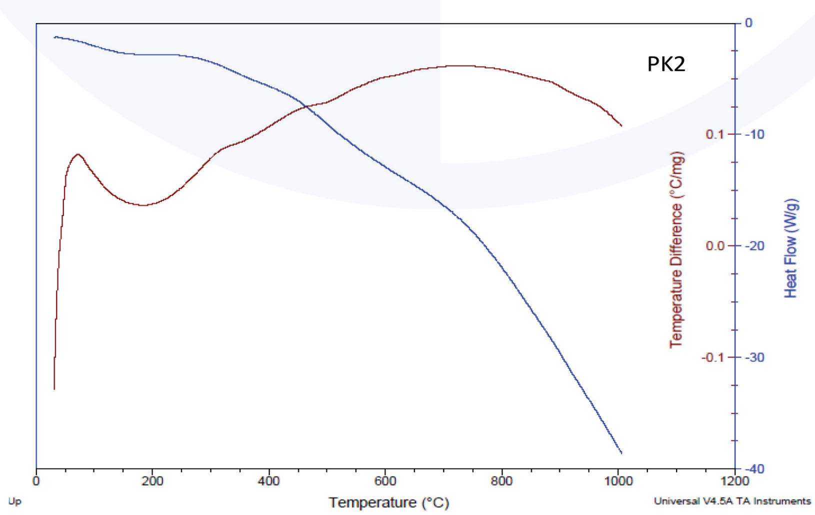

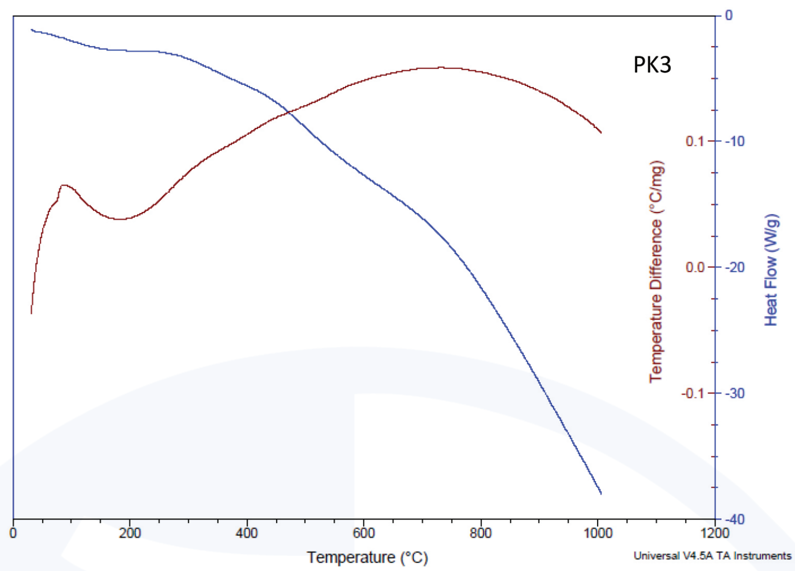

Figure 4. The DTA-DSC analysis graph of the TCF samples (PK1, PK2, PK3)

DTA analysis is a method that has a lot in common with the DSC. In this method, both the sample and the reference are heated precisely the same in order to change the phase. The temperature difference between the reference and the sample is checked in this process. DSC and DTA both give us the same information about thermal analysis. The DTA analysis method is based on measuring the temperature difference between the unknown sample and the control sample according to the same heating program [15].

In the DSC test, the control and unknown samples are kept at the same temperature, and the energy difference required to maintain isotherm is plotted in terms of temperature changes. The DSC method is slightly more quantitative than the DTA method [15].

By examining the results of the analyses, the physical properties of the material, such as melting and evaporation temperatures, and other phase changes of the material, such as crystal structure change temperature, can be obtained, or as a chemical-thermal analysis, the decomposition or oxidation temperature of the material or enthalpy changes can be calculated [15, 16].

In order to obtain information about the structural changes of matter, it is necessary for certain peaks to occur in these graphs, the surfaces below the peak and their angles representing the acquisition of changes. The graphs of the control sample and under the TCF Show that the material has not had any structural and specific changes up to the temperature of 1000 °C. Given the purity of silica at this temperature and the melting point of around 1700 °C, this behavior is expected [14].

The TGA (Thermal Gravimetric Analysis) Analysis

Thermal analysis or thermal gravimetric analysis is a thermal decomposition method that is measured by changing the temperature over a mass of a sample. Figures 5 and 6 show the details of the TGA analysis as follows:

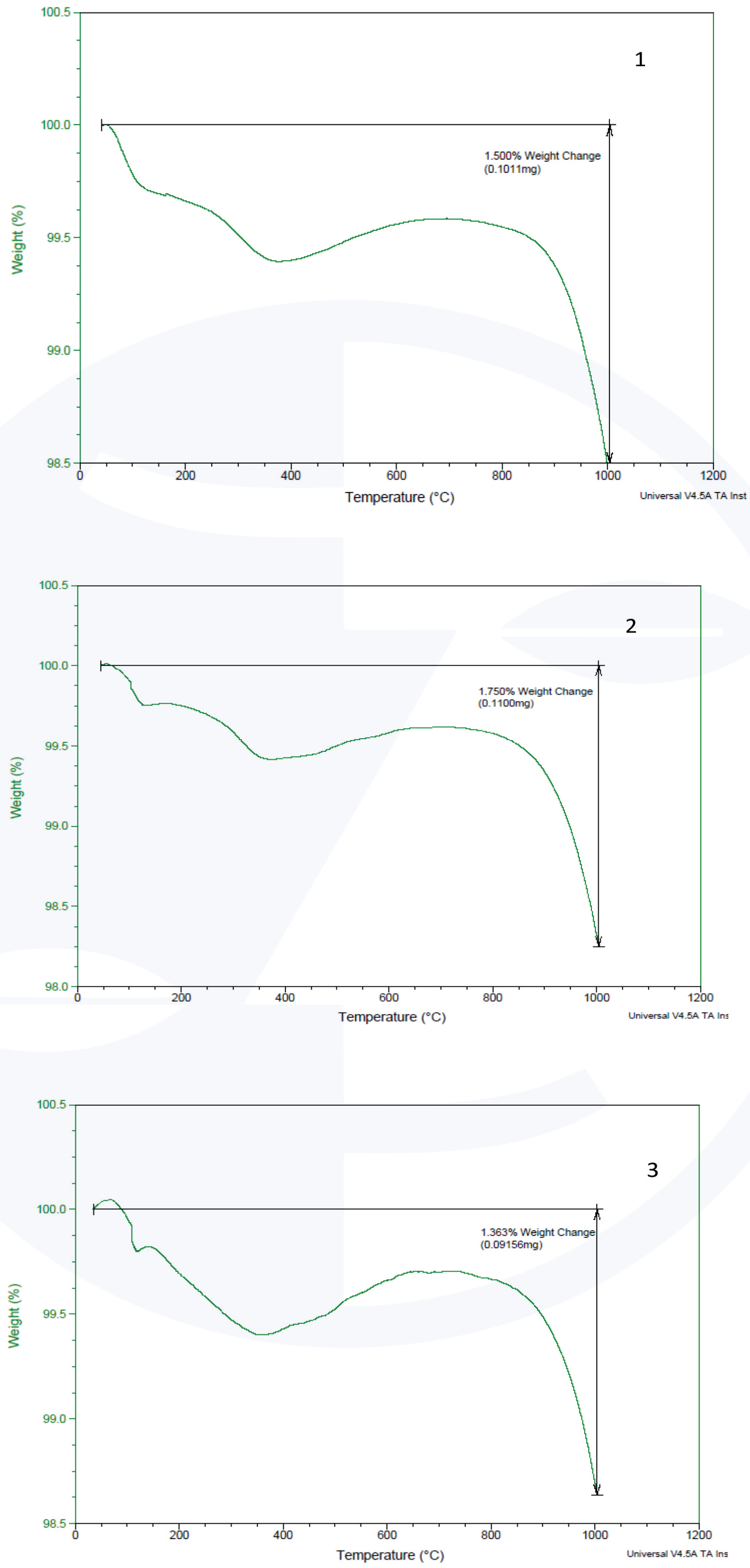

Figure 5. The mass reduction diagram (TGA), the codes 1 to 3 under the control.

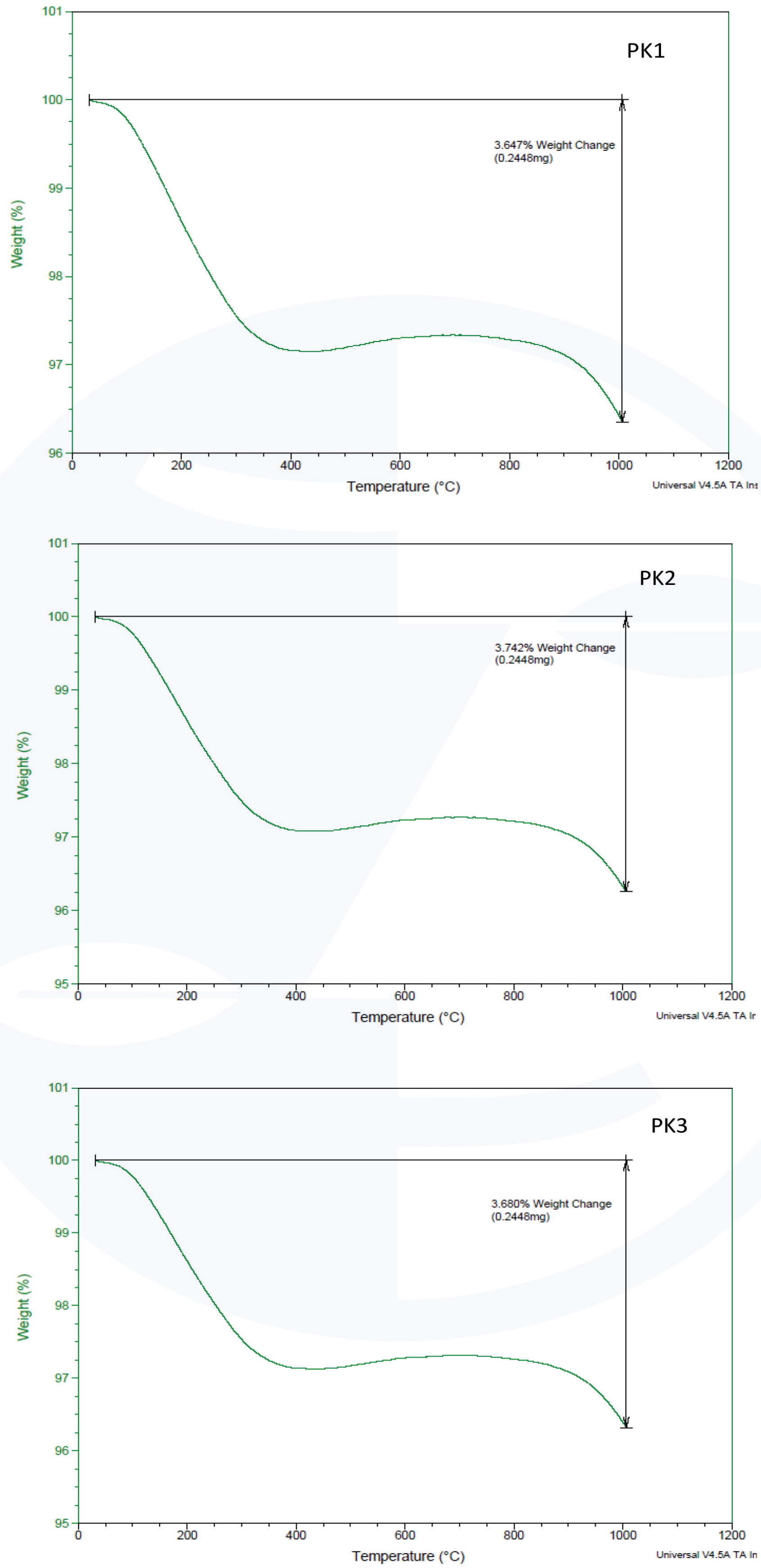

Figure 6. The mass reduction diagram (TGA), the codes PK1 toPK3 under the TCF

Figure 7 illustrates the results of the TGA test of control samples to investigate their thermal properties considering the mass loss.

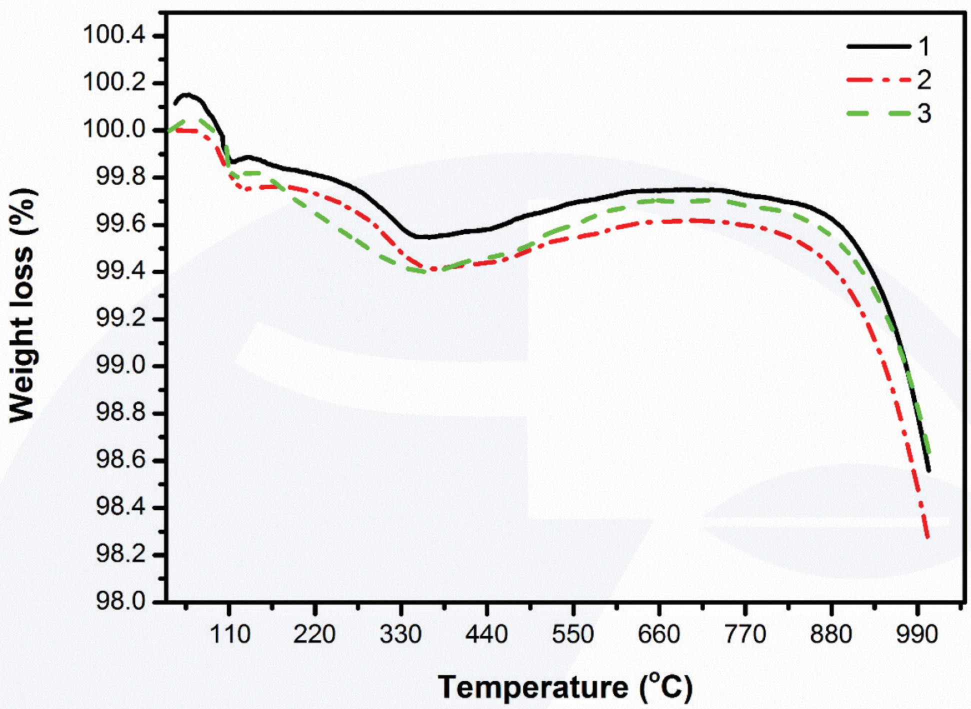

Figure 7. The TGA curves for control samples

According to Figure 7, three stages of the weight loss and one stage of the weight gain can be seen in the samples. In the first stage of the weight loss, at temperatures, less than 120 ° C, the physically absorbed water evaporates to the surface of the samples [17]. At this stage, the values of 0.14, 0.20, and 0.25% of their initial mass have been reduced, in samples 1, 2, and 3 respectively. In the second stage of the weight loss, at temperatures between 120 °C to 350 °C, the structurally absorbed water may have evaporated [18, 19]. As a result of its location within the pores of the structure, this water requires a higher temperature to evaporate. Therefore, the weight loss that occurred in the second stage for samples 1, 2, and 3 was equal to 0.32%, 0.34%, and 0.40% by weight of the raw material, respectively. The weight gain of the samples in the temperature range of 350 to 880 °C may be due to a test error (warm air error) [20].

In fact, with the heating of the air in contact with the body of the chamber, and the movement of this air with a lower density upwards and back again, after cooling at the top of the chamber, from the middle to the bottom to the collision of this airflow to the sampling vessel in the middle of the chamber, the apparent mass of the sample increases. The weight loss diagram moves upwards (weight gain). This effect can only be seen in samples where the amount of weight loss caused by heating is very small, such as the silica samples used in this study [21].

The final weight loss stage was observed at temperatures ranging between 880 and 1000 °C. At the end of this stage, the total weight loss of all stages for samples 1, 2, and 3 was 1.5%, 1.75%, and 1.36%, respectively. The samples' mean mass reduction of all these phases, including surface absorption water and structural absorption, was 1.53%. This behavior is generally expected from the natural behavior of pure silica with a melting point of around 1700 °C.

The results of the TGA test for the PK samples are shown in Figure 8.

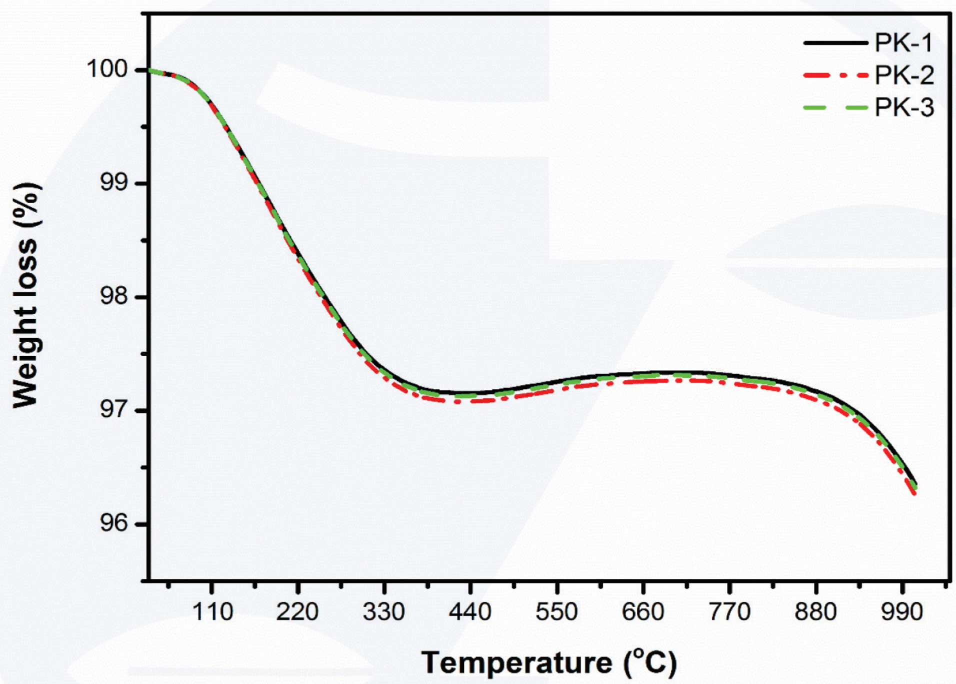

Figure 8. The TGA curves for the PK samples under the TCF

According to Figure 8, two stages of the weight loss and one stage of the weight gain can be seen in the samples. According to the figure, it is understood that, unlike numerical samples, the weight changes in each stage are very close to each other in these samples. In the first stage, the weight loss at temperatures below 350 °C has been again in the surface water absorption range and probably the structural water in these samples [18,19]. Therefore, the weight loss that occurred in the first stage for the PK1, PK2, and PK3 samples was equal to 2.85, 2.93, and 2.87% respectively by weight of the raw material. This is while all samples had the same structure and the same storage conditions. The results demonstrate that the mass reduction in these samples was higher than in the control samples. The weight gain of the samples in the temperature range of 350 to 880 °C, may also be the result of a test error (warm air error) [20].

The final weight loss stage was observed in the temperature range of 880 to 1000 °C. At the end of this stage, the total weight loss of all stages for PK1, PK2, and PK3 samples was 3.65%, 3.74%, and 3.68%, respectively. The mean value of the total mass reduction was 3.69%, which was significantly higher than the control samples. A comparison of mass changes is summarized in Table 4:

Table 4 . Numerical comparison of mass changes

Groups	Total mass reduction Mean in 350 °C	Total mass reduction Mean
The mean mass reduction in the samples under the TCF	2.88	3.69
The mean mass reduction in the control samples	0.35	1.53
Changes percent	722.85%	141%

Conclusion

The results demonstrate that the samples exposed to the T-Consciousness Field lost a significantly higher amount of mass, compared to the control samples. A 722.85% mass difference is remarkably observed up to 350 °C. As the temperature rises, eventually, 141% more mass is lost in the samples under the TCF. Due to the sameness of the material used in the experiment and the test conditions, the difference cannot be explained by material factors. According to the XRF analysis, pure silica lost less than 3% of mass weight after being placed at a temperature of 1100 °C for 1.5 hours. This mass reduction was a result of water and light elements., while the silica samples under the effect of TCF lost higher amounts of mass weight at a lower temperature compared to the control samples in a similar condition.

Overall, it was found that the Consciousness Bond Field has affected the thermal behavior of Silica and the weight mass according to Phase-0 and Taheri's theory:

T-Consciousness transforms into matter and energy, and vice versa.

It appears that these changes have not been solely the result of the burning of reaction of pure silica, although this requires further investigation. Considering that this study took place based on Taheri's theory of T-Consciousness, and is not bound to any specific material, the authors suggest the investigation of TCFs on other materials.

References

1. Taheri, M. A. (2020). The main monitoring center for T-Consciousness Fields research and studies based on Sciencefact. www.Cosmointel.com.
2. Taheri, M. A. (2012). General Connection of Particles. Interuniversal Publishing Erfan-Halgheh. ID: 978-1-940491-03-5.
3. Taheri, M. A. (2013). Human from Another Outlook (2nd Edition). ISBN-13: 978-1939507006, ISBN- 10: 1939507006.
4. Kazazi, B., & Taheri, M. A. (2021). Influence of Consciousness Bond Field (CF) on crystallization and strength of cement mortar (concrete). Retrieved from www.cosmointel.com.
5. Kazazi, B., & Taheri, M. A. (forthcoming 2022). Comparison of the behavior of concrete made under the influence of Taheri Consciousness Fields (TCFs), and under gamma and neutron radiations, with ordinary concrete, when receiving TCF and gamma and neutron radiations simultaneously.
6. Kazazi, B., & Taheri, M. A. (forthcoming 2022). Investigation of chlorine ion penetration in concrete under the influence of Taheri Consciousness Fields.
7. Kazazi, B., & Taheri, M. A. (2021). Effects of the T-Consciousness Field on Concrete (ASR. Retrieved from www.cosmointel.com.
8. Kazazi, B, & Taheri, M. A. (2021). Effect of the Consciousness Bond Field on the structure and properties of Aluminum. Retrieved from www.cos-mointel.com
9. Kazazi. B,̄ & Taheri. M. A. (2021). Effect of the Consciousness Bond Field on the structure and properties of 1000- series Aluminum –with preheating Retrieved from www.cosmointel.com.
10. Kazazi. B, & Taheri. M. A. (2021). Influence of Consciousness Bond Field on the plant synthesis of nano-silver preheating Retrieved from www.cos-mointel.com.
11. Kazazi. B, & Taheri. M. A. (2021). Study of the effect of the Consciousness Bond Field on mechanical crushing of silica particles preheating Retrieved from www.cosmointel.com.
12. Kazazi. B, & Taheri. M. Ā. (2021). - Study of changes in cement mass under Consciousness Bond Field according to Taheri's theory. Retrieved from www.cosmointel.com.
13. Kazazi. B, & Taheri. M. A. (2021). Study of density changes and increase in the length of pure copper up to 300 °C in Consciousness Bond Field. Retrieved from www.cosmointel.com.
14. Khalil. K.M, Elsamahy. A. A, & Elanany. M. S. (2002). Formation and Characterization of High Surface Area Thermally Stabilized Titania/Silica Composite Materials via Hydrolysis of Titanium (IV) tetra-Isopropoxide in Sols of Spherical Silica Particles. Journal of Colloid and Interface Science, 249, 359–365. doi:10.1006/jcis.2002.8268.
15. Hill. J. O. (2005). THERMAL ANALYSIS Temperature-Medulated Techniques. Encyclopedia of Analytical Science (Second Edition).
16. Bhadeshia, K. H. D. H. (2002). Thermal analyses techniques. Differential thermal analysis. University of Cambridge, Material Science and Metallurgy. Retrieved from www.msm.cam.ac.uk/phase-trans/2002/Thermall.pdf.
17. Yadav. M, & Ahmad. S. (2015). Montmorillonite/graphene oxide/chitosan composite: Synthesis, characterization and properties. International Journal of Biological Macromolecules, 79, 923–933. doi:10.1016/j.ijbiomac.2015.05.055.
18. Vidyadhar, A.V. (2013). Influence of Zn 2+ doping on the structural and surface morphological properties of nanocrystalline Ni-Cu spinel ferrite, International Nano Letters, 1–8. Retrieved from http://www.inl-journal.com/content/3/1/29.
19. Photisan. M. S. (2018). Influence of Calcium Aluminate Cement and Ground Granulated Blast Furnace Slag on the Synthesis of Rice Husk Ash-Based Geopolymer Mortars. (PhD thesis). The University of Kassel.
20. Saadatkhah. N, Garcia. A. C, & Ackermann. S. (2019). Experimental methods in chemical engineering: Thermogravimetric analysis—TGA. Canadian Society for Chemical Engineering. DOI: 10.1002/cjce.23673.

Examining the Length and Density Changes of Copper up to 300 °C under the Influence of Consciousness Bond Field: A Study of Taheri Consciousness Theory

Bahareh Kazazi[1*], Mohammad Ali Taheri[2]

1. Civil Engineering, CEO of Hoobe Construction Company, Tehran, Iran.

2. Sciencefact R&D Department, Cosmointel Inc. Research Center, Ontario, Canada.

*Corresponding author:

Bahareh Kazazi
Civil Engineering, CEO of Hoobe Construction Company, Tehran, Iran.

Email: baharkazazi@gmail.com

ABSTRACT

According to Taheri's theory of Consciousness, T-Consciousness can be converted into matter and energy and vice versa. Consciousness Bond Field is one of many Taheri Consciousness Fields (TCFs) founded and introduced by Mohammad Ali Taheri as new Fields. These Fields are neither matter nor energy; therefore, they do not possess a quantity, but they have direct effects on both matter and energy. In other words, although TCFs cannot be directly measured, we can investigate their effects indirectly through reproducible experiments. In this study, pure copper was selected to study its density and thermal behavior in the presence of the Consciousness Bond Field. Two meters of wire were cut from a cable and divided into two equal parts. Diffusion spectrometry was performed on the samples, and 15 pieces of 19.5 ±0.25 mm were cut from each sample. The density of the samples was examined by the Archimedes method. The samples were then heated up to 300 °C. The relative increase in their lengths was examined at targeted temperatures, and the density of the samples was measured once more. Radiographic examination was performed on the 12 samples. The test results showed that all parts were healthy and free of defects. The changes in density followed a pattern opposite to those of the control samples and inconsistent with the known laws of material physics. Considering the increase in length, the density should have been decreased significantly compared to the control samples following dilatometry, but this was not the case. The density of the samples under the Consciousness Bond Field increased despite the increase gained in length. As the samples were undamaged and intact, the sample mass must have increased according to the concept of density and its increase. An XRD sample from each group was investigated. The observed changes gave the possibility of higher defects in the sample under TCF.

Keywords: Consciousness Bond Field, Taheri Consciousness Fields, Copper Dilatometry, Densitometry

INTRODUCTION

Humans have always been curious to know the world around them. Many efforts have been made in this direction, which has led to the knowledge of various laws and fields such as gravitational field, electromagnetic field, electric field, etc. The term "field" has been used frequently in theories of physics.

The nature of consciousness and its place in science has received much attention in the current century. Many philosophical and scientific theories have been proposed in this area. In the1980s, Mohammad Ali Taheri introduced novel fields with a non-material/ non-energetic nature named Taheri Consciousness Fields (TCFs). In this perspective, T-Consciousness is one of the three existing elements of the universe apart from matter and energy. According to this theory, there are various TCFs with different functions, which are the subcategories of a networked universal internet called the Cosmic Consciousness Network (CCN). The major difference between the theory of TCFs and other theoretical concepts about consciousness is related to the practical application of the TCFs. TCFs can be applied to all living and non-living creatures, including plants, animals, microorganisms, materials, etc.

Mohammad Ali Taheri, the founder of Erfan Keyhani Halqeh, a school of thought, introduced a new science in 2020 as a branch of this school. He coined the term Sciencefact for this new science because it utilizes scientific investigations to prove the existence of T-Consciousness as an irrefutable phenomenon and a fact. Although science focuses solely on the study of matter and energy and Sciencefact, by contrast, explores the effects of the [non-material/ non-energetic] TCFs, Sciencefact has provided a common ground between the two by conducting reproducible laboratory experiments in various scientific fields, and it has used the scientific approach in proving TCFs.

The influence of the TCFs begins with the Connection between CCN as the Whole Taheri Consciousness of the universe and the subjects of study as a part. This Connection called "Ettesal" is established by the Announcer's mind (a certified and trained individual who has been entrusted with the TCFs). The human mind has an intermediary role (Announcer) which plays a part by fleeting attention to the subject of study and then the main achievement obtained as a result of the effects of the TCFs. These Fields cannot be directly measured by science, but it is possible to investigate their effects on various subjects through reproducible laboratory experiments.

The research methodology in the study of T-Consciousness has been founded on the process of Assumption, Argument, and Proof, in which the Assumption is: The Cosmos was formed by a third element called T-Consciousness that is different from matter and energy.

The Argument is the existence of TCFs can be demonstrated by its effects on matter and energy (e.g., humans, animals, plants, microorganisms, cells, materials, etc.)

The Proof is the scientific verification of the effects of TCFs on matter and energy (according to the Argument) through various reproducible scientific experiments.

Accordingly, to investigate and verify the existence, effects, and mechanisms of TCFs, the following five research phases (Phases 0 through 4), and the aims of each phase are outlined below.

Phase-0 studies aim to prove the existence of TCFs by observing their effects. The nature of T-Consciousness and what it is will not be addressed in this phase. Phase-1 explores the varied effects of different TCFs. Phase-2 examines the reason behind the varied effects of these fields. Phase-3 investigates the mechanism of TCFs effects on matter and energy. Finally, Phase-4 draws significant conclusions, particularly with regard to the mind and memory of matter and their relation to the T-Consciousness, etc. [1, 2, 3].

Since any change in the structure and function of materials requires matter or energy, it is obvious that the study of the behavior of materials and their intrinsic, mechanical, and chemical properties in the presence of TCFs would be of value to scientific researchers. This research on the function and behavior of materials began over a decade ago and has yielded considerable results including the following.

Extensive research has also been conducted on cement mortar-based materials under the influence of TCFs. Although the purpose of previous research was to investigate the overall function, properties, and behavior of concrete and cement mortar, such as strength, concrete cancer, chloride diffusion coefficient, bending of concrete beams, penetration of gamma-neutron radiation, etc. under the influence of TCFs, in the present study, the process of internal changes revealed a number of details about how TCFs influence materials, including mass change during the application of TCFs [4-13].

In addition, different methods of nanomaterial synthesis, the study of tensile properties of metals, the study of angles of contact of water with a surface and change of silica mass in the thermal analysis due to the effects of TCFs without force or energy and matter, offer a revision of known laws and definitions of the behavior of the matter [1].

In the casting of pure 1000 series aluminum from a single ingot, after examining the crystal defects using two methods, it was found that the internal defects in some cases grew up to 1000%. In those samples, the only factor was the application of TCFs which had a significant effect on grid irregularities [3, 1]. Clearly, creating this level of displacement otherwise requires energy supply [4-13].

In the molecular software simulation of the behavior of aluminum, it was found that electron volts energy is created in the samples under the TCF if we consider the defects in half epsilon, assuming the mass remains constant per atom as (-3.10 eV) [13]. Given the background of the studies, the fundamental question was whether it is possible that underlying changes have taken place in the realm of the matter, and this is we have been overlooked due to the software limitations and the fact that mass has been kept constant?

Given these results, in the present research, pure copper was selected to investigate the thermal behavior and density changes before and after dilatometry up to 300 °C.

Materials and test methods

Preparation of the copper wire and analysis

It was unknown what effect the TCF would have on the matter. Also, the possibility of a change in volume, length, mass or distortion, etc., was given. This is because, in practice, the matter may not have the same expansion in all dimensions. For us, however, the basis for comparison was directly the measurement of volume. Therefore, considering any possible effects, the frequency, and the wire's diameter and length should have been measured at close intervals. This enabled us to measure the possible volume change over approximately two centimeters. However, such a test would have created a measurement error. In addition, the measurement alone was not effective due to the unknown mechanism of volume change under the TCF. Therefore, Archimedes' density was used as the initial measurement. This experiment was performed in three sets as follows:

Two meters of copper-filled solid wire with a diameter of 8 mm were cut. Emission spectrometry according to the BS EN 15079- 15 standard was performed. The wire was di-vided into two equal parts. One of the piec es was assigned to the Consciousness Bond Field test by the project executor and the other was assigned to the control by the laboratory of-ficial. Fifteen samples, each 19.5±0.25 mm in length, were cut from each wire by the laboratory official. The density of each of the 9 samples e was measured by the Archimedes method. All fifteen samples were then

dilat-ed by the ASTM E289-17 standard up to 300 °C and after the changes, densitometry was performed again. To investigate the surface defects, industrial radiography before and after dilatometry was used for each group. A sample from each group was examined in order to evaluate the crystal changes. A 3mm piece was cut from one side. The two 3 mm pieces were then cut again (for 3mm) to bring the probe closer to the center of the pieces, and they were examined crystallographically (XRD).

Application of the Taheri Consciousness Field

One of the TCFs, called the Consciousness Bond Field, was applied to the samples according to the protocols regulated by the COSMOintel research center (www.COSMOintel.com). A request for Connec tion to the CCN to utilize TCFs can be placed through the COSMOintel website in the "Assign Announcement" section. This access is available for everyone at no cost. In order to study and experience this Connection, the researchers can register on the website at any time in order to report the experiment to the COSMOintel research center. Certain details of the experiment must be provided to the center; for example, the characteristics or number and name of samples and controls must be spec-ified. This entire experiment was carried out as a double-blind method where lab techni-cians were completely unaware of the TCFs theory, and the Announcer at the COS-MOintel research center who established the Connection was unaware of the details of the study. Double-blind is a gold standard that is common in science experiments.

Results and discussion

Spectrochemical analysis

The result of the spectrochemical analysis test shows the percent abundance of possible ele-ments in the sample and the purity level of the copper sample. It was determined from the re-sults that the copper sample was 99.9% pure. The details are shown in Table 1.

Table 1 . The sample spectrometry

Zn	Pb	Sn	P	Mn
<0.01	0.01	<0.01	<0.005	Trace
S	**Ag**	**Co**	**Be**	**Cu**
None	Trace	0.01	<0.001	99.9
Fe	**Ni**	**Si**	**Cr**	**Al**
<0.005	0.03	<0.005	Trace	0.004

Increase in length

Following are the results of dilatometric analysis, as well as the relative increase in length due to heat and the difference in density before and after dilatometry for the two groups (Table 2).

Table 2 . Increase in copper length due to heat and density changes

	Name	100 °C	200 °C	300 °C		Before	After	
Change in Length (mm) of Control Samples	1	0.015	0.035	0.051	Density (±0.05) (g/cm³)	8.84	8.83	-0.113
	2	0.015	0.036	0.051		8.85	8.83	-0.225
	3	0.016	0.034	0.051		8.85	8.84	-0.112
	4	0.008	0.032	0.066		8.85	8.80	-0.564
	5	0.009	0.034	0.067		8.81	8.81	0
	6	0.008	0.032	0.066		8.82	8.79	-0.340
	7	0.009	0.032	0.066		8.85	8.81	-0.451
	8	0.008	0.036	0.068		8.86	8.81	0.564
	9	0.006	0.032	0.063		8.85	8.80	-0.564
	10	0.007	0.031	0.068				-0.488
	11	0.007	0.032	0.065				
	12	0.005	0.033	0.071				
	13	0.006	0.031	0.06				
	14	0.006	0.034	0.067				
	15	0.006	0.032	0.067				
	Average	0.008733	0.033067	0.063133				
Change in Length (mm) of TCF Samples	fs1	0.016	0.037	0.055	Density (±0.05) (g/cm³)	8.83	8.85	0.226
	fs2	0.015	0.032	0.049		8.83	8.86	0.339
	fs3	0.016	0.038	0.059		8.82	8.85	0.340
	ck1	0.008	0.034	0.068		8.82	8.83	0.113
	ck2	0.007	0.032	0.065		8.84	8.85	0.113
	ck3	0.008	0.033	0.067		8.82	8.83	0.113
	ck4	0.01	0.036	0.068		8.83	8.83	0
	ck5	0.008	0.033	0.066		8.82	8.81	-0.113
	ck6	0.009	0.034	0.069		8.82	8.82	0
	c1	0.007	0.032	0.068				0.226
	c2	0.008	0.035	0.07				
	c3	0.007	0.031	0.066				
	c4	0.006	0.034	0.067				
	c5	0.005	0.035	0.071				
	c6	0.006	0.033	0.065				
	Average	0.009067	0.033933	0.064867				
	%Change	3.80%	2.61%	2.74%				

To account for potential variability and minimizing possible errors, the experiment was repeated in three separate groups with multiple samples. The results of the changes in each group were compared and examined with the average of the changes in the group, as shown in Table 3.

Table 3 . Comparison of average length changes in the tested groups ncrease in copper length due to heat and density changes

Series	100 C	200 C	300 C
Control -Group1 average	0.015333	0.035000	0.051000
TCF-Group1 average	0.015667	0.035667	0.054333
Change %	**2.70%**	**2%**	**6.50%**
Control-Group2 average	0.008000	0.033000	0.066000
TCF-Group2 average	0.008333	0.033667	0.067167
Change%	**4%**	**2%**	**1.70%**
Control-Group3 average	0.006167	0.032167	0.066333
TCF-Group3 average	0.006500	0.033333	0.067833
Change%	5.30%	3.60%	2.30%

A laboratory official provided the num-bers. According to the official protocol of the laboratory, the results are usually reported to the three decimal places. However, copper's longitudinal expansion coefficient is $17\times10^{-6}(1/k)$ and because of the very small length and the very low test temperature, the results were reported with differences up to 6 decimal places. It was in order to be able to understand the length change properly.

In Table 4, the mean changes in the length of all samples under the influence of the Con-sciousness Bond Field are compared with the mean of the control samples.

Table 4 . Comparison of mean changes in the length of all the samples under the influence of Consciousness Bond Field compared to the control

All Controls Ave.	0.008733	0.033067	0.063133
All TCFs Ave.	0.009067	0.033933	0.064867
%Change	3.80%	2.61%	2.74%

According to the total results, the parts un-der the TCF seemingly had a relative increase in length compared with the control samples. This is because one factor that characterizes the behavior of materials under heat is the lin-ear thermal expansion coefficient of the mate-rial presented by the laboratory.

Linear expansion coefficients

Linear expansion coefficients are the rate of change of unit length per unit degree change in temperature. The coefficient of linear expan-sion of materials is found from the following formula:

$$\alpha = (dl/dT)*l/1$$

Linear expansion coefficient is inversely related to the initial length of the sample and directly related to the length changes. In this study, the temperature was constant, and the results of linear expansion coefficients of sam-ples are shown in Table 5 [14].

Table 5 . Linear expansion coefficients of the sample (All of the results are in 10-6 range)

Linear Thermal Expansion Coefficients 1/C mm/mm			
Control		TCF	
Name	$\alpha\times10^{-6}$	Name	$\alpha\times10^{-6}$
1	18.2	fs1	18.8
2	18.2	fs2	17.4
3	17.8	fs3	19.0
Average	**18.0**	**Average**	**18.4**
4	15.6	ck1	15.6
5	14.8	ck2	15.5
6	16.6	ck3	15.1
7	13.8	ck4	15.6
8	15.6	ck5	16.8
9	15.6	ck6	15.1
Average	**15.3**	**Average**	**15.6**
10	14.9	c1	15.0
11	15.0	c2	14.6
12	14.6	c3	14.8
13	14.6	c4	14.5
14	15.1	c5	14.6
15	14.7	c6	15.1
Average	**14.8**	**Average**	**14.9**

Considering the linear expansion coefficients of pure copper that are 17×10-6(1/k), the length of samples tends to increase under the effect of the Consciousness Bond Field.

Obviously, given the length of the samples, the small temperature changes relative to the melting point of copper (1085 ºC) [14], and only applying the TCF without any other external process, large changes are not expected. We will elaborate on the possibility of large changes later.

Comparison of density before and after dilatometry

This research is based on laboratory experiments on the possibility of changes in materials, on the other hand, any produced material, even if it is standard and high quality, has a few changes in the structure. Therefore, the best way to analyze the results is to compare the behavior of each piece before and after exposure to the Consciousness Bond Field. In order to do this, the density of each sample was compared before and after exposure. Figure 1 and Table 6 show the results.

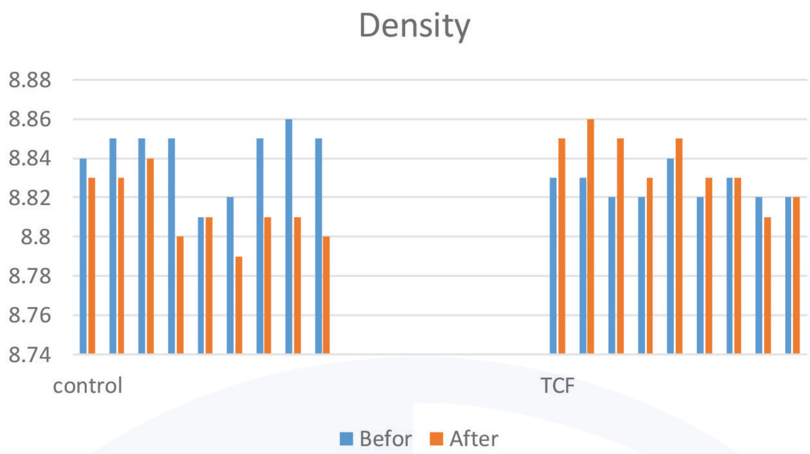

Figure 3. Comparison of changes in the density of samples

As results demonstrate, the samples under the Consciousness Field show an increase in the density after the application of heat. The comparison of these changes is presented in Table 6.

Table 6 . The comparison of density changes in samples

	300 °C Control			300 °C TCF		
Sample	Before	After	Difference	Before	After	Difference
1	8.84	8.83	**-0.113**	8.83	8.85	**0.226**
2	8.85	8.83	**-0.225**	8.83	8.86	**0.339**
3	8.85	8.84	**-0.112**	8.82	8.85	**0.340**
4	8.85	8.80	**-0.564**	8.82	8.83	**0.113**
5	8.81	8.81	**0**	8.84	8.85	**0.113**
6	8.82	8.79	**-0.340**	8.82	8.83	**0.113**
7	8.85	8.81	**-0.451**	8.83	8.83	**0**
8	8.86	8.81	**0.564**	8.82	8.81	**- 0.113**
9	8.85	8.80	**-0.564**	8.82	8.82	**0**
Average	8.84	8.81	**-0.488**	8.83	8.84	**0.226**
	average difference of density%		**-5.4%**	average difference of density%		**+2.5%**
	difference-in-difference of average density in two groups					**7.9%**

Theoretical Discussion

The results of Table 2 show that the samples under the Consciousness Bond Field had an increase in the relative length. The linear thermal expansion coefficient of pure copper means that a unit of copper will have a relative increase of 0.000017 per unit of length. This coefficient depends on the magnitude of the temperature difference. Also, the melting temperature of copper is 1080 °C, which is 780 °C higher than the temperature of this experiment. As an example, the linear thermal expansion coefficient of cast Copper from ambient temperature to 100 °C from 17 to 18× 10^{-6} [14].

These changes provide a better understand-ing of the effect of the T-consciousness Field which is non-material and non-energetic. It is very difficult to change the density of the crys -talline solids. Copper has the atomic structure of FCC and is one of the most compact atom-ic lattices. In these atomic lattices, the copper atom contacts 12 other atoms, and 74% of the atomic lattice space is filled [16]. To better understand the required energy to change the density of copper, refer to an example where a copper sample with a length of 10 mm and a cross-section radius of 2.4 mm with a cold-rolled coil equivalent to the strain of 4.5 with a magnitude of difference up to 4 decimal places had a density change of only 0.8% [16]. Therefore, any change in the structure of atomic lattices requires a considerable amount of energy.

Heating or cooling affects all the dimensions of a body of material, with a resultant change in volume. Volume changes may be determined from:

$$\Delta V / V_0 = \alpha_V \Delta T$$

where ΔV and V_0 are the volume change and original volume, respectively, and α_V represents the volume coefficient of thermal expansion. In many materials, the value of α_V is anisotropic.

that is, it depends on the crystallographic direction along which it is measured. For materials in which the thermal expansion is isotropic, α_V is approximately 3α [14].

Therefore, based on the principle of material and energy conservation and with the mass remaining constant, a 5.4% decrease in the average density difference was observed in the control group before and after dilatometry. On the contrary, the density has increased in the samples under the Consciousness Field. This is despite the fact that the average density of these samples before dilatometry was 0.01 (g/cm3) less than the control samples. A 1.5% higher linear expansion coefficient leads to a 4.5% higher volumetric thermal expansion coefficient. Therefore, the volume of the samples under the TCF has theoretically become much larger. If the mass remained constant, theoretically, the density of the samples under the TCF after dilatometric should have had a much smaller density than the control sample ($\rho = m/V$). The difference in differences in the density of the samples compared with the control group was (-5.4%) + (2.505) = 7.9% which is a much higher density. This change is only possible by creating a heavier mass. However, for both groups, part of the increase in volume has returned to normal after cooling.

In this study, there is one sample with high dispersion in each group, and if only numerical and theoretical studies were considered, these samples would have been removed and the difference would have been much larger. But our basis in this study is only experimental data and no observation was excluded. According to Taheri's theory of T-Consciousness, the third factor, which is neither energy nor matter but can be converted into matter and energy, is T-Consciousness. Despite the compactness of the copper atomic lattice, how T-Consciousness has made matter denser and what changes have taken place in the copper atomic lattice needs more research.

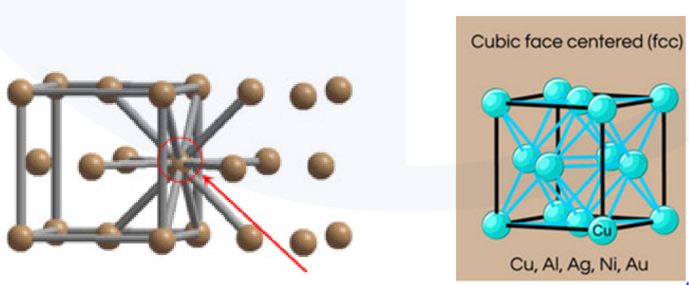

Figure 2. Schematic picture of the copper crystal lattice

Radiographic results

Among the factors checked for accuracy was the accuracy of the parts before and after dilatometry. A check was made to ensure that they were free of cracks and holes. For this reason, radio-graphs were taken of the second series. The original radiographic reports are provided in the following in figures 3 and 4.

Revision number : 0		Radiographic test report							Reference code/standard : —			
Nominal Thickness (mm)	No. of film	Film Size (cm)	Visible IQI	Repair		Reject	Accept	Order No.	Segment	Type of defect(s) / location / Dimension		
---	1	10*20	Wire 12	---		•		38157 1~6	B-CK 1~6	Not Seen		
Source Type	Source size (mm*mm)	Total film length(cm)	IQI Type	Film type	Screen Type	Exposure Technique	Ug (mm)	Sensitivity %	Density	SFD (cm)	Exposure Time (minute)	Source Strength(K
X-RAY	2*2	20	10-16 Cu	Kodak AA400	Lead	SWSI	≤0.51	1-2	1.8-4	60	0.4	170
Abbreviation		Type of Weld Defects				Technique			Other			
		LOP: Lack of Penetration				SWSI: Single Wall Single Image			SFD: Source To Film Distance			
		LOF: Lack of Fusion				DWSI: Double Wall Single Image			IQI: Image Quality Indicator			
		Ti: Tungsten Inclusion				DWDI: Double Wall Double Image			No.: Number			
*REMARK: Test result shall be considered by the customer.												

Revision number : 0		Radiographic test report							Reference code/standard : —			
Nominal Thickness (mm)	No. of film	Film Size (cm)	Visible IQI	Repair		Reject	Accept	Order No.	Segment	Type of defect(s) / location / Dimension		
---	1	10*20	Wire 12	---		•		38157 1~6	A-CK 1~6	Not Seen		
Source Type	Source size (mm*mm)	Total film length(cm)	IQI Type	Film type	Screen Type	Exposure Technique	Ug (mm)	Sensitivity %	Density	SFD (cm)	Exposure Time (minute)	Source Strength(K
X-RAY	2*2	20	10-16 Cu	Kodak AA400	Lead	SWSI	≤0.51	1-2	1.8-4	60	0.4	170
Abbreviation		Type of Weld Defects				Technique			Other			
		LOP: Lack of Penetration				SWSI: Single Wall Single Image			SFD: Source To Film Distance			
		LOF: Lack of Fusion				DWSI: Double Wall Single Image			IQI: Image Quality Indicator			
		Ti: Tungsten Inclusion				DWDI: Double Wall Double Image			No.: Number			
*REMARK: Test result shall be considered by the customer.												

Figure 3. Radiography before and after dilatometry of ck samples under the T-Consciousness Field

Revision number : 0		Radiographic test report							Reference code/standard : —			
Nominal Thickness (mm)	No. of film	Film Size (cm)	Visible IQI	Repair		Reject	Accept	Order No.	Segment	Type of defect(s) / location / Dimension		
---	1	10*20	Wire 12	---		•		38157 7~12	B-1~6	Not Seen		
Source Type	Source size (mm*mm)	Total film length(cm)	IQI Type	Film type	Screen Type	Exposure Technique	Ug (mm)	Sensitivity %	Density	SFD (cm)	Exposure Time (minute)	Source Strength(K
X-RAY	2*2	20	10-16 Cu	Kodak AA400	Lead	SWSI	≤0.51	1-2	1.8-4	60	0.4	170
Abbreviation		Type of Weld Defects				Technique			Other			
		LOP: Lack of Penetration				SWSI: Single Wall Single Image			SFD: Source To Film Distance			
		LOF: Lack of Fusion				DWSI: Double Wall Single Image			IQI: Image Quality Indicator			
		Ti: Tungsten Inclusion				DWDI: Double Wall Double Image			No.: Number			
*REMARK: Test result shall be considered by the customer.												

Revision number : 0		Radiographic test report							Reference code/standard : —			
Nominal Thickness (mm)	No. of film	Film Size (cm)	Visible IQI	Repair		Reject	Accept	Order No.	Segment	Type of defect(s) / location / Dimension		
---	1	10*20	Wire 12	---		•		38157 7~12	A-1~6	Not Seen		
Source Type	Source size (mm*mm)	Total film length(cm)	IQI Type	Film type	Screen Type	Exposure Technique	Ug (mm)	Sensitivity %	Density	SFD (cm)	Exposure Time (minute)	Source Strength(K
X-RAY	2*2	20	10-16 Cu	Kodak AA400	Lead	SWSI	≤0.51	1-2	1.8-4	60	0.4	170
Abbreviation		Type of Weld Defects				Technique			Other			
		LOP: Lack of Penetration				SWSI: Single Wall Single Image			SFD: Source To Film Distance			
		LOF: Lack of Fusion				DWSI: Double Wall Single Image			IQI: Image Quality Indicator			
		Ti: Tungsten Inclusion				DWDI: Double Wall Double Image			No.: Number			

Figure 4. Radiography before and after dilatometry of the control samples

The test results showed that all parts were healthy and free of defects. Density numbers and length changes depended on the healthy part and were not because of the cavities or cracks. The radiographic images of the samples are provided here.

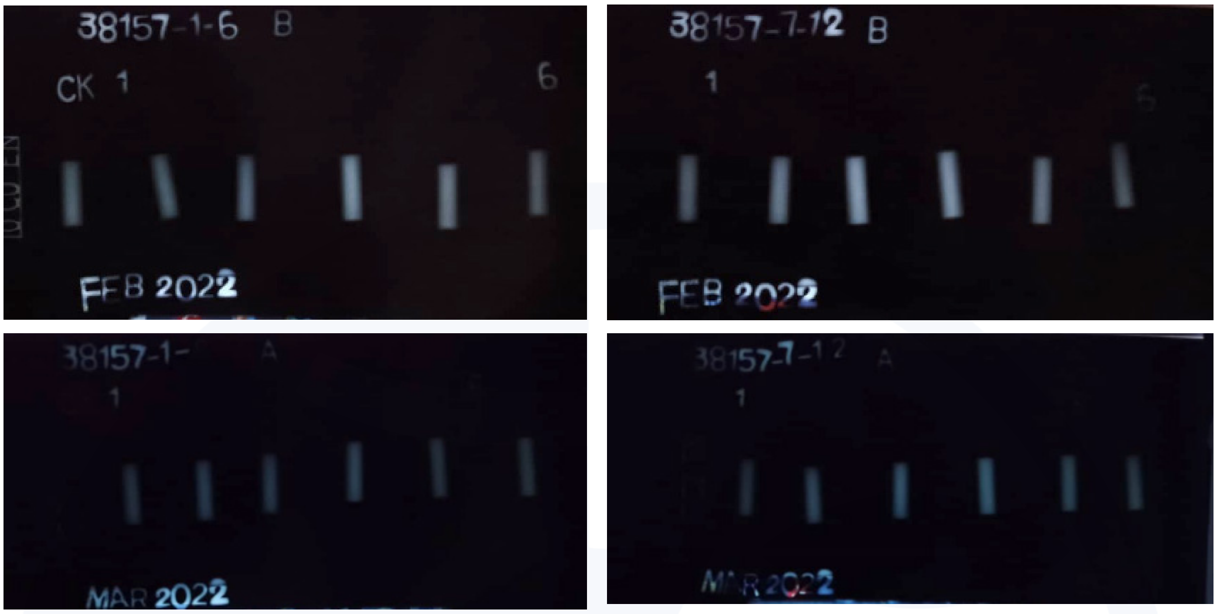

Figure 5. Radiography of the samples. The images on the right are the control samples, and the images on the left are the samples under the influence of the Consciousness Bond Field. The images on the top are before dilatometry and the images on the bottom are after dilatometry.

XRD (X-Ray Diffraction Crystallography)

XRD test was used to evaluate the changes in the crystal structure of the two experimental samples. The X-ray diffraction patterns of these two samples are shown in Figure 6. Tests were performed with a copper anode at a voltage of 30 mA and a current of 40 kV. Step size was 0.05° and counting time per step was 0.5 sec.

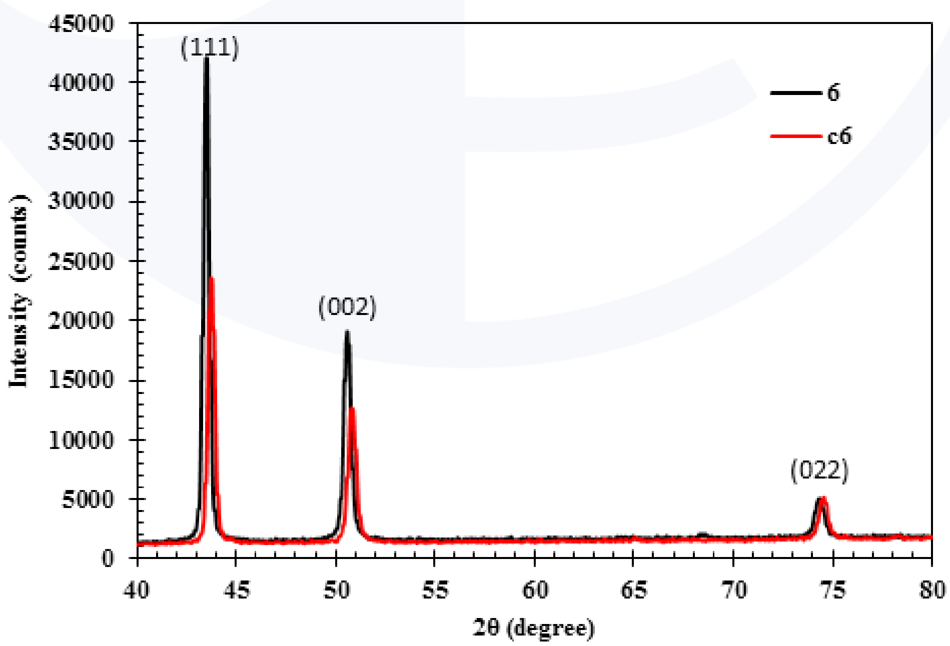

Figure 6. The X-ray diffraction pattern of the experimental samples (C6:TCF & 6: Control)

X'Pert Highscore Plus software was used to identify the phase from the results of the X-ray diffraction pattern of these samples. According to Figure 6, it is clear that in these samples only one crystalline phase is formed. By adapting these peaks to the reference diffraction patterns by the mentioned software, it was found that these two samples had the highest compliance with the copper structure with the reference code JCPDS No. 968-431-3208 has a cubic crystal structure and Fm-3m space group (FCC structure). The diffraction plates of each peak are shown on the same peak in Figure 6. According to Figure 6, two major changes in diffraction patterns are observed for these two samples. The first change is related to the higher diffraction intensity of some peaks in sample 6 than in sample c6 and the second change is the displacement of peaks related to sample c6 to the higher angles. In general, the increase in the intensity of crystalline peaks can be attributed to the increase in the degree of crystallinity of the structure [17]. Therefore, the lower crystallinity of sample c6 may be due to the presence of crystal defects in the structure of this material. On the other hand, displacement of the peaks can be attributed to the distance between the plates and the lattice parameter according to Bragg law [18].

$$(n\lambda = 2d\sin\theta) \quad (1)$$

Where n is a constant value (here equal to 1), λ is the X-ray wavelength (here 1.54 angstroms), d is the spacing of the diffraction between the graphene oxide plates and θ is the location of the peak. Accordingly, the distance between the crystal plates decreases with the increasing angle of the peak. Thus, the distance between the diffraction plates (111), (002), and (022) decreased from 2,091, 1,811, and 1,281 angstroms in sample 6 to 2,090, 1.810 and 1,280 angstroms in sample c6, respectively. On the other hand, the value of the distance between the plates according to Equation 2 in the cubic crystal lattice is related to the lattice parameter (the distance between two atoms in the crystal lattice) [19].

$$d = a / (h^2 + k^2 + l^2)^{0.5} \quad (2)$$

Where d is the distance between the crystal plates, a is the lattice parameter, and h, k, and l are the Miller indices of the diffraction plates. Accordingly, and due to the fact that the Miller indices are constant for the two samples, the reduction of the plate spacing in sample c6 compared to sample 6 can be attributed to the lower lattice parameter in this sample than in sample 6. According to this relation, the lattice parameters for samples c6 and 6 are equal to 3.622 and 3.620 angstroms, respectively. This lower lattice parameter may be due to defects such as gaps in the c6 crystal structure.

The size of the crystal and the macrostrain related to the structure of the two materials can also be calculated from the results of the XRD test. To calculate these parameters, the MAUD Rietveld software was used. It is a technique introduced by Hugo Rietveld for identification of the crystalline materials. In this technique, the height, width, and position of each peak in its X-ray diffraction pattern can be used to determine many structural aspects of the material. Rietveld's technique uses the least-squares method to better fit the theoretical values on the measured values [20,21]. According to the results of this method, the crystal size of samples 6 and c6 are 100.5 and 95.4 nm, respectively. Also, the micristrain of the structure of these two samples are equal to 0.0020 and 0.0022, respectively. The higher micristrain of the c6 structure can be considered another reason for the lattice distortion due to the structural defects.

Conclusion

In this study, 99.9% pure copper was used. According to the results of the dilatometric test, the samples under the influence of the Consciousness Bond Field had a significant increase in length. Therefore, the first result was a change in length of pure copper up to 300 °C in the presence of the Consciousness Bond Field compared to the control sample. Also, the samples whose density was measured before and after dilatometry showed a pattern of density change opposite to that of the control samples. Due to the increase in length, it is obvious that the sample volume has increased and according to the definition of density, the density should have decreased after dilatometry, which was the case in the control samples. But in the samples under the influence of the Consciousness Bond Field, the density increased. This is related to the increase in the mass of samples under the influence of the Consciousness Bond Field.

Moreover, radiographs of the samples showed that an increase in the length did not cause destruction in the samples and the samples were all intact. And the increase in length and changes in density were not a result of changes in appearance or defects in the samples. Given that the experimental conditions were constant and that the only variable was the presence of the Consciousness Bond Field, we can attribute the results to Taheri's theory of T-Consciousness which states T-Consciousness can be converted to both matter and en-ergy, and so the increased density. According to the XRD results, the crystal size of samples 6 and c6 are 100.5 and 95.4 nm, respectively. Also, the micristrain of the structure of these two samples are equal to 0.0020 and 0.0022, respectively. The higher micristrain of the c6 structure can be considered another reason for the lattice distortion due to the structural defects.

One of the possible reasons for the increase in mass could be the effect on the crys-tal lattice distortion. Considering the compact atomic lattices of copper, any further compaction would lead to higher defects.

Due to the novelty of this idea and its comprehensiveness, it is recommended to examine the possibility of changes in the atomic structure and crystal lattices of other materi-als as well as subatomic changes and theories for denser particles. The investigation will en-able us to further findings on the effects of the Consciousness Bond Field on the matter.

Acknowledgment

We appreciate the sincere cooperation of the Razi Metallurgy Research Center.

References

1. Taheri, M. A. (2020). The main monitoring center for T-Consciousness Fields research and studies based on Sciencefact. www.Cosmointel.com.
2. Taheri, M. A. (2012). General Connection of Particles. Interuniversal Publishing Erfan-Halgheh. ID: 978-1-940491-03-5.
3. Taheri, M. A. (2013). Human from Another Outlook (2nd Edition). ISBN-13: 978-1939507006, ISBN- 10: 1939507006.
4. Kazazi, B, & Taheri, M. A. (2021). Effect of the Consciousness Bond Field on the structure and properties of Aluminum. Retrieved from www.cosmointel.com.
5. Kazazi. B, & Taheri. M. A. (2021). Effect of the Consciousness Bond Field on the structure and properties of 1000- series Aluminum–with preheating Retrieved from www.cosmointel.com.
6. Kazazi. B, & Taheri. M. A. (2021). Study of density changes and increase in the length of pure copper up to 300 °C in Consciousness Bond Field. Retrieved from www.cosmointel.com.
7. Kazazi. B, & Taheri. M. A. (2021). Study of the effect of the Consciousness Bond Field on mechanical crushing of silica particles preheating Retrieved from www.cosmointel.com.
8. Kazazi. B, & Taheri. M. A. (2021). Influence of Consciousness Bond Field on the plant synthesis of nano-silver preheating Retrieved from www.cosmointel.com.
9. Kazazi, B., & Taheri, M. A. (2021). Influence of Consciousness Bond Field (CF) on crystallization and strength of cement mortar (concrete). Retrieved from www.cosmointel.com.
10. Kazazi, B., & Taheri, M. A. (forthcoming 2022). Comparison of the behavior of concrete made under the influence of Taheri Consciousness Fields (TCFs), and under gamma and neutron radiations, with ordinary concrete, when receiving TCF and gamma and neutron radiations simultaneously.
11. Kazazi, B., & Taheri, M. A. (forthcoming 2022). Investigation of chlorine ion penetration in concrete under the influence of Taheri Consciousness Fields.
12. Kazazi, B., & Taheri, M. A. (2021). Effects of the T-Consciousness Field on Concrete (ASR. Retrieved from www.cosmointel.com.
13. Kazazi. B, & Taheri. M. A. (forthcoming 2022). Molecular software simulation of the behavior of aluminum under TCFs.
14. ASM International. www.asminternational.org
15. WWW.nano.ir
16. Forouzanmehr N, Nili-Ahmadabadi M, Abdous H, Fallahi B.(2020). On the free volumes of severely deformed pure Fe and Cu, similarities and differences. Metallurgical Engineering, 23(1): 4-15 http://dx.doi.org/10.22076/me.2020.112690.1255
17. Inoue M, Hirasawa I. (2013). The relationship between crystal morphology and XRD peak intensity on CaSO4·2H2O. Journal of Crystal Growth; 380:169–75. doi:10.1016/J.JCRYSGRO.2013.06.017.
18. Fish PW. (1971). Electron diffraction and the Bragg equation. Physics Education;6:002. doi:10.1088/0031-9120/6/1/002.
19. Mousa AM, Haider AJ, Al-jawad SMH. (2011). Optical Properties of Nanostructure in CdS at Different Condition Bath Optical Properties of Nanostructure in CdS at Different Condition Bath Deposition. Journal of Materials Science and Engineering ;5:184–91. doi:10.17265/2161-6213/2011.02.011.
20. Hernandez CC, Ferreira FF, Rosa DS. (2018). X-ray powder diffraction and other analyses of cellulose nanocrystals obtained from corn straw by chemical treatments. Carbohydrate Polymers;193:39–44. doi:10.1016/j.carbpol.2018.03.085.
21. Ju X, Bowden M, Brown EE, Zhang X. (2015). An improved X-ray diffraction method for cellulose crystallinity measurement. Carbohydrate Polymers;123:476–81. doi:10.1016/j.carbpol.2014.12.071.

Changes in Cement Mass under the Influence of Consciousness Bond Field: A Study of Taheri Consciousness Theory

Bahareh Kazazi[1*], Mohammad Ali Taheri[2]

1. Civil Engineering, CEO of Hoobe Construction Company, Tehran, Iran.

2. Sciencefact R&D Department, Cosmointel Inc. Research Center, Ontario, Canada.

* Corresponding author:

Bahareh Kazazi
Civil Engineering, CEO of Hoobe Construction Company, Tehran, Iran.

Email: baharkazazi@gmail.com

ABSTRACT

Taheri Consciousness (T-Consciousness) was introduced and defined by Mohammad Ali Taheri as one of the constituent components of the Cosmos in addition to matter and energy, from which Taheri Consciousness Fields (TCFs) are derived. TCFs are not matter or energy, but they can be proven by scientific experiments. In this regard, extensive research on materials indicates that the occurred changes require energy. As no energy was applied during the experiment, the only reason for these changes was the existence of T-Consciousness. By examining the behavior of cement in various functions, it was found that in many cases, the water absorption of cement was reduced or remained constant while the number of elements had changed. This finding raised the possibility of a change in the mass of the matter. This study investigated the volume and mass of 9 identical cement samples up to 28 days old. It was found that water absorption under T-Consciousness Field was still lower (-2.8%, -2.6%), the mass of the samples increased (3 to 4%), and the percentage of crystalline phase was higher in the samples under the Field. TGA (Thermal gravimetric analysis), DTA (Differential thermal analysis), and DSC (Differential scanning calorimetry) analysis results were consistent with XRF (X-Ray Fluorescence) and XRD (X-ray Diffraction).

Keywords: Consciousness Bond Field, Taheri Consciousness Fields, Crystal changes, Cement, Mass change, Thermal analysis

The First Journal in T-Consciousness Research
Journal of CosmoIntel

INTRODUCTION

Throughout history, humans have been curious about the world around them. Many efforts have been made in this direction, leading to the discovery of many principles, laws, and fields, such as gravitational field, electromagnetic field, electric field, etc.

The nature of consciousness and its place in science has received much attention in the current century. Many philosophical and scientific theories have been proposed in this area. In the 1980s, Mohammad Ali Taheri introduced novel fields with a non-material/non-energetic nature named Taheri Consciousness Fields (TCFs). In this perspective, T-Consciousness is one of the three existing elements of the universe apart from matter and energy and can be converted into matter and energy and vice versa [1,2].

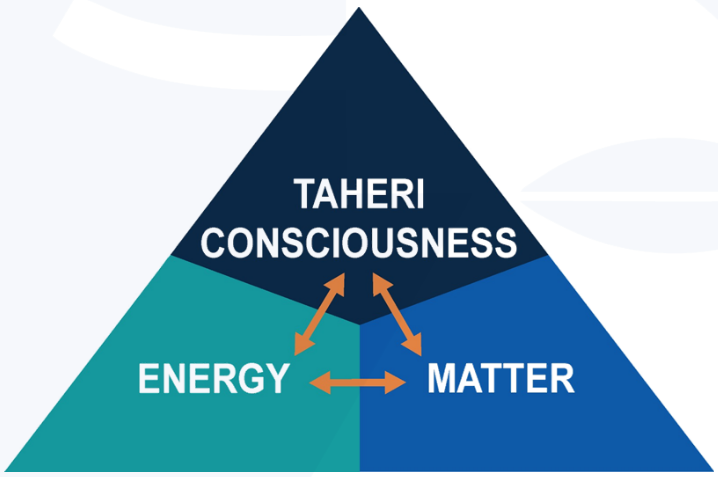

Figure 1. The relationship between T-Consciousness, matter, and energy in the theory of TCFs

According to this theory, there are various TCFs with different functions, which are the subcategories of a networked universal internet called the Cosmic Consciousness Network (CCN). The major difference between the theory of TCFs and other theoretical concepts about consciousness is related to the practical application of the TCFs. TCFs can be applied to all living and non-living creatures, including plants, animals, microorganisms, materials, etc.

Mohammad Ali Taheri, the founder of Erfan Keyhani Halqeh, a school of thought, introduced a new science in 2020 as a branch of this school. He coined the term Sciencefact for this new science because it utilizes scientific investigations to prove the existence of T-Consciousness as an irrefutable phenomenon and a fact. Although science focuses solely on the study of matter and energy and Sciencefact, by contrast, explores the effects of the [non-material/non-energetic] TCFs, Sciencefact has provided a common ground between the two by conducting reproducible laboratory experiments in various scientific fields, and it has used the scientific approach in proving TCFs.

The influence of the TCFs begins with the Connection between CCN as the Whole Taheri Consciousness of the universe and the subjects of study as a part. This Connection called “Ettesal” is established by a certain and trained individual who has been entrusted with the TCFs. The human mind has an intermediary role (Announcer) which plays a part by fleeting attention to the subject of study and then the main achievement obtained as a result of the effects of the TCFs. These Fields cannot be directly measured by science, but it is possible to investigate their effects on various subjects through reproducible laboratory experiments.

The research methodology in the study of T-Consciousness has been founded on the process of Assumption, Argument, and Proof, in which the basic Assumption is: The Cosmos was formed by a third element called T-Consciousness that is different from matter and energy.

The Argument: The existence of TCFs can be demonstrated by their effects on matter and energy (e.g., humans, animals, plants, microorganisms, cells, materials, etc.)

The Proof: is the scientific verification of the effects of TCFs on matter and energy (according to the Argument) through various reproducible scientific experiments.

Accordingly, to investigate and verify the existence, effects, and mechanisms of TCFs, the following five research phases (Phases 0 through 4), and the aims of each phase are outlined below.

Phase-0 studies aim to prove the existence of TCFs by observing their effects. The nature of T-Consciousness and what it is will not be addressed in this phase. Phase-1 explores the varied effects of different TCFs. Phase-2 examines the reason behind the varied effects of these fields. Phase-3 investigates the mechanism of TCFs effects on matter and energy. Finally, Phase-4 draws significant conclusions, particularly with regard to the mind and memory of matter and their relation to the T-Consciousness, etc. [1, 2,3]

Research on the function and behavior of materials under the influence of TCFs began a decade ago. In one study, the crystal defects in two methods were examined. The findings indicated that the crystal reached by casting pure 1000 series aluminum from a single ingot at ambient temperature, increased the mold volume, and applying 300 ° C preheating, had higher growth in the internal defects, up to 1000% in some cases [4,5]. As we know, the formation of defects requires the transfer of energy, which is mainly provided in the form of mechanical thermal behavior, by creating external stress for the material [6]. In these samples, as the material, energy-based factors were constant, the only influential factor must be something beyond energy and material, which according to Taheri it is the third element of the universe; T-Consciousness. The previous study revealed that TCFs had significant effects on lattice irregularities [4,5]. As we can see, creating this level of displacement requires an energy supply [6].

In the previous dilatometric study on the 99.9% pure copper, we examined the samples of the same length, under the same conditions and heated them up to 300 ° C. Compared with the samples under the T-Consciousness Field, relative increases in the length of the control samples were reported. Also, a reverse trend of density changes was identified in the samples under T-Consciousness Field compared with controls [7].

Moreover, in a repeated experiment, the mechanical crushing of pure silica samples was tested to measure its properties. The application of mechanical force simultaneously under the same conditions, and using the same device created the same silica powder, which was 80% lower than the average micro-strain of the crystal lattice [8,9]. This decrease indicated that the internal stresses in the crystal structure of the samples were significantly reduced, and the obtained crystalline structures had very little lattice distortion. This finding indicated that despite the application of external force, the samples under the T-Consciousness Field were still much more able to keep the structure of their crystal lattice without distortion compared to the control.

Continuation of the research over the years has resulted in the examination of many pieces of cement made according to international standards under the influence of TCFs. The aim of previous research was to investigate the overall function and behavior of concrete and cement mortar in increasing strength, concrete cancer, penetration of chloride ions, bending of concrete beams, penetration of gamma-newer radiation, and some other factors. However, in this study, the process of internal change revealed many points about how T-Consciousness Fields influences materials. Among the points is that in XRF (X-Ray Fluorescence) analysis, in addition to changing the water content percentage of the samples, the weight percentage of the elements of the samples had parallel changes [10-13].

In fact, in the XRF test, a part of the sample is first weighed and then placed in a furnace and heated to 1100 ° C for 2 hours, then weighed again and the percentage of weight loss due to heat is reported by LOI (Loss on Ignition).

Given that the total percentage of all phases along with the value (Loss on Ignition) of LOI should be equal to 100, increasing or decreasing the percentage (Loss on Ignition) of LOI causes the percentage of other phases to change. However, a significant point was observed in all cases, i.e., sometimes with the report of less or equal water absorption, extensive, purposeful, and reproducible changes have been made in the type and number of elements.

Studying the changes in the strength of cement samples on the 90th day, although these samples were made with the standard sand and the LOI average ± 1% LOI was the same in the experimental and control samples, the percentage of elements had changed. It makes it more probable that these changes lead to mass change, particularly since the calcium element constitutes more than 60% by weight of cement and in some cases has shown 13% changes [10]. Obviously, T-Consciousness affected the chemical composition and function of matter, and the fundamental question was whether these changes led to a change in mass in the samples.

Materials and methods

Analyses

For the first stage, a random bag of cement was selected. In order to analyze the chemical and elemental properties of the sample, XRF analysis was carried out. Then 9 cement samples with the Normal concentration were prepared according to the ASTM C187 standard and were categorized, and labeled into three groups of three by the laboratory official (Figure 2)

One group was identified as the control group (OPC), and two groups were selected as the experimental groups to be examined under the influence of TCFs 1 and 2 (different TCFs) labeled as N and M, respectively. The dimensions and mass of all samples were measured on the first, seventh, fourteenth, and twenty-eight days using a scale. On the 28th day, XRF and XRD (X-ray Diffraction) tests, a technique for analyzing the cement's crystal structures, were done on all samples in the same instrument, under the same conditions, and with the same amount of material.

All cement samples were pulverized by the laboratory prior to analysis (Figure 3).

Due to the similarity of the results of the trend changes, the second sample NO.2 of each group was selected and examined more thoroughly, and the following thermal analysis tests were carried out. In the analysis, the mass amount of all samples was 6 mg and the temperature growth rate was 10 °C, in the temperature range of 25 to 1000 °C, by ASTM-E1131 and was in the American (TA): SDT Q600 V20.9 Build20, in Air, with the following specifications: Three thermal analyses of TGA (Thermal Gravimetric Analysis), DTA (Differential Thermal Analysis), and DSC (Differential Scanning Calorimetry) were carried out to quantitatively examine the compounds present in these samples.

Before starting the main experiment, the weight percentage of elements and the water adsorption of the dry powder cement used in this research were measured. The details are presented in Table 1: A small amount of LOI (≈1.7%) in the untreated sample indicates the existence of the heat-resistant ceramic structures, and a minimal amount of these structures have been decomposed by heat.

Table 1. Results of XRF test related to cement before hydration

Na_2O%	0.11	MgO%	1.7	$Al_2O_{3\%}$	2.22	$SiO_{2\%}$	19.5	$SO_{3\%}$	2.8
K_2O%	0.66	CaO%	66.0	$TiO_{2\%}$	0.35	$Fe_2O_{3\%}$	5.0	L.O.I%	1.66

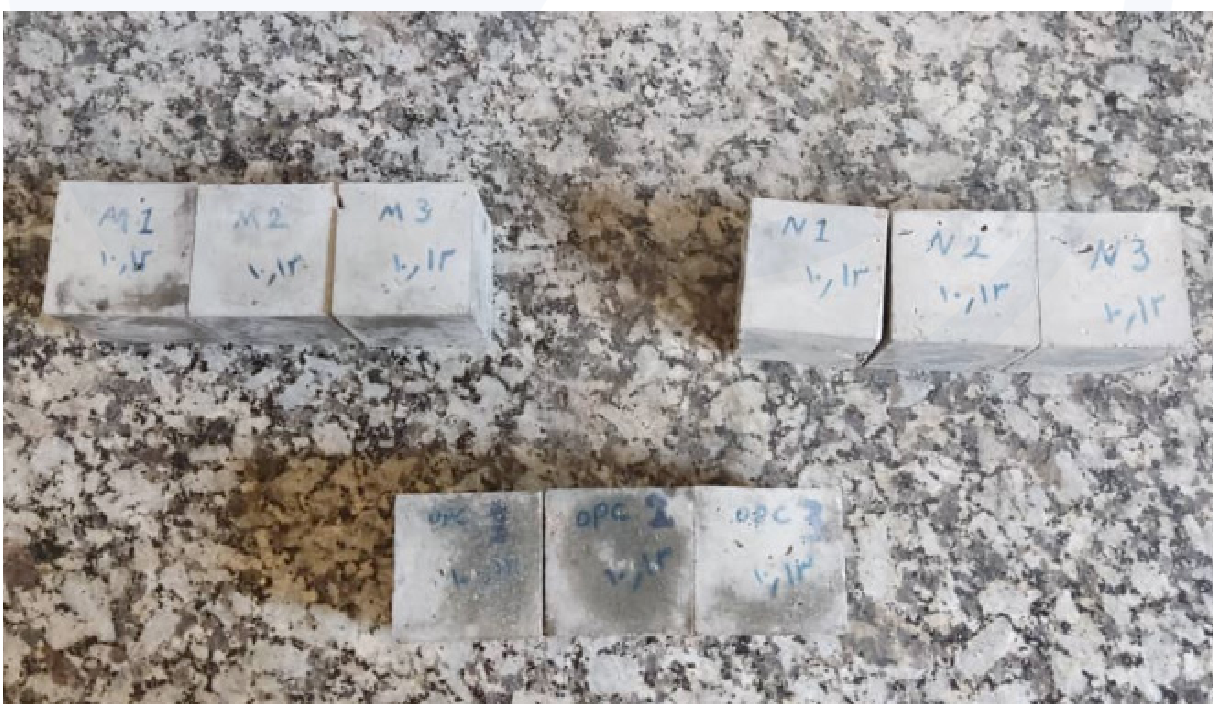

Figure 2. The Cement samples

Figure 3. The Powder Cement samples NO.2 of each sample after hydration. Samples from right to left, respectively: Control2, M2, N2

Application of the Taheri Consciousness Field

One of the TCFs, called the Consciousness Bond Field, was applied to the samples according to the protocols regulated by the COSMOintel research center (www.COSMOintel.com). A request for Connection to the CCN to utilize TCFs can be placed through the COSMOintel website in the "Assign Announcement" section. This access is available for everyone at no cost. In order to study and experience this Connection, the researchers can register on the website at any time in order to report the experiment to the COSMOintel research center. Certain details of the experiment must be provided to the center; for example, the characteristics or number and name of samples and controls must be specified. This entire experiment was carried out as a double-blind method where lab technicians were completely unaware of the TCFs theory, and the *Announcer* at the COSMOintel research center who established the Connection was unaware of the details of the study. Double-blind is a gold standard common in science experiments.

Results and discussion

Changes in the dimensions and mass of the cement samples up to 28 days of age are collected in tables 2 and 3. Table 4 summarizes the comparison of the groups for the days 7,14,28.

Table 2 . Changes in the dimensions of the samples up to 28 days of age

Groups	Samples	1-day(cm)	7-day(cm)	14-day(cm)	28-day(cm)
The OPC Control	OPC1	5.05×5.00×5.25	5.05×5.00×5.25	5.05×5.00×5.25	5.05×5.00×5.25
	OPC2	5.18×5.00×5.07	5.18×5.00×5.07	5.18×5.00×5.07	5.18×5.00×5.07
	OPC3	5.20×5.00×5.00	5.20×5.00×5.00	5.20×5.00×5.00	5.20×5.00×5.00
N (TCF1)	N1	5.10×5.00×5.18	5.10×5.00×5.18	5.10×5.00×5.18	5.10×5.00×5.18
	N2	5.24×5.13×5.02	5.24×5.13×5.02	5.24×5.13×5.02	5.24×5.13×5.02
	N3	5.25×5.10×5.00	5.25×5.10×5.00	5.25×5.10×5.00	5.25×5.10×5.00
M(TCF2)	M1	5.15×5.05×5.00	5.15×5.05×5.00	5.15×5.05×5.00	5.15×5.05×5.00
	M2	5.18×5.05×5.00	5.18×5.05×5.00	5.18×5.05×5.00	5.18×5.05×5.00
	M3	5.00×5.10×5.24	5.00×5.10×5.24	5.00×5.10×5.24	5.00×5.10×5.24

The First Journal in T-Consciousness Research
Vol . 01
No . 08
April
2022

Table 3 . Mass changes of the cement samples up to 28 days of age

Groups	Samples	1-day (gr)	Mean	7-day (gr)	Mean	14-day (gr)	Mean	28-day (gr)	Mean
OPC Control	OPC1	285.50	277.93	287.06	281.71	287.97	284.51	288.62	285.15
	OPC2	276.90		282.69		283.56		284.21	
	OPC3	275.40		275.4		282.01		282.64	
N(TCF1)	N1	274.44	280.90	280.32	286.74	281.32	287.76	281.93	288.36
	N2	285.92		291.60		292.66		293.25	
	N3	282.35		288.3		289.31		289.92	
M(TCF2)	M1	271.39	276.01	277.27	281.85	278.25	282.85	278.83	283.46
	M2	278.13		284.18		285.2		285.76	
	M3	278.51		284.12		285.11		285.72	

Table 4 . Mean mass changes compared to the first day and percentage change compared to the control

Groups	7-day	14-day	28-day
OPC-control	3.78	6.58	7.22
N-TCF1	5.84	6.86	7.46
M-TCF2	5.84	6.84	7.45
Changes%	56%	4.3%	3.3%

Considering that the N samples had an average of about 1% higher mass on the first day, it is obvious that the mold volume was larger by an average of 3 mm^3. As the average of the three M samples had 0.6% less mass than the control sample, it can be said that at 28 days of age, the samples exposed to TCF2 have a higher mass increase rate of about 3 to 4% compared to the controls. Since the samples are kept in water until the age of 28 days, one of the reasons for this increase could be higher water absorption. For this purpose, the Loss on Ignition (LOI) test was carried.

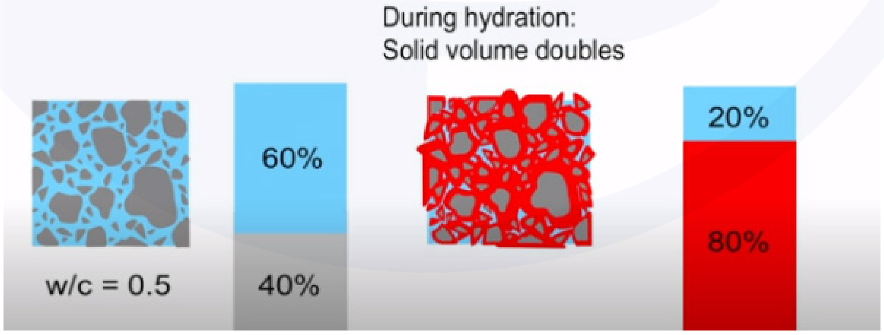

Figure 4. Schematic illustration of cement hardening

XRF (X-Ray Fluorescence) analysis

During the XRF test, part of the sample is first weighed and then placed in a furnace and heated to 1100 ° C for 2 hours, then weighed again and the percentage of weight loss due to heat is reported by LOI (Loss on Ignition).

Table 5 . XRF test of weight percentage of elements and water absorption LOI

Name		Control			TCF1			TCF2	
OXID%	OPC1	OPC2	OPC3	N1	N2	N3	M1	M2	M3
Na2O	0.07	0.07	0.05	0.05	0.09	0.07	-	-	-
MgO	1.5	1.51	1.5	1.3	1.5	1.5	1.2	1.2	1.1
AL_2O_3	2.14	1.9	1.9	1.8	1.9	1.9	1.43	1.67	1.6
SiO_2	15.2	14.9	14.9	15.1	15.7	15.6	15.2	14.9	13.4
P_2O_5	0.08	0.08	0.09	0.1	0.09	0.09	0.16	0.19	0.21
SO_3	1.9	1.6	1.6	1.5	1.5	1.6	1.7	1.5	1.7
K_2O	0.56	0.58	0.56	0.53	0.56	0.60	0.6	0.567	0.56
CaO	51.7	52.6	52.5	50.5	52.1	52.3	52.6	53.6	54.6
TiO_2	0.27	0.28	0.27	0.26	0.27	0.27	0.32	0.31	0.31
Fe_2O_3	3.5	3.3	3.4	3.3	3.4	3.3	3.8	3.4	3.5
LOI	23.08	23.18	23.23	22.56	22.89	22.07	22.09	22.66	22.97
Average LOI		**23.16**			**22.5**			**22.5**	

Table 6 . The average weight percentage of some elements obtained after heat loss and the percentage change in them compared to the control

Name	Na	%	Mg	%	AL	%	Ca	%	P	%	Ti	%	LOI	%
OPC	0.06	*	1.5		1.98		52.26		0.08		0.27		23.16	
N(TCF1)	0.07	-	1.4	-6	1.86	-6	51.63	-1	0.09	12.5	0.27		22.5	-2.8
M(TCF2)	-	100%	1.1	-26.6	1.56	-15	53.6	2.5	0.18	125	0.31	14.8	22.57	-2.6

The LOIs show that sample M and sample N have lost less weight of water on average 2.6% and 2.8%, respectively. That is, the wa-ter absorption of the samples is less than the control. Therefore, the mass of 3 to 4% is not more dependent on the water absorption.

The Results of the XRD (X-Ray Diffraction)

XRD test was used to investigate the crystal structures in the three samples of processed cement. The diffraction patterns are provided below. It should be noted that the following data include two parts: qualitative (phase identification) and quantitative (amount of compounds). The quantitative part can only be used as a reference point for the general understanding, and other well-known methods should be used if you want to examine the quantitative.

Raw Data Origin:	XRD measurement (*.XRDML)
Start Position [°2Th.]:	3.0011
End Position [°2Th.]:	79.9091
Step Size [°2Th.]:	0.0260
Scan Step Time [s]:	37.9950
Scan Type:	Continuous
PSD Mode:	Scanning
PSD Length [°2Th.]:	3.35
Offset [°2Th.]:	0.0000
Divergence Slit Type:	Fixed
Divergence Slit Size [°]:	1.0000
Specimen Length [mm]:	10.00
Measurement Temperature [°C]:	25.00
Anode Material:	Cu
K-Alpha1 [Å]:	1.54060
K-Alpha2 [Å]:	1.54443
K-Beta [Å]:	1.39225
K-A2 / K-A1 Ratio:	0.50000

Generator Settings: 40 mA, 40 Kv

The crystal, chemical composition, and their presence percentage in the samples by the de-vice are given in table 7. The details show that most of the crystals are in the same category. In order to examine more carefully, one from each sample is analyzed qualitatively.

Table 7. Compositions and percentage of cement crystals

OPC1	H2 Ca1 O2 Portlandite 98-004-6197 36.9%	Ca3 O5 Si1 Hatrurite 98-001-2728 36.4%	Ca2 O4 Si1 Dicalcium Silicate 98-003-6706 24.6%	Mg1 O1 Periclase 98-007-4470 4.2%
OPC2	H2 Ca1 O2 Portlandite 98-004-6197 40.8%	Mg1 O1 Periclase 98-007-4470 4.5%	Ca3 O5 Si1 Hatrurite 98-001-2728 33.2%	Ca2 O4 Si1 Dicalcium Silicate 98-003-6706 21.5%
OPC3	H2 Ca1 O2 Portlandite 98-004-6197 40.9%	Ca3 O5 Si1 Hatrurite 98-001-2728 35.2%	Mg1 O1 Periclase 98-007-4470 4.7%	Ca2 O4 Si1 Dicalcium Silicate 98-003 19.3%
N1	H2 Ca1 O2 Portlandite 98-004-6197 42.1%	Ca3 O5 Si1 Hatrurite 98-001-2728 33.4%	Mg1 O1 Periclase 98-007-4470 4.4%	Ca2 O4 Si1 Dicalcium Silicate 98-003-6706 20.1%
N2	Ca3 O5 Si1 Hatrurite 98-001-2728 33.3%	Ca2 O4 Si1 Dicalcium Silicate 98-003-6706 22.4%	H2 Ca1 O2 Portlandite 98-004-6197 39.6%	Mg1 O1 Periclase 98-007-4470 4.7%
N3	H2 Ca1 O2 Portlandite 98-004-6197 49.5%	Ca3 O5 Si1 Hatrurite 98-001-2728 45.5%	Mg1 O1 Periclase 98-007-4470 5.0%	
M1	H2 Ca1 O2 Portlandite 98-004-6197 34.5%	Ca3 O5 Si1 Hatrurite 98-001-2728 30.1%	Mg1 O1 Periclase 98-003-6706 7.6%	Ca2 O4 Si1 Dicalcium Silicate 98-003-6706 27.9%
M2	H2 Ca1 O2 Portlandite 98-001-7623 39.1%	Ca3 O5 Si1 Hatrurite 98-001-2728 34.2%	Mg1 O1 Periclase 98-007-4470 4.8%	Ca2 O4 Si1 Dicalcium Silicate 98-003-6706 21.9%
M3	H2 Ca1 O2 Portlandite 98-004-6197 38.3%	Ca3 O5 Si1 Hatrurite 98-001-2728 36.8%	Mg1 O1 Periclase 98-007-4470 4.7%	Ca2 O4 Si1 Dicalcium Silicate 98-003-6706 20.2%

Table 8. Ratio of crystalline phase

sample ID	the sum of the net area	the sum of the total area	crystallinity%
M1	2253.87	22970.43	9.812049666
M2	1726.017	22069.28	7.820903083
M3	1738.32	22031.15	7.890282623
N1	1843.147	24797	7.432943501
N2	1761.05	20298.36	8.675824057
N3	1935.57	25028.08	7.733593628
OPC1	1983.51	28272.99	7.015565032
OPC2	2001.59	23851.35	8.391935886
OPC3	1900.64	24369.66	7.799206062

Table 9 . Comparison of the average ratio of crystalline phase

Group	Ave. crystallinity%	Changes%
M	8.50%	9.96%
N	7.94%	2.72%
OPC	7.73%	

The results demonstrate that the percentage of crystallinity in the samples under the T-Consciousness Field is higher than in the controls; and in sample M, it is significantly higher than in the other two groups. M and N are two different fields. For qualitative evaluation, sample number 2 of each group was selected and analyzed qualitatively since the variations of all three samples from each group are very close to each other.

A qualitative review of the second sample No. 2 of each group

X'Pert Highscore Plus software was used to identify the phase from the results of the X-ray diffraction pattern of these samples. According to Figure 5, it is clear that the main phases are the same in all three samples and the peaks are diffracted at almost the same angles, which indicates that the main compounds are almost the same in all three samples.

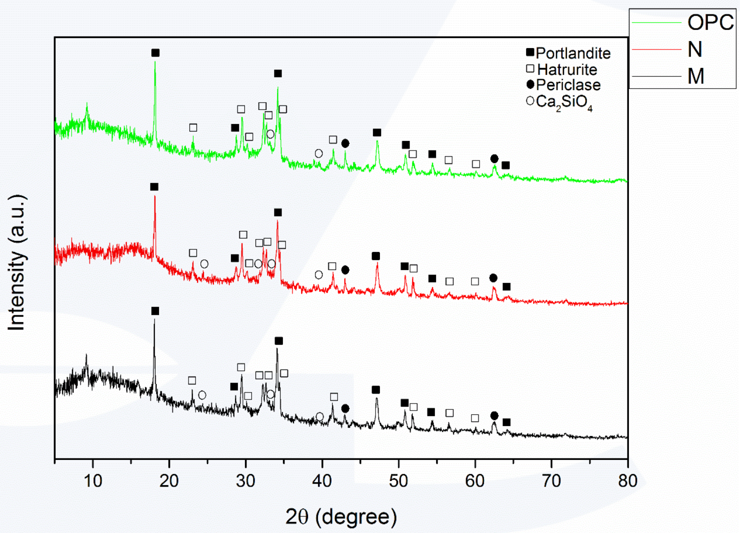

Figure 5. Figure 5- The X-ray diffraction patterns of the hydrated cement samples

According to these diffraction patterns and by matching the visible peaks in these patterns on the reference diffraction patterns by the mentioned software, it was determined that all samples had four phases, which are:

(A) Portlandite phase with the chemical formula Ca (OH)2 and reference code JCPDS No: 98-004-6197 with hexagonal crystal structure and spatial group P-3m1. In this structure, the diffraction plates (001), (100), (101), (102), (110), (111), and (112) are observed at angles of 18.1 °, 28.6 °, 34.1 °, 47.1 °, 50.8 °, 54.3 °, and 64.2 °, respectively.

(B) Harturite phase with chemical formula Ca3SiO5 and reference code JCPDS No: 98-001-2728 with orthorhombic crystal structure and C-E space group. In this structure, the diffraction plates (115), (221), (401), (224), (225), (319), (620), (224) and (629) are observed at angles of 23.1 °, 29.5 °, 30.2 °, 32.3 °, 32.7 °, 34.5 °, 41.4 °, 51.8 °, 59.7 ° and 60.1 °, respectively.

(C) Periclase phase with chemical formula MgO and reference code JCPDS No: 98-007-4470 with cubic crystal structure and space group Fm-3m. In this structure, diffraction plates (200) and (220) are observed at angles of 42.9 ° and 62.3 °, respectively.

(D) Calcium silicate phase with chemical formula Ca_2SiO_4 and reference code JCPDS No: 98-003-6706 with orthorhombic crystal structure and spatial group Pbmn. In this structure, diffraction plates (111), (040), (112), and (211) are observed at angles of 24.4 °, 31.8 °, 33.3 °, and 39.5 °, respectively.

To better compare the intensity of the peaks in each sample, some specified peaks are magnified in the range of specific angles, as shown in Figure 6.

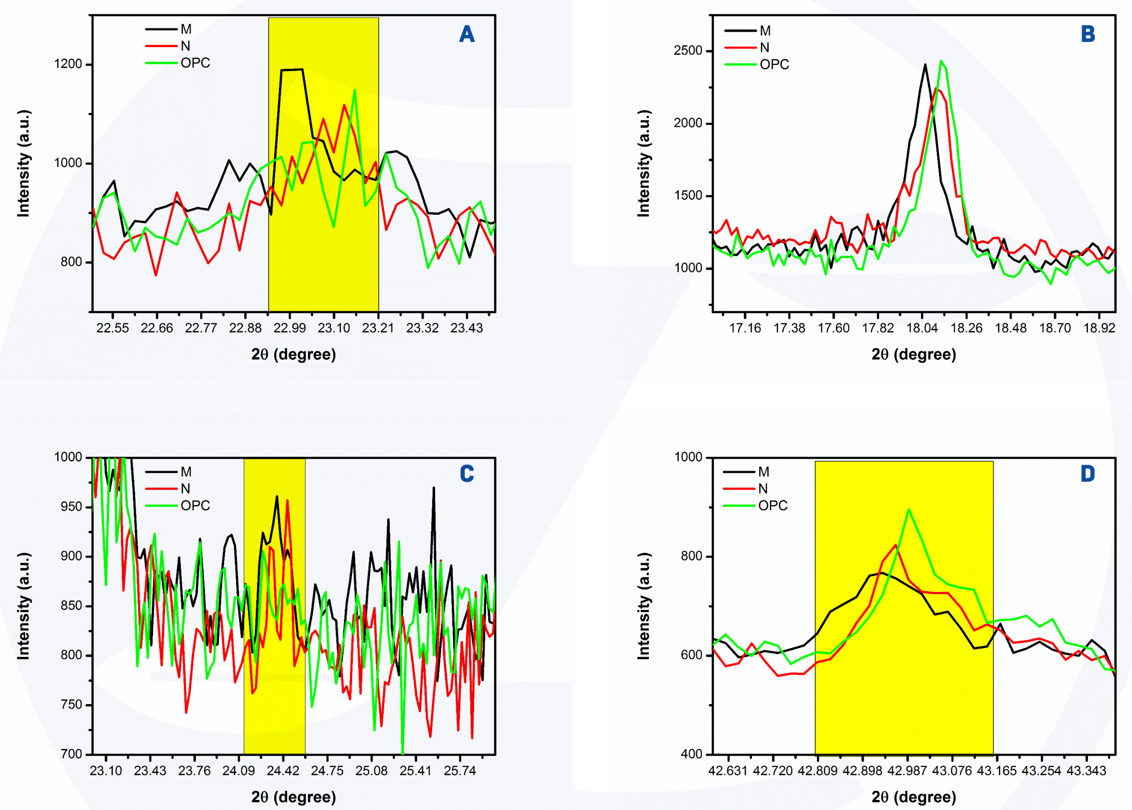

Figure 6. X-ray diffraction patterns were magnified and stacked for peaks related to phases of (a) harturite, (b) portlandite, (c) calcium silicate, and (d) periclase.

According to Figure 6 (A), the harturite phase is almost the same intensity in samples N and OPC, but in sample M the intensity of this peak is higher than in the other two samples. Figure 6 (C) also shows that for the calcium silicate phase, sample M has a relatively higher intensity than the other two samples. The results of the XRF test also show that the CaO phase, which constitutes these two phases, is higher in sample M than in the other two samples. Therefore, it can be concluded from the results that the calcium silicate-based phases, one of which being the harturite phase with the chemical formula Ca_3SiO_5, in sample M are more than the other two samples. In addition, Figure 6 (C), shows that the phase intensity of calcium silicate in the OPC sam-ple is lower than in the other two samples.

In fact, according to the results of the XRF test, it is observed that the amount of SiO_2, which is another compound of the two constituents of calcium silicate, in sample N is higher than in the other two samples, and it can be concluded that after sample M, sample N has the most silicate phases. Figure 6 (B) shows the peak intensities of the portlandite phase, and it is clear that among the three samples, the peak intensity in sample N is less than in the other two samples. Considering that the results of the XRF test also show that the percentage of CaO in this sample is less than the other two samples, from the results of these two tests, it can be concluded that sample N has less portlandite content than the other two samples.

Figure 6 (D) also shows the intensity of the peaks related to the periclase phase. By comparing the peak intensities, it is clear that the peak intensities in the OPC are higher than the others, followed by the N and M samples. By comparing the MgO values in the XRF test results, the exact order was observed, and therefore it can be concluded that the periclase phase in the OPC sample is more than the other two samples, followed by the N and M samples.

Figure 7 shows that the results of thermal analyses (TGA / DTA / DSC) were carried out for quantitative examination of the compounds of these samples.

Comparison of sample No. 2 of each group and the results of TGA-DTA-DSC analyses

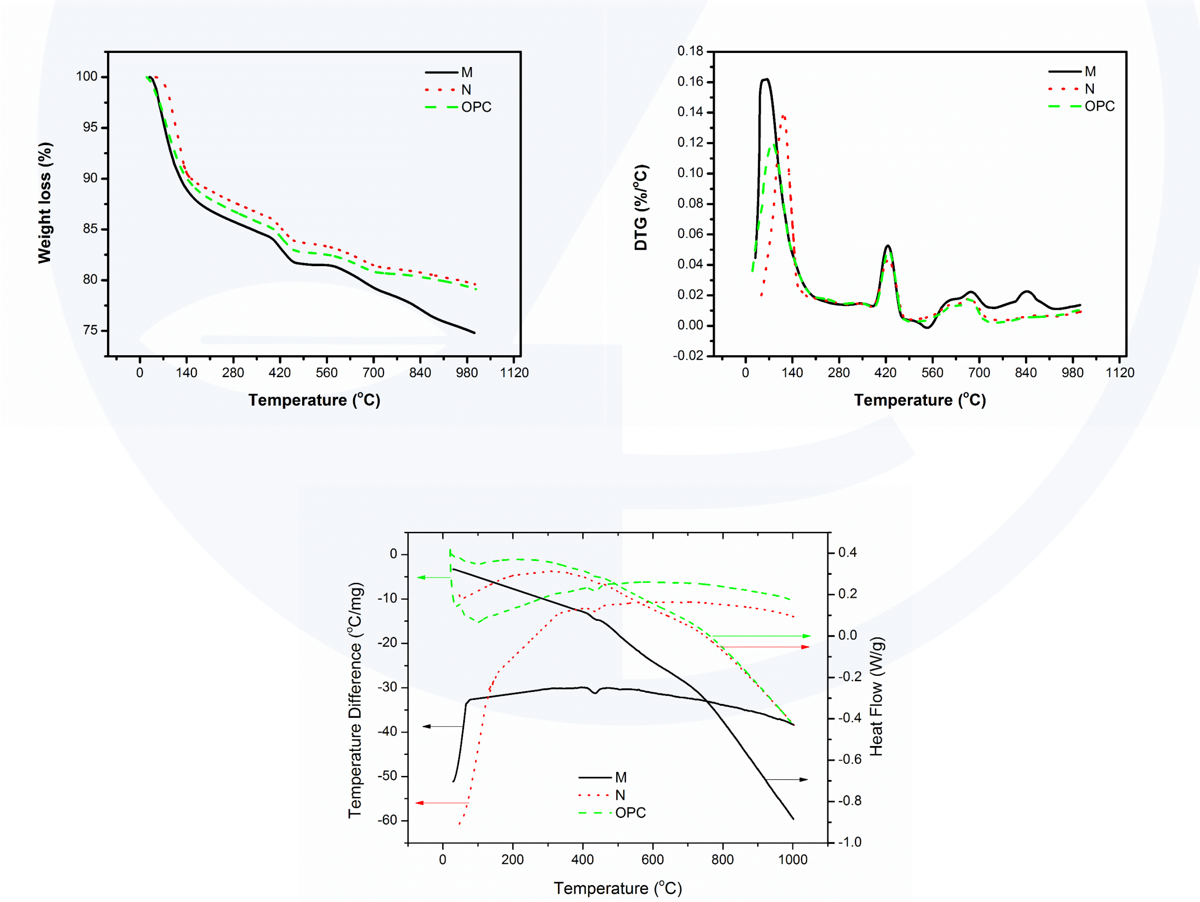

Figure 7. Results of tests (1) TGA, (2) DTG and (3) DTA / DSC on the samples M (TCF), N (TCF), and OPC (Control)

The First Journal in T-Consciousness Research
Vol. 01
No. 08
April
2022

According to Figure 7, Graph (1) shows a weight-loss stage at temperatures below 200 ° C, which is related to the evaporation of structural water and water absorbed in the samples [14]. About 13% of sample M, 12% of sample OPC, and 11% of sample N lost weight in this temperature range. Therefore, it is clear that the difference is small, but it is reasonably meaningful. Considering the importance of the Portlandite phase in water absorption of cement, the lower phase of this phase in sample N than the other two samples, proven in the results of previous tests, can be the most important reason for lower water absorption in this sample. This finding could be the reason for the higher water absorption in sample M because the amount of CaO in the XRF test results was higher than in the other two samples.

The second stage of weight loss, which caused a peak in the DTG diagrams at 420 ° C, and also in the DTA / DSC diagrams, also showed an endothermic peak related to the thermal decomposition of the Portlandite phase [15]. From the intensity of the peaks in the DTG diagrams, it is clear that the value of this phase in all three samples is approximately close to each other. However, the TGA results show that the weight loss in the temperature range of 380 to 490 ° C for the M, N, and OPC samples was about 2.8%, 2.5%, and 2.6%, respectively. The next weight loss stage is in the temperature range of 560 to 700 ° C, which is related to the thermal decomposition of phases based on calcium silicate [16]. The weight reduction of M, N, and OPC samples in this temperature range was about 2.6%, 2.1 and 1.7%, respectively. Sample M has 50%, and sample N has 23% more calcium silicate compared with the control group. This trend is precisely in line with the trend of the values obtained by the results of XRF tests and shows that the silicate phases in samples M and N are more than in the OPC sample.

In addition, in sample M, another weight-loss stage can be observed at a temperature of about 840 °C, which has not been observed in the other two samples of this stage. At this stage, in sample M, about 2.1% of the initial mass of the sample is thermally decomposed. This stage of weight loss is usually related to the calcium carbonate removal from the sample [17], which can be justified by the higher amount of CaO in the XRF test results. Therefore, it can be concluded that in sample M, unlike the other two samples, there is some calcium carbonate.

Conclusion

All results showed that the dimensions of the samples did not change significantly, and the volume remained the same. Regarding the increase in mass, one of the control samples did not show much difference until the age of 7 days, which caused the rate of increase in mass to be 50% higher up to the age of 7 days than the one-day age, the reason for this is not apparent. Then the cement samples enter the hydration process naturally, and the mass changes begin according to Figure (4). The rate of mass growth is 3 to 4% higher in the samples under T-Consciousness Field when their age goes up. According to the results (Tables 5 and 6), the presence of L.O.I in the Control is more than in the TCF. This implies that the weight change is not dependent on water absorption and light elements. From the XRD results (Tables 7 and 8), it is clear that the chemical compounds are composed of different percentages, and the percentage of crystalline phases is higher in the samples under the TCF (Tables 9).

There was about ~10% more crystalline phase in sample M than in the control group.

As can be seen from the image of this sample, the pulverized cement also had a different tex-ture and color (Figure 3). The thermal analy-sis (Figure 7) shows that the lost water in the samples is not significant, and the differences depen d on the changes in matter. Sample M has 50%, and sample N has 23% more calcium silicate compared with the control group. In sample M, unlike the other two samples, there is some calcium carbonate. These changes can be examined from two perspectives. First, the cement hardening process has been so that under the T-Consciousness Fields, the tendency to absorb less water and to create denser compounds in it has intensified. Second, according to the results of the XRF, which show a repetitive pattern in the samples, as seen in the other studies, the cement elements have changed in addition to low water absorption. That is, the composition of the cement substance has changed, and then the chemical reactions have also changed.

This possibility is debatable since the primary cement, and all conditions were the same in this experiment. The difference in water absorption in the samples under the T-Consciousness Field is almost zero. However, their constituent elements' type and weight percentage are different after hydration. For example, Na is not reported in any M group samples. Aluminum or phosphorus, for example, reports the same change pattern, which is almost repetitive. This implies a conversion between T-Consciousness, matter and energy. Not only are the reactivities different, but the degree of presence of the elements has also changed under the T-Consciousness in a different way. Obviously, not all cement elements can be obtained exactly, but given the process of these changes in other research on cement, the results of both probabilities are reported.

From t he results of extensive changes in the behavior and structure of various materials, i t is concluded that T-Consciousness, according to Taheri's theory, can be converted into matter and energy [1, 2].

T-Consciousness ↔ Wave (Matter and Energy)

References

1. Taheri, M. A. (2020). The main monitoring center for T-Consciousness Fields research and studies based on Sciencefact. www.Cosmointel.com.
2. Taheri, M. A. (2012). General Connection of Particles. Interuniversal Publishing Erfan-Halgheh. ID: 978-1-940491-03-5.
3. Taheri, M. A. (2013). Human from Another Outlook (2nd Edition). ISBN-13: 978-1939507006, ISBN- 10: 1939507006.
4. Kazazi, B, & Taheri, M. A. (2021). Effect of the Consciousness Bond Field on the structure and properties of Aluminum. Retrieved from www.cosmointel.com.
5. Kazazi. B, & Taheri. M. A. (2021). Effect of the Consciousness Bond Field on the structure and properties of 1000- series Auminum with preheating Retrieved from www.cosmointel.com.
6. Rawdon H.R., Krynitski A.I., Berliner J.F., Brittleness developed in aluminium and duralumin by stress and corrosion, Chemical Metallurgy Engineering, vol. 26 (1922), p. 154–160.
7. Kazazi. B, & Taheri. M. A. (2021). Study of density changes and increase in the length of pure copper up to 300 °C in Consciousness Bond Field. Retrieved from www.cosmointel.com.
8. Kazazi. B, & Taheri. M. A. (2021). Study of the effect of the Consciousness Bond Field on mechanical crushing of silica particles preheating Retrieved from www.cosmointel.com.
9. Kazazi. B, & Taheri. M. A. (2021). Influence of Consciousness Bond Field on the plant synthesis of nano-silver preheating Retrieved from www.cosmointel.com.
10. Kazazi, B., & Taheri, M. A. (2021). Influence of Consciousness Bond Field (CF) on crystallization and strength of cement mortar (concrete). Retrieved from www.cosmointel.com.
11. Kazazi, B., & Taheri, M. A. (forthcoming 2022). Comparison of the behavior of concrete made under the influence of Taheri Consciousness Fields (TCFs), and under gamma and neutron radiations, with ordinary concrete, when receiving TCF and gamma and neutron radiations simultaneously.
12. Kazazi, B., & Taheri, M. A. (forthcoming 2022). Investigation of chlorine ion penetration in concrete under the influence of Taheri Consciousness Fields.
13. Kazazi, B., & Taheri, M. A. (2021). Effects of the T-Consciousness Field on Concrete (ASR. Retrieved from www.cosmointel.com.
14. Soares.L.W.O, R.M. Braga, J.C.O. Freitas, R.A. Ventura, D.S.S. Pereira, D.M.A. Melo,.(2015). The effect of rice husk ash as pozzolan in addition to cement Portland class G for oil well cementing, Journal of Petroleum Science and Engineering. 131 - 80–85. doi:10.1016/j.petrol.2015.04.009.
15. Sharma.D.K , Sharma.R,.(2018). Influence of rice husk ash and rice tiller ash along with chromate reducing agents on strength and hydration properties of Ordinary Portland Cement, Construction and Building Materials. 169 - 843–850. doi:10.1016/j.conbuildmat.2018.03.044.
16. Tantawy.M.A , Shatat.M.R, El-Roudi.A.M , Taher.M.A, Abd-El-Hamed.M ,.(2014). Low Temperature Synthesis of Belite Cement Based on Silica Fume and Lime, International Scholarly Research Notices. 1–10. doi:10.1155/2014/873215.
17. Sabeur.H , Saillio.M, Vincent.J ,.(2019). Thermal stability and microstructural changes in 5 years aged cement paste subjected to high temperature plateaus up to 1000 °C as studied by thermal analysis and X-ray diffraction, Heat and Mass Transfer. 55 - 2483–2501. doi:10.1007/s00231-019-02599-w.

Effects of Taheri Consciousness Fields on Concrete (ASR)

Bahareh Kazazi[1*], Mohammad Ali Taheri[2]

1. Civil Engineering, CEO of Hoobe Construction Company, Tehran, Iran.

2. Sciencefact R&D Department, Cosmointel Inc. Research Center, Ontario, Canada.

*Corresponding author:

Bahareh Kazazi
Civil Engineering, CEO of Hoobe Construction Company, Tehran, Iran.

Email: baharkazazi@gmail.com

ABSTRACT

The Alkali-silica reaction of concrete is known as one of the destructive reactions. There are many studies in this area. Taheri Consciousness Fields (TCFs) were founded and introduced by Mohammad Ali Taheri as new Fields. These Fields are neither matter nor energy, therefore, do not possess a quantity, but they have direct effects on both matter and energy. In other words, although TCFs cannot be directly measured, we can investigate their effects indirectly through various controlled experiments. In this study, cement mortar samples were examined by using the ASTM C1260 standard and under the effect of a type of TCF known as TCF(H). Additional experiments, aggregate petrography, L.O.I (Loss on Ignition), SEM (Scanning electron microscopy), XRD (X-ray Diffraction), XRF (X-Ray Fluorescence), FT-IR (Fourier-transform infrared spectroscopy) were performed to further investigate the effect of TCF(H). It was found that the TCF (H) was able to reduce the expansion and improve the cement mortar function by up to 10% (average ~ 7% P-value= 0.008) and make observable changes in chemical and elemental compositions.

Keywords: ASR concrete silica alkali reaction, Taheri Consciousness Fields, T-Consciousness, Intelligence

INTRODUCTION

Concrete is one of the most widely used building materials in the world. Aggregates make up about 60 to 70% of the concrete volume. Aggregates have a great impact on the physical and chemical properties of concrete. In principle, their properties affect the performance, reliability, and behavior of concrete. One of the major effects of aggregate on concrete is the chemical reactions of aggregate with cement inside concrete [1]. One of the most important reactions is the alkaline reaction of aggregate, which is known as concrete cancer. The main cause of this reaction is the chemical composition of the aggregate, which is surrounded by the hydrated cement paste and thus internal pressures are created, which eventually cause expansion and cracking, and disintegration of the concrete. It has also been observed that some of the gel leaks out with the water and settles in cracks that have been already formed due to the swelling of the aggregates, causing other destructive agents to penetrate.

The alkaline reaction is especially important in dam construction projects because the cost of repairing a dam is very high. In previous years, in Canada, after 20 years, the cost of repairing a dam was more than the initial cost of construction [2]. Therefore, different countries put identification, prevention, and repair methods on their agenda. Of course, it should be noted that the best method is to study the history of the aggregate performance during 15 years of operation, and it is necessary to study it beyond just the physical characteristics and include the components and functional environment of concrete. In this way, a comprehensive solution may be suggested. In the absence of such conditions, the design of an alternative test to simulate aggregate behavior and prevention is necessary [3]. To find the proposed solution, it is necessary to know how the aggregate functions in concrete. In general, aggregates cause alkaline reactions in two ways:

A. Alkaline carbonate reaction

The cause of this reaction is the alkali in cement and a group of dolomitic lime aggregates that cause cracks in wet conditions [1-4]. and is less studied due to its rarity.

B. Alkaline silica reaction (ASR)

This reaction was first known in California in 1930, [5] the Alkaline-silica reaction (ASR) is a chemical process in which OH^- ions present in the solution of the concrete pores are combined with the weakly crystalline and amorphous silica in the aggregates in concrete; and ASR compounds are then produced. The presence of water and constant swelling leads to an increase in stress and fracture of the concrete. When the internal stress reaches more than the tensile strength of the concrete, cracks are generated [6].

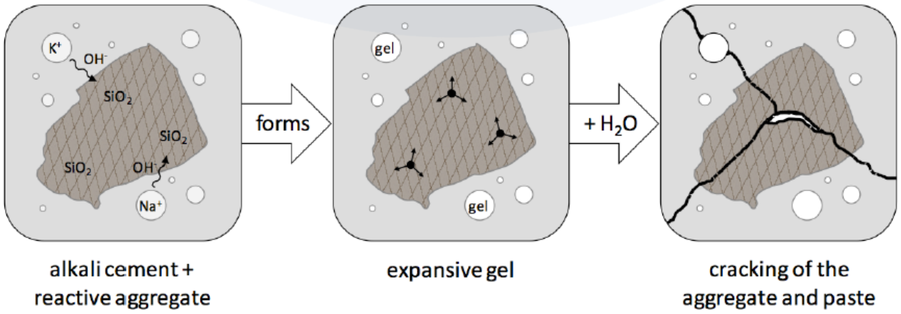

Figure 1 - Schematic drawing of the concrete cracking process by alkali-silica reaction

In general, the effective factors in this reaction are the presence of unstable silicas, and aluminosilicates, [7-8] sufficient alkaline compounds in the water inside the concrete pores, and the presence of moisture. Research has been done regarding the details and the extent of the effect of each of these factors in performing the reaction. The latest research has examined their effect, particularly water, on the size and structure, and growth of gels at the nanoscale [9].

In addition to the cases that are required for gel formation, the rate of expansion of the reaction depends on factors such as the number of ions in concrete, type of cement, pozzolans used, conditions of the performance environment, sources, and ion accumulation sites along with ambient humidity and ambient temperature [10-12]. The main subject of this research, considering the extent of this destruction, is further studied in this section.

Methods of Control and prevention of concrete cancer

The most well-known methods of controlling or preventing alkaline silica reaction

Given the importance of this destructive response, engineers from the beginning thought of solutions to control and repair structures, many of which have been used in industry for years and are constantly being improved. One of the most well-known methods is the use of gel-controlling pozzolans, the most famous of which are:

Use of low alkali cement and the addition of minerals and chemicals such as fly ash [13], Silica fume [14-15], Slag of smelting iron and copper furnaces [16], and use of nano-silicates silica powder [17], Lithium salts [18-19], and even environmentally friendly methods such as the use of rubber fragments [20] or rice husk [21]. In Iran, zeolite has been also used for many years due to its availability in the structure of dams [22-23].

The extent of application of all the above methods depends on parameters such as the type of cement and environmental conditions on the one hand and the study of other mechanical and chemical properties of concrete on the other hand. Therefore, all methods have limitations and a distinct range of effects. According to the recommendation of research institutes, the best method is still to identify destructive aggregates and prevent their use or control the amount of alkali in cement. A good solution for this problem is a method of control that is simple, comprehensive, and independent of other constraints [24].

Taheri Consciousness Fields

The nature of consciousness and its place in science has received much attention in the current century. Many philosophical and scientific theories have been proposed in this area. In the1980s, Mohammad Ali Taheri introduced novel fields with a non-material/non-energetic nature named Taheri Consciousness Fields (TCFs). In this perspective, T-Consciousness is one of the three existing elements of the universe apart from matter and energy. According to this theory, there are various TCFs with different functions, which are the subcategories of a networked universal internet called the Cosmic Consciousness Network (CCN). The major difference between the theory of TCFs and other theoretical concepts about consciousness is related to the practical application of the TCFs. TCFs can be applied to all living and non-living creatures, including plants, animals, microorganisms, materials, etc.

Mohammad Ali Taheri, the founder of Erfan Keyhani Halqeh, a school of thought, introduced a new science in 2020 as a branch of this school. He coined the term Sciencefact for this new science because it utilizes scientific investigations to prove the existence of T-Consciousness as an irrefutable phenomenon and a fact. Although science focuses solely on the study of matter and energy and Sciencefact, by contrast, explores the effects of the [non-material/non-energetic] TCFs, Sciencefact has provided a common ground between the two by conducting reproducible laboratory experiments in various scientific fields, and it has used the scientific approach in proving TCFs.

The influence of the TCFs begins with the Connection between CCN as the Whole Taheri Consciousness of the universe and the subjects of study as a part. This Connection called "Ettesal" is established by a certified and trained individual who has been entrusted with the TCFs. The human mind has an intermediary role (Announcer) which plays a part by fleeting attention to the subject of study and then the main achievement obtained as a result of the effects of the TCFs. These Fields cannot be directly measured by science, but it is possible to investigate their effects on various subjects through reproducible laboratory experiments.

The research methodology in the study of T-Consciousness has been founded on the process of Assumption, Argument, and Proof, in which the basic Assumption is: The Cosmos was formed by a third element called T-Consciousness that is different from matter and energy.

The Argument: The existence of TCFs can be demonstrated by its effects on matter and energy (e.g., humans, animals, plants, microorganisms, cells, materials, etc.)

The Proof: is the scientific verification of the effects of TCFs on matter and energy (according to the Argument) through various reproducible scientific experiments.

Accordingly, to investigate and verify the existence, effects, and mechanisms of TCFs, the following five research phases (Phases 0 through 4), and the aims of each phase are outlined below.

Phase-0 studies aim to prove the existence of TCFs by observing their effects. The nature of T-Consciousness and what it is will not be addressed in this phase. Phase-1 explores the varied effects of different TCFs. Phase-2 examines the reason behind the varied effects of these fields. Phase-3 investigates the mechanism of TCFs effects on matter and energy. Finally, Phase-4 draws significant conclusions, particularly with regard to the mind and memory of matter and their relation to the T-Consciousness, etc. [25-28]

Materials and Methods

ASTM C 1260

There are different methods for testing the reactivity of aggregates, and in this research standard ASTM C 1260 is the basis of the work [29]. On the other hand, due to the novelty of the knowledge of the CF(H), from each mold that included 4 samples, one sample was selected for the following experiments: Group XI No. 3- Group XII No. 4- Group XIII No. 4- Control Group No. 4. From now on each sample briefly introduces its group and is named by the same group name and is examined for the following tests.

Petrography

The samples and the rock and mortar sections were examined in terms of mineralogy; the shape and form of silica crystals were examined by petrographic imaging.

SEM (Scanning electron microscopy)

Examination of SEM photography and preparation of images and investigation of the construction and the presence of basic elements.

L.O.I (Loss on Ignition)

Doing L.O.I test to reduce the weight of the sample due to heat.

XRF (X-Ray Fluorescence)

A quantitative and qualitative investigation of oxides of XRF samples.

XRD (X-ray Diffraction)

crystallography study; investigation and identification of crystalline phases and changes in the crystalline structure.

FT- IR (Fourier-transform infrared spectroscopy)

Infrared examination of FT- IR

Methodology of the ASTM C 1260 test

Aggregate used: In order to better investigate the effects of the CF(H), the aggregates were selected from a Kish Island rock mine in Iran, which have high reactivity.

Method: The test was performed according to the ASTM C1260 standard by preparing 4 series, which according to the standard, each series included 4 prism samples. This method was accelerated and strict.

Cement: The Portland cement used for all samples was type II cement from one bag. Since the samples were exposed to NaOH, the number of alkalis in the cement was not a significant factor in expansion.

First, all aggregates were graded according to the requirements of Table1.

Table 1 . Requirements for the grading of the aggregate

Sieves Size (mm)		Weight Percentage
Passed	Remained	
4.75	2.36	10
2.36	1.18	25
1.18	0.600	25
0.600	0.300	25
0.300	0.150	15

Then four molds of each series including 4 standard samples were prepared for each aggregate and cement composition.

Mortar components ratio

The ratio of dry materials for the mortar test was one part of cement to 2.25 parts of aggregate by weight, and the ratio of water to cement was equal to 0.47.

Mixing

Mixing of mortars was performed in accordance with the requirements of the ASTM C305 standard method.

Molding the samples

Immediately after making the mortar, the samples were molded.

Application of Taheri Consciousness Fields

One of the introduced TCFs is called the Consciousness Bond Field and was applied to the samples according to the protocols regulated by the COSMOintel research center (www.COSMOintel.com). A request for Connection to the CCN to utilize TCFs can be placed through the COSMOintel website in the "Assign Announcement" section. This access is available for everyone at no cost. In order to study and experience this Connection, the researchers can register on the website at any time in order to report the experiment to the COSMOintel research center. Certain details of the experiment must be provided to the center; for example, the characteristics or number and name of samples and controls must be specified. This entire experiment was carried out as a double-blind method where lab technicians were completely unaware of the TCFs.

Storage and measurement of samples

Initial storage and reading

Samples were placed in a wet chamber immediately after molding. They were removed from the mold after 24 hours and the initial reading was performed with an accuracy of 0.002 mm. The samples made with one type of aggregate were placed in a sealed chamber that had enough water to drown the samples, and the chamber was placed in an oven at a temperature of 80 ° C ±2 for 24 hours.

Zero base reading

After 24 hours, each of the chambers was removed from the oven in turn, and then the base reading of each of the prisms was done immediately after drying their surfaces, and then they were returned to the chamber, then all samples made from the aggregates were placed in a chamber with a sufficient amount of normal NaOH at a temperature of 80 ° C ±2 so that the samples were completely drowned and the chamber was sealed and returned to the oven.

Subsequent reading and storage

The change in length of the samples was read periodically for 14 days after the baseline reading.

Calculation Method

The difference between base reading (zero) and reading in each time period of the samples was calculated and the expansion of the samples for each period was recorded. The average expansion of four samples for each cement and aggregate composition was reported to be approximately 0.01% of the read periods.

Results and Discussion

Examination of the results in Table 2 shows an average reduction of the rate of expansion of 0.6.6% was observed in the samples under the TCF (H).

Table 2 . The average expansion rate of each series, which is itself an average of the 4 samples, during 16 days

Days	Sand Expansion			
	XI	XII	XIII	Control
2	0.00	0.00	0.00	0.00
9	0.48	0.48	0.43	0.48
14	0.60	0.60	0.56	0.63
16	0.64	0.63	0.60	0.67

Table 3 . Expansion rate of 4 internal samples in each series, at 16 days compared to the control

Name	Sand Expansion			
	XI	XII	XIII	Control
Sample No.1	0.622	0.625	0.614	0.673
Sample No.2	0.614	0.626	0.579	0.671
Sample No.3	0.654	0.635	0.592	0.658
Sample No.4	0.669	0.621	0.606	0.661
The Average percentage of 16-day expansion	**0.64**	**0.63**	**0.6**	**0.67**
Percentage of Change Compared to control at 16 days old	**-4.5%**	**-6%**	**-10.5%**	-------

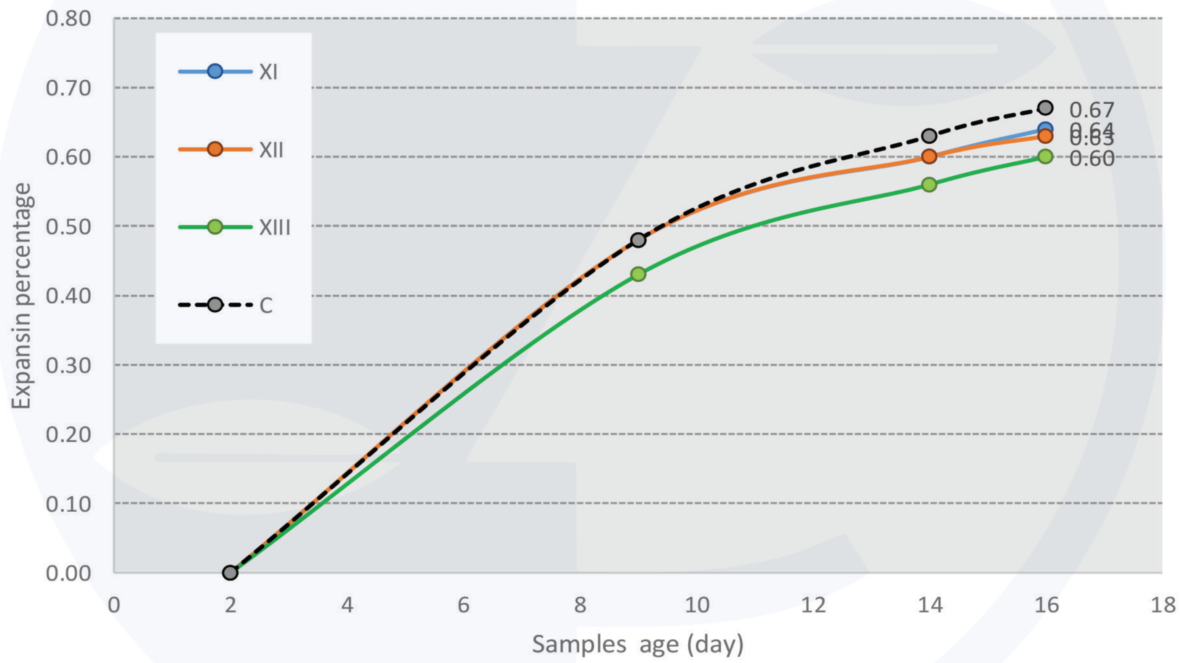

Figure 2 - Comparison of the expansion percentage of samples

Aggregate petrography

Petrography or descriptive petrology is a branch of petrology that discusses the naming, classification, construction, and texture of rock collections. Rocks are heterogeneous natural objects that result from the accumulation of one or more minerals. Usually, in most rocks, the constituent minerals are in balance with each other. The thermodynamic conditions governing the rocks limit the possibility of the presence of minerals together, so it is possible to identify, classify and name the rocks by studying the twin minerals and how they relate to each other in petrography [30].

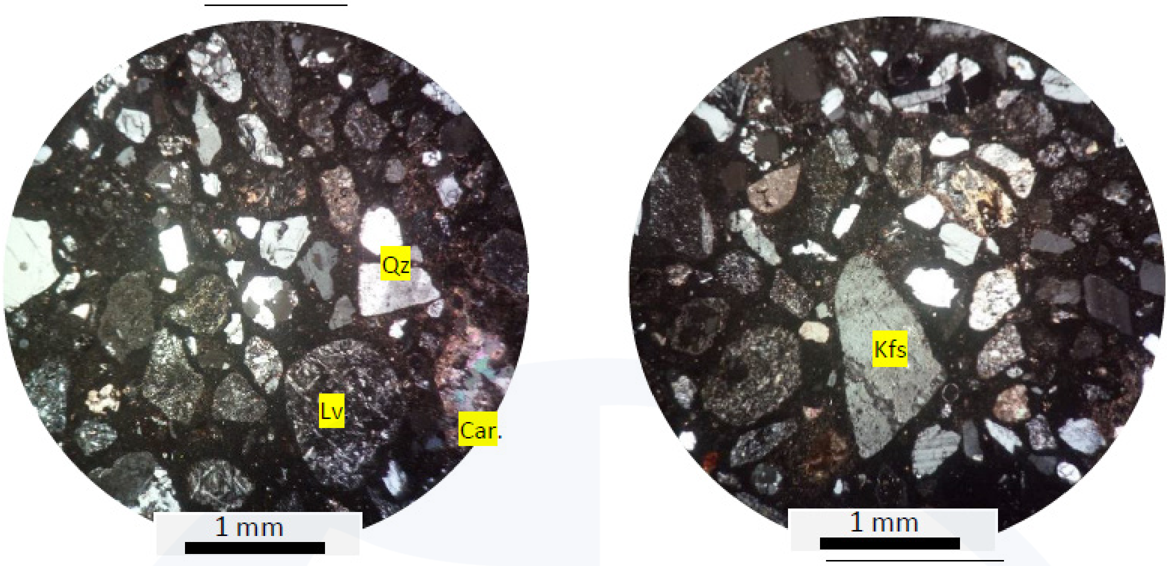

Figure 3 - The Control Sample

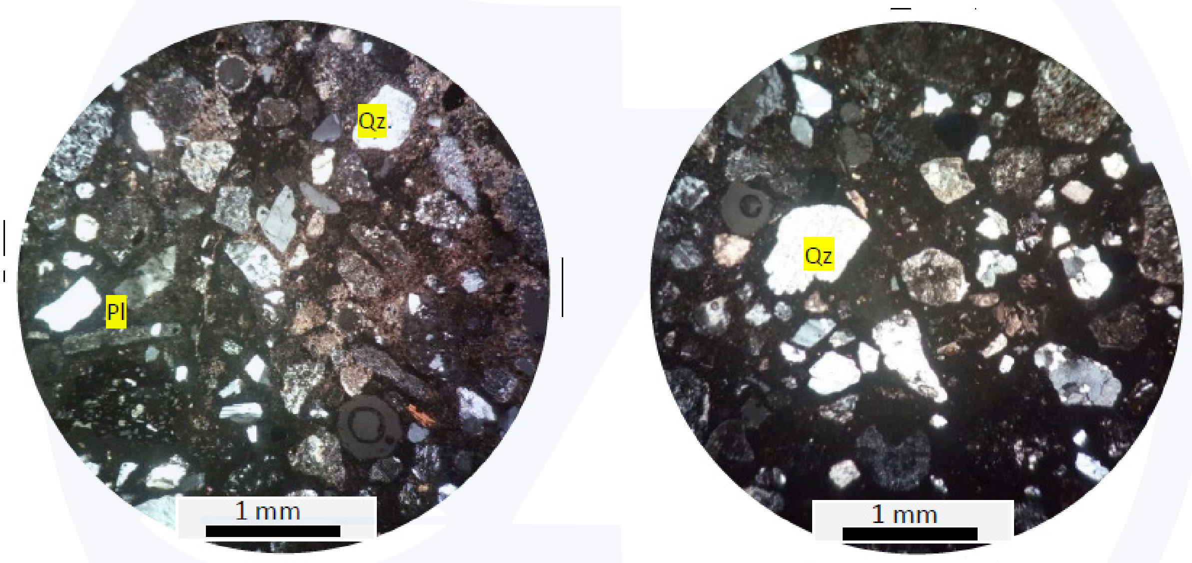

Figure 4 - Sample XI

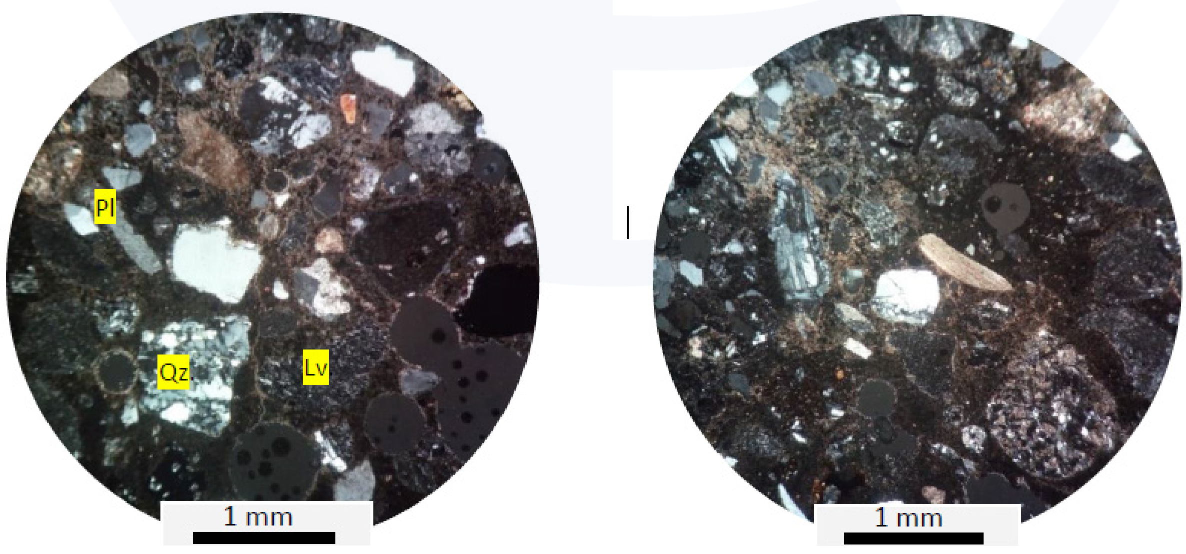

Figure 5 - Sample XII

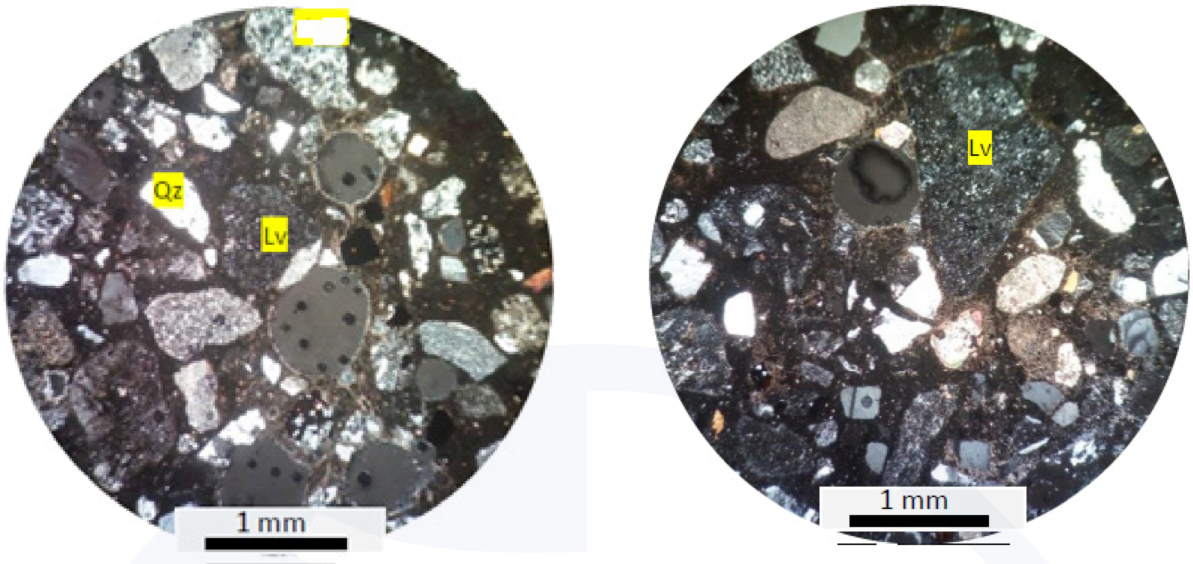

Figure 6- Sample XIII

The identified grains are igneous, sedimentary, and single minerals. The main minerals of the samples are quartz, plagioclases, and potassium feldspar. Igneous components are mainly intermediate to Mafic in composition. Their constituent minerals are plagioclase and pyroxene and are in the form of Photo Cryst in the microcrystalline to glass background. Sedimentary parts are mainly chert, quartz, sandstone, and conglomerate grains as well as carbon parts. Some grains, which are mostly clearer in the samples under the TCF (H), have good roundness, but most of the ones that are more evident in the control sample are more angular. Since the aggregates are freely selected and graded, and according to the full description of how this reaction appears, one of the events is the appearance changes of siliceous minerals. Igneous grains are mainly alteration, and their main minerals are feldspar and quartz minerals. The background of igneous minerals has been completely altered to chlorite. Most of these minerals are quartz and feldspar. Grains' dimensions vary from 100 micrometers to larger than 2 millimeters. The cement background between the grains is completely microcrystalline and covers the space between the grains.

SEM (Scanning Electron Microscopy)

After measuring the expansion rate, the samples were examined by SEM scanning electron microscope, and determination of the chemical composition by point and bulk analysis as an element from different sections.

As it can be seen in figure 8, the apparent difference in the photos is quite obvious. The crystals formed in the control sample are clear and it can be noted that gels are formed around the aggregate. The spaces around the aggregate in the samples under the TCF(H) have a better connection with cement, and less empty and dark space is seen.

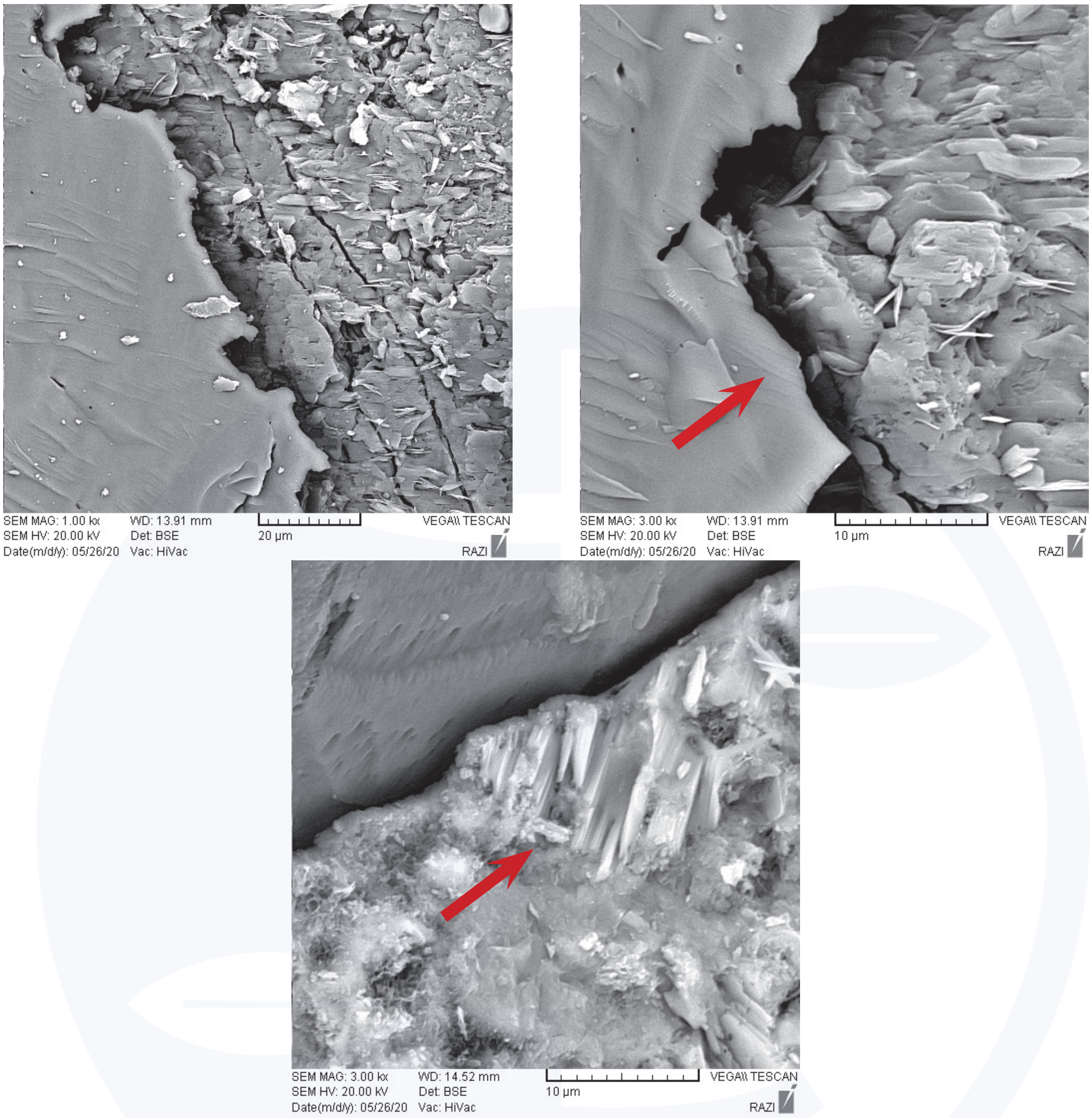

Spectra: SHAHED

Element	Series	unn. C [wt.-%]	norm. C [wt.-%]	Atom. C [at.-%]
Carbon	K series	1.12	1.24	2.13
Oxygen	K series	46.21	51.10	66.30
Sodium	K series	1.79	1.99	1.79
Magnesium	K series	0.41	0.46	0.39
Aluminium	K series	3.09	3.42	2.63
Silicon	K series	21.37	23.63	17.47
Calcium	K series	15.63	17.29	8.95
Iron	K series	0.80	0.88	0.33
	Total:	90.4 %		

Figure 7 - Control sample at the gel formation place, around the aggregates, and weight percentage and atomic number percentage of the elements present in this sample

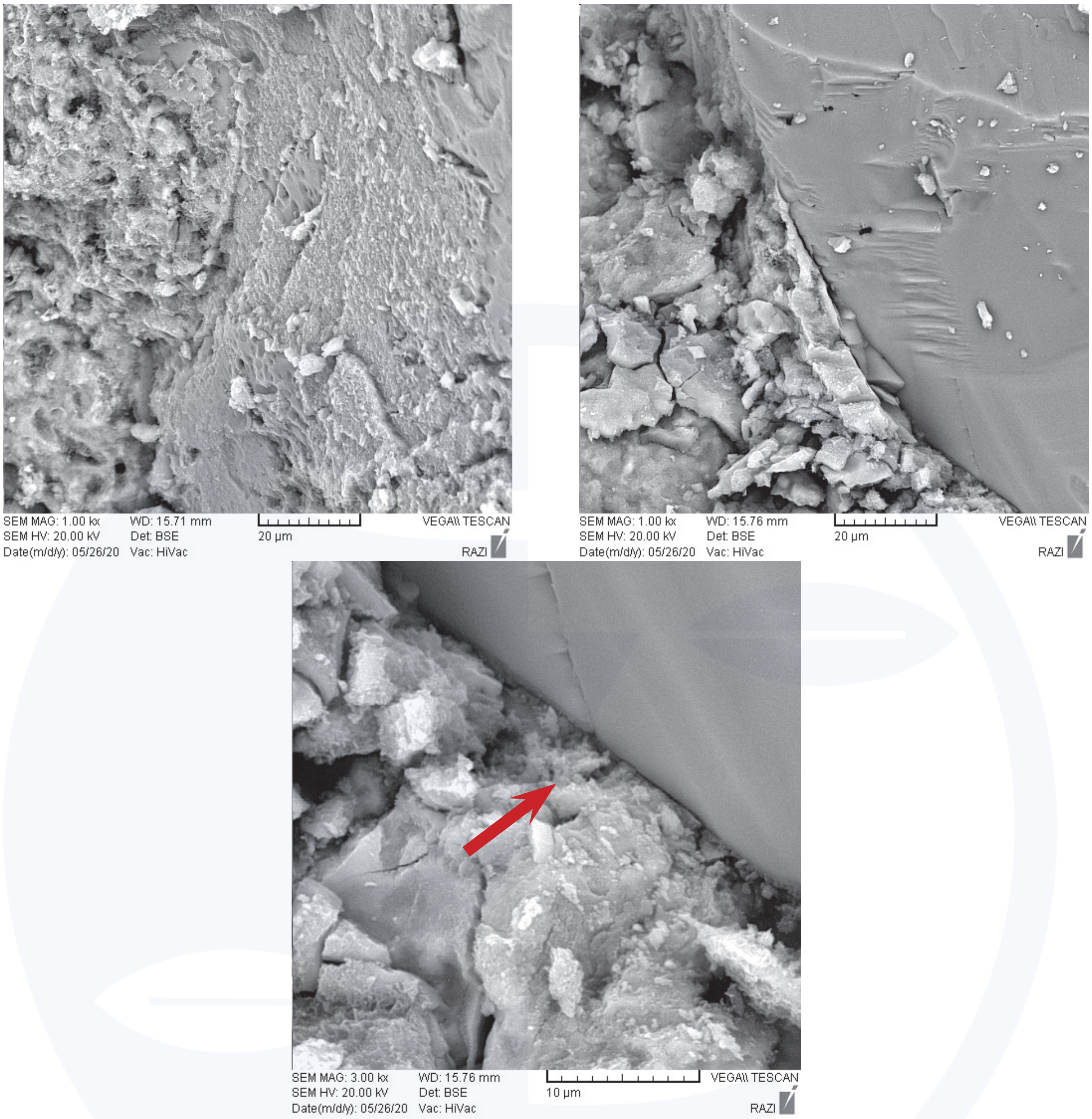

Spectra: SAMPLE 1

Element	Series	unn. C [wt.-%]	norm. C [wt.-%]	Atom. C [at.-%]
Carbon	K series	2.18	2.44	4.50
Oxygen	K series	39.46	44.12	61.12
Sodium	K series	1.00	1.12	1.08
Magnesium	K series	0.65	0.73	0.67
Aluminium	K series	2.32	2.59	2.13
Silicon	K series	14.05	15.71	12.40
Potassium	K series	0.76	0.84	0.48
Calcium	K series	27.05	30.24	16.72
Titanium	K series	0.50	0.56	0.26
Iron	K series	1.47	1.64	0.65
	Total:	89.4 %		

Figure 8 - Sample XI at the gel formation place, around the aggregate, and weight percentage and atomic number percentage of the elements present in this sample

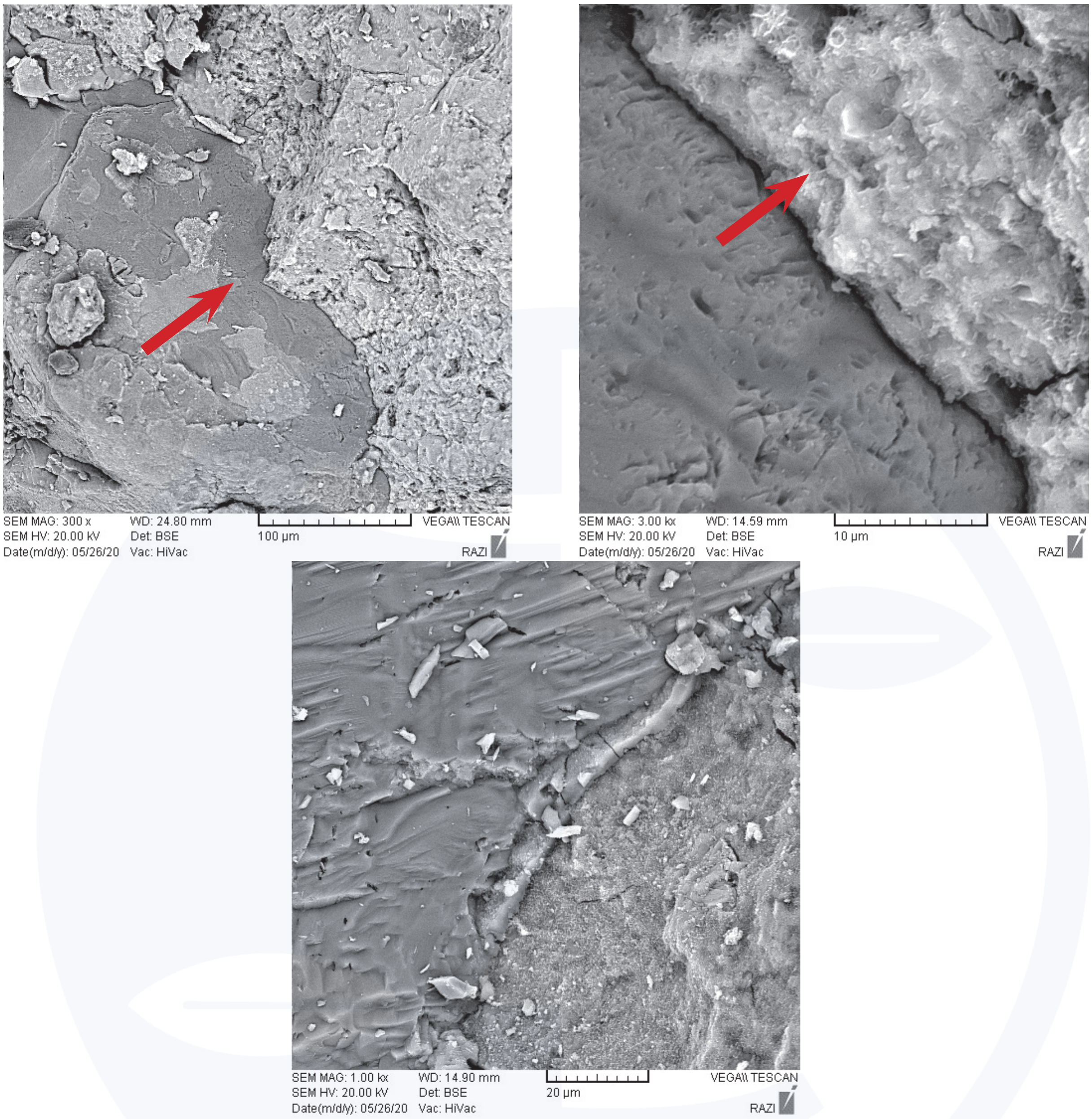

Spectra: SAMPLE 2

Element	Series	unn. C [wt.-%]	norm. C [wt.-%]	Atom. C [at.-%]
Carbon	K series	3.75	4.66	7.95
Oxygen	K series	40.15	49.93	63.95
Sodium	K series	1.57	1.96	1.74
Magnesium	K series	0.54	0.67	0.56
Aluminium	K series	2.07	2.57	1.96
Silicon	K series	12.96	16.12	11.76
Potassium	K series	0.73	0.91	0.48
Calcium	K series	17.23	21.43	10.96
Iron	K series	1.41	1.76	0.64
	Total:	80.4 %		

Figure 9 - Sample XII at the gel formation place, around the aggregate, and weight percentage and atomic number percentage of the elements present in this sample

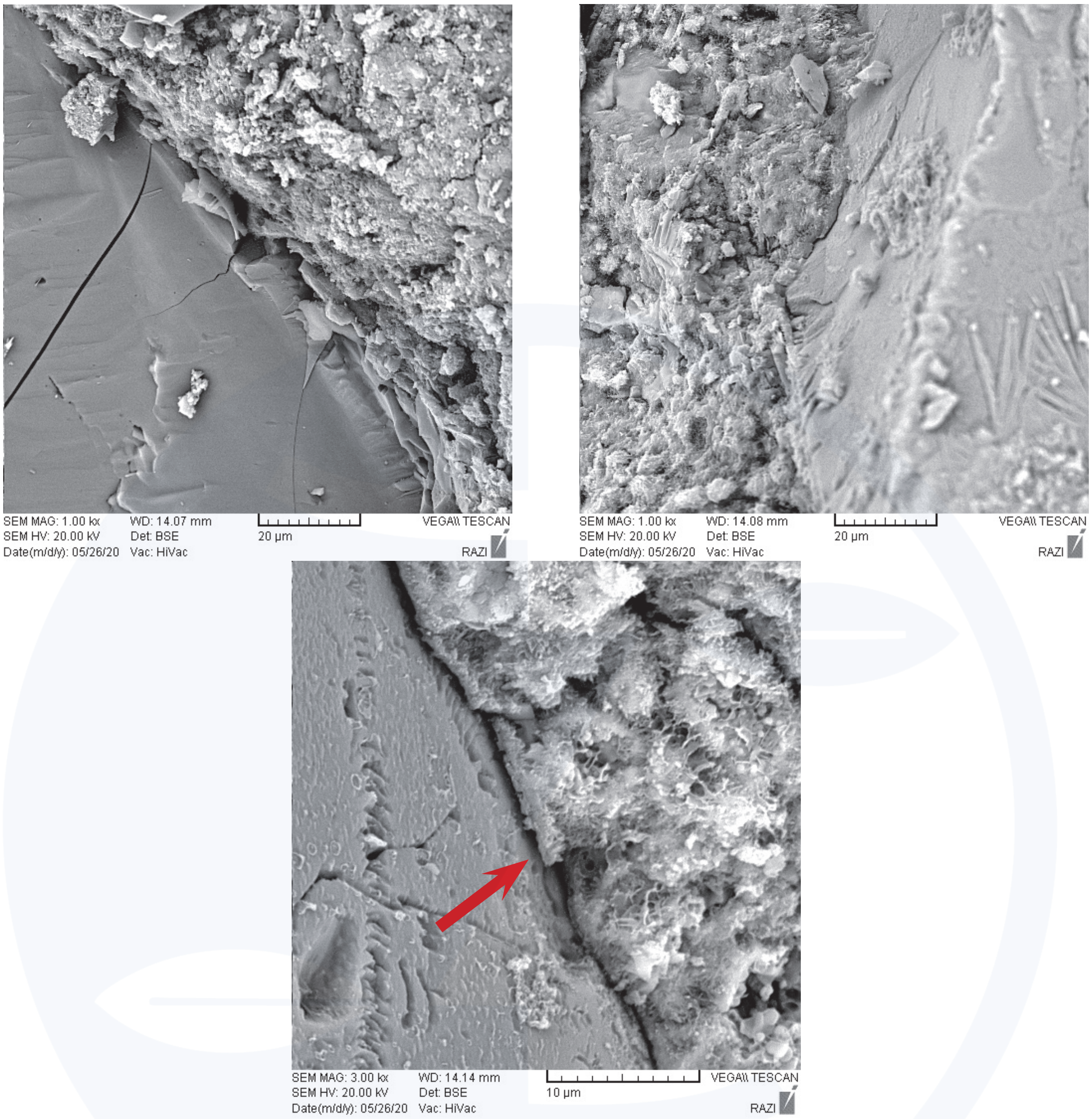

Spectra: SAMPLE 3

Element	Series	unn. C [wt.-%]	norm. C [wt.-%]	Atom. C [at.-%]
Carbon	K series	2.43	2.81	5.07
Oxygen	K series	39.51	45.79	61.97
Sodium	K series	1.48	1.72	1.62
Magnesium	K series	0.52	0.60	0.54
Aluminium	K series	2.55	2.96	2.37
Silicon	K series	13.98	16.21	12.49
Potassium	K series	1.14	1.32	0.73
Calcium	K series	23.37	27.08	14.63
Iron	K series	1.31	1.51	0.59
	Total:	86.3 %		

Figure 10 - Sample XIII in the gel formation place, around the aggregate, and weight percentage and atomic number percentage of the elements present in this sample

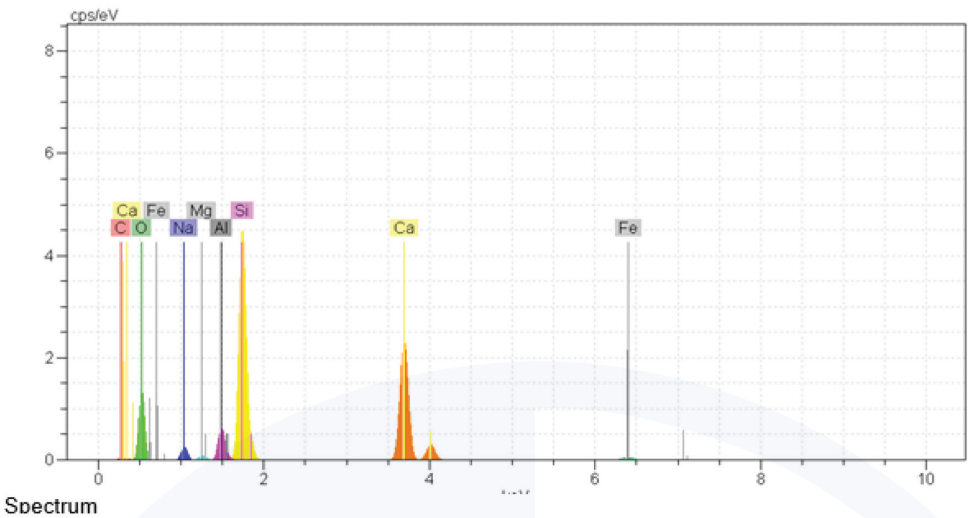

Figure 11 - Identification and abundance of the elements present in the control sample

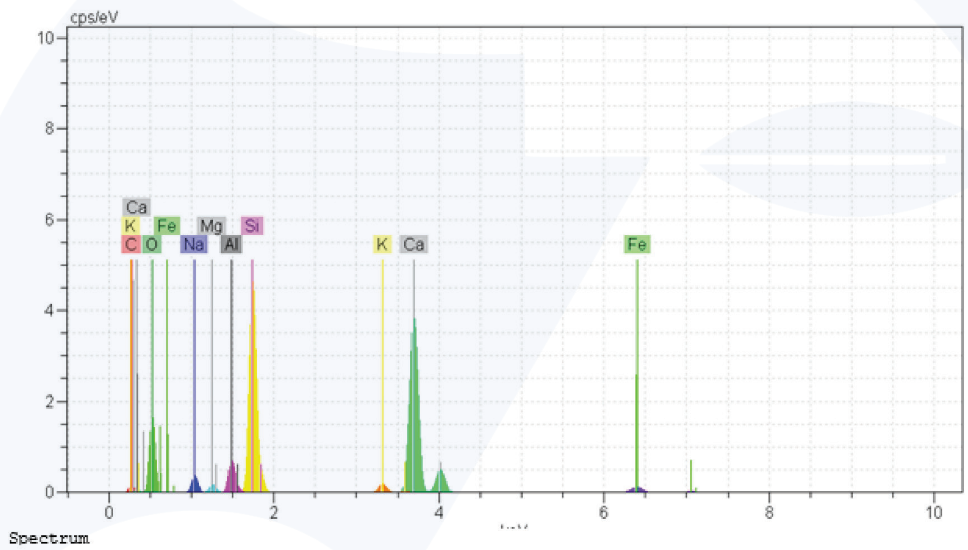

Figure 12 - Identification and abundance of the elements present in sample XI

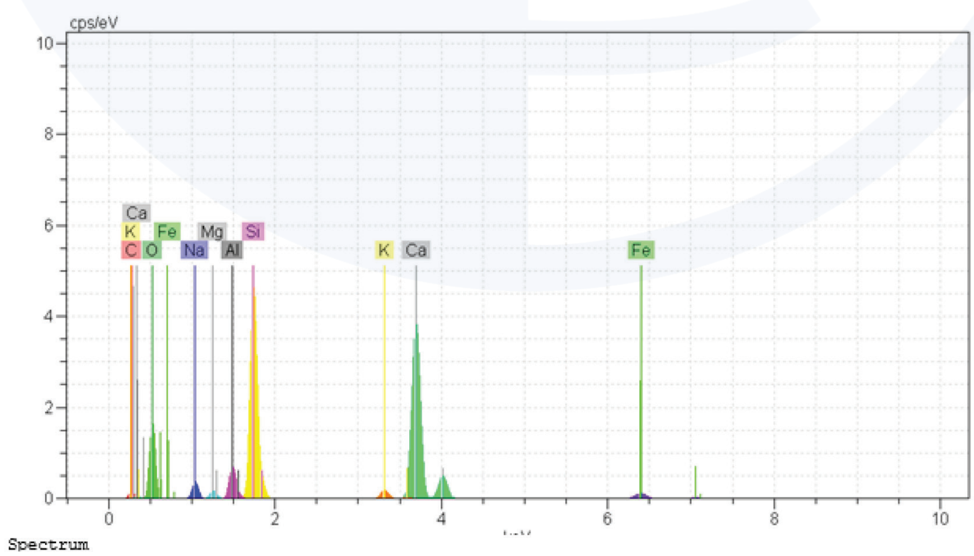

Figure 13 - Identification and abundance of the elements present in sample XII

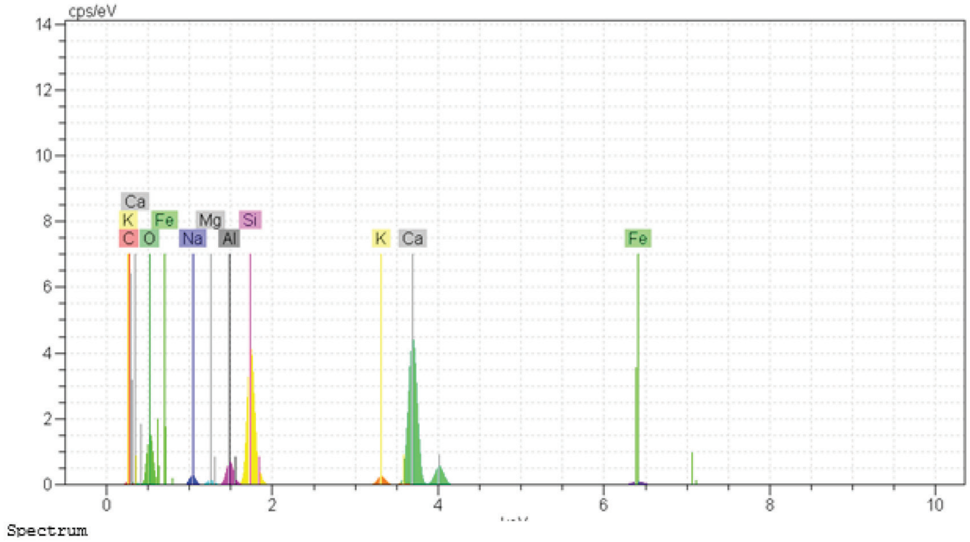

Figure 14 - Identification and abundance of the elements present in sample XIII

Table 4 . Weight percentage of the identified elements compared to the control

Name	Carbon	Oxygen	Silicon	Iron	Calcium
Control	-	-	-	-	-
TCF XI	96.77%+	13.7%-	33.5%-	86.4%+	74.9%+
TCF XII	275%+	2.3%-	31.8%-	100%+	24%+
TCF XIII	126.5%+	10.4%-	31.4%-	71.6%+	56.7%+

As mentioned earlier, silica gels begin to spread around the aggregate, usually creating a dark space around the aggregate. It can be seen in the photos that this distance is greater in the control sample. In order to ensure the qualitative analysis of SEM, which shows the intensity and amount of the identified elements, a quantitative comparison of the maximum presence of elements have been presented. Although the silica phase has a comparative priority and the gels are alkali-silica, the purposeful changes of the other elements can be considered. These can be the criteria for how the TCF(H) works.

Loss on Ignition (L.O.I)

L.O.I test was used to determine the levels of water or carbonates. The cement sample was heated to 950$^{\circ C}$ for 1.5 hours until the sample mass was stabilized. Then the amount of the lost mass was calculated.

Table 5 . Comparison of the amount of mass reduction due to combustion compared to the control

Test	XI	XII	XIII	Control
L.O.I	10.38	10.41	11.16	9.85
Percentage of the changes compared to the control	5.4%+	5.7%+	13.3%+	0---

This mass loss may indicate the presence of more materials in the samples under the TCF (H) that evaporates earlier due to heat; materials such as carbon or water from the hydration of cement or other possible materials.

XRF (X-ray fluorescence)

From each series, a sample was selected according to the maximum to minimum expansion compared to the control and the samples under the reference standard ASTM E 1621-13 and at a temperature of 21℃, the humidity of 51% based on the weight percentage of elements, and constituents by Semi-Quantitative method were analyzed by XRF.

Table 6 . Weight percentage of the oxide elements identified in the samples

Oxide	XI	XII	XIII	Control
Na_2O	2.4	2.2	2.4	2.4
MgO	1.6	1.5	1.45	1.58
Al_2O_3	7.6	7.42	7.3	8.2
SiO_2	43.7	42.5	43.2	45.5
P_2O_5	0.15	0.16	0.17	0.17
SO_3	0.48	0.57	0.54	0.42
K_2O	2.1	2.1	2.2	2.3
CaO	25.6	26.8	25.2	23.6
TiO_2	0.79	0.84	0.88	0.78
Fe_2O_3	5.2	5.5	5.5	5.2

Table 7 . Percentage of the changes of the elements compared to the control sample in XRF

Oxide	XI	XII	XIII	Control
Al_2O_3	7.13%-	9.5%-	11%-	0
SiO_2	4%-	6.6%-	5%-	0
SO_3	14.3%+	35.7%+	28.6%+	0
CaO	8.5%+	13.6%+	6.8%+	0
TiO_2	1.5%+	5.8%+	5.8%+	0

XRD (X-ray diffraction)

XRD test was taken from the samples for more accurate identification. The results of this test with respect to the general composition of cement [31-32]. are given in Table (8).

Similar to the previous test, a sample from each series was selected depending on the maximum and minimum changes compared to the control. The test was performed according to the standard BS EN 13925-1:2008 at 21℃ and 51% humidity, electric current: 30 mA, voltage Kv40, anode: Cu, operating angle θ2: (10-100) degrees. Rietveld's analysis method was considered for quantitative analysis.

Step Size: 0.02, counting time: 0.5 sec

Table 8 . Identified phases in the samples under XRD

Phase	X1%	XII%	XIII%	Control%
Albite	**0.16134055**	**0.30215344**	**0.16134055**	**0.048718713**
Aluminate	6.552184	7.252681	6.552184	8.082461
Anhydrate	3.9395797	5.3288217	3.9395797	3.495407
Calcite	**11.64169**	**6.4741564**	**11.64169**	**16.603098**
Calciumsilicate	4.4278374	2.773415	4.4278374	5.016588
Dolomite	**4.7871003**	**6.83844**	**4.7871003**	**8.888318**
Ferrite	38.724575	28.624723	38.724575	29.967413
Gypsum	**2.3371325**	**15.209964**	**2.3371325**	**0.05992761**
Hemihydrate	**1.3149565**	**6.19433**	**1.3149565**	**0.08419773**
Microcline	7.396136	6.7929025	7.396136	8.271617
Periclase	12.425677	7.641237	12.425677	13.771777
Portlandite	2.3961468	2.2504933	2.3961468	2.2082295
Quartz	3.8956416	4.316682	3.8956416	3.5022485
Total	100	100	100	100

Comparison of the chemical compounds of XRD analysis

Albite contains silicon and oxygen compounds and belongs to the silicate family and has a triclinic crystal structure [33]. This compound is further developed in samples under the TCF (H).

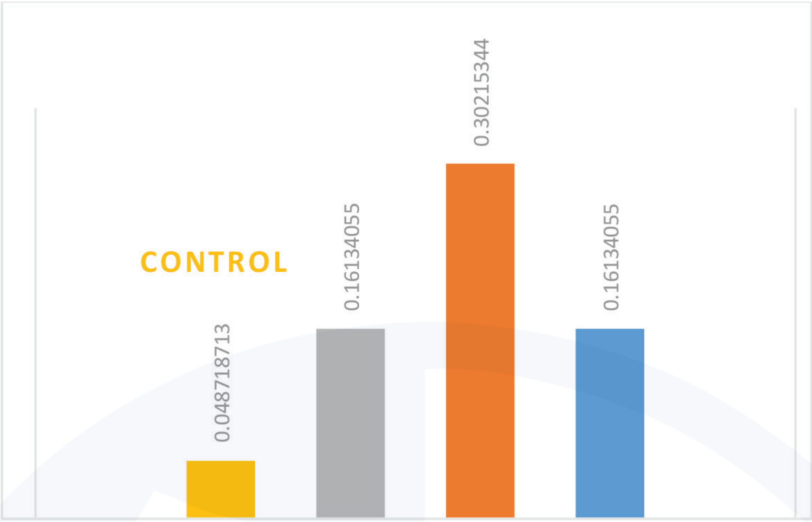

Figure 15 - Abundance of Albite in the samples

Calcite ($CaCO_3$) is a well-known form of calcium silicate. One of the parameters to which sulfates react is Ca $(OH)_2$. It is a product of cement hydration.

Ca $(OH)_2$ + cement gels (C_3S, C2S) water →+cement

Rainwater penetrates into the concrete and as it exits the capillary tubes, dissolves the Ca $(OH)_2$ created in the concrete and brings it out

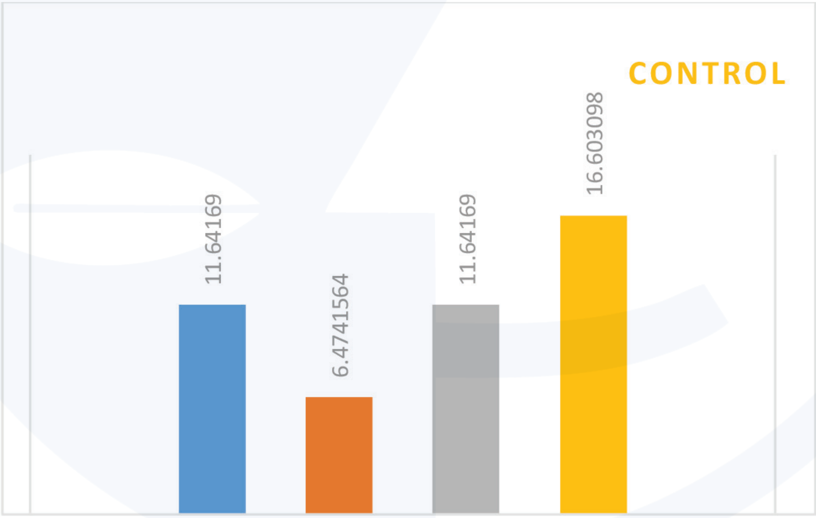

Figure 16 - Abundance of crystalline calcite in the samples

of the concrete. In the presence of air, Ca $(OH)_2$ combines with carbon dioxide and CaCO3 is formed.

After evaporation of water, $CaCO_3$ appears as white powder on the concrete surface. It also leaves a void that prepares the concrete for the sulfate's reaction. On the other hand, ambient sulfates react with $CaCO_3$ and form gypsum and aluminate gypsum compounds, which increase the volume and some specific type of sulfates reaction. In the samples under the TCF (H), we saw a sharp decrease in $CaCO_3$ [34].

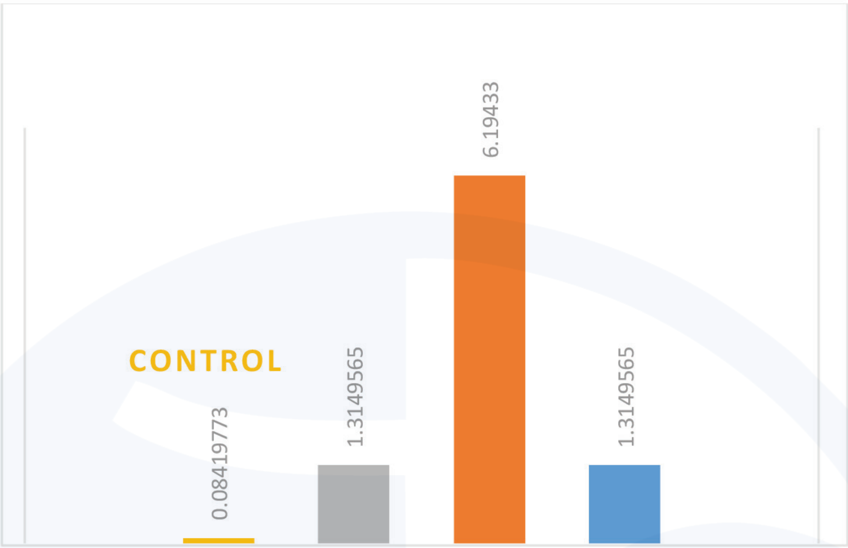

Figure 17 - Abundance of crystalline dolomite in the samples

Dolomite with the formula CaMg $(CO_3)_2$. Studies show that dolomite has a limited effect on the behavior of cement; its small amounts can improve the properties of cement and its large amounts have a reducing effect [35], And since in this process all cement has the same structure what is found after the chemical silica alkali analysis is somehow the residue of the material. assuming that the amount of dolomite is the same in all samples, after the reaction, less dolomite is seen in the sample un-der the TCF (H). And dolomite on a small scale plays an alternative role to cement in increas-ing hydration.

Gypsum ($CaSO_4$. $2H_2O$) is allotropy with two molecules of calcium sulfate. In the cement industry, gypsum is used to increase the set-ting time of cement. Gypsum particles mixed with cement are very fine, forming a coating on the cement grains and preventing the rapid growth of cement crystals and instantaneous setting because the instantaneous setting is irreversible.

Sulfates attack various compounds of hydrated cement. Sodium and potassium sulfates combine with calcium hydroxide and calcium hydroaluminate. The interaction of sodium sulfate with calcium hydroxide can be summarized as follows:

$$\mathbf{Ca\ (OH)_2+Na_2SO_4.10HO_2 \rightarrow CaSO_4.2H_2O +2NaOH + 8H_2O}$$

And the interaction of sodium sulfate with calcium hydroaluminate is as follows:

$$\mathbf{2(3CaO.AL_2O_3.12H_2O) +(NaSO4.10H_2O) \rightarrow 3CaO.AL_2O_3.3CaSO_3.31H_2O+2AL(OH)_3 +6NaOH+17H_2O}$$

One of the products of the above reactions is gypsum with the formula CaSO4·2H2O. This gypsum increases its volume and also causes resistance [2].

The chemical composition of gypsum has been seen more in the samples under the TCF (H).

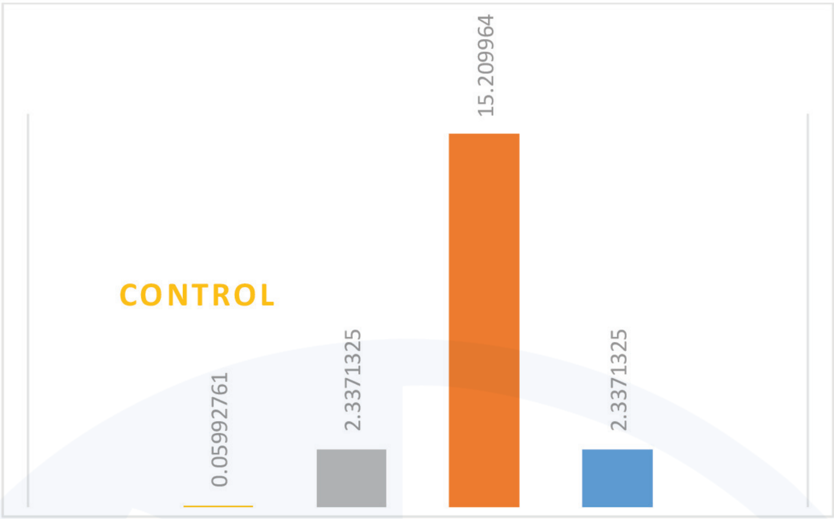

Figure 18 - Abundance of GYPSUM crystal in the samples

Hemihydrate is allotropy from calcium sulfate with the formula $CaSO_4 * 1 / 2H_2O$ and has half a unit of the water molecule. This chemical composition has been seen more in the samples under the TCF (H).

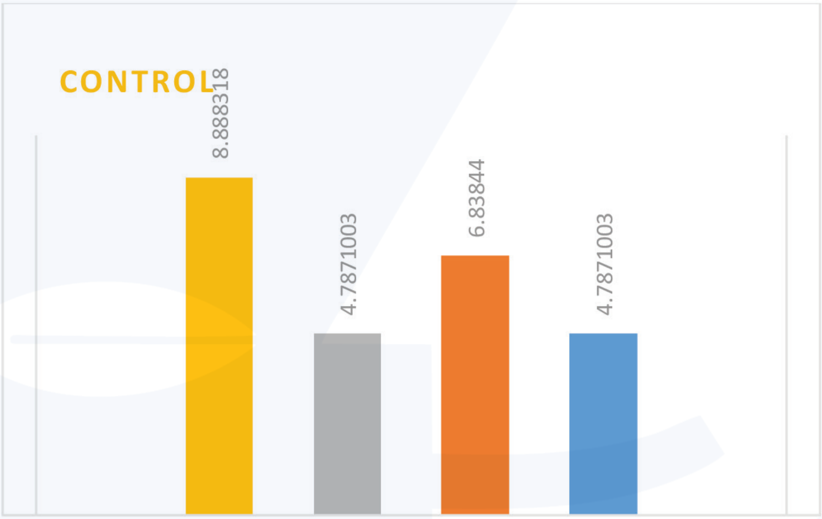

Figure 19 - Abundance of Hemihydrate crystals in the samples

The FT-IR test of infrared spectroscopy

A sample from each series was selected for FT-IR analysis. This analysis can detect vibrations in the functional groups of a sample. Existing chemical bonds stretch or bend when infrared radiation strikes the sample. Therefore, the chemical group in the sample, regardless of the structure of the rest of the molecule, tends to absorb infrared radiation in a certain range of wavelengths. As a result, based on the relationship between wavelength position and chemical structure, it is possible to easily identify different statistical groups in the sample. The position of the functional groups is almost constant. To investigate the chemical structure of the samples, the FT-IR test was used, and the results are shown in Figure 20. Also, for better comparison, the results of the magnified image of these spectra in the range of 400 cm^{-1} to 1800 cm^{-1} are also shown.

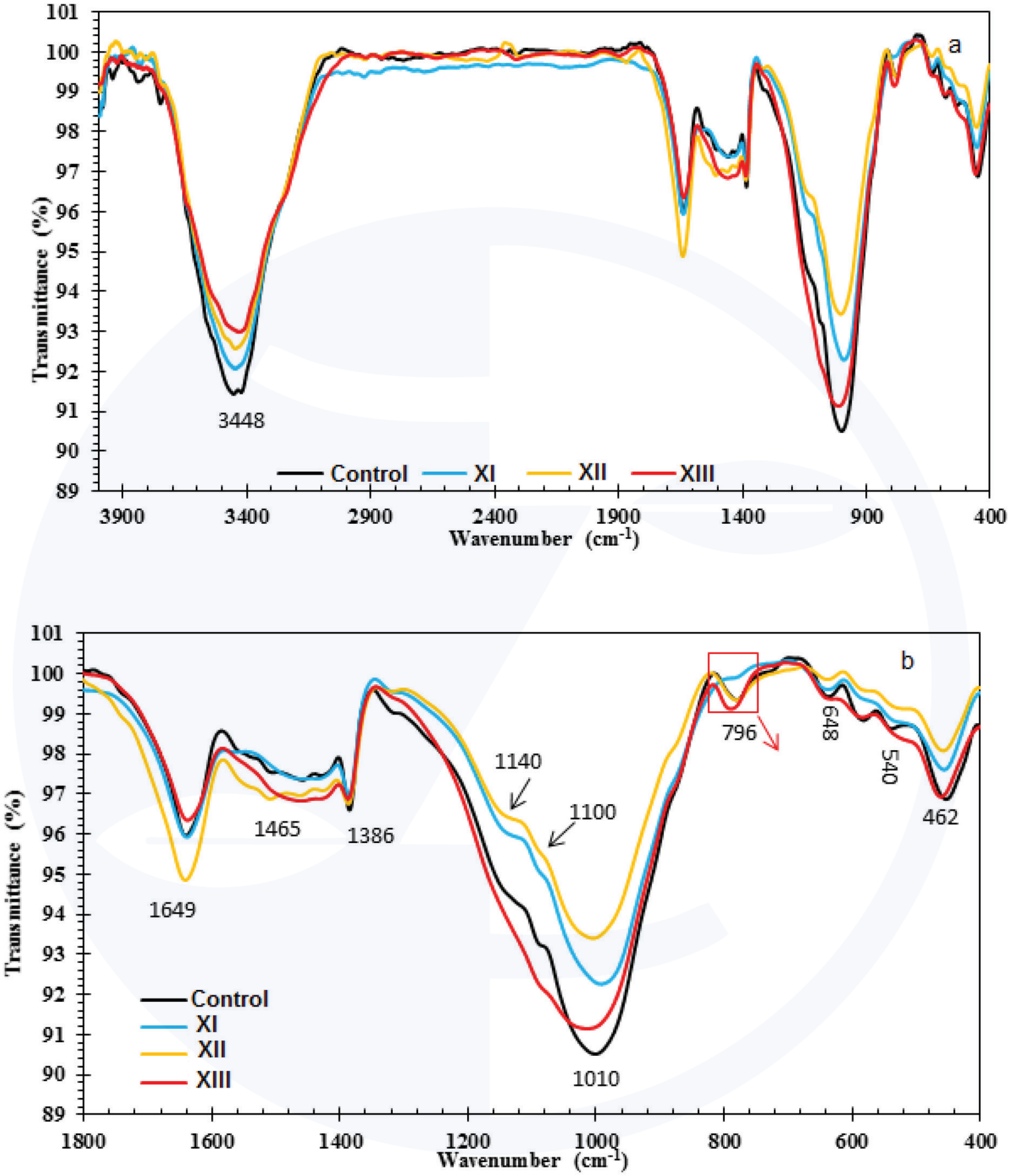

Figure 20 - Figure 20- FT-IR test results related to cement samples (a) of the whole spectrum and (b) range of 400 cm^{-1} to 1800 cm^{-1}

According to the spectra shown in Figure 20, in the studied samples, the peaks in the wave number of about 3460 cm^{-1} related to the tensile vibration of O-H bonds have been adsorbed on water molecules [36]. The same O-H bonds can vibrate at a certain frequency in the form of bending that the absorption resulting from the flexural vibration of O-H bonds has occurred in the wave number 1649 cm^{-1} [37]. The tensile vibration of the O-H bonds in the control and the flexural vibration of the O-H bonds in the samples under the TCF (H) have more pronounced peaks. Tensile vibrations of bonds in the carbonate group have shown the structure of calcium carbonate at the wave number 1465 cm^{-1}absorption peak [38]. Also, the tensile vibrations of Si-O bonds in the units of $SiO4^{-4}$ anions at the 1386 cm^{-1} wave number have shown an absorption peak [39]. The peaks appearing in the wave numbers of 1100 cm^{-1} and 1010 cm^{-1} are related to the tensile vibration of Si-O-Si and Si-O-Al bonds in the compounds present in cement, respectively [40]. This peak is seen more intensely in the control sample. The two peaks located at 648 cm^{-1}, 462 cm^{-1} and 540 cm^{-1} are also related to the flexural vibration of Si-O bonds in different compounds [40-41].

As identified in the spectrum in Figure 20, a peak is also located at wave number of 796 cm^{-1}, which is observed in samples containing high amounts of alkali in production cements. [40]. By comparing the peak intensity of this wave number, it is clear that sample XI had the lowest, and sample XIII had the highest amount of alkali in the structure. This is while the amount of alkali in control and XII were nearly identical. The amount of alkali in cement can be one of the most important parameters in cement cancer. In our experiment, the cement is the same and low-alkali and the analysis was after exposure to stimulant alkali, therefore, according to the nature of FT-IR, it can be concluded that despite the reactive medium, some amount of alkali is still seen in the XIII sample, which did not react. And this study is consistent with the results of the rate of expansion. However, according to the test conditions, the alkali of the cement must react with Normal NaOH and aggregate at the maximum state, produce an alkaline silica gel, and cause expansion. It should be noted; that this peak is usually checked to compare the alkalinity of the cement before the reaction. However, this conclusion requires an extensive review of low-alkali cement is damaging the environment.

Conclusion

In the first step, we realized that the TCF (H) was able to affect the rate of expansion of cement due to the alkaline reaction, and this effect was in the range of expansion reduction and the average of 7% (P-value0.008 -Table 3, Figure 2). According to the petrography of cement sections, it was observed that the roundness of the minerals was more noticeable in the samples under the CF(H) (Figures 3-4-5-6). Also, in SEM photography, the normal space between aggregate and cement, which is the place of gel formation, was examined. And if we examine the 10 µ scale together in the photos, in the control sample, clear crystals are seen and a larger dark space is created between the aggregate and the cement (Figures 7-8-9-10).

Elemental analysis around the aggregate clearly reveals the difference between the elements affecting this reaction (Table 4). Carbon is up to 97% higher, silicon is up to 31% lower, and iron is up to 100% higher. In the LOI test, the samples are first oxidized at 950℃ and then the mass drop is calculated. This drop is greater in the samples under the CF (H), and maybe water or carbon or materials that evaporate more easily at heat have been formed (Table 5).

Also, according to the results of the XRF analysis, there is a difference in the elements presented in Tables (6 and 7) and we see SO_3 up to 28% more and SiO2 average 5% less, CaO between 6 to 13% more, and Al_2O_3 average 9% more. The differences between the crystals seen in the XRD analysis are detailed in Table (8) and we found some compounds such as Hemihydrate, Albite, and Gypsum in the samples under the TCF (H) more and Dolomite and Calcite compounds decreased. (Figures15-16-17-18-19)

It should be noted that the way to identify phases is the possibility of the presence of elements from X-ray diffraction analysis, and since the TCF (H) has a new way of operation, what is created may not be in known formats of materials and cement. Consciousness, matter, and energy are three execution elements in our research. Therefore, we are always faced with the assumption that not all the effects of the TCF (H) can be deduced from the known custom calculations, which are limited to the laws of matter in the field of matter and energy.

These effects are more evident in the analysis of FT-IR results (Figure20). The tensile vibration of the O-H bonds in the control samples and the flexural vibration of the O-H bonds in the samples under the TCF (H) have clearer peaks. The peaks appearing in the wavenumbers of 1100 cm^{-1} and 1010 cm^{-1} are related to the tensile vibration of Si-O-Si and Si-O-Al bonds in the compounds in cement, respectively, which can be seen more intense in the control sample. And in general, the difference between control graphs and the ones under the TCF (H) can be seen which has taken a different way.

As was mentioned at the beginning, the basis of the current research is to investigate the effects of TCF (H). In this theory, Although, TCFs are not measurable, it is possible to investigate their effects through various scientific research.

In this research, all the experiments have been conducted by experts unfamiliar with the theory of TCFs. Our results showed that the composition of the materials, the presence of elements, and their chemical compounds changed under the influence of TCF, and these changes were purposeful in order to control the expansion and the rate of concrete destruction. Therefore, it can be concluded that the TCF has the ability to change the behavior of materials and was able to affect favorably the process of controlling the alkaline reaction of silica by changing the chemical composition. TCF is applicable to all living (and non-living) creatures including plants, animals, microorganisms, molecules, etc. We suggest that other researchers investigate the effect of TCFs on different living and non-living creatures.

Acknowledgments

We would like to thank the international laboratories officials of Iran who patiently helped us in this research. Many thanks to Professor Ramezanianpor. Dr. Mojtahedi and Dr. Nasiri for their scientific advice and Ms. Jalayer for her work in literary and translation matters.

References

1. Mohammad. A, Ghiyasvand . E, & Nili .M. (2020). Relation between mechanical properties of concrete and alkali-silica reaction (ASR); a review. Construction and Building Materials Vol.253: 30 119189
2. Zandi .Y.(2009). Advanced Concrete Technology. ISBN:978-964-547-221-2. PP55-65
3. Kashi. M.G. (2005). Mitigation of Alkali-Silica Reactivity (ASR) for Saymareh dam Project. Soil, Rock & Structure Consulting Engineers
4. Abd-Elssamad. A, Ma. Z.J, Hou. H, Le Pape. Y. (2020). Influence of mineralogical and chemical compositions on alkali-silica-reaction of Tennessee limestones. Construction and Building Materials. Vol. 261, 20 119916
5. Stanton. T.E. (1940). Expansion of Concrete Through Reaction Between Cement and Aggregate. Proceedings of the American Society of Civil Engineers 66: 1781–1811
6. Pan. J, Feng. Y.T, Wang. J, Sun. Q.C. (2012). Modeling of alkali-silica reaction in concrete: A review. Frontiers of Structural and Civil Engineering. 6(1): 1–18 DOI 10.1007/s11709-012-0141-2
7. Lindgard. J, Andic-Caki.r O, Fernandes. I, Ronning. T. F, Thomas M D A. (2012). Alkali-silika reaction (ASR). Literature review on parameters influence laboratory performance testing, Cement and Concrete Research.Vol.42: pp.223-243
8. St John. D.A, Poole. A.B, Sims. I. (1998). Concrete Petrography-A Handbook of Investigative Techniques. Arnold, UK. pp 474.
9. Wu. H, Pan. J, Wan.g J. (2020). Nano-scale structure and mechanical properties of ASR products under saturated and dry conditions. www.nature.com/scientificreports
10. Diamond. S, et al. (1918). On the physics and chemistry of alkali-silica reaction, 5th Conf. Alkali Aggregate Reaction in concrete
11. Buck. A.D, Houston. B.J, Pepper. L. (1953). Effectiveness of mineral admixture in preventing excessive expansion of concrete due to alkali- aggregate reaction. Journal of the American Concrete Institute. Vol.30: 11-60.
12. Ramlochana. T, Thomasa. M, Grruberb. K.A. (2003). The effect of metakaolin on alkali-silica reaction in concrete. Cement and Concrete Research. Vol. 30: 339-344.
13. Rodrigue. A, Duchesne. J, Fournier. B, Champagne. M, Bissonnette.B.(2020). Alkali-silica reaction in alkali-activated combined slag and fly ash concretes: The tempering effect of fly ash on expansion and cracking. Construction and Building Materials. Vol. 251: 118968
14. Bolouri. A, Haji-Aghababayi. M. (2009). Investigation of the effect of microsilica on reducing the alkali-silica reactivity of silica in concrete aggregates of Shamil and Nian dams, First International Concrete Technology Conference, Tabriz.
15. Sedghi. P. (2009). Alkaline reaction of aggregates in concrete with a view to Gavoshan tunnel. The first national concrete conference, Tehran.
16. Singh. J, Singh. S.P.(2020). Evaluating the alkali-silica reaction in alkali-activated copper slag mortars. Construction and Building Materials. Vol. 253: 119-189
17. Delnavaz. M, Family. H, Khaksari. M, Alipour. B.(2010). Investigating the effect of using nano-silica, silica fume and metakaolin on reducing alkali-silica reactions of concrete aggregates, 2nd National Concrete Conference Tehran-Iran . https://civilica.com/doc/152568
18. Feng. X, Thomas. M.D.A, Bremner. T.W, Balcom. B.J, Folliard K. J. (12005). Studies on lithium salt to mitigate ASR-induced expansion in new concrete: a critical review, Cement and Concrete research. Vol.35: 1789-1796
19. Kim. T, Olek. J. (2016). The effects of lithium ions on chemical sequence of alkali-silica reaction. Cement and Concrete Research. 79: 159-168.
20. Afshinnia. K, Poursaee. A. (2015). The influence of waste crumb rubber in reducing the alkali-silica reaction in mortar bars. Journal of Building Engineering. 4: 231-236
21. Le .H.T, Ludwig. H. M. (2020). Alkali silica reactivity of rice husk ash in cement paste. Construction and Building Materials Vol. 243: 118145.
22. Ahmadi. B, Shekarchi .M. (2010).Use of natural zeolite as a supplementary cementitious material. Cement and concrete composites. Vol.32 (2) pp134-141
23. Najmi. M, Sobhani. J, Ahmadi. B, Shekarchi. M.(2012). An experimental study on durability properties of concrete containing zeolite as a highly reactive natural pozzolan. Construction and Building Material. Vol. 35: pp 1023-1033.
24. Snyder. K. A, Lew. H. S. (2013). Alkali-Silica Reaction Degradation of Nuclear Power Plant Concrete Structures: A Scoping Study. Materials and Structural Systems Division Engineering Laboratory. NISTIR 7937
25. WWW.cosmointel.com
26. Taheri. .M. A. (2013). Human from another outlook. Interuniversal Press. 2nd Edition. ISBN-13: 978-1939507006, ISBN-10: 193950700
27. Taheri. M.A. (2012). General Connection of particles. Interuniversal Publishing.Erfan-Hlgheh. ID: 978-1-940491-03-5
28. Torabi.S., Taheri. M. A., & Semsarha, F. (2020). Alleviative effects of Faradarmani Consciousness Field on Triticum aestivum L. under salinity stress. F1000Research, 9(1089), 1089.
29. Astm. ASTM C1260-Standard test method for potential alkali reactivity of aggregates (mortar-bar method). ASTM Int. 2012. 1-5.
30. Esfahani. A.N, Ahmadi.M,(2005). Petrography of igneous rocks, Islamic Azad University. (Khorasgan). ISBN:964-95173-7-5
31. Stutzman. P, Feng. P, Bullard . J. (2016). Phase Analysis of Portland Cement by Combined Quntitative X-Ray Powder Diffraction and Scanning Electron Microscopy. Journal of Research of the National Institute of Standards and Technology. Vol. 121 http://dx.doi.org/10.6028/jres.121.004,
32. Le Saoût. G, Kocaba. V, Scrivener. K. (2011). Application of the Rietveld method to the analysis of anhydrous cement. Cement and Concrete Research. 41 133–148
33. Khodam. F. (2018). X Ray Diffraction (XRD) Spectroscopy. NAIS. vol. 2: pp 11-19. Print ISSN: 2588-6401., Online ISSN: 2588-641X
34. Zandi. Y.(2009). Advanced Concrete Technology. ISBN:978-964-547-221-2.,PP 2-10
35. Sybilskia. M, Nocun-Wczelikb. W, Gorazdze. C. (2015). The effect of dolomite additive on cement hydration. Peer-review under responsibility of organizing committee of the 7th Scientific-Technical Conference Material Problems in Civil Engineering. DOI 10.1016/j.proeng.06.136
36. Javidparvar. A.A, Ramezanzadeh .B, Ghasemi. E. (2016). The effect of surface morphology and treatment of Fe3O4 nanoparticles on the corrosion resistance of epoxy coating, J. Taiwan Inst. Chem. Eng. 61. https://doi.org/10.1016/j.jtice.2016.01.001
37. Anchieta .C, Cancelier. A, Mazutti. M, Jahn .S, Kuhn .R, Gündel .A, Chiavone-Filho .O, Foletto E.(2014). Effects of Solvent Diols on the Synthesis of ZnFe2O4 Particles and Their Use as Heterogeneous Photo-Fenton Catalysts, Materials (Basel). 7 (2014) 6281–6290. https://doi.org/10.3390/ma7096281.
38. Sasnauskas. V. (2013). Cement hydration with zeolite-based additive, Chemija. 24 -271–278.
39. Hassan. M, J. M. Khatib, P. S. Mangat, and P. H. E. Gardiner. (2014). "FTIR and XRD Characterized Portland Cement Stabilised Lead Contaminated Soil." .
40. Tyler. S. (2001). Application of FTIR for Quantification of Alkali in Cement. The University of North Texas.
41. Trezza M. A. (2007). Hydration study of ordinary portland cement in the presence of zinc ions. Materials research. Dec;10(4):331-4.

Effect of Taheri Consciousness Bond Field on the Structure and Properties of Aluminum

Bahareh Kazazi[1*], Mohammad Ali Taheri[2]

1. Civil Engineering, CEO of Hoobe Construction Company, Tehran, Iran.

2. Sciencefact R&D Department, Cosmointel Inc. Research Center, Ontario, Canada.

1. Civil Engineering, CEO of Hoobe Construction Company, Tehran, Iran.

2. Sciencefact R&D Department, Cosmointel Inc. Research Center, Ontario, Canada.

* Corresponding author:

Bahareh Kazazi
Civil Engineering, CEO of Hoobe Construction Company, Tehran, Iran.

Email: baharkazazi@gmail.com

ABSTRACT

The properties and structure of aluminum in various known fields have been already studied. The aim of this study was to investigate the behavior and properties of unalloyed aluminum under the influence of the Consciousness Bond Field. Consciousness Bond Field is one of many Taheri Consciousness Fields (TCFs) that were founded and introduced by Mohammad Ali Taheri as new Fields more than four decades ago. These Fields are neither material nor energetic. Therefore, they do not have the quantity, but they have direct effects on both matter and energy. In other words, although TCFs cannot be directly measured, we can investigate their effects indirectly through various reproducible experiments. The present study is an attempt to examine this theory. In this research, aluminum metal has been used as a sample. Nine aluminum samples were cast under the same conditions and divided into three equal groups. Two groups were put under the influence of TCFs, and the third group was considered the control group. In order to study the effect of TCFs, the structure and properties of the metal samples were investigated. X-ray diffraction (XRD) analysis test was performed for structural analysis of aluminum samples. In terms of properties, Brinell hardness tests, electrical conductivity determination, and corrosion resistance tests were performed using the potentiodynamic method. Changes in the structure of the samples were observed. The TCF has increased lattice strain, twin defects, and intrinsic defects and reduced the size of crystalline areas and extrinsic defects.

Keywords: Concrete, Taheri Consciousness Fields, Consciousness Bond Field, Alkaline reaction

INTRODUCTION

Scientific understanding of the nature of matter began in the early twentieth century, and since then significant advances have been made in this field. Understanding the law of conservation of mass and energy, recognizing fundamental particles, quantum view of these particles, and relativistic view of the universe have been among the achievements of this scientific movement. The question can be raised whether our fundamental understanding of the nature of matter and the universe is fully developed and whether further research should continue only based on existing science or if it is possible to open a fundamentally new look at matter and the universe. There has already been debate about Cosmic Intelligence, and attempts have been made to explain it in the world of science. One of the concepts related to Cosmic Intelligence is black holes [1]. It seems that most of the discussions on "cosmic intelligence" have been philosophical and argumentative, and based on common sense, and there is a lack of empirical or computational studies in this regard. It should be noted that intelligence in this context refers to the presentation of new theories that provide a more general understanding of existence and can be examined and verified by scientific methods.

The nature of consciousness and its place in science has received much attention in the current century. Many philosophical and scientific theories have been proposed in this area. In the1980s, Mohammad Ali Taheri introduced novel fields with a non-material/non-energetic nature named Taheri Consciousness Fields (TCFs). In this perspective, T-Consciousness is one of the three existing elements of the universe apart from matter and energy. According to this theory, there are various TCFs with different functions, which are the subcategories of a networked universal internet called the Cosmic Consciousness Network (CCN). The major difference between the theory of TCFs and other theoretical concepts about consciousness is related to the practical application of the TCFs. TCFs can be applied to all living and non-living creatures, including plants, animals, microorganisms, materials, etc.

Mohammad Ali Taheri, the founder of Erfan Keyhani Halqeh, a school of thought, introduced a new science in 2020 as a branch of this school. He coined the term Sciencefact for this new science because it utilizes scientific investigations to prove the existence of T-Consciousness as an irrefutable phenomenon and a fact. Although science focuses solely on the study of matter and energy and Sciencefact, by contrast, explores the effects of the [non-material/non-energetic] TCFs, Sciencefact has provided a common ground between the two by conducting reproducible laboratory experiments in various scientific fields, and it has used the scientific approach in proving TCFs.

The influence of the TCFs begins with the Connection between CCN as the Whole Taheri Consciousness of the universe and the subjects of study as a part. This Connection called "Ettesal" is established by a certified and trained individual who has been entrusted with the TCFs. The human mind has an intermediary role (Announcer) which plays a part by fleeting attention to the subject of study and then the main achievement obtained as a result of the effects of the TCFs. These Fields cannot be directly measured by science, but it is possible to investigate their effects on various subjects through reproducible laboratory experiments.

The research methodology in the study of T-Consciousness has been founded on the process of Assumption, Argument, and Proof, in which the basic Assumption is: The Cosmos was formed by a third element called T-Consciousness that is different from matter and energy.

The Argument: The existence of TCFs can be demonstrated by its effects on matter and energy (e.g., humans, animals, plants, microorganisms, cells, materials, etc.)

The Proof: is the scientific verification of the effects of TCFs on matter and energy (according to the Argument) through various reproducible scientific experiments.

Accordingly, to investigate and verify the existence, effects, and mechanisms of TCFs, the following five research phases (Phases 0 through 4), and the aims of each phase are outlined below.

Phase-0 studies aim to prove the existence of TCFs by observing their effects. The nature of T-Consciousness and what it is will not be addressed in this phase. Phase-1 explores the varied effects of different TCFs. Phase-2 examines the reason behind the varied effects of these fields. Phase-3 investigates the mechanism of TCFs effects on matter and energy. Finally, Phase-4 draws significant conclusions, particularly with regard to the mind and memory of matter and their relation to the T-Consciousness, etc. [2-5]

Aluminum with the highest abundance in the earth's crust after silicon is one of the strategic metals that are the most used after steel. It has many applications in almost all industries. Any change in the position of atoms is directly related to the properties and application of this material [6]. While "Consciousness Bond Field" as a variable TCFs influences materials, it is expected that pure materials, which are not composed of different chemical compounds and alloys, still have stable behavior under the influence of TCF.

According to the theory of TCFs, T-Consciousness can be converted into matter and energy, so in re-cooling, a change in the crystalline lattice of atoms is probable. The present study examines the mentioned cases.

Methodology

Melted Aluminum made from AA1XXX series aluminum ingots was cast in nine uniform molds (Cylinders with a diameter of 3 cm and height of 1cm). Samples were arbitrarily named by those doing the experiment. Two groups of samples were under TCF, and one group of the samples was considered the control. According to Table (1), the groups under TCF were identified as X1 and X2 and the control group was identified as Control. Each group consisted of three samples coded with numbers (1 to 9). Then, to apply TCF, the names of the first and second series were, declared to the second author of this article.

Table 1 . Grouping of 9 cast aluminum samples

Group Name	X1			X2			Control		
Sample Number	1	2	3	4	5	6	7	8	9

Application of Taheri Consciousness Fields

One of the introduced TCFs is called the Consciousness Bond Field and was applied to the samples according to the protocols regulated by the COSMOintel research center (www.COSMOintel.com). A request for Connection to the CCN to utilize TCFs can be placed through the COSMOintel website in the "Assign Announcement" section. This access is available for everyone at no cost. In order to study and experience this Connection, the researchers can register on the website at any time in order to report the experiment to the COSMOintel research center. Certain details of the experiment must be provided to the center; for example, the characteristics or number and name of samples and controls must be specified. This entire experiment was carried out as a double-blind method where lab technicians were completely unaware of the TCFs.

All samples were cast from one molten pot. Samples 1, 4, and 7 samples 2, 5, and 8, and samples 3, 6, and 9 were cast simultaneously to uniformly distribute any possible error. Then, chemical analysis was performed on the samples to investigate any possibility of unwanted impurities and their effect on the properties. For this purpose, a sample from each series was randomly selected and subjected to spectrochemical analysis [7]; the results of which are given in Table (2). The result shows that the composition of the samples is in the same category and there is no difference in the composition in a way that can significantly affect the properties.

Table 2 . Chemical composition of cast samples (one random sample from each group)

One random sample of the group X1

Si	Fe	Cu	Mn	Mg	Cr	Ni	Zn	Ti	Be	Ca	Li
0.06	0.11	0.01	0.009	0.002	0.002	0.01	0.02	Trace	Trace	Trace	Trace
Pb	Sn	Sr	V	Na	Bi	Co	Zr	B	Ga	Cd	Al
0.01	< 0.005	Trace	0.008	0.005	0.01	0.02	Trace	0.0015	0.005	0.005	99.75

One random sample of the group X2

Si	Fe	Cu	Mn	Mg	Cr	Ni	Zn	Ti	Be	Ca	Li
0.06	0.11	0.02	0.009	0.002	0.004	0.01	0.02	Trace	Trace	Trace	Trace
Pb	Sn	Sr	V	Na	Bi	Co	Zr	B	Ga	Cd	Al
0.01	< 0.005	Trace	0.008	0.005	0.01	0.01	Trace	0.0022	0.004	0.004	99.75

One random sample of the control group

Si	Fe	Cu	Mn	Mg	Cr	Ni	Zn	Ti	Be	Ca	Li
0.06	0.11	0.01	0.009	Trace	0.005	0.01	0.02	Trace	Trace	Trace	Trace
Pb	Sn	Sr	V	Na	Bi	Co	Zr	B	Ga	Cd	Al
0.01	< 0.005	Trace	0.009	0.004	0.02	0.01	Trace	0.0022	0.004	0.004	99.75

Some of the main properties of aluminum metal are high electrical conductivity, softness, and ductility as well as relatively good corrosion resistance at medium pH. Therefore, these properties were compared in the control samples and those under TCF.

Brinell hardness test was performed under ASTM E10 (2018) standard [8]. A constant load of 31.25 Kg for the specified time of 10 – 15 seconds was applied using a 2.5mm diameter tungsten carbide ball. The test was performed at three points on each sample and its location was the core of the sample [8].

Also, the electrical conductivity test was performed according to ASTM E1004 (2017) [9]; and the electrical specific resistance was determined by reversing the specific conductivity. Corrosion behavior was also investigated by potentiodynamic polarization test according to ASTM G1-03 (Re.17) & ASTM G3-14 standards [9]. For this purpose, 3.5% NaCl solution, which is a common medium in corrosion tests, was used. The Ag / AgCl reference electrode and the scanning rate of 0.5 mV / S were used at ambient temperature. The samples were immersed in the solution for 60 minutes before the test. Samples 1, 4, 7, samples 2, 5, 8, and samples 3, 6, and 9 were tested simultaneously.

Crystalline structure and lattice defects of atoms investigated by X-ray diffraction (XRD). The tests were performed with a copper anode at a voltage of 30 mA and a current of 40 kV. Step size was 0.05 ° and counting time per step was 0.5 sec. Structure analysis was performed by the Rietveld refinement method using Maud software [10].

Results and discussion

Hardness test

The results of the Brinell hardness test are shown in Table (3). The hardness of each sample was determined by averaging three points. Then, using the hardness of each sample, the mean and standard deviation of the results in each series were determined (Figure 1). The average hardness in the X1 group is less than the control group but in the X2 group is slightly higher than the control group, so they are not in the same direction. On the other hand, there is a common dispersion of results in all-metal hardness tests and the difference between the obtained data is not large enough to be considered a significant change.

Table 3 . Brinell hardness test results of 9 aluminum samples

Name	Sample Code	Point 1	Point 2	Point 3	Mean	Mean of Each Series	Standard Deviation
	1	21	20	21	20.67		
Group X1 (TCF)	2	20	21	20	20.33	20.56	0.16
	3	21	20	21	20.67		
	4	23	22	23	22.67		
Group X2 (TCF)	5	21	20	21	20.67	21.67	0.82
	6	22	21	22	21.67		
	7	22	21	21	21.33		
Control Group	8	21	20	21	20.67	21.44	0.68
	9	23	22	22	22.33		

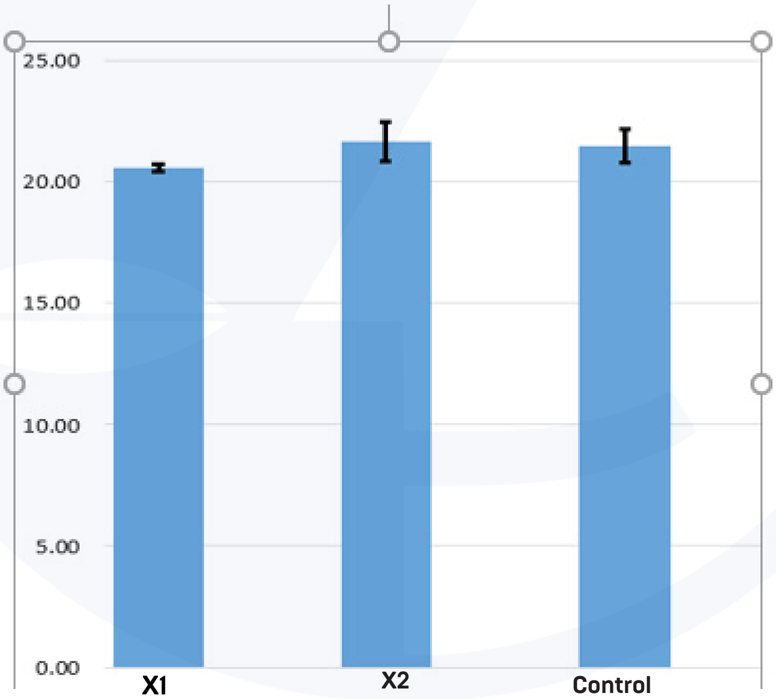

Figure 1. Mean values and standard deviation of hardness in three groups

Electrical conductivity

The results of the conductivity test and the calculation of electrical resistance are shown in Table (4). It can be seen that the results are the same for all samples, so in the measurement accuracy range, no difference in this property was observed between the samples. Unalloyed aluminum is almost exclusively used for electrical applications, and electrical conductivity is one of the properties of this aluminum series [11].

Table 4 . Results of specific resistivity test (10-8Ω m)

Name	Sample Code	Specific Resistivity (10^{-8} Ω.m)	Electrical Conductivity (10^7 S/m)	Electrical Conductivity (%IACS)
	1	2.87	3.48	60±0.5
Group X1(TCF)	2	2.87	3.48	60±0.5
	3	2.87	3.48	60±0.5
	4	2.87	3.48	60±0.5
Group X2(TCF)	5	2.87	3.48	60±0.5
	6	2.87	3.48	60±0.5
	7	2.87	3.48	60±0.5
Control Group	8	2.87	3.48	60±0.5
	9	2.87	3.48	60±0.5

Corrosion resistance

The diagrams for the nine samples are shown in (Figure 2). The formation of a small surface area has been seen in the samples which, after some fluctuations in current, disappeared and the intensity of the current increased rapidly (approximately horizontal line in the graph equivalent to critical pitting potential or Epit). After some corrosion, a layer of aluminum oxide was formed, and the graph tends to be vertical. This is a common process in aluminum corrosion testing [11].

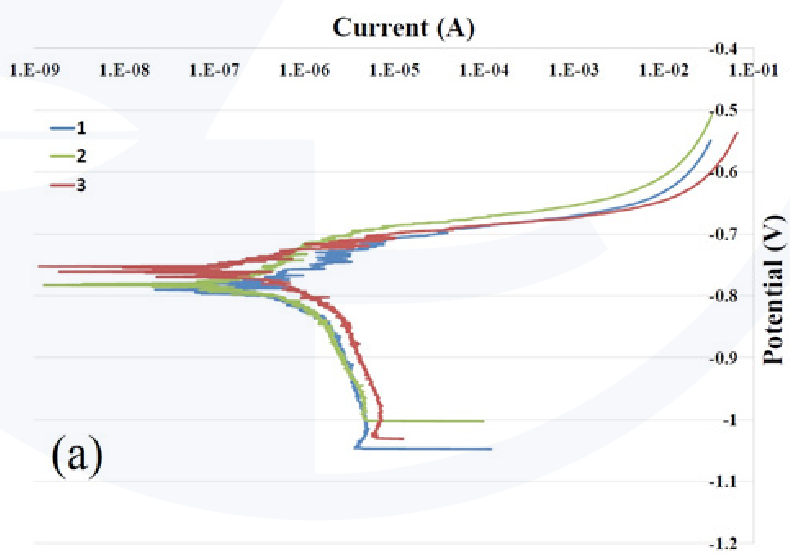

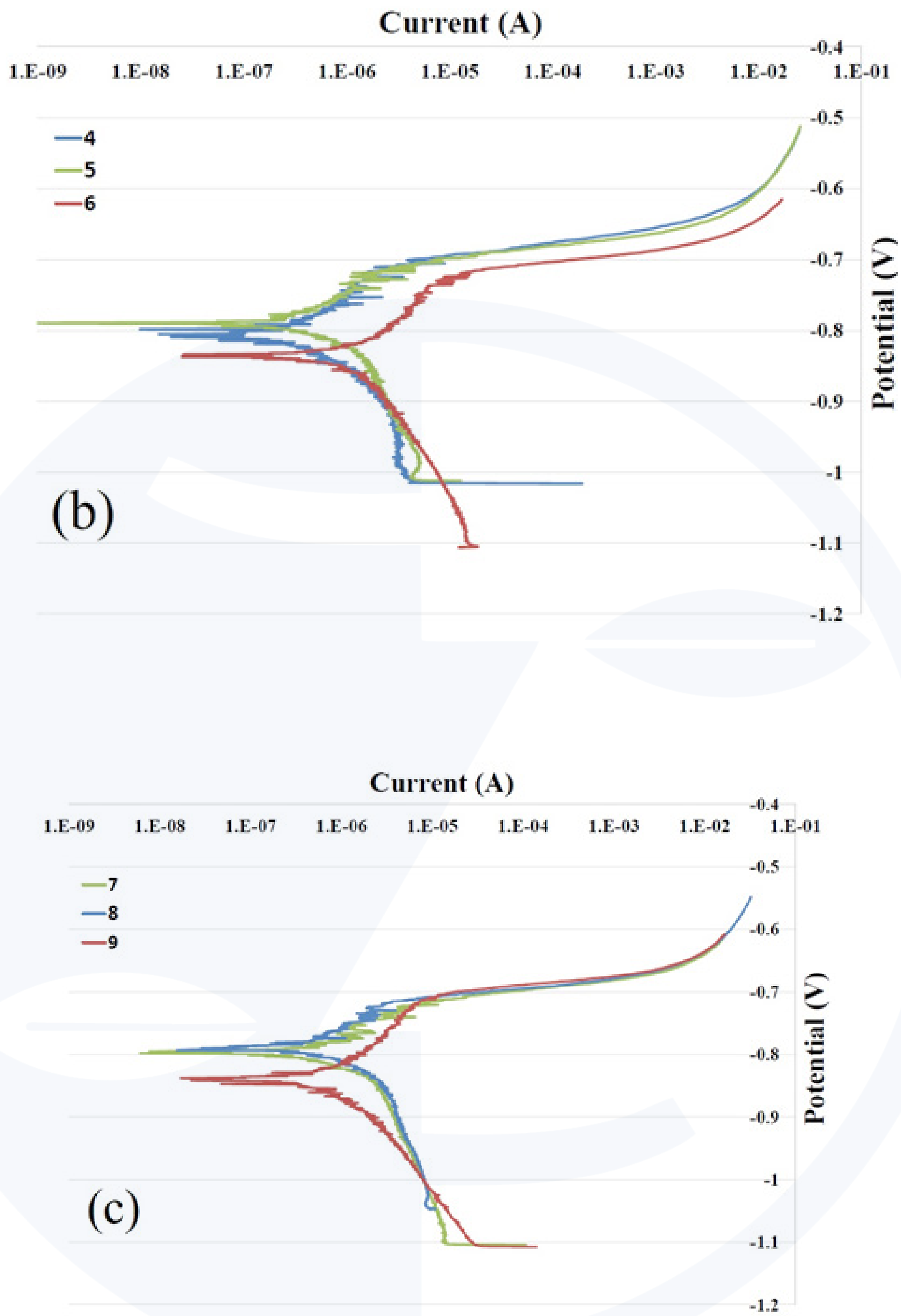

Figure 2. Potentiodynamic polarization curves for three groups of samples (a): X1, (b): X2, (C): Control

In order to compare the corrosion intensity in three groups of samples, the corrosion current intensity parameter can be used. High corrosion resistance in this test is demonstrated as low corrosion current intensity and low corrosion rate. The values extracted from the graphs are given in Table (5). Also, the mean values and standard deviation of corrosion potential (Ecorr) and the corrosion current density (icorr) for each sample are shown in

Table (6). The average intensity of corrosion current in the two groups under influence of TCF is lower than the control group, indicating better corrosion resistance. The results of the corrosion test are numerical and there is an inherent variation in the results. Therefore, it is important to check if the changes are statistically significant.

Table 5 . Results of Potentiodynamic corrosion test of 9 aluminum samples in 3.5% NaCl medium

Name	Sample Code	Corrosion Current Intensity i_{corr} (μA/cm²)	Corrosion Potential E_{corr} (mV)	Corrosion Rate mpy (mm/year)
	1	0.593	-772.52	0.253 (6.43E-3)
Group **X1 (TCF)**	2	0.337	-773.149	0.144 (3.66E-3)
	3	0.597	-826.191	0.255 (6.48E-3)
	4	0.376	-801.837	0.161 (4.08E-3)
Group X2 (TCF)	5	0.498	-784.754	0.213 (5.40E-3)
	6	0.877	-835.944	0.375 (9.5E-3)
	7	0.877	-785.809	(9.52E-3) 0.375
Control Group	8	0.597	-780.926	(6.47E-3) 0.255
	9	0.566	-843.362	(6.13E-3) 0.242

Table 6 . Average of current intensities and corrosion potentials, along with standard deviation

Name	Current Intensity Mean i_{corr} (μA/cm²)	Standard Deviation	Change from Control (%)	Potential Mean E_{corr} (mV)	Standard Deviation	Change from Control (%)
Group X1 (TCF)	0.509	0.121	-0.25%	-790.62	25.15	-1.5%
Group X2 (TCF)	0.584	0.213	-14%	-807.51	21.28	-0.5%
Control group	0.680	0.140		-803.36	28.35	

Aluminum metal is prone to various corrosions, including Pitting Corrosion [12-13], Exfoliation Corrosion [14], Stress Corrosion [15], Filiform Corrosion [16], Water Line Corrosion [11], Crevice Corrosion [17], Cavitation [11], Erosion [18], Microbiological Corrosion [19], Transgranular and Intergranular (Intercrystalline) Corrosion [20].

Each series of aluminum alloys is more prone to a certain type of corrosion. The (1000-series) aluminum used in this study is susceptible to intercrystalline corrosion. This corrosion is not visible to the naked eye and spreads at the border of grains and crystals. It is effective in changing the mechanical properties and the possibility of rupture. In water at a temperature above 60–70℃, the sensitivity to intercrystalline corrosion increases with the increasing purity of the metal.

To study this change, it is necessary to design more complete experiments to intensify the environment and more accurate equipment [20,11]. However, in the routine standard examination in this experiment, we see small changes in the corrosion process. The (1000-series) aluminum is inherently resistant to this type of (tested) corrosion.

Microstructure analysis by XRD method

In order to investigate the effect of TCF on the structure of matter in atomic dimensions, the effects of a type of TCF on the structure of aluminum were evaluated using the XRD method. Crystalline lattice information such as lattice parameter, size of crystalline areas, Lattice strain, and the possibility of some crystalline defects that can be examined by XRD analysis have specific effects on the behavior of materials [21-28].

Parameters related to the crystalline structure of aluminum samples and mean values of the three groups and their standard deviation for each group were calculated (Table 7).

Table 7 . Parameters related to the crystalline structure of aluminum samples

X1(TCF)									
	1	**Std.Dev.**	**2**	**Std.Dev.**	**3**	**Std.Dev.**	**Average**	**Std.Dev.**	**%**
Lattice Parameter	**4.0503**	5.82E-05	**4.0504**	6.31E-05	**4.0511**	3.64E-05	4.0506	3.30E-04	0.0%
crystallite size	**2764.85**	212.70	**1733.82**	85.67	**1733.18**	64.11	2077.28	4.86E+02	-13.3%
Microstrain	**3.01E-04**	1.26E-05	**2.76E-04**	1.64E-05	**4.59E-04**	1.77E-05	3.45E-04	8.11E-05	27.6%
Intrinsic	2.22E-06		1.23E-11		3.61E-06		1.94E-06	1.49E-06	23.2×10^{3}%
Extrinsic	1.19E-06		1.01E-11		5.23E-05		1.78E-05	2.44E-05	-61.1%
Twin defect	1.65E-06		2.27E-12		9.94E-06		3.86E-06	4.35E-06	47.1×10^{3}%
X2(TCF)									
	4	**Std.Dev.**	**5**	**Std.Dev.**	**6**	**Std.Dev.**	**Average**	**Std.Dev.**	**%**
Lattice Parameter	**4.0496**	7.01E-05	**4.0399**	7.29E-05	**4.0503**	4.89E-05	4.0466	4.76E-03	-0.1%
crystallite size	**1682.66**	0.72	**1648.96**	0.46	**2810.63**	201.59	2047.42	5.40E+02	-14.5%
Microstrain	2.92E-04	1.66E-05	**4.83E-04**	4.22E-06	**2.06E-04**	1.53E-05	3.27E-04	1.16E-04	20.9%
Intrinsic	8.07E-07		2.26E-05		1.49E-10		7.80E-06	1.05E-05	93.5×10^{3}%
Extrinsic	1.16E-07		1.13E-04		6.92E-07		3.79E-05	5.32E-05	-17.2%
Twin defect	3.18E-07		3.57E-06		1.80E-10		1.30E-06	1.61E-06	15.7×10^{3}%
Control									
	7	**Std.Dev.**	**8**	**Std.Dev.**	**9**	**Std.Dev.**	**Average**	**Std.Dev.**	
Lattice Parameter	**4.0503**	4.73E-05	**4.0497**	6.48E-05	**4.0500**	5.79E-05	4.0500	2.40E-04	
crystallite size	**2810.79**	189.98	**2124.27**	68.98	**2251.82**	155.36	2395.63	2.98E+02	
Microstrain	**3.06E-04**	1.10E-05	**4.06E-04**	1.32E-05	**9.97E-05**	3.39E-05	2.71E-04	1.28E-04	
Intrinsic	2.46E-08		3.91E-10		1.02E-12		8.33E-09	1.15E-08	
Extrinsic	3.38E-08		1.32E-04		5.43E-06		4.58E-05	6.10E-05	
Twin defect	2.42E-08		3.36E-10		4.96E-13		8.18E-09	1.13E-08	

Discussion and review of changes for XRD

Lattice parameter

The lattice parameter refers to the physical dimension of the unit cell in a crystalline lattice. If the ratio is smaller, it means that the lattice is more compact, and if it is larger, it means that the lattice is more expanded [21-28]. No significant changes were observed in this parameter for the samples.

Lattice strain (Microstrain)

Lattice strain is the difference between crystalline lattice sizes that led to the formation of lattice strain [21-28]. An average of approximately (~ 20%) increase in lattice strain was observed in the samples under TCF.

Crystallite size

This factor is partly representative of the crystalline cells that must be created without strain or defect [21-28]. The size of crystalline areas decreased in TCF cases, except for one case (sample number 6), this reduction was up about (~ 13%) on average.

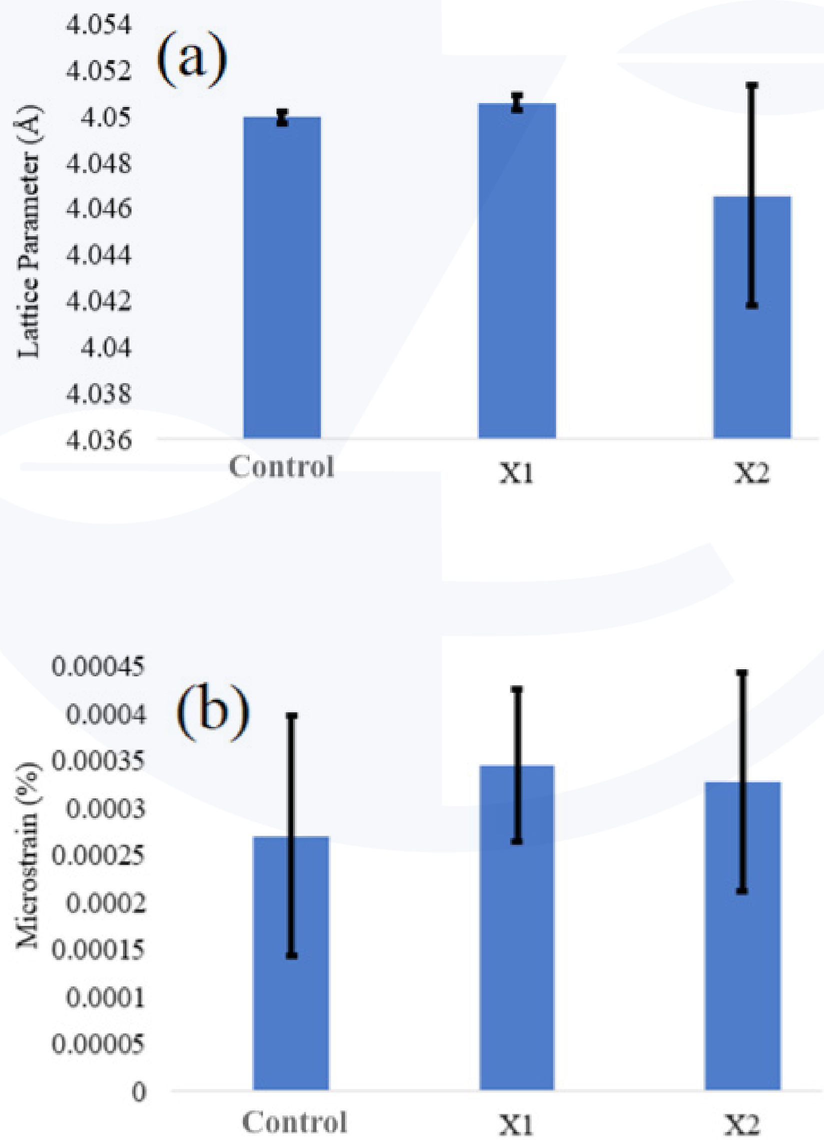

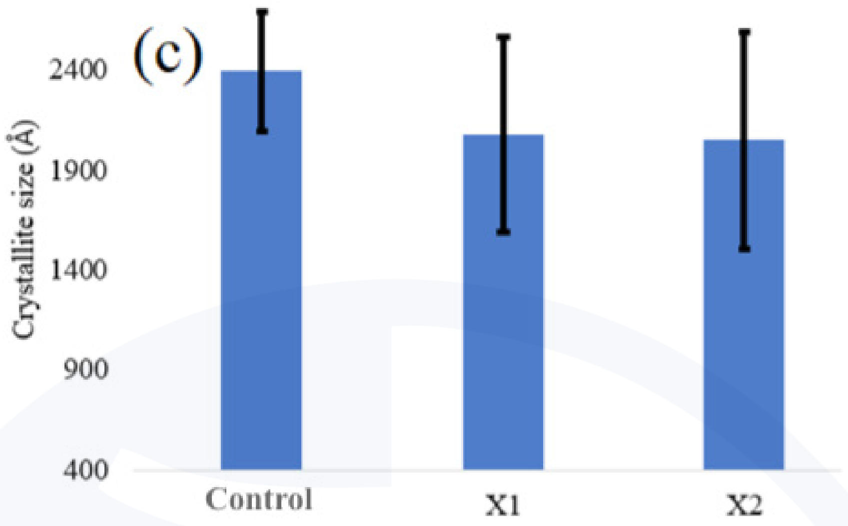

Figure 3. Mean and standard deviation calculated for (a) lattice parameter (b) lattice strain (c) crystal area size.

Intrinsic defects

As in TCF groups, this defect is occurring with a difference of about average (~ 58×10^3%).

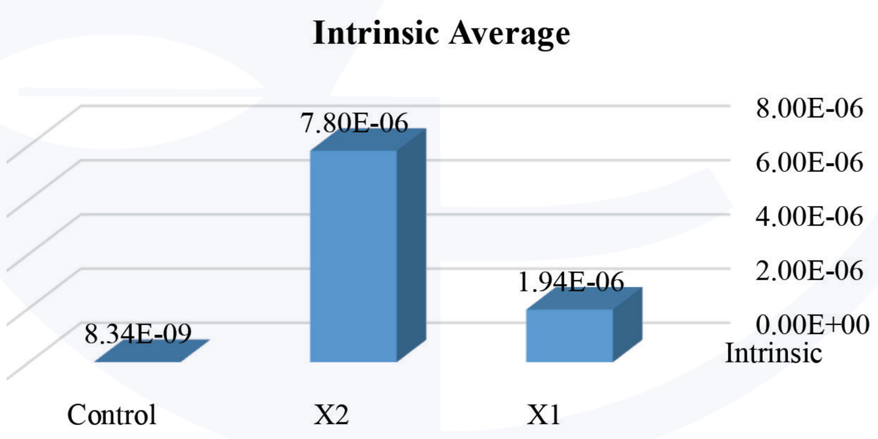

Figure 4. The average of Intrinsic defects

Extrinsic Defects

This disorder has decreased under TCF by an average of (~ 39%).

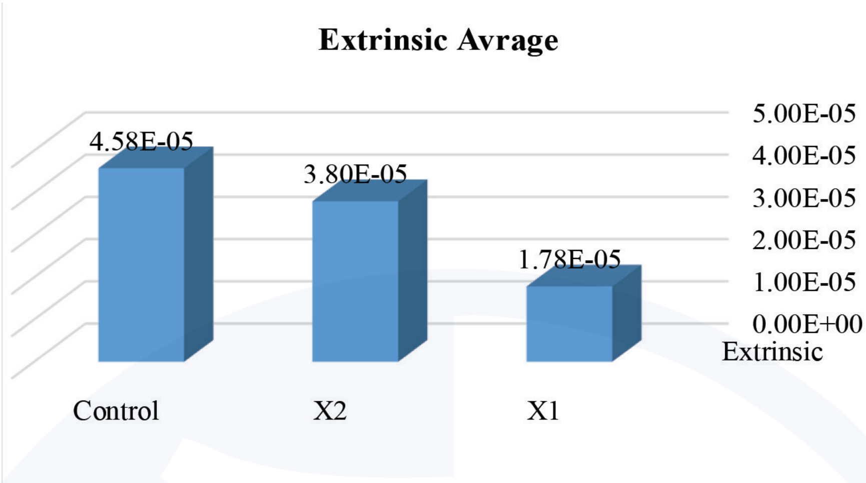

Figure 5. The average of extrinsic defects

Twin Defects

Twin defects represent a special type of boundary that is created by the symmetry of the crystalline lattice mirrors.

Twin boundary increases the strength of the material, causes plastic deformation in materials with BCC and HCP structure, has higher energy than the intragranular and is suitable for chemical interaction [21-28].

Except for one case under the CF, in most samples as well as in the average data, this factor shows a significant increase of about (~30×10^3%).

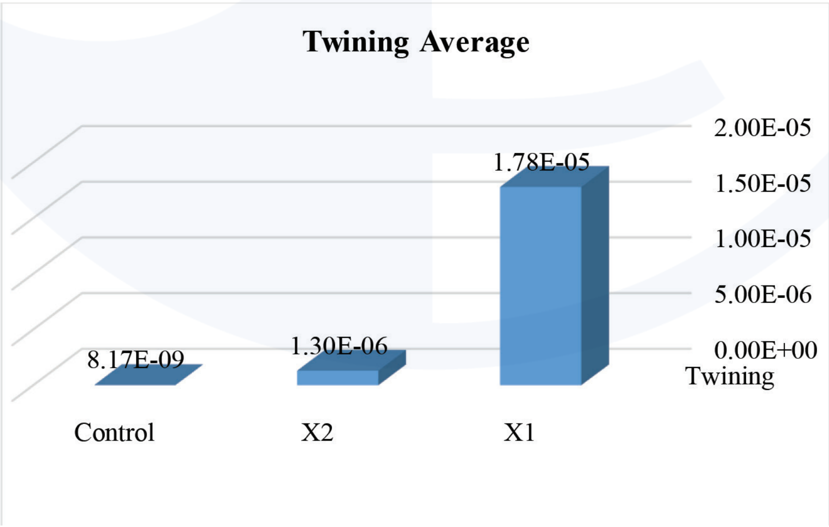

Figure 6. The average of extrinsic defects

Conclusion

- In X-ray diffraction analysis (XRD), the average mean lattice strain (lattice disorder) was higher (~ 20% on average - Table 7) in both X1 and X2 groups than in the control group.
- In contrast, the average crystallite sizes in both groups were less than the control group, which was consistent with lattice strain change (~ 13% on average - Table 7).
- There were some differences in the lattice parameter.
- Extrinsic defects in X1 and X2 groups decreased (~ 39%) on average compared to the control group (Table7)
- Intrinsic and Twin defects in X1 and X2 groups increased (~ 103 %) on average compared to the control group (Table7).

In general, a crystalline defect is a disorder of the atoms and ions' order in a part of the crystalline lattice of matter. Manufacturing processes, such as mechanical work and metal deformation, can increase lattice defects and strain. Entering alloy elements can also affect atomic distances and lattice parameters [29-30].

Being one-element, similarities in composition and impurities in the samples and no difference in how they are processed, make the factor of Consciousness Bond Field to be recognized as the possible cause for these changes. Also, in pure aluminum (1000-series), electrical conductivity, ductility, and corrosion resistance are among the inherent properties [11].

Since pure aluminum (99.75%) purity, according to spectrochemical analysis after casting) is used in this research and according to the principles of T-Consciousness and T-Consciousness Fields, the pure elements of the Mendeleev table are included in the category of fixed T-Consciousness Fields, the pure aluminium is not influenced by the variable T-Consciousness Fields, which is Consciousness Bond Field in this study. In other words, participation in reaction by pure aluminium due to the influence of this Field is not expected, and some of the principal factors of this metal remain in a stable state.

The structure of crystal lattice is related to the collection of atoms and the above experiment shows that the variable T-Consciousness Field of Consciousness Bond Field influences the collective properties and not the individual properties (variable T-Consciousness Field). It should be noted that the effect of variable T-Consciousness Fields such as Consciousness Bond Field on materials with chemical compounds is to change the reactions [4]. But in the case of pure materials from the point of view of the matter, changes in the principal factors are not expected. However, the same material is a collection of millions of atoms, and in terms of atomic structure, changes in the collection of atoms are possible. Therefore:

Unalloyed aluminum under Consciousness Bond Field was more disordered in terms of crystalline lattice structure and no significant changes were observed in the properties.

Determining the physical and microstructural mechanisms that have occurred to alter properties under the TCF requires more specialized studies using more equipment. But preliminary results show that TCF as a factor independent of matter and energy and even information could have measurable effects on matter.

References

1- Lefebvre V.A, Efremov Y.N, Cosmic intelligence and black holes*World Futures,* 64(8) (2008) 563-576.

2- Taheri, M. A*Human from another outlook.* Interuniversal Press; 2nd Edition ISBN-13: 978-1939507006, ISBN- 10: 1939507006. (2013)

3- Taheri MA*General Connection of particles.* Interuniversal Publishing. Erfan-Halgheh. ID: 978-1-940491-03-5. (2012)

4- Kazazi. B, Taheri. M. A; Meshkin-Far. A, Influence of the Consciousness Field on the Cement Properties and Behavior", Science of Consciousness, Tucson, Arizona, (2020)

5- www.cosmointel.com

6- Nowtash. M.R, World and aluminum and Iran, stand in the perspective horizon of Islamic Republic of Iran1404/ Technology *Development Quarterly Journal* (2005).

7- Busch. K.W, Bush. M. A, Multielement Defection Systems for Spectrochemical Analysi(1990) ISBN 0-47-81974-3

8- ASTM E10-14: Standard method for Brinell hardness of metallic materials". www.ASTM.org

9- www.ASTM.org , ASTM E1004

10- Lutterotti. L , Total pattern fitting for the combined size–strain–stress–texture determination in thin-film diffraction Nucl. Instrum. Methods Phys.(2010). Res, Sect. B 268 334–40

11- Vargel.Ch, CORROSION OF ALUMINIUM, Elsevier (2004), ISBN 008044495-4 ,p 28-150

12- Kaesche H., Me´canisme de la corrosion par piqu^res, Corrosion Traitements Protection Finition, vol. 17 (1969), p. 389–396.

13- Reboul M., Warner T., Mayet H., Baroux B., A ten step mechanism for the pittingcorrosion of aluminium alloys, Corrosion Reviews, vol. 15, nos 3–4 (1997), p. 471–496.

14- Ketcham S.J., Shaffer I.S., Exfoliation corrosion of aluminum alloys, ASTM, STP, vol. 516, (1972), p. 3–16.

15- Rawdon H.R., Krynitski A.I., Berliner J.F., Brittleness developed in aluminium and duralumin by stress and corrosion, Chemical Metallurgy Engineering, vol. 26 (1922), p. 154–160.

16- Rique J.P., La corrosion filiforme dans les peintures pour l'ae´ronautique, Surfaces, vol. 117, (1984), p. 55–66.

17- Reboul M.,Touche M., Examen de deux radeaux en aluminium apre`s 8 et 35 ans en mer,rapport Pechiney CRV, (1983).

18- Dillon R.L., Hope R.S., Erosion–corrosion of aluminum alloys, REV, rapport HW-74359,April (1953).

19- Hedrick H.G., Crum M.G., Reynolds R.J., Culver S.C., Mechanism of microbiological corrosion of aluminum alloys, *Electrochemical Technology* (1967), p. 75–77.

20. Rohrmann F., Transactions of the Electrochemical Society, vol. 66, (1934), p. 229.

21- Snyder.R.L., Fiala.J., Bunge.H.J., Defect and Microstructure Analysis by Diffraction, Oxford Science Publication ISBN.0198501897(Hbk)

22- Scardi.P., Ermrich.M., Fitch.A., Wen Huang.E., Jardin.R., Kuzel.R., Leineweber.A., Mendoza Cuevas.A., Misture.S.T., Rebuffi.L., Schimp.CH., Size - strain separation in diffraction line profile https://doi.org/10.1107/S1600576718005411(2018)

23- Soleimanian.V.,Mojtahedi.M.,AcomparisonbetweendifferentX-raydiffractionlinebroadeninganalysismethodsfornanocrystallineball-milled FCC powders, (2015) DOI 10.1007/s00339-015-9054-y

24- Zheng. Yu. Jie., Ying Quek .Su., First Principles Study of Intrinsic and Extrinsic Point Defects in Monolayer WSe2 , (2019) , arXiv:1901.05238

25- Warren.B.E., X-RAY STUDIES OF DEFORMED METALS (1959)- Review of a research programme sponsored by the U.S. Atomic Energy Oommi~sion.

26- Feret. F.R, Selected applications of Rietveld analysis in the aluminium industry. *International Tables for Crystallography* (2019). Vol. H, ch. 7.6, doi:10 .1107/97809553602060000980

27- Huang.Y.,LangdonT.G.,"Usingatomicforcemicroscopytoevaluatethedevelopmentofmesoscopicshearplanesinmaterialsprocessedby severe plasticdeformation*MaterialsScienceandEngineering,Vo*l.A358,(2003).

28- WWW.EDU.nano.ir

29- Jafaril.M, Jamshidian.M, Ziaei-Rad.S, Investigating the Stored Deformation Energy Distribution in a Polycrystalline Metal using a Dislocation Densi-ty-based Crystal ViscoplasticityTheory/ Computational Methods in Engineering, Isfahan University of Technology (IUT)/ DOI: 20.1001.1.22287698.1397.37.2.5.1/ (2019)

30- Humphreys. M., Hatherly. F., Recrystallization and Related Annealing Phenomena, Second Edition.*Elsevier,* (2002), ISBN:0080426859

Influence of Taheri Consciousness Bond Field on the Crystallization and Strength of Cement Mortar (Concrete)

Bahareh Kazazi[1*], Mohammad Ali Taheri[2]

1. Civil Engineering, CEO of Hoobe Construction Company, Tehran, Iran.

2. Sciencefact R&D Department, Cosmointel Inc. Research Center, Ontario, Canada.

ABSTRACT

In this study, the behavior of cement mortar was investigated under the Consciousness Bond Field. Taheri Consciousness Fields (TCFs) were founded and introduced by Mohammad Ali Taheri as new Fields more than four decades ago. These Fields are neither material nor energetic. Therefore, they do not have quantity, but they have direct effects on both matter and energy. In other words, although TCFs cannot be directly measured, we can investigate their effects indirectly through various reproducible experiments. In all tests of this research, type II cement and standard sand were used. The samples preparation and their strength measurement were done under the ISIR 393 standard, and each group included 3 prism samples. Three series of experiments were performed with a number of different groups, in each series one group was as control and the others were the study samples under the effect of Consciousness Bond Field. Series 1 included five groups of cement sand mortar. Compres-sive and flexural strengths were measured at 7, 28, and 42 days of age. Series 2 included four groups of cement sand mortar which were measured at 7, 28, and 42 days of age. Series 3 included four groups of cement sand mortar made exactly according to the above-said condition. And strength was measured at 7, 28, 42, and 90 days of age. Due to the results received from FT-IR (Fourier-transform infrared spectros-copy), SEM (Scanning electron microscopy), XRF (X-Ray Fluorescence), and XRD (X-ray Diffraction), the growth trend of the strength of the samples under the Consciousness Bond Field were more significant than the control samples. The results of other analyzes showed that the abundance of chemical compounds containing calcium ($CaCO_3$ from 20 to 80% and Ca_3SiO_5 from 25 to 75%) in the samples under the Consciousness Bond Field at 90 days was higher than the control. While silicon-containing compounds were higher in control samples at the same age. Sodium (Na), Potassium (K), and Phosphorus (P) were reduced by approximately (an average of 30%) in samples under Con-sciousness Bond Field at 90 days, while the abundance of Aluminum and Calcium was increased (about 7% on average). Differences in the appearance and chemical composition of the crystals, including the amount of ettringite formation in the samples under the Consciousness Bond Field, were observable in SEM imaging.

* Corresponding author:

Bahareh Kazazi
Civil Engineering, CEO of Hoobe Con-struction Company, Tehran, Iran.

Email: baharkazazi@gmail.com

Keywords: Cement-sand mortar, Consciousness Bond Field, Taheri Consciousness Fields, Strength of cement

INTRODUCTION

Cement was invented in 1824 and no material has been able to replace it yet [1]. The combination of aggregate cement and water as concrete is one of the most widely used materials in the world, and more than 4 million tons of cement is produced annually in the world [2]. Due to the dependence of industry on the properties of this material, various methods are offered to increase its efficiency. It should be noted that the first performance of this material is hardening which is out of chemical reactions. Because of the importance of cement, the study of its changes trend under the Consciousness Bond Field was the subject of this study. Consciousness Bond Field is expected to increase chemical reactions of the composites and improve their behavior in direction of their fundamental character (According to the Theory of General Connection of Particles introduced by Taheri) [3].

To get acquainted with the theoretical foundations of T-Consciousness Fields, it is worth mentioning that The nature of consciousness and its place in science has received much attention in the current century. Many philosophical and scientific theories have been proposed in this area. In the1980s, Mohammad Ali Taheri introduced novel fields with a non-material/non-energetic nature named Taheri Consciousness Fields (TCFs). In this perspective, T-Consciousness is one of the three existing elements of the universe apart from matter and energy. According to this theory, there are various TCFs with different functions, which are the subcategories of a networked universal internet called the Cosmic Consciousness Network (CCN). The major difference between the theory of TCFs and other theoretical concepts about consciousness is related to the practical application of the TCFs. TCFs can be applied to all living and non-living creatures, including plants, animals, microorganisms, materials, etc.

Mohammad Ali Taheri, the founder of Erfan Keyhani Halqeh, a school of thought, introduced a new science in 2020 as a branch of this school. He coined the term Sciencefact for this new science because it utilizes scientific investigations to prove the existence of T-Consciousness as an irrefutable phenomenon and a fact. Although science focuses solely on the study of matter and energy and Sciencefact, by contrast, explores the effects of the [non-material/non-energetic] TCFs, Sciencefact has provided a common ground between the two by conducting reproducible laboratory experiments in various scientific fields, and it has used the scientific approach in proving TCFs.

The influence of the TCFs begins with the Connection between CCN as the Whole Taheri Consciousness of the universe and the subjects of study as a part. This Connection called “Ettesal” is established by a certified and trained individual who has been entrusted with the TCFs. The human mind has an intermediary role (Announcer) which plays a part by fleeting attention to the subject of study and then the main achievement obtained as a result of the effects of the TCFs. These Fields cannot be directly measured by science, but it is possible to investigate their effects on various subjects through reproducible laboratory experiments.

The research methodology in the study of T-Consciousness has been founded on the process of Assumption, Argument, and Proof, in which the basic Assumption is: The Cosmos was formed by a third element called T-Consciousness that is different from matter and energy.

The Argument: The existence of TCFs can be demonstrated by its effects on matter and energy (e.g., humans, animals, plants, microorganisms, cells, materials, etc.)

The Proof: is the scientific verification of the effects of TCFs on matter and energy (according to the Argument) through various reproducible scientific experiments.

Accordingly, to investigate and verify the existence, effects, and mechanisms of TCFs, the following five research phases (Phases 0 through 4), and the aims of each phase are outlined below.

Phase-0 studies aim to prove the existence of TCFs by observing their effects. The nature of T-Consciousness and what it is will not be addressed in this phase. Phase-1 explores the varied effects of different TCFs. Phase-2 examines the reason behind the varied effects of these fields. Phase-3 investigates the mechanism of TCFs effects on matter and energy. Finally, Phase-4 draws significant conclusions, particularly with regard to the mind and memory of matter and their relation to the T-Consciousness, etc. [4-6]

Materials and methods

Preparation of cement mortar and evaluation of increase in their strength in all tests were based on ISIR 393 [7]. In all samples, standard sand and type II cement were used. And all of them made samples were kept in exactly the same environmental conditions from the beginning to the strength measurement.

According to the above standard, the method of measuring flexural and compressive strength was determined with prism samples with dimensions of 160 × 40 × 40 mm. These samples were molded using a paste mixture consisting of one weight unit of standard sand and one-half weight unit of water (water to cement ratio 0.05). To determine the flexural strength, a three-point loading device was used in which the prism sample was inserted into the machine from the side that was in contact with the mold, and then the load was applied to the opposite sides of the prism by a high roller at a speed of 50 ± 10 N /S until the sample was broken. The two prism samples were then covered with a damp cloth until the compressive strength test was performed.

Flexural strength R_f was calculated according to the following equation:

$$R_f = b^3 / L \times F_f \times 1.5$$

where R_f: Flexural strength in Mpa

b: Dimensions of the square section of the prism in millimeters

Ff: The load applied to the prism at the time of failure in N

L: The distance from the center to the center of the rollers or loading openings in millimeters.

For measuring the compressive strength, the test was performed on half of the flexural strength samples. Each sample was placed inside the machine and the load was gently applied to the sample at a speed of 2400 ± 20 N/S until the sample was broken.

Compressive strength in Mpa was calculated from the following equation:

$$R_C = F_C / 1600$$

where

R_C: Compressive strength in Mpa

F_c: Maximum load during failure in Newton and

1600: The surface of the loading jaw or the surface of the auxiliary plates (40 × 40 mm) in square millimeters.

The results of the flexural strength test were calculated according to the numerical mean of three unique results and each test was reported with an approximation of 0.1 Mpa and the numerical average of the results of the three tests was reported with an approximation of 0.1 Mpa.

group was calculated for the compressive strength. Each result was presented with an approximation of 0.1 Mpa and was obtained by performing six compressive strength tests on three broken prisms. If each of the six results alone was more than 10% different from the average, it was removed and the average of the remaining five samples was presented. And if one of the results of the five samples differed by more than 10% from the numerical average, all results were deleted, and no result was provided for that group [7].

Naming the samples

Before preparing the samples, each group of molds was named randomly and by meaning-less names by the laboratory manager. One group was considered as the control and the rest as experimental. The names were declared to the administrator of establishing TCF.

Application of Taheri Consciousness Fields

One of the introduced TCFs is called the Consciousness Bond Field and was applied to the samples according to the protocols regulated by the COSMOintel research center (www.COSMOintel.com). A request for Connection to the CCN to utilize TCFs can be placed through the COSMOintel website in the "Assign An-nouncement" section. This access is availa ble for everyone at no cost. In order to study and experience this Connection, the researchers can register on the website at any time in order to report the experiment to the COSMOintel research center. Certain details of the experiment must be provided to the center; for example, the characteristics or number and name of samples and controls must be specified. This entire experiment was carried out as a double-blind method where lab technicians were completely unaware of the TCFs.

Flexural and compressive strength measurement test - Series 1

Five groups of cement sand mortar were prepared according to the mentioned standard and conditions, each group consisted of three samples. They were all kept in exactly the same physical and environmental conditions such as temperature, humidity, and pressure. Then compressive and flexural strengths were measured at the ages of 7, 28, and 42 days.

Flexural and compressive strength measurement test - Series 2

Four groups of cement mortar were prepared according to the above-mentioned standard and conditions, each group containing three samples. The strength was measured at the ages of 7, 28, and 42 days.

Flexural and compressive strength measurement test – Series 3

Four groups of cement-sand mortar, each group consisting of three samples, were made exactly in accordance with the mentioned conditions. Their strengths were measured at the ages of 7, 28, 42 and 90 days. FT-IR (Fourier-transform infrared spectros-copy) was analyzed at the ages of 28, 42, and 90 days. And SEM (Scanning electron micros-c opy), XRF (X-Ray Fluorescence), and XRD (X-ray Diffraction), analyses were conducted at the age of 90 days.

Results and discussion

Strength measurement of all samples

Table 1 . The measured flexural and compressive strengths.

	Name	Flexural strength (Mpa)				Compressive strength (Mpa)			
		Age-day				Age-day			
		7	28	42	90	7	28	42	90
series 1	B-control	*	7.3	7.1		29.5	46.9	42.9	
	A	6.1	7.5	7.7		34.8	51.2	47.2	
	F	6.1	7	7.1		32	45.8	46.6	
	a	5.5	7.2	7.6		29.1	38.8	48.6	
	b	5.6	7	7.7		29.3	44.3	56	
Series 2	SH-control	6.1	9.05	10.8		31.7	45.6	48.8	
	A1	6	8.1	10.7		31	45.1	52	
	B1	6.1	*	10.8		30.2	44.5	51.5	
	C1	*	*	10.7		29.3	44.4	49.5	
series 3	Sh-control	7.5	8.1	8.2	8.6	32.5	41.4	42.8	45.9
	a1	7.3	8.6	8.3	8.8	31.4	42.1	41.8	48.1
	b1	7	8.2	8.3	8.7	30.8	41.7	44.3	47.8
	c1	7.5	8.1	7.7	7.9	31.8	44.7	44	46.4

Table 2 . Percentage of change in compressive and flexural strengths compared to the 7-day-old age of the samples in their own group.

	Name	Percentage change of flexural strength				Percentage change in compressive strength			
		Age-day				Age-day			
		7	28	42	90	7	28	42	90
series1	B-Control	*	7.30%	7.10%		*	59%	45.40%	
	A	*	23%	26.20%		*	47.10%	35.60%	
	F	*	14.75%	16.40%		*	43.10%	45.60%	
	a	*	31%	38.20%		*	33.33%	67%	
	b	*	26.80%	37.50%		*	51.20%	91.10%	
series 2	SH-Control	*	48.30%	77%		*	43.80%	53.90%	
	A1	*	35%	78%		*	45.50%	67.70%	
	B1	*	*	77%		*	47.40%	70.52%	
	C1	*	*	*		*	51.50%	69%	
series 3	Sh-Control	*	8%	9.30%	14.665	*	27.40%	31.70%	41.23%
	a1	*	17.80%	13.70%	20.50%	*	34.10%	33.12%	53.18%
	b1	*	17.14%	8.57%	24.30%	*	35.40%	43.80%	55.20%
	c1	*	8%	3%	5.30%	*	40.56%	38.36%	46%

Considering the way of presenting the results based on the used standard, some samples have been removed at the discretion of the test technician and taking the test error into account. As shown in the tables, in the samples of Series 1, the increase in strength started from the first measurement at the age of 7 days. While the samples of other Series showed a decrease in strength at the age of 7 days in subsequent measurements the growth rate of strength increased compared to the age of 7 days.

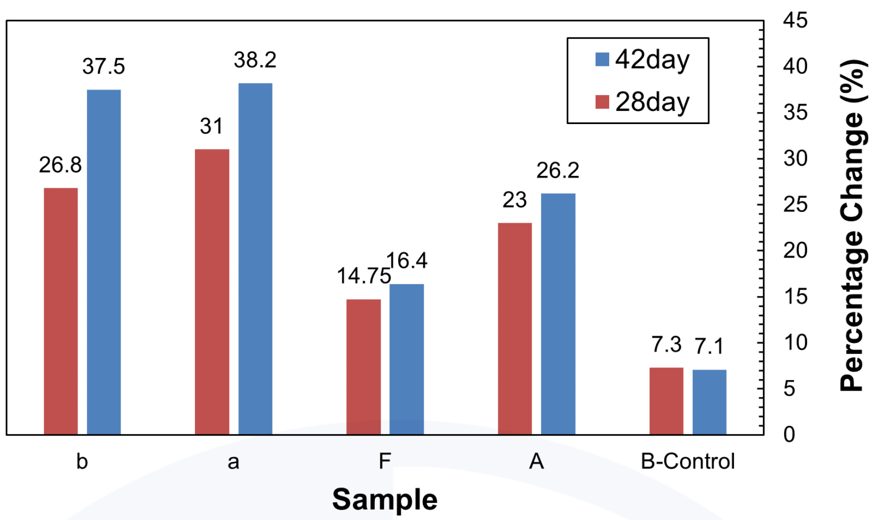

Figure 1- Percentage of flexural strength growth in Series 1 compared to seven-day age in its own group

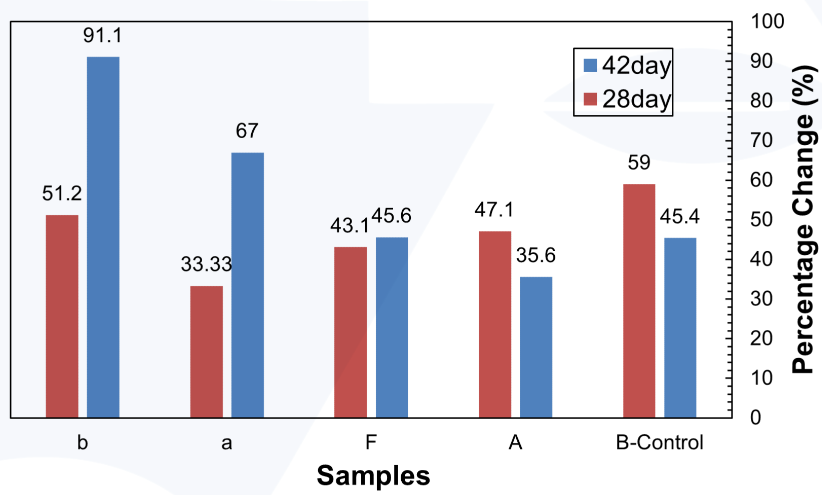

Figure 2- Percentage of compressive strength growth in Series 1 compared to seven-day age in its own group

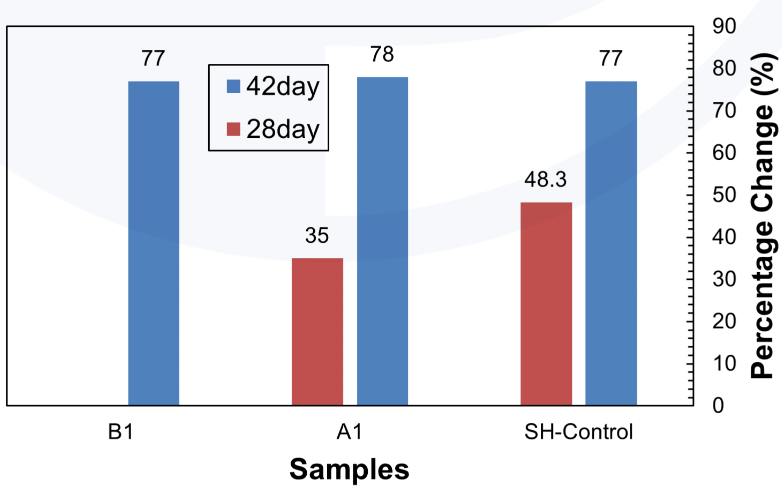

Figure 3- Percentage of flexural strength growth in Series 2 compared to seven-day age in its own group

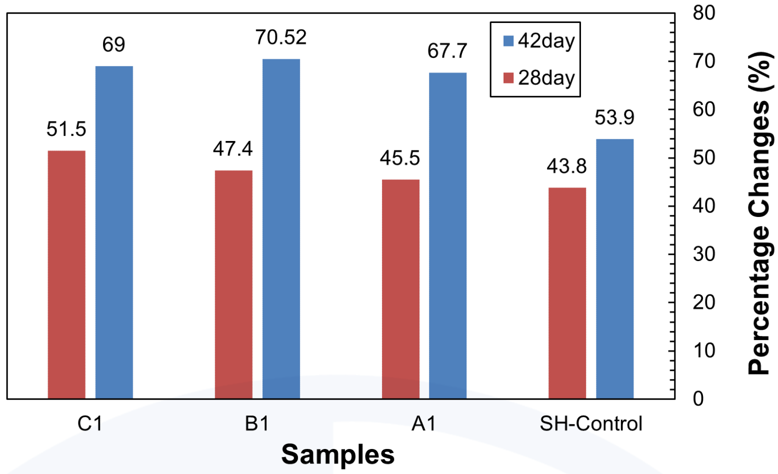

Figure 4- Percentage of compressive strength growth in Series 2 compared to seven-day age in its own group

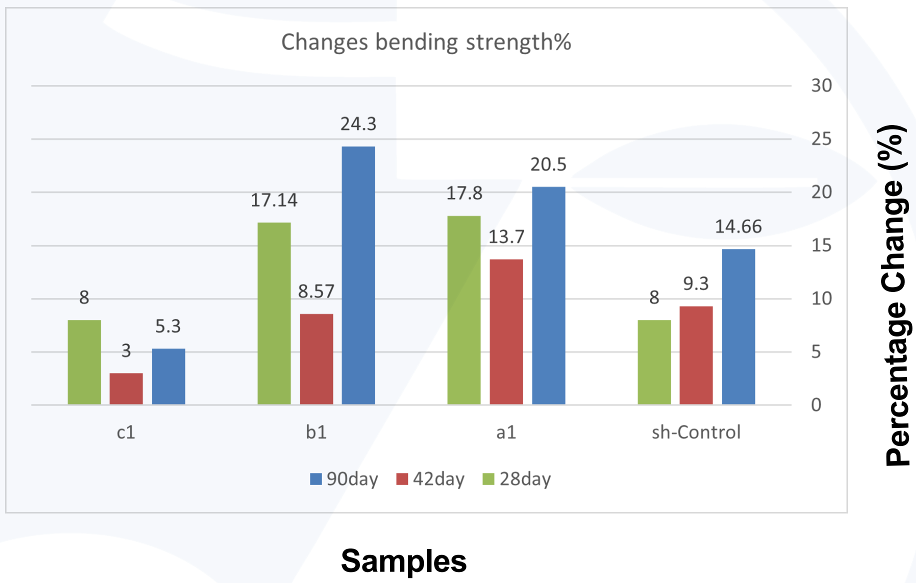

Figure 5- Percentage of flexural strength growth in Series 3 compared to seven-day age in its own group

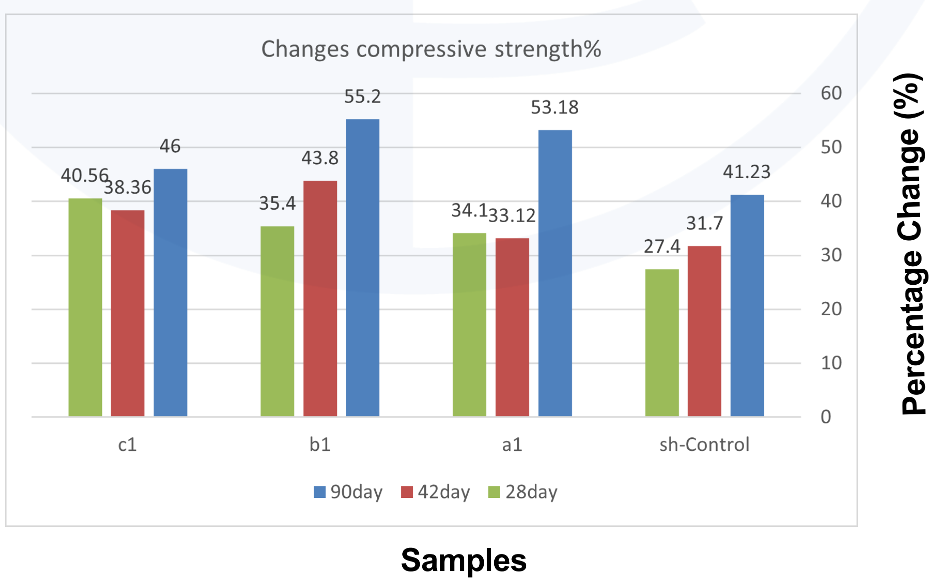

Figure 6- Percentage of compressive strength growth in Series 3 compared to the seven-day age in its own group

As seen, in most samples under TCF, the growth rate of strength over time compared to the age of 7 days was more than the control samples. This phenomenon indicates changes in the structure of chemical compounds. Also, in recent years, due to the environmental pollution caused by cement, the use of cement with new and green chemical compounds has flourished to replace Portland cement in the industry [8], which the growth pattern of their strength is different from the known Portland cement used in this study. For example, Lc3-50 cement, which is going to be replaced by Portland cement in the industry [8], shows a decrease in strength in the first days and then in the ages of 28 to 42 days shows more strong growth and again in 90 days shows a decrease in strength compared to Portland cement [8-9]. The TCF may have intelligent-ly altered the behavior of the cement.

FT-IR analysis of the samples - Series 3

To investigate the chemical structure of cement mortar, FT-IR test was used, and the results are shown in the figure 7. Also, to compare the results better, the magnified image of these spectra in the range of 400 cm-^{1} to 1800 cm-1 is shown.

In all graphs, the control samples are demarked as "Sh".

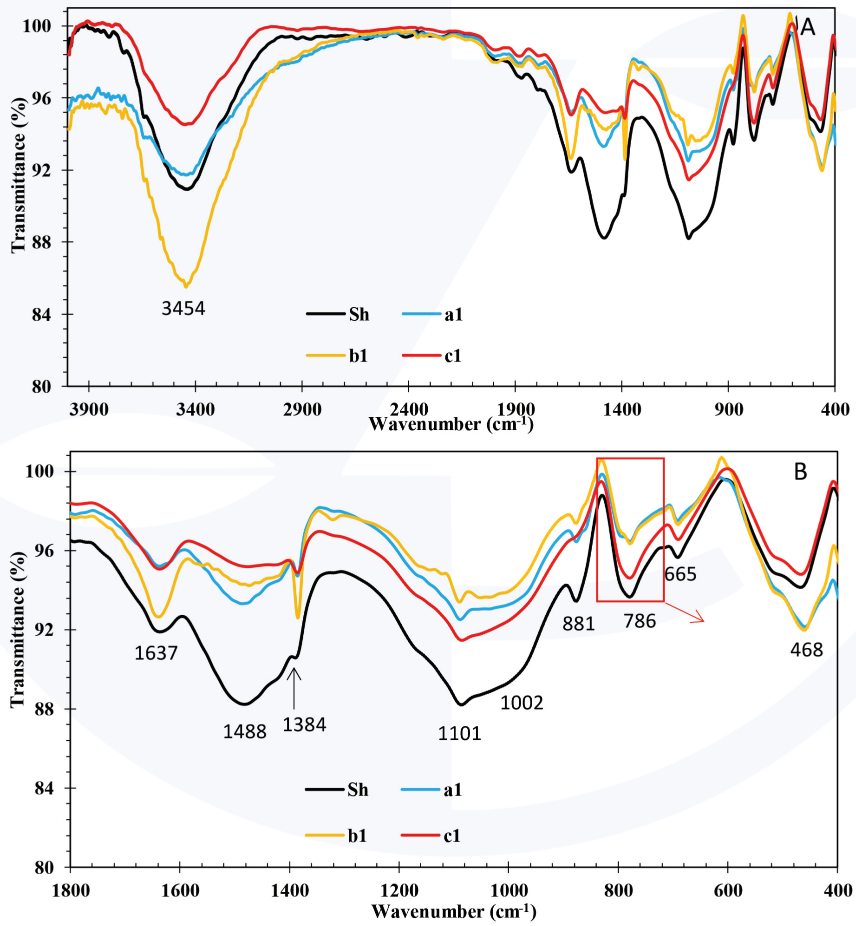

Figure 7- FTIR test results related to 28-day cement mortar sample. (A) the whole spectrum and (B) the range of 400 cm^{-1} to 1800 cm^{-1} (Sh is the Control)

In the spectra shown in Figure 7, in the studied samples, the peaks at wavelengths of about 3450 cm-1 and 1637cm-1 are related to the tensile and flexural vibrations of O-H bonds in adsorbed water molecules, respectively [10, 11]. Also, in these samples, the tensile vibrations of the bonds in the carbonate group have shown the structure of calcium carbonate in the cement at a wave number of 1488 cm-1 absorption peak [12]. In addition, at the wavenumber 1384cm-1 the absorption peak related to the tensile vibrations of Si-O bonds in the anion units of SiO_4^{4-} can be seen [13]. The peaks at the wave numbers 1101 cm-1and 1002 cm-1 are related to the tensile vibration of Si-O-Si and Si-O-Al bonds in cement compounds, respectively [14]. In addition, at wave number 881 cm^{-1} the absorption peak is relat-ed to the tensile vibrations of the existing C-O bonds of calcite [15]. Comparing the peaks of calcium carbonate and silica peaks, it is clear that the control sample has more calcite and silica than the other samples.

The two peaks positioned at the wave numbers 665 cm^{-1} and 468 cm^{-1} are related to the flexural vibration of Si-O bonds in different compounds [13-16]. Also, as mentioned, the peak positioned at the wave number of 786 cm^{-1} is observed in the samples containing high amounts of alkali [13]. By comparing the peak intensity in this wave number, it is clear that samples a1 and b1 had the lowest, and control samples had the highest amount of alkali in the structure.

Another parameter introduced by Berra et al. is the Coefficient of Structural Disorder [17]. This coefficient is proposed to evaluate the sensitivity to alkaline reaction in cement before use and hydration. According to this coefficient, if the value of this parameter is less than 120, it means that the sample is inactive, if, between 120 and 200, it means the sample has little activity, if, between 200 and 300, it means it is highly active, and if more than 300, it means the sample has pozzolanic activity [17]. Since the used cement is type II and although it is inactive, the study of this factor during the reaction, which can indirectly represent CaOH2 or other alkaline compounds, can be useful. According to this theory, the value of this coefficient is obtained from Equation (1). [17]

$$C_d^{\,1} = \Delta v / A'_b \quad (1)$$

In this equation, Cd is the coefficient of structural disorder and Δv is the peak width positioned at the wave number 796 cm-1and the value of A'b is extracted from Equation (2).

$$A'_b = \log\left[(P+Z)/Z\right] \quad (2)$$

In this equation, P is the minimum peak point positioned at 796 cm^{-1} and Z is the difference between the minimum peak positioned at wave numbers 796 cm^{-1} and 1100 cm^{-1}. The value obtained for this coefficient is shown in the form of bar graphs in Figure 8 for better comparison.

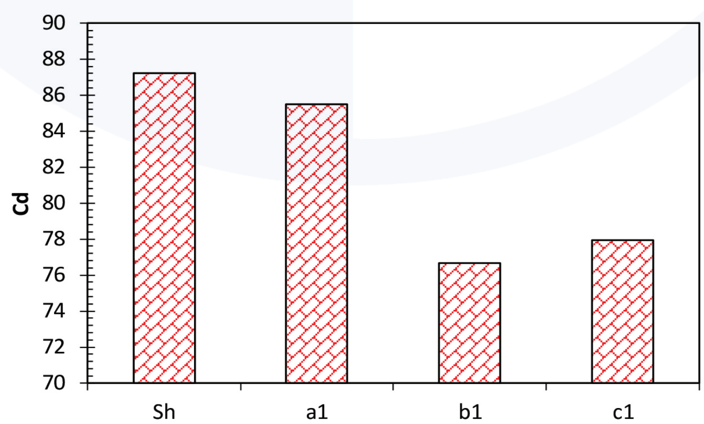

Figure 8- Values obtained for the Coefficient of the Structural Disorder for different samples at the age of 28 days. (Sh is the control)

According to the results obtained for this co-efficient, it is clear that the value of Cd for the control samples is the highest and for b1 samples is the lowest. Therefore, the obtained results in this study showed that the studied samples were in-active and that was consistent with the structure of the used cement. And the least chemical activ-ity belonged to sample b1 and the most chemi-cal activity belonged to the control sample. This coefficient is used for the degree of alkalinity of different cements and here, despite the use of the same type of cement, a different amount of chemical composition is created.

The results of FT-IR test of samples 42 and 90 are shown in Figures 9 and 10. For better comparison, the results of the magnified im-age of these spectra in the range of 400 cm^{-1} to 1800 cm^{-1} are also shown.

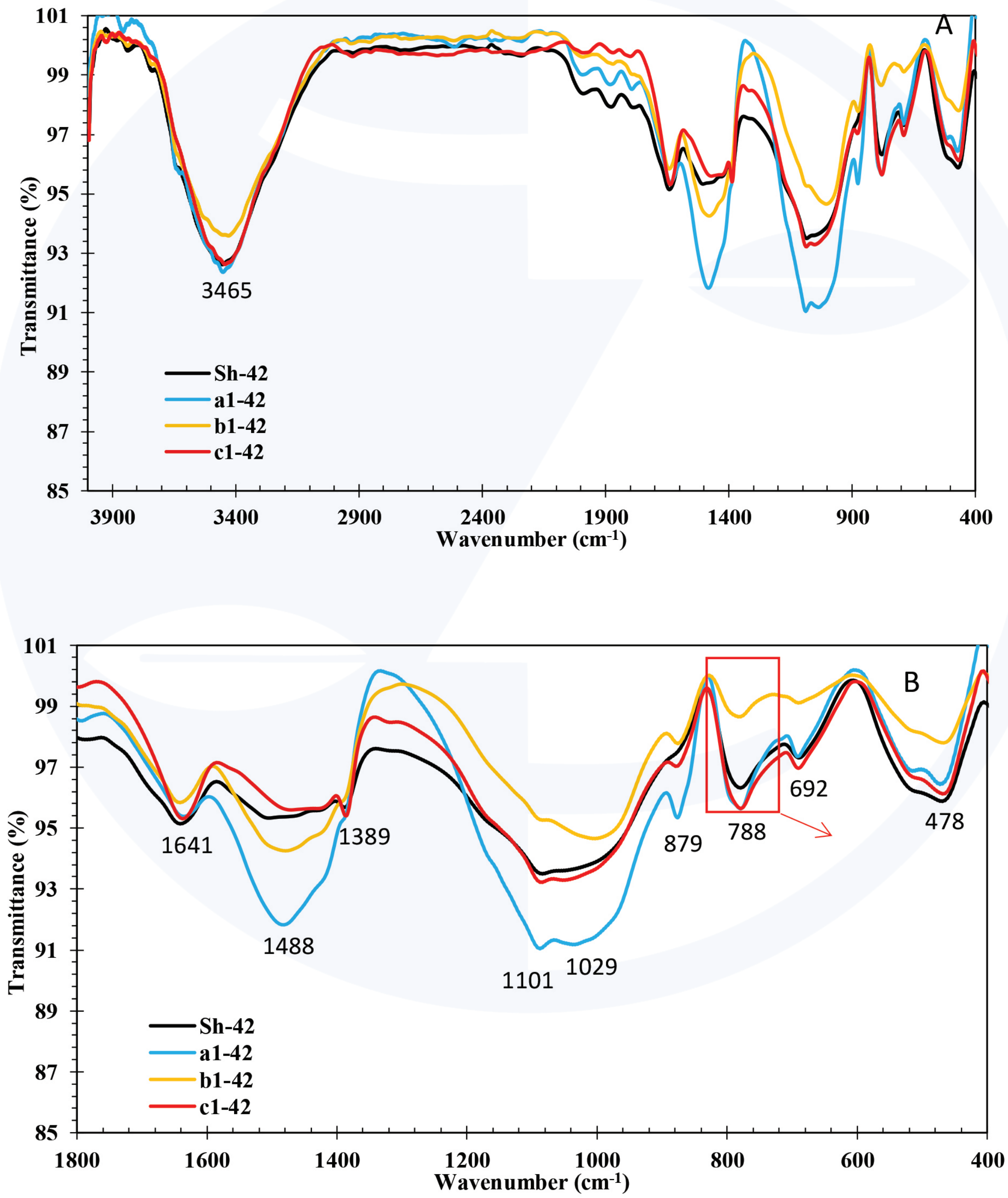

Figure 9- FTIR test results for sample 42 (A) of the whole spectrum and (B) the range of 400 cm^{-1} to 1800cm^{-1}. (Sh is the control)

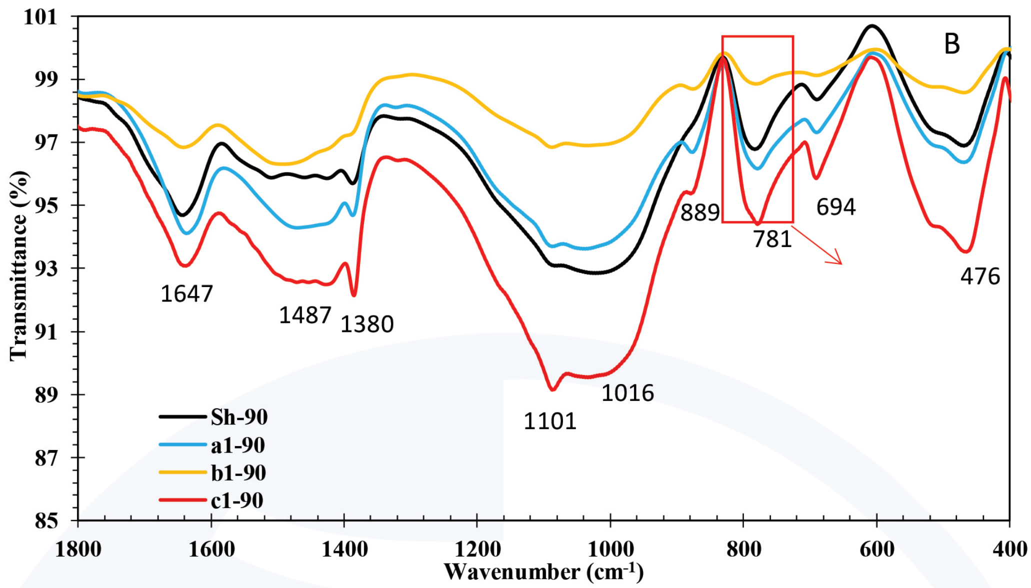

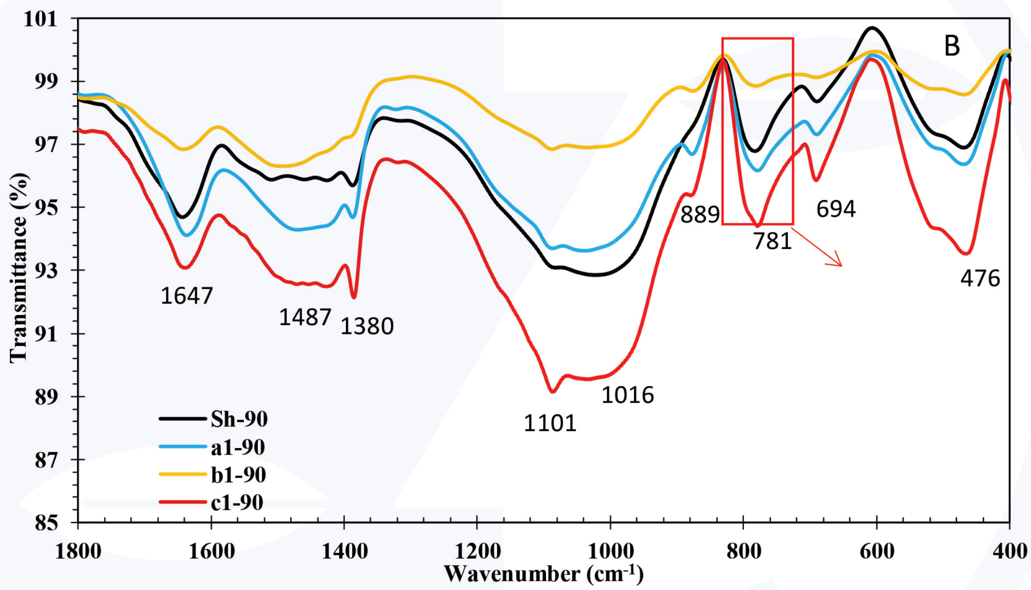

Figure 10- FTIR test results for sample 90 (A) of the whole spectrum and (B) the range of 400cm^{-1} to 1800cm^{-1} (Sh is the control)

In these two samples, the peaks at wave numbers of about 3450 cm^{-1} and 1640 cm^{-1} are again related to the tensile and flexural vi-brations of O-H bonds in adsorbed water molecules, respectively [10,11]. Also in these samples, the tensile vibrations of the bonds in the carbonate group have shown the structure of calcium carbonate in the cement at a wave num-ber of 1488 cm^{-1} [12]. In the 42 day samples, the amounts of calcium carbonate in sample a1 are higher than in other samples.

This is while, in the 90-day samples, the amount of this substance was more in sample c1 than in sample a1. In addition, in the wave number of 1380 cm^{-1} to 1389 cm^{-1}, the absorption peak related to the tensile vibrations of Si-O bonds in the units of SiO44- anions can be seen in both samples [13]. However, in sample 90, this peak is intensified, which could indicate more abundance of sul-fate anion in this sample. The peaks at the wave numbers about 1100 cm-1and 1020 cm^{-1} are related to the tensile vibration of Si-O-Si and

Si-O-Al bonds in the compounds in cement, respectively [14]. Here again, it is observed that the siliceous structures in samples a1 and c1 were the higher after 42 and 90 days, respec-tively. In addition, at a wave number of about 885 cm^{-1}, the absorption peak is related to the tensile vibrations of the existing C-O bonds of calcite [15].

The two peaks at wave numbers about 690 cm^{-1} and 470 cm^{-1} are also related to the flexural vibration of Si-O bonds in different compounds [13,16]. Also, as mentioned before, the peak positioned at the wave number about 781 cm^{-1} is observed in samples containing high amounts of alkali [13]. By comparing the peak intensity in this wave number, it is clear that sample b1 in both groups of 42 days and 90 days had the least amount of alkali in the structure. However, in the 42-day sample, the alkalinity of samples c1 and a1 was the same and more than the control value. Also, after 90 days, the amount of alkali in sample c1 was significantly more than in other samples. The value obtained for the Coefficient of the Structural Disorder of 42-day and 90-day samples is shown in the form of bar graphs in Figure 11,12 for better comparison [17].

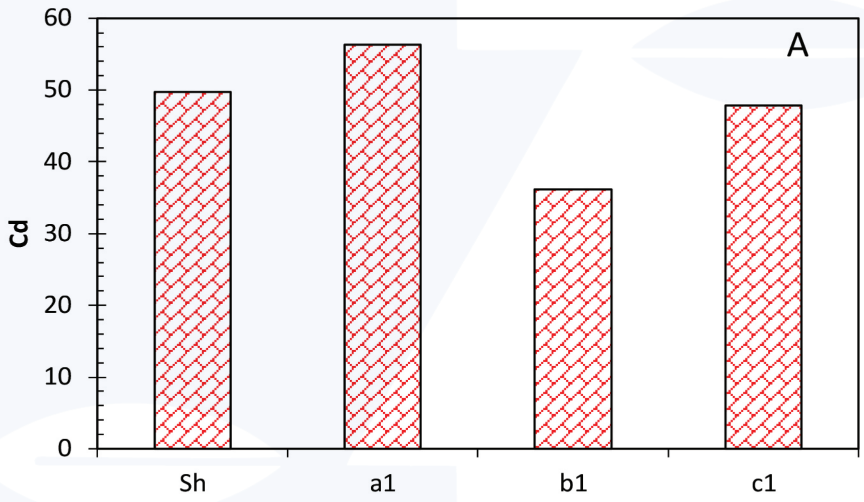

Figure 11- Values obtained for the Structural Disorder Coefficient of different samples at the age of 42 days (sh is the control)

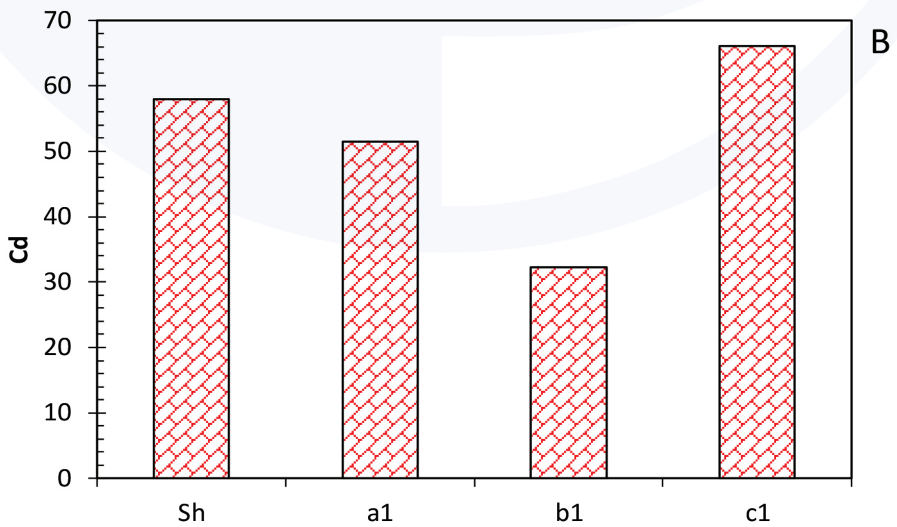

Figure 12- Values obtained for the Structural Disorder Coefficient of the samples at the age of 90 days (sh is the control)

According to the results obtained for this coefficient, it is clear that the value of Cd for samples a1 and c1 was higher after 42 and 90 days, respectively. Also, in both sample categories, the lowest value of this this coefficient belonged to sample b1. As previously stated, the value of Cd can be considered a measure of the alkaline-silica activity of a sample. And the least chemical activity, as mentioned before, be-longed to sample b1. These differences occurred while the used cement was the same in all samples. It should be noted that this coefficient can represent any type of alkali in these samples and the type of chemical composition cannot be explained.

XRD test of samples at the age of 90 days- Series 3

XRD test was used to investigate the crystal structure of the studied samples. The diffraction patterns are shown in Figure 13. The analysis information is as follows:

Reference Standard of the test:

BS EN 13925-1: 2008, Anode: Cu, Voltage: 40 KV, Current: 30 mA

Counting time:

0.5 sec, Step Size: 0.02, 2ɵ: 2-100°

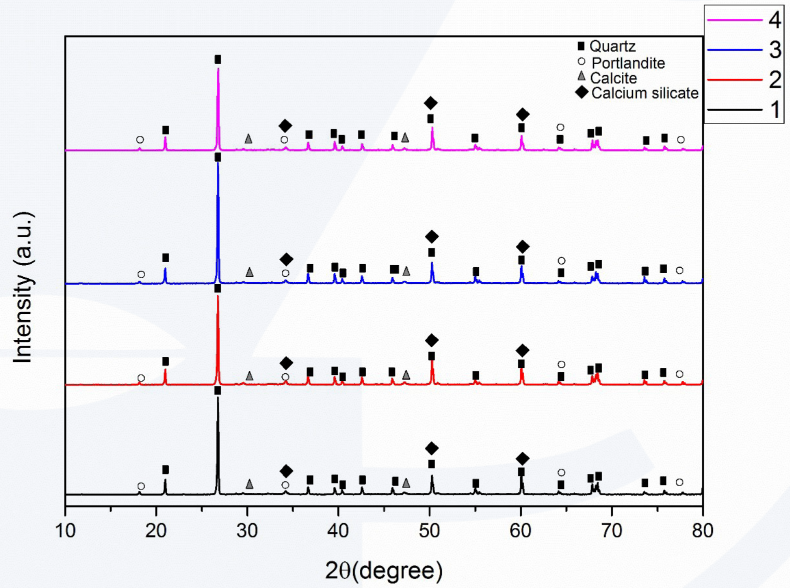

Figure 13- The diffraction patterns obtained from the four samples under study. (Control:4, 1:cl, 2: al, 3: bl)

According to Figure 13, in all four samples, there were two predominant phases and two small phases. The predominant phases included one quartz phase (SiO_2) with referen ce code JCPDS No: 05-0490 and one portlandite phase (Ca (OH) 2) with reference code JCPDS No: 44-1481. Also, the other two phases present in the samples with a much lower value were calcite ($CaCO_3$) with reference code JCPDS No: 05-0586 and calcium silicate (Ca_3SiO_5) with reference code JCPDS No: 42-0551. The Rietveld method was used to measure the values of each phase in the samples. In this technique, by the least-squares method, the theoretical diffraction patterns are adapted to the values obtained from the test and thus the values of each phase are calculated. The results of this adaptation are reported in Table 3.

Table 3 . Percentage of chemical compounds in 90-day cement (4-sh is the control)

Sample name	SiO_2 (%)	Change to control %	$Ca(OH)_2$ (%)	Change to control %	$CaCO_3$ (%)	Change to control %	Ca_3SiO_5 (%)	Change to control %
1-c1	66.2	5%-	32.2	10.6%	0.9	80%	0.7	75%
2-a1	67.2	3.7%-	31.5	8%	0.8	60%	0.5	25%
3-b1	69.4	*	29.5	1%	0.6	20%	0.5	25%
4-sh	69.8	*	29.1	*	0.5	*	0.4	*

According to Table 3, it is clear that from samples 1 to 4, the value of SiO2 in the cement increased and the percentage of Ca $(OH)_2$ de-creased. Also, the other two phases from sam-ples 1 to 4 either decreased or did not change. Sample No. 4 is the control sample. In general, calcium-containing compounds have higher values under TCF.

During the hydration of cement after 90 days, it is expected that the chemical compounds con-taining CH and C-S-H to grow, as shown in Figure (14). Compared to the control sample, it seems that the formation of chemical com-pounds occurred more intensely, or, in other words, more complete hydration was formed under TCF.

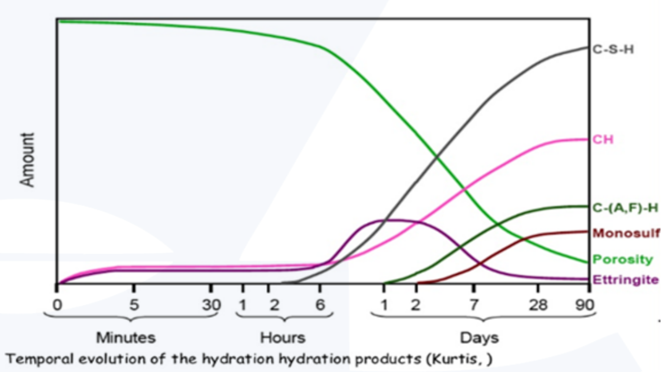

Figure 14- The process of creating chemical compounds in cement [18]

XRF and L.O.I analysis of 90-day sample -Series 3

XRF analysis was performed to evaluate the abundance of elements in the samples. Also, to examine the L.O.I (Loss on Ignition) of weight loss due to combustion, the samples were exposed to 950° C for 1.5 hours. The results of Percentage changes are presented in Table 4· Reference standard: ASTM E1621-13

Table 4 . Percentage of the elements in cement samples and amount of weight loss due to combustion

	Samples			
%Oxide/Name	c1	a1	b1	Sh-Control
Na_2O	0.04	0.06	0.08	0.11
Mg_2O	0.54	0.46	0.48	0.54
Al_2O_3	1.6	1.5	1.49	1.43
Si_2O_3	66.1	67	68.6	68.4
P_2O_5	0.07	0.14	0.14	0.18
SO_3	0.87	0.88	0.96	0.93
K_2O_3	0.11	0.14	0.09	0.16
Ca O	20.6	19.6	18.1	18.2
Fe2O3	3.1	2.9	2.9	3
L.O.I	6.97	7.32	7.16	7.05

Table 5 . Comparison of the percentage of the most elemental changes compared to the control

Oxide%	Samples			
	c1	a1	b1	Sh-Control
Na_2O	-64%	-45.45%	-27.27%	*
Al_2O_3	12%	5%	4%	*
$P2O_5$	-61%	-22%	-22%	*
K_2O_3	-45.50%	-12.50%	-43.80%	*
CaO	13.20%	7.70%	0	*

Table 5 shows the comparison of the percentage of some element changes in comparison to the control samples. One of the important points in Table 5 is the significant reduction of Potassium, Sodium, and Phosphorus in the samples under CF. Sodium (Na) and Potassium oxides (K) play an active role in the alkaline reaction of con-crete with aggregates and cause cracking and destruction of concrete [19]. The abundance of alkalis in cement is limited and mainly below 4%, however, this small amount has certain ef-fects on hardening behavior. With the increase of alkalis including Sodium and Potassium, the initial strengths increase, and the 28-day strengths decrease.

The reason is the effect of Potassium on the hydration of C3S [20]. The higher the C3S content in Portland cement, the faster this type of cement hardens. While, if the C2S is higher, the cement hardens at a lower rate. But in the end, it reaches a higher strength [20-21]. According to Table 5, in the samples under CF, the amount of Sodium (Na) and Potassium (K) has been reduced by approximately (~ 30%), and instead more CaO has been reported. Cement with more CaO starts to harden at a slower rate but reaches higher final strengths [20-21]. If this process has taken place from the be-ginning of hydration, it can be considered ef-fective in justifying the slow process of starting strength at 7 days and continuing to increase strength at older ages.

SEM analysis of the 90-day samples-Series 3

Finally, the SEM images are shown in figures 15-19. The images were taken from the samples in order to observe the crystal differences.

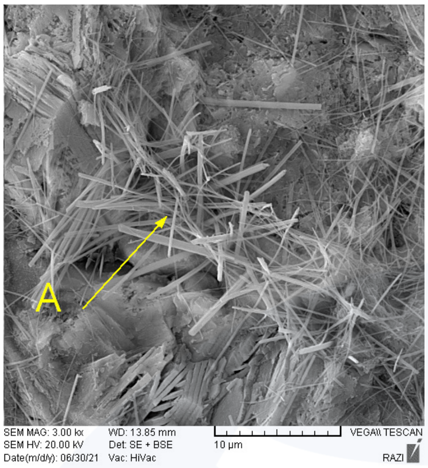

Spectra: sample A-A.spx

Element	Series	unn. C [wt.-%]	norm. C [wt.-%]	Atom. C [at.-%]
Oxygen	K series	34.05	37.40	57.07
Magnesium	K series	0.77	0.85	0.85
Aluminium	K series	4.57	5.02	4.54
Silicon	K series	10.66	11.71	10.18
Sulfur	K series	3.44	3.78	2.88
Calcium	K series	34.11	37.46	22.82
Iron	K series	3.45	3.79	1.66
	Total:	91.0 %		

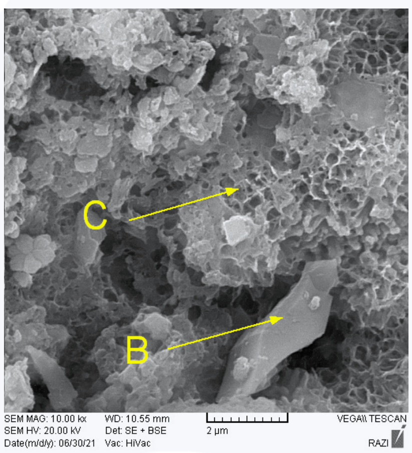

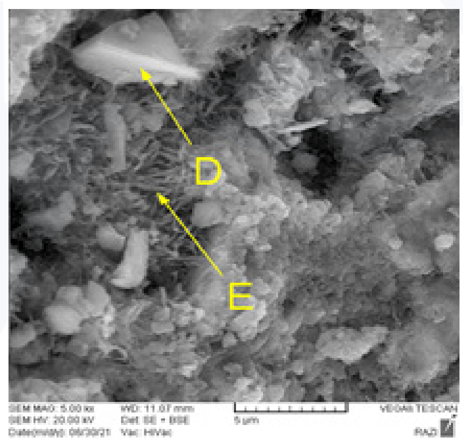

Spectra: sample A-B.spx

Element	Series	unn. C [wt.-%]	norm. C [wt.-%]	Atom. C [at.-%]
Oxygen	K series	37.61	45.46	67.19
Silicon	K series	16.48	19.92	16.77
Sulfur	K series	2.06	2.49	1.84
Calcium	K series	2.91	3.52	2.08
Iron	K series	23.68	28.61	12.12
	Total:	82.7 %		

Spectra: sample A-D.spx

Element	Series	unn. C [wt.-%]	norm. C [wt.-%]	Atom. C [at.-%]
Oxygen	K series	65.72	62.04	75.66
Silicon	K series	28.69	27.09	18.82
Sulfur	K series	1.97	1.86	1.13
Calcium	K series	9.54	9.01	4.38
	Total:	105.9 %		

Spectra: sample A-C.spx

Element	Series	unn. C [wt.-%]	norm. C [wt.-%]	Atom. C [at.-%]
Oxygen	K series	26.08	30.90	58.77
Silicon	K series	3.10	3.68	3.98
Sulfur	K series	1.98	2.35	2.23
Calcium	K series	2.55	3.02	2.29
Iron	K series	50.69	60.06	32.72
	Total:	84.4 %		

Spectra: sample A-E.spx

Element	Series	unn. C [wt.-%]	norm. C [wt.-%]	Atom. C [at.-%]
Oxygen	K series	36.02	42.27	61.33
Magnesium	K series	3.00	3.52	3.36
Aluminium	K series	3.32	3.90	3.35
Silicon	K series	9.41	11.04	9.12
Sulfur	K series	1.58	1.85	1.34
Calcium	K series	30.94	36.31	21.03
Iron	K series	0.95	1.12	0.46
	Total:	85.2 %		

Figure 15- Sample al

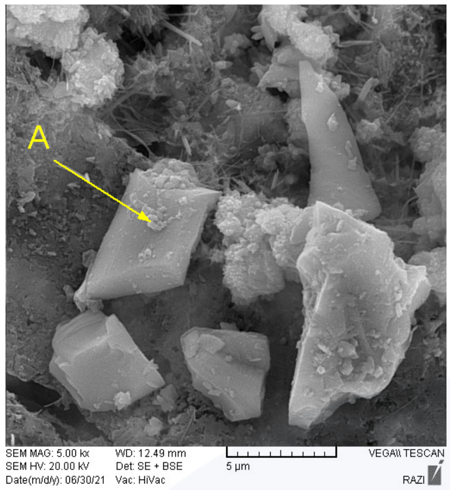

Spectra: sample B-A.spx

Element	Series	unn. C [wt.-%]	norm. C [wt.-%]	Atom. C [at.-%]
Oxygen	K series	52.96	58.90	73.20
Aluminium	K series	0.55	0.61	0.45
Silicon	K series	26.91	29.93	21.19
Calcium	K series	8.96	9.97	4.96
Iron	K series	0.53	0.59	0.21
	Total:	89.9 %		

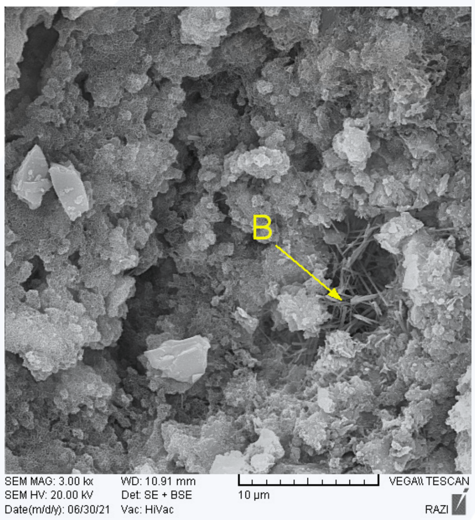

Spectra: sample B-B.spx

Element	Series	unn. C [wt.-%]	norm. C [wt.-%]	Atom. C [at.-%]
Oxygen	K series	32.20	41.31	61.74
Magnesium	K series	0.59	0.75	0.74
Aluminium	K series	1.79	2.30	2.04
Silicon	K series	4.29	5.50	4.68
Sulfur	K series	6.23	7.99	5.96
Calcium	K series	31.40	40.29	24.04
Iron	K series	1.45	1.85	0.79
	Total:	77.9 %		

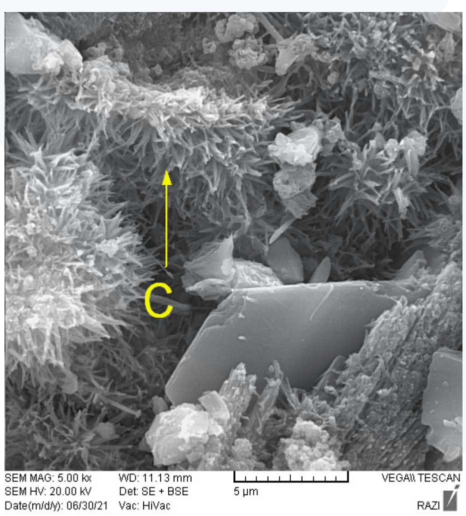

Spectra: sample B-C.spx

Element	Series	unn. C [wt.-%]	norm. C [wt.-%]	Atom. C [at.-%]
Oxygen	K series	46.45	51.06	70.31
Aluminium	K series	0.99	1.09	0.89
Silicon	K series	8.48	9.32	7.31
Sulfur	K series	3.51	3.86	2.65
Calcium	K series	30.24	33.24	18.27
Iron	K series	1.31	1.44	0.57
	Total:	91.0 %		

Figure 16- Sample b1

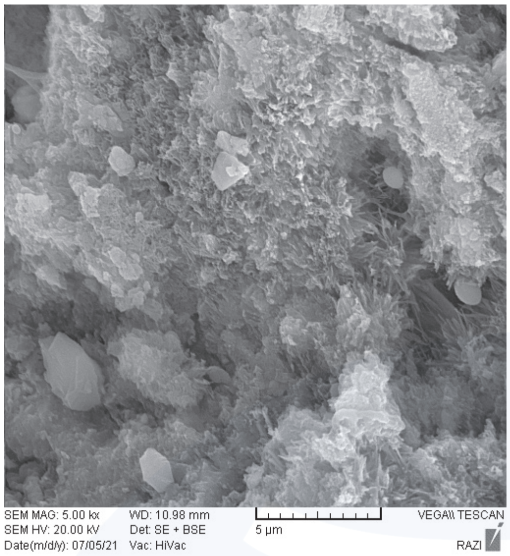

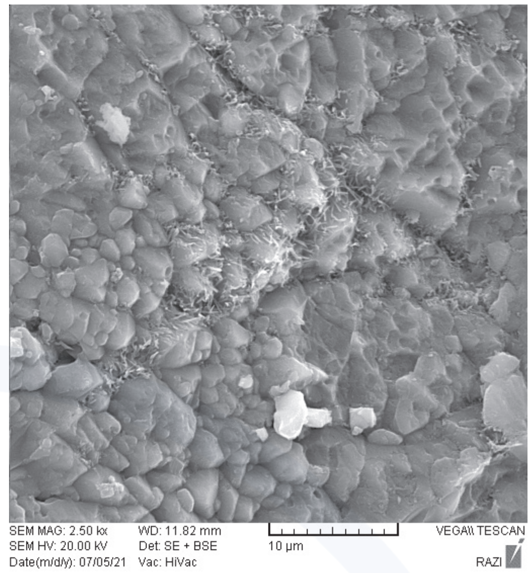

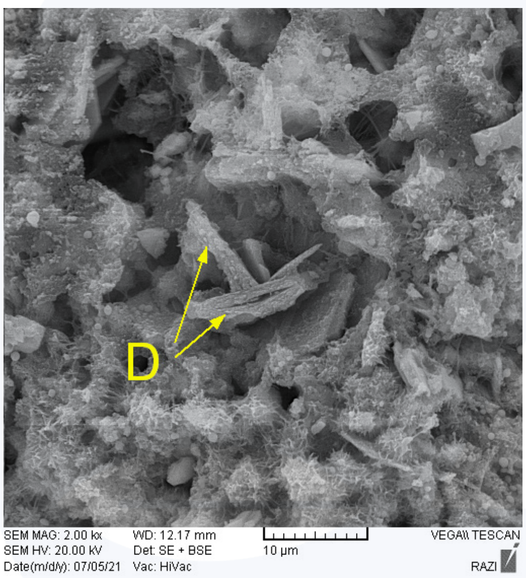

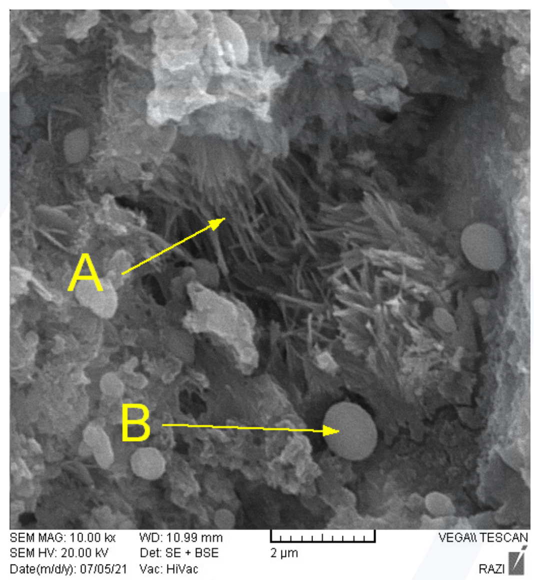

Spectra: sample C-D.spx

Element	Series	unn. C [wt.-%]	norm. C [wt.-%]	Atom. C [at.-%]
Oxygen	K series	47.79	50.79	69.95
Aluminium	K series	9.88	10.50	8.58
Silicon	K series	1.21	1.28	1.01
Calcium	K series	34.51	36.68	20.17
Iron	K series	0.71	0.75	0.30
	Total:	94.1 %		

Spectra: sample C-A.spx

Element	Series	unn. C [wt.-%]	norm. C [wt.-%]	Atom. C [at.-%]
Oxygen	K series	7.76	9.16	17.58
Magnesium	K series	2.39	2.82	3.56
Aluminium	K series	4.35	5.14	5.85
Silicon	K series	24.84	29.33	32.06
Sulfur	K series	3.99	4.71	4.51
Calcium	K series	37.52	44.29	33.93
Titanium	K series	0.20	0.23	0.15
Iron	K series	3.65	4.31	2.37
	Total:	84.7 %		

Spectra: sample C-B.spx

Element	Series	unn. C [wt.-%]	norm. C [wt.-%]	Atom. C [at.-%]
Oxygen	K series	9.53	14.08	28.10
Aluminium	K series	0.55	0.81	0.96
Silicon	K series	7.55	11.16	12.68
Sulfur	K series	2.32	3.43	3.42
Calcium	K series	43.43	64.18	51.13
Titanium	K series	0.57	0.84	0.56
Iron	K series	3.72	5.50	3.14
	Total:	67.7 %		

Figure 17- Sample cl

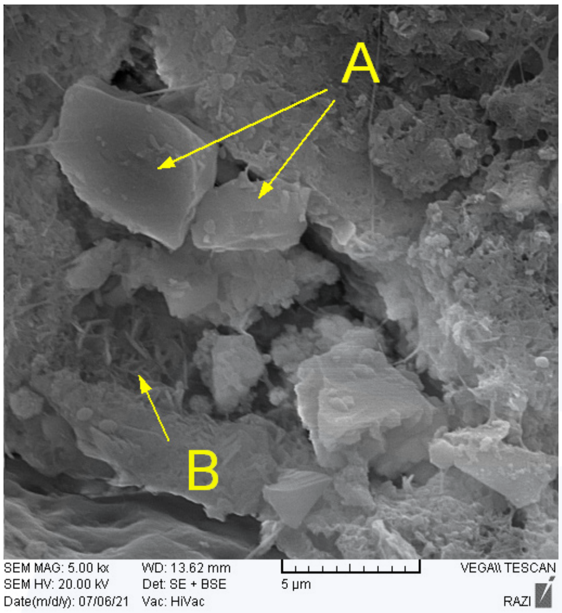

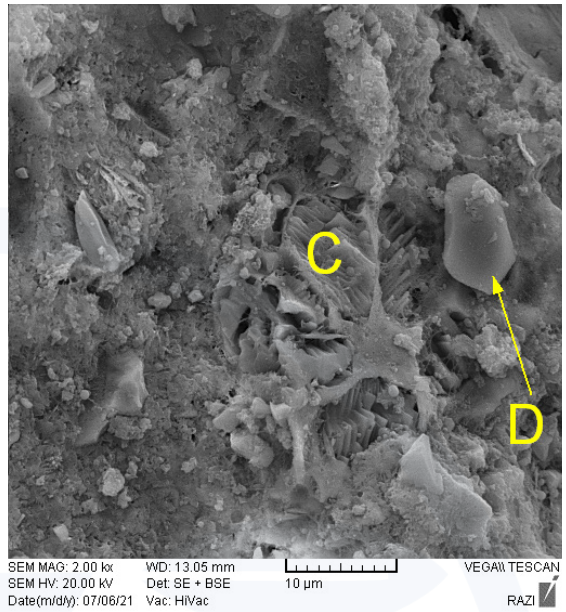

Spectra: sample SH-A.spx

Element	Series	unn. C [wt.-%]	norm. C [wt.-%]	Atom. C [at.-%]
Oxygen	K series	45.61	48.47	62.56
Sodium	K series	5.07	5.38	4.84
Magnesium	K series	0.20	0.22	0.18
Aluminium	K series	9.24	9.82	7.52
Silicon	K series	27.21	28.91	21.26
Potassium	K series	0.20	0.21	0.11
Calcium	K series	6.09	6.48	3.34
Iron	K series	0.48	0.51	0.19
	Total:	94.1 %		

Spectra: sample SH-C.spx

Element	Series	unn. C [wt.-%]	norm. C [wt.-%]	Atom. C [at.-%]
Oxygen	K series	36.86	38.10	57.38
Magnesium	K series	1.95	2.02	2.00
Aluminium	K series	0.85	0.88	0.79
Silicon	K series	15.30	15.82	13.57
Sulfur	K series	2.72	2.81	2.11
Calcium	K series	38.38	39.67	23.85
Iron	K series	0.68	0.70	0.30
	Total:	96.7 %		

Spectra: sample SH-B.spx

Element	Series	unn. C [wt.-%]	norm. C [wt.-%]	Atom. C [at.-%]
Oxygen	K series	27.30	32.89	51.07
Magnesium	K series	3.70	4.46	4.56
Aluminium	K series	2.56	3.09	2.84
Silicon	K series	14.52	17.49	15.47
Sulfur	K series	1.39	1.67	1.30
Calcium	K series	32.23	38.83	24.07
Iron	K series	1.30	1.56	0.70
	Total:	83.0 %		

Spectra: sample SH-D.spx

Element	Series	unn. C [wt.-%]	norm. C [wt.-%]	Atom. C [at.-%]
Oxygen	K series	55.31	54.76	68.68
Aluminium	K series	0.36	0.36	0.26
Silicon	K series	39.11	38.72	27.67
Sulfur	K series	2.48	2.45	1.54
Calcium	K series	3.74	3.71	1.86
	Total:	101.0 %		

Figure 18- Sample control Sh

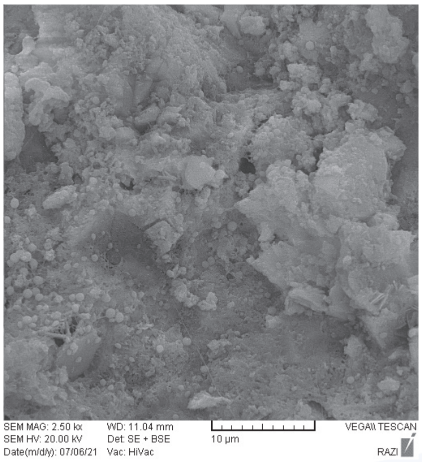

Spectra: sample SH-E.spx

Element	Series	unn. C [wt.-%]	norm. C [wt.-%]	Atom. C [at.-%]
Oxygen	K series	56.09	62.60	76.46
Silicon	K series	22.81	25.45	17.71
Calcium	K series	10.70	11.95	5.83
	Total:	89.6 %		

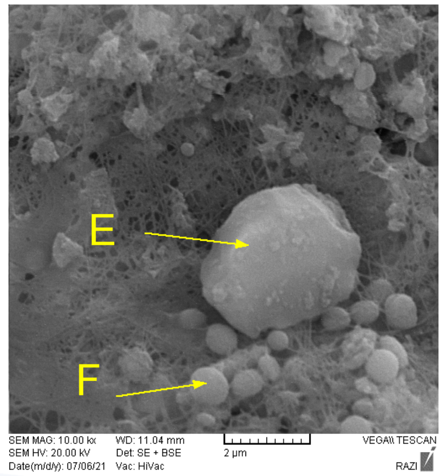

Spectra: sample SH-F

Element	Series	unn. C [wt.-%]	norm. C [wt.-%]	Atom. C [at.-%]
Oxygen	K series	48.52	49.14	68.04
Magnesium	K series	0.91	0.92	0.84
Aluminium	K series	1.77	1.80	1.47
Silicon	K series	12.99	13.16	10.38
Sulfur	K series	3.34	3.38	2.34
Calcium	K series	27.75	28.10	15.53
Iron	K series	3.46	3.50	1.39
	Total:	98.7 %		

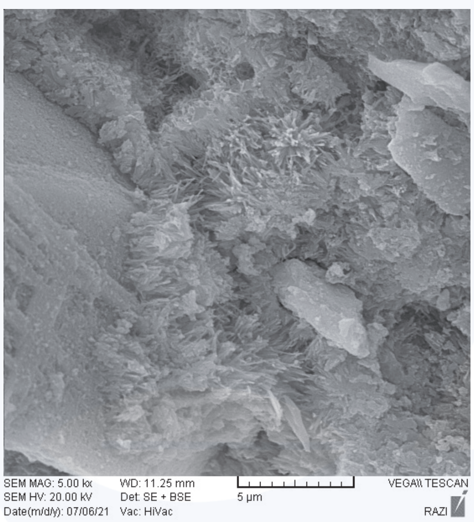

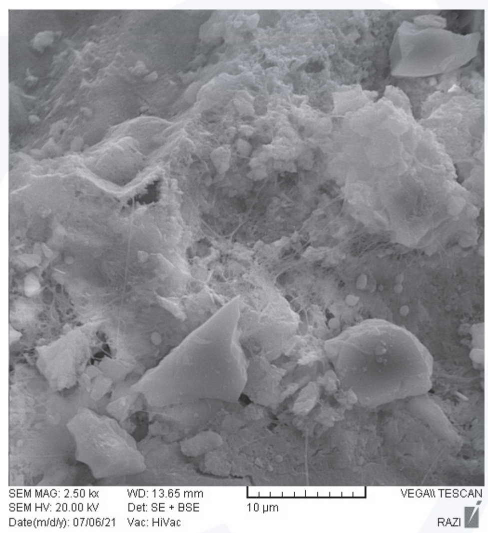

Figure 19- Sample control Sh

In the SEM images, the process of formation of crystals containing calcium, iron, aluminum, and sulfur is more clearly seen in the samples under the TCF and can indicate the formation of ettringite (Figures 15 to 19). The importance of this difference is illustrated in Figure (20) of the 90-day cement sample with 5 and 20% of fly ash, which shows the difference in ettringite formation. Wind ash is added to cement to reduce CO_2 and preserve the environment [22]. Ettringite is also a product of the combination of calcium aluminate with calcium sulfate, and its small amounts increase the strength, and high amounts will have a negative effect on the durability of concrete. Of course, the dimensions of the effect of Ettringite on the efficiency of cement are of interest to the industry and there is still a lot of work to be done in this regard. Some studies have been done to use the heat capacity of this compound in cement to optimize building heating [23-24].

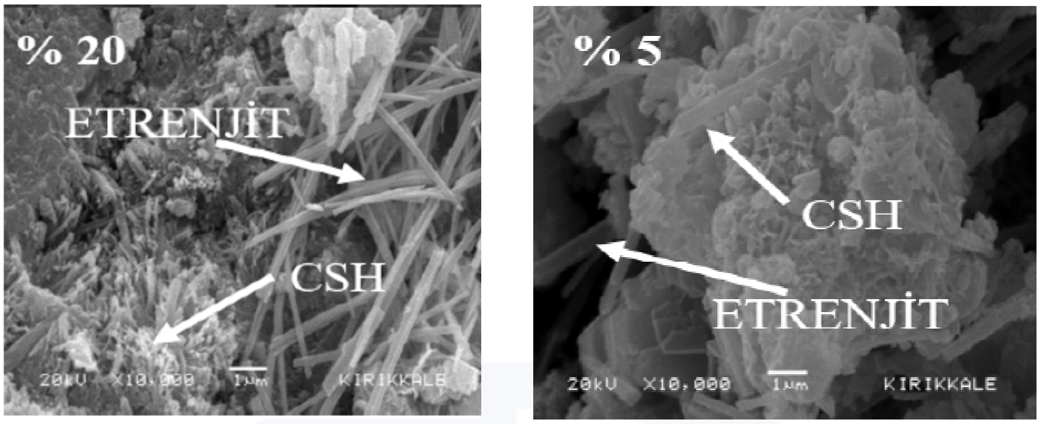

Figure 20- How crystals are formed in modified cement (green) with 5 and 20% fly ash at the age of 90 days [22]

Conclusion

As seen, in most of the samples under the TCF, the growth rate of strength over time compared to the age of 7 days was higher than in the control samples. This phenomenon shows changes in the structure of chemical compounds [25-26]. Examining the supplementary analyzes of Series 3, the followings are seen:

In XRD results, the abundance of silicon-containing compounds in the control sample is higher at 90 days. While, in the samples under the TCF, the predominant chemical compounds are mainly calcium. In the samples under CF, $CaCO_3$ compounds are 20 to 80% and Ca_3SiO_5 compounds are 25 to 75%, and also Ca (OH)2 is more formed.

From the XRF results, it is clear that the abundance of calcium and aluminum in the samples under TCF was higher (about 7% on average). Sodium (Na), Potassium (K), and Phosphorus (P) are about 30% on average (between 13 and 64%) less in the samples under TCF, which have special effects on delaying the hydration process (increasing long-term strength).

In SEM images, the process of ettringite mation is more clearly seen in the samples under TCF. Due to the fact that the composition of cement elements under the CF has changed (Table 5-6), the creation of new chemical compounds has a new trend and is not comparable to the conventional chemistry of cement.

A noteworthy point in the results of FT-IR analysis is that the change in chemical bonds for each sample is unique to that sample.

In general, the present study presents the following general points:

- From the SEM images and XRD results and comparison with the expected hydration process, it can be said that in total, at 90 days, we see more complete hydration in the samples under Consciousness Bond Field.
- XRF result show the change of the amount of elements in the samples under TCF. Considering that all samples are made of one material, change of elements is possible through the transformation of T-Consciousness into matter. One of the challenges of the concrete industry is to achieve the chemical compositon, the processing of materials close to the cement structure, which can be combined with known cements and have a favorable effect on the properties of cement. Consciousness Bond Field can create appropriate structural changes by making changes in the cement base using T-Consciousness and not material.
- In this research, the process of internal changes for each series and group is independent of others. However, the general change is in the direction of increasing strength, and this is in accordance with the theory of the General Connection of Particles,

which states that changes in the behavior of materials under the Consciousness Bond Field in order to improve their fundamental character [4]. And since the basic character of

- So far, in the experience of working with TCFs, we have found that the dimensions of achievement in their implementation are much more than a specific function. It means that when cement is placed under the TCF, other parameters and chemical compounds change in a multifaceted and completely targeted way [27-28].

This directly means changing behavior in different situations. In this respect, we are faced with a multifaceted technology that creates the possibility of different functions at the lowest cost, and this has always been the focus of the industry.

Acknowledgments

The authors would like to thank Dr. Bakhshi for his cooperation over the years.

References

1. Locher F.W. (2006) .Cement: principles of production and use ISBN9789642917020,pp13
2. U.S. (2012).Geological Survey, Mineral Commodity Summaries, January
3. Taheri.M.A . (2012).*General Connection of particles* .Interuniversal Publishing.Erfan-Halgheh. ID: 978-1-940491-03-5
4. Taheri.M., Payervand, F., Ahmadkhanlou, F., Torabi, S., & Semsarha, F. (2021). Distinction of Consciousness Fields According to Taheri from Other Conventional Physical Fields: Evaluating the Magnetic Properties of Materials.
5. Taheri M.A, (2013) .*Human from another outlook.* Interuniversal Press; 2nd Edition ISBN-13: 978-1939507006, ISBN- 10: 1939507006
6. WWW.Cosmointel.com
7. http://www.isiri.gov.ir, Iran Institute of Standards and Industrial Research
8. Joseph.Sh,Joseph.A.Mand Bishnoi.Sh,(2015). EconomicImplicationsofLimestoneClinkerCalcinedClayCement(LC3)inIndia,CalcinedClaysfor SustainableConcrete,RILEMBookseries10,DOI10.1007/978-94-017-9939-3_62
9. Scrivener K, FREng. Cement chemistry and sustainable materials(2018).Edx
10. Javidparvar A.A, Ramezanzadeh.B, Ghasemi.E,(2016). The effect of surface morphology and treatment of Fe3O4 nanoparticles on the corrosion resistance of epoxy coating, J. Taiwan Inst. Chem. Eng. 61 . https://doi.org/10.1016/j.jtice.2016.01.001.
11. Anchieta.C, Cancelier.A, Mazutti.M, Jahn. S, Kuhn.R, Gündel. A, O. Chiavone-Filho. O, Foletto.E,.(2014). Effects of Solvent Diols on the Synthesis of Zn-Fe2O4 Particles and Their Use as Heterogeneous Photo-Fenton Catalysts, Materials (Basel). 7 -6281–6290. https://doi.org/10.3390/ma7096281.
12. Sasnauskas. V,.(2013). Cement hydration with zeolite-based additive, Chemija. 24 - 271–278
13. Hassan.M,Khatib.J.M,Mangat.P.S,Naseef.A,Gardiner.P.H.E,.(2014).FTIRandXRDCharacterizedPortlandCementStabilisedLeadContaminatedSoil, in: Int. Conf. Nat.Sci.Environ.(ICNSE2014),Dubai,(:pp.102–106.)
14. Springfield.T;(2021). Application of FTIR for Quantification of Alkali in Cement, (2011) https://www.researchgate.net/publication/313389380_FTIR_and_ XRD_Characterized_Portland_Cement_Stabilised_Lead_Contaminated_Soil
15. Chollet.M,Horgnies.M;(2011). AnalysesofthesurfacesofconcretebyRamanandFT-IRspectroscopies:Comparativestudyofhardenedsamplesafter demoulding andafterorganicpost-treatment,Surf.InterfaceAnal.43-714–725.https://doi.org/10.1002/sia.3548.
16. Trezza M.A;(2007). Hydration study of ordinary Portland cement in the presence of zinc ions, in: Mater. Res. Universidade Federal de Sao Carlos, (pp. 331–334).https://doi.org/10.1590/S1516-14392007000400002.
17. Berra M, MangialardiT, Paolini A.E;.(1999). Rapid evaluation of the threshold alkali level for alkali-reactive sliceaous aggregates in concrete", Cement and Concrete Composites 21 -325-333
18. Scrivener K, FREng. Cement chemistry and sustainable materials, Edx-Introuction &Hydration(2018)
19. Zandi Y . (2009). Advanceed ConcreteTechnology (2009). ISBN:978-964-547-221-2. PP5-25
20. Locher F.W, (2006). Cement: principles of production and use ISBN:9789642917020-pp206
21. Taylor H.F.W, .(1997). Cement Chemistry, 2nd Ed. Academic Press, London
22. Demir. I, Guzelkuck.S, Sevim.O, Filaze.A, Sengul.C.G.(2017),Mortar Examination of Microstracture of Fly Ash in Cement Proceedings ofThe IRES International Conference, Lisbon, Portugal, 11th-12th December
23. Ndiaye K, Ginestet. S, Cyr.M;(2017). Durability and stability of an ettringite-based material for thermal energy storage at low temperature. Cem Concr Res(99:106–15) https://doi.org/10.1016/j.cemconres.2017.
24. Khadim.P, Gineste.N.S, Cyr.M, (2018). Experimental evaluation of two low temperature energy storage prototypes based on innovative cementitious material https://doi.org/10.1016/j.apenergy.2018.02.136
25. Locher. F.W, (2006) .*Cement: principles of production and use* -ISBN9789642917020,pp204
26. Double.D.D,(1983). New developments in understanding the chemistry of cement hydration, Published: Royal Societyhttps://doi.org/10.1098/
27. Kazazi.B,Taheri.M.A , (2001) Effects of the Consciousness Field on Concrete (ASR).
28. Kazazi.B, Taheri.M.A,(2021). Influence of the Consciousness Bond Field on alkaline reaction of Concrete

Effect of Taheri Consciousness Bond Field on the Structure and Properties of 1000-Series Aluminum with Preheating

Bahareh Kazazi[1*], Mohammad Ali Taheri[2]

1. Civil Engineering, CEO of Hoobe Construction Company, Tehran, Iran.

2. Sciencefact R&D Department, Cosmointel Inc. Research Center, Ontario, Canada.
1. Civil Engineering, CEO of Hoobe Construction Company, Tehran, Iran.

2. Sciencefact R&D Department, Cosmointel Inc. Research Center, Ontario, Canada.

* Corresponding author:

Bahareh Kazazi
Civil Engineering, CEO of Hoobe Construction Company, Tehran, Iran.

Email: baharkazazi@gmail.com

ABSTRACT

The properties and structure of aluminum in various known fields have been already studied. The aim of this study was to investigate the behavior and properties of unalloyed aluminum with 300 °C preheating under the Consciousness Bond Field. Taheri Consciousness Fields (TCFs) were founded and introduced by Mohammad Ali Taheri as new Fields more than four decades ago. These Fields are neither material nor energetic. Therefore, they do not have the quantity, but they have direct effects on both matter and energy. In other words, although TCFs cannot be directly measured, we can investigate their effects indirectly through various reproducible experiments. The present study is an attempt to examine this theory. For this purpose, aluminum metal was used as a sample. Six aluminum samples were cast under the same conditions and divided into two groups. One group was put under the influence of TCF, and the other group was the control. Then, in order to record the effect of the Consciousness Bond Field, the structure and properties of the metal samples were investigated. X-ray diffraction (XRD) analysis was performed for structural analysis of the samples. In terms of properties, corrosion resistance was investigated in a standard SBF solution. Some changes in the structure, such as reduction of twin defects and increase of extrinsic and intrinsic defects were observed under the influence of TCF.

Keywords: Consciousness Bond Field, Taheri Consciousness Fields, Twin defects, Intrinsic defects, Extrinsic defects, Corrosion resistance

INTRODUCTION

Aluminum, with the highest abundance in the earth's crust after silicon, is one of the strategic metals, and the most used after steel. It has many applications in almost all industries. Any change in the position of atoms is directly related to the properties and application of this material [1]. "Consciousness Bond Field" is one of many Taheri Consciousness Fields (TCFs) that influence materials. It is expected that pure materials, which are not composed of different chemical compounds and alloys, have stable behavior under the influence of the Consciousness Bond Field. However, in re-cooling, a change in the crystalline lattice of atoms is probable according to the theory of TCFs by which T-Consciousness can be converted into matter and energy. The present study examines the mentioned cases. In previous studies, 1000-series aluminum was investigated only by casting without preheating. In this study, the aim was to investigate the effect of preheating and increasing the mold length and, in a way, prolonging the cooling process and TCFs [2].

The nature of consciousness and its place in science has received much attention in the current century. Many philosophical and scientific theories have been proposed in this area. In the 1980s, Mohammad Ali Taheri introduced novel fields with a non-material/non-energetic nature named Taheri Consciousness Fields (TCFs). In this perspective, T-Consciousness is one of the three existing elements of the universe apart from matter and energy. According to this theory, there are various TCFs with different functions, which are the subcategories of a networked universal internet called the Cosmic Consciousness Network (CCN). The major difference between the theory of TCFs and other theoretical concepts about consciousness is related to the practical application of the TCFs. TCFs can be applied to all living and non-living creatures, including plants, animals, microorganisms, materials, etc.

Mohammad Ali Taheri, the founder of Erfan Keyhani Halqeh, a school of thought, introduced a new science in 2020 as a branch of this school. He coined the term Sciencefact for this new science because it utilizes scientific investigations to prove the existence of T-Consciousness as an irrefutable phenomenon and a fact. Although science focuses solely on the study of matter and energy and Sciencefact, by contrast, explores the effects of the [non-material/non-energetic] TCFs, Sciencefact has provided a common ground between the two by conducting reproducible laboratory experiments in various scientific fields, and it has used the scientific approach in proving TCFs.

The influence of the TCFs begins with the Connection between CCN as the Whole Taheri Consciousness of the universe and the subjects of study as a part. This Connection called "Ettesal" is established by a certified and trained individual who has been entrusted with the TCFs. The human mind has an intermediary role (Announcer) which plays a part by fleeting attention to the subject of study and then the main achievement obtained as a result of the effects of the TCFs. These Fields cannot be directly measured by science, but it is possible to investigate their effects on various subjects through reproducible laboratory experiments.

The research methodology in the study of T-Consciousness has been founded on the process of Assumption, Argument, and Proof, in which the basic Assumption is: The Cosmos was formed by a third element called T-Consciousness that is different from matter and energy.

The Argument: The existence of TCFs can be demonstrated by its effects on matter and energy (e.g., humans, animals, plants, microorganisms, cells, materials, etc.)

The Proof: is the scientific verification of the effects of TCFs on matter and energy (according to the Argument) through various reproducible scientific experiments.

Accordingly, to investigate and verify the existence, effects, and mechanisms of TCFs, the following five research phases (Phases 0 through 4), and the aims of each phase are outlined below.

Phase-0 studies aim to prove the existence of TCFs by observing their effects. The nature of T-Consciousness and what it is will not be addressed in this phase. Phase-1 explores the varied effects of different TCFs. Phase-2 examines the reason behind the varied effects of these fields. Phase-3 investigates the mechanism of TCFs effects on matter and energy. Finally, Phase-4 draws significant conclusions, particularly with regard to the mind and memory of matter and their relation to the T-Consciousness, etc. [2-6]

Methodology

The molten aluminum made from AA1XXX series aluminum ingot was cast in six uniform molds (Cylinders with a diameter of 6 cm and a height of 1.5 cm). The molds were placed in a tray before casting and preheated to 300 °C. The six samples were divided into two equal groups, each consisting of three samples. The samples were arbitrarily named by those doing the experiment. One group of the samples was put under TCF, and the other group of samples was considered the control. According to Table (1), the group under TCF was identified as X1 and the control group was identified as Control. Each group consisted of three samples, and they were coded with numbers 1 to 6 for ease of work. Then, the names of the group under the TCF were declared to the person establishing the connection, i.e., the second author of the article, for the announcement of the connection.

Table 1 . Grouping of 6 cast aluminum samples

Group Name		Control			X1(CF)	
Sample Number	1	2	3	4	5	6

Application of the Consciousness Bond Field

One of the introduced TCFs is called the Consciousness Bond Field and was applied to the samples according to the protocols regulated by the COSMOintel research center (www.COSMOintel.com). A request for Connection to the CCN to utilize TCFs can be placed through the COSMOintel website in the "Assign Announcement" section. This access is available for everyone at no cost. In order to study and experience this Connection, the researchers can register on the website at any time in order to report the experiment to the COSMOintel research center. Certain details of the experiment must be provided to the center; for example, the characteristics or number and name of samples and controls must be specified. This entire experiment was carried out as a double-blind method where lab technicians were completely unaware of the TCFs.

All samples were cast from one molten pot. Then, chemical analysis was performed on the samples to investigate any possibility of unwanted impurities and their effect on the properties. For this purpose, a sample from each series was randomly selected and subjected to spectrochemical analysis [7], the results of which are given in Table (2). The result shows that the composition of the samples is in the same category and there is no difference in the composition in a way that can significantly affect the properties.

Table 2 . Chemical composition of cast samples (one random sample from each group)

One random sample of the group X1(TCF)

Si	Fe	Cu	Mn	Mg	Cr	Ni	Zn	Ti	Be	Ca	Li
0.06	0.11	0.01	0.009	0.002	0.002	0.01	0.02	Trace	Trace	Trace	Trace
Pb	Sn	Sr	V	Na	Bi	Co	Zr	B	Ga	Cd	Al
0.01	< 0.005	Trace	0.008	0.005	0.01	0.02	Trace	0.0015	0.005	0.005	99.75

One random sample of the control group

Si	Fe	Cu	Mn	Mg	Cr	Ni	Zn	Ti	Be	Ca	Li
0.06	0.11	0.01	0.009	Trace	0.005	0.01	0.02	Trace	Trace	Trace	Trace
Pb	Sn	Sr	V	Na	Bi	Co	Zr	B	Ga	Cd	Al
0.01	< 0.005	Trace	0.009	0.004	0.02	0.01	Trace	0.0022	0.004	0.004	99.75

Some of the main properties of aluminum metal are high electrical conductivity, softness, and ductility as well as relatively good corrosion resistance at medium pH. Therefore, these properties were compared with the control samples and those under TCF.

Corrosion behavior was also investigated by potentiodynamic polarization test according to ASTM G1-03 (Re.17) & ASTM G3-14 standards [8]. For this purpose, SBF solution, which is a common medium in corrosion tests, was used. The Ag / AgCl (KCL-sat) reference electrode and the scanning rate of 0.5 mVs-1 were used at 37± 2º C temperature in one cm2 area and Counter Electrode: Graphite.

X-ray diffraction (XRD) by the reference standard BS EN 13925-1: 2008 was used to investigate the crystalline structure and lattice defects of atoms. The tests were performed with a copper anode at a voltage of 30 mA and a current of 40 kV. Step size was 0.02 and counting time per step was 0.5 sec. Structure analysis was performed by the Rietveld refinement method using Maud software [9].

Results and discussion

Corrosion resistance

The diagrams for the six samples are shown in (Figure 1). The formation of a small surface area has been seen in the samples which, after some fluctuations in current, disappeared and the intensity of the current increased rapidly (approximately horizontal line in the graph equivalent to critical pitting potential or Epit). After some corrosion, a layer of aluminum oxide was formed, and the graph tended to be vertical. This is a common process in aluminum corrosion testing [10].

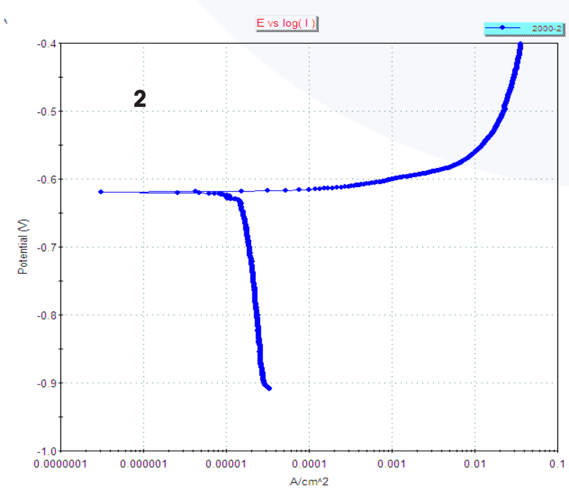

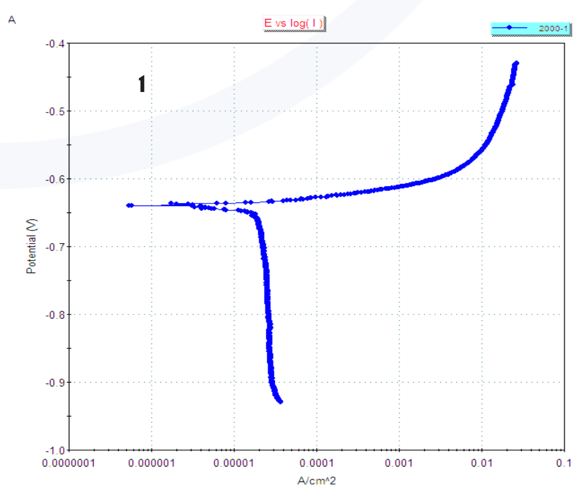

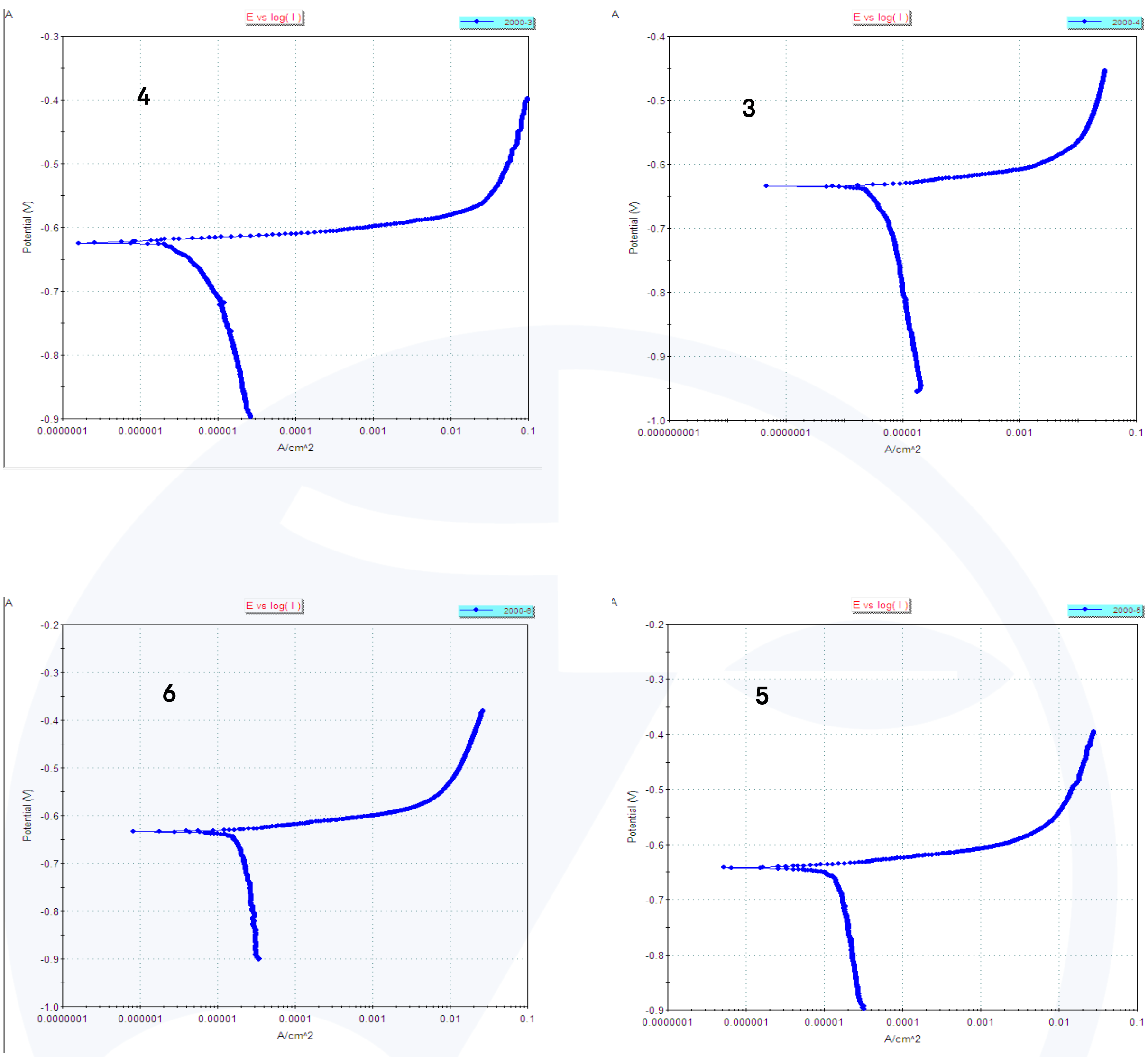

Figure 1. Graph of potential changes in terms of corrosion intensity for the three control samples 1, 2, and 3, and the samples 4, 5, and 6 under TCF.

In order to compare the corrosion rate in the two groups of samples, the corrosion current rate parameter can be used. High corrosion resistance in this test is demonstrated as low corrosion current density and low corrosion rate. The values extracted from the graphs are given in Table (3). Also, the mean values and standard deviation of corrosion potential (Ecorr) and the corrosion current density (icorr) for each sample are shown in Table (4). The corrosion rates average of the group under the TCF is lower than that of the control group, indicating better corrosion resistance. But the results of the corrosion test, which is an electrochemical process, are statistical, and in which there is an inherent dispersion in the results. Therefore, it is important to check if the differences are statistically significant.

Table 3 . Results of potentiodynamic corrosion test of the 6 aluminum samples in SBF

Name	Sample Code	Corrosion Current Density i_{corr} ($\mu A/cm^2$)	Corrosion Potential E_{corr} (mV)	Corrosion Rate mpy (mm/year)
Control Group	1	18.96	-651.482	8.10 (2.06E-1)
	2	14.86	-636.037	6.34 (1.61E-1)
	3	4.793	-624.367	2.05 (5.20E-2)
Group X1(TCF)	4	2.845	-643.658	1.26 (3.09E-2)
	5	13.24	-646.390	5.65 (1.44E-1)
	6	17.33	-650.501	7.04(1.88E-1)

Table 4 . Mean of current densities and corrosion potentials

Name	Current Densities Mean i_{corr} ($\mu A/cm^2$)	Change From Control %	Corrosion Potentials Mean E_{corr} (mV)	Change From Control %
X1(TCF)	11.138	**- 13.46%**	-646.852	**-1.5%**
Control	12.871		-637.507	

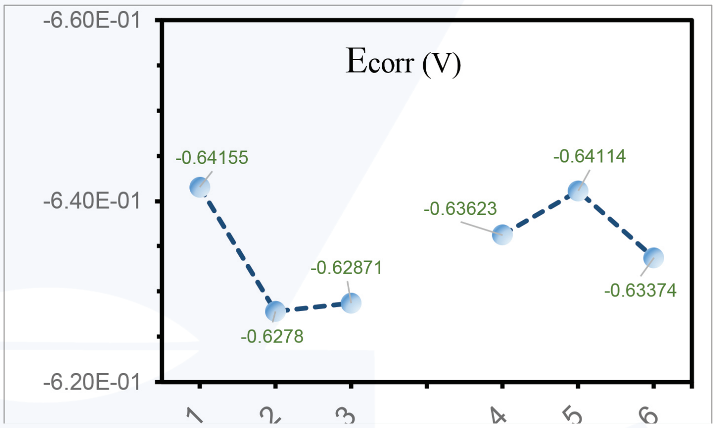

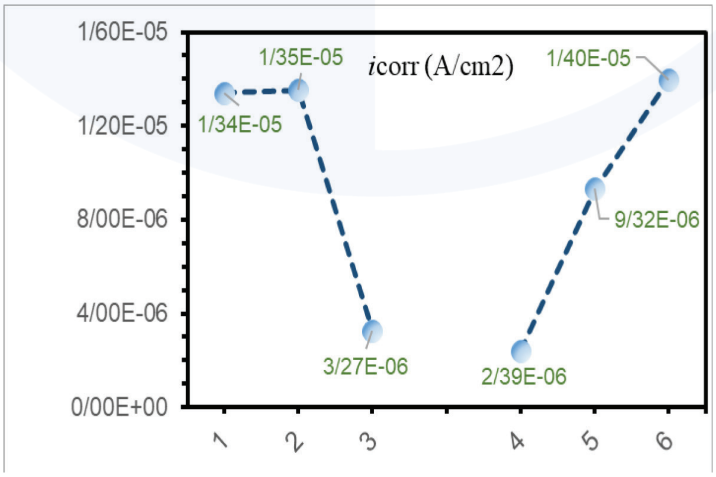

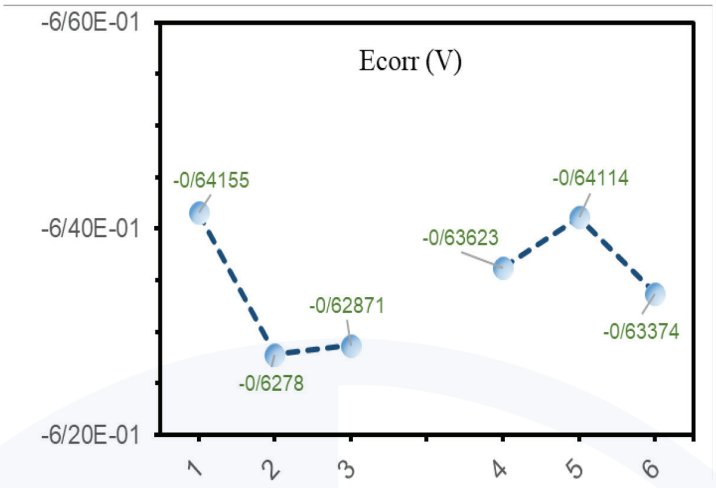

Figure 2. Graph of current density and corrosion potential based on the comparison between two groups, numbers 1, 2, and 3 are control samples, and 4, 5, and 6 are samples under the TCF.

As found in the pictures, the scattering of changes can be seen in the samples under the TCF as well as the control samples, and it is certainly not possible to comment on the effectiveness of this process in creating change.

Aluminum metal is prone to various corrosions, including Pitting Corrosion [11-12], Exfoliation Corrosion [13], Stress Corrosion [14], Filiform Corrosion [15], Water Line Corrosion [10], Crevice Corrosion [16], Cavitation [10], Erosion [17], Microbiological Corrosion [18], Transgranular and Intergranular (Intercrystalline) Corrosion [19].

Each series of aluminum alloys is more prone to a certain type of corrosion. The 1000 series aluminum used in this study is susceptible to intercrystalline corrosion. This corrosion is not visible to the naked eye and spreads at the border of grains and crystals. It is effective in changing the mechanical properties and the possibility of rupture. In water at a temperature of 60–70 ºC, the sensitivity to intercrystalline corrosion increases with the increasing purity of the metal.

To study this change, it is necessary to design more complete experiments to intensify the environment and more accurate equipment [19,10]. However, in the routine standard examination in this experiment, we see small changes in the corrosion process. The 1000-series aluminum is inherently resistant to this type of (tested) corrosion.

Microstructure analysis by XRD method

In order to investigate the possibility of affecting Consciousness Bond Field on the structure of matter in atomic dimensions, the XRD method was used to examine the structure of aluminum. Crystalline lattice information such as lattice parameter, size of crystalline areas, Lattice strain, and the possibility of some crystalline defects that can be examined by XRD analysis have specific effects on the behavior of materials [20-27].

Parameters related to the crystalline structure of aluminum samples and mean values groups and standard deviation for each group were calculated (Table 5).

Table 5 . Parameters related to the crystal structure of aluminum samples

Control									
	1	S.U.	**2**	S.U.	**3**	S.U.	**Mean**	Standard Deviation	%
Lattice Parameter	**4.0526676**	4.99E-05	**4.0526237**	5.18E-05	**4.050832**	5.18E-05	**4.0520411**	0.00	
crystallite size	**4626.9634**	384.4204	**4768.3184**	1.2199256	**3140.2742**	11.013911	**4178.518**	7.36E+02	
Microstrain	**2.24E-04**	1.48E-05	**3.44E-04**	1.06E-05	**3.47E-04**	1.11E-05	**3.05E-04**	5.71E-05	
intrinsic	1.79E-11		2.36E-06		3.41E-06		**1.92E-06**	1.42E-06	
extrinsic	3.91E-05		3.86E-05		3.84E-05		**3.87E-05**	3.062E-07	
Twin defect	5.21E-10		2.37E-07		1.52E-05		**5.16E-06**	7.128E-06	
X1(TCF)									
	4	S.U.	**5**	S.U.	**6**	S.U.	**Mean**	**Standard Deviation**	%
Lattice Parameter	**4.021798**	4.63E-05	**4.0499344**	4.63E-05	**4.051243**	4.97E-05	**4.0409918**	0.01	
crystallite size	**3543.1538**	9.770131	**5329.5815**	37.58558	**3506.65**	207.1544	**4126.461**	8.51E+02	
Microstrain	**3.49E-04**	1.01E-05	**2.44E-04**	1.20E-05	**3.05E-04**	1.23E-05	**2.99E-04**	4.32E-05	
Intrinsic	9.00E-06		2.57E-05		5.79E-10		1.16E-05	1.07E-05	504%
Extrinsic	5.04E-05		4.88E-05		6.62E-05		5.51E-05	7.844E-06	40.24%
Twin defect	4.83E-07		6.92E-06		1.97E-09		2.47E-06	3.155E-06	-50.21%

Discussion and review of the changes of XRD

Lattice parameter

The lattice parameter refers to the physical dimensions of the unit cell in a crystalline lattice. If the ratio is smaller, it means that the lattice is more compact, and if it is larger, it means that the lattice is more expanded [20-27]. No significant changes were observed in this parameter for the samples.

Lattice strain (Microstrain)

Crystalline lattice size differences lead to the formation of lattice strain [20-27], and in the average of the samples under the CF a slight difference has arisen.

Crystalline size

This factor is partly representative of the crystalline cells that must be created without strain or defect [20-27]. This parameter is somewhat representative of crystalline cells that are considered almost without strain or defect [20-27]. It is related to the lattice strain and has changed slightly under the CF just like strain.

Intrinsic defects

In the CF group, this defect is seen more with a difference by an average of (~504%).

Extrinsic Defects

This disorder has increased under the CF by an average of (~ 40%).

Twin Defects

Twin defects represent a special type of boundary that is created by the mirror symmetry of the crystalline lattice. The twin boundary increases the strength of the material. This parameter has decreased on average (~ % 50).

Conclusion

- Extrinsic defects in the TCF group increased on average (~ 40%) compared to the control group.
- Intrinsic defects in the group under the TCF increased by an average of (~ 504%) compared to the control group.
- Twin defects in the group under the TCF decreased by (~ 50%).

In general, a crystalline defect is a disorder of the atoms and ions' order in a part of the crystalline lattice of matter. Manufacturing processes, such as mechanical work and metal deformation, can increase lattice defects and strain. Entering alloy elements can also affect atomic distances and lattice parameters [28-29].

Being one-element, similarities in composition and impurities in the samples and no difference in how they are processed, make the factor of Consciousness Bond Field to be recognized as the possible cause for these changes. Also, in pure aluminum (1000-series), electrical conductivity, ductility, and corrosion resistance are among the inherent properties [10].

According to the study of aluminum without preheating [30] Since pure aluminum (99.75% purity, according to spectrochemical analysis after casting) is used in this research and according to the principles of T-Consciousness and TCFs, the pure elements of the Mendeleev table are included in the category of fixed TCFs, the pure aluminium is not influenced by the variable TCFs, which is Consciousness Bond Field in this study. In other words, participation in reaction by pure aluminium due to the influence of this Field is not expected, and some of the principal factors of this metal remain in a stable state [30].

The structure of crystal lattice is related to the collection of atoms and the above experiment shows that the variable TCFs of Consciousness Bond Field influence the collective properties and not the individual properties. It should be noted that the effect of the variable TCFs, such as Consciousness Bond Field on materials with chemical compounds is to change the reactions [5]. But in the case of pure materials from the point of view of the matter, changes in the principal factors are not expected. However, the same material is a collection of millions of atoms, and in terms of atomic structure, changes in the collection of atoms are possible. Therefore:

Unalloyed aluminum under the Consciousness Bond Field was more disordered in terms of crystalline lattice structure and no significant changes were observed in the properties [30].

Determining the physical and microstructural mechanisms that have occurred to alter properties under the TCF requires more specialized studies using more equipment. But preliminary results show that TCF as a factor independent of matter and energy and even information could have measurable effects on matter.

Acknowledgment

We are very grateful for the support and advice of Dr. Mojtahedi in this research.

References

1- Nowtash. M.R, World and aluminum, and Iran stand in the perspective horizon of Islamic Republic of Iran1404/ Technology Development Quarterly journal. (2005)
2- Kazazi. B, Taheri. M. A; Effect of the Consciousness Bond Field on the structure and properties of Aluminum. (2021)
3- Taheri, M. A. Human from another outlook Interuniversal Press; 2nd Edition ISBN-13: 978-1939507006, ISBN- 10: 1939507006. (2013)
4- Taheri MA. General Connection of particles. Interuniversal Publishing.Erfan-Hlgheh. ID: 978-1-940491-03-5.(2012)
5- Kazazi.B, Taheri.M.A; Meshkin-Far.A, Influence of the Consciousness Field on the Cement Properties and Behavior", Science of Consciousness, Tucson, Arizona, (2020)
6- www.cosmointel.com
7- Busch. K.W, Bush.M.A, Multielement Defection Systems for Spectrochemical Analysi. (1990) ISBN 0-47-81974-3
8- www.ASTM.org , ASTM E1004
9- Lutterotti . L , Total pattern fitting for the combined size–strain–stress–texture determination in thin film diffraction Nucl. Instrum. Methods Phys. (2010) Res, Sect. B 268 334–40
10- Vargel.Ch, CRROSION OF ALUMINIUM, Elsevier. (2004), ISBN 008044495-4 ,p 28-150
11- Kaesche H., Me´canisme de la corrosion par piqu^res, Corrosion Traitements Protection
Finition, vol. 17 (1969), p. 389–396.
12- Reboul M., Warner T., Mayet H., Baroux B., A ten step mechanism for the pitting corrosion of aluminium alloys, Corrosion Reviews, vol. 15, nos 3–4 (1997), p. 471–496.
13- Ketcham S.J., Shaffer I.S., Exfoliation corrosion of aluminum alloys, ASTM, STP, vol. 516, (1972), p. 3–16.
14- Rawdon H.R., Krynitski A.I., Berliner J.F., Brittleness developed in aluminium and duralumin by stress and corrosion, Chemical Metallurgy Engineering, vol. 26. (1922), p. 154–160.
15- Rique J. P., La corrosion filiforme dans les peintures pour l'ae´ronautique, Surfaces, vol. 117, (1984), p. 55–66.
16- Reboul M., Touche M., Examen de deux radeaux en aluminium apre`s 8 et 35 ans en mer,
rapport Pechiney CRV. (1983).
17- Dillon R.L., Hope R.S., Erosion–corrosion of aluminum alloys, REV, rapport HW-74359,
April. (1953).
18- Hedrick H.G., Crum M.G., Reynolds R.J., Culver S.C., Mechanism of microbiological
corrosion of aluminum alloys, Electrochemical Technology. (1967), p. 75–77.
19- Rohrmann F., Transactions of the Electrochemical Society, vol. 66 ,(1934), p. 229.
20- Snyder. R. L., Fiala.J., Bunge. H. J., Defect and Microstructure Analysis by Diffraction, Oxford Science Publication ISBN.0198501897(Hbk). (2000).
21- Scardi. P., Ermrich. M., Fitch. A., Wen Huang.E., Jardin.R., Kuzel.R., Leineweber. A., Mendoza Cuevas.A., Misture. S. T., Rebuffi.L., Schimp.CH., Size - strain separation in diffraction line profile https://doi.org/10.1107/S1600576718005411.(2018).
22- Soleimanian.V., Mojtahedi.M., A comparison between different X-ray diffraction line broadening analysis methods for nanocrystalline ball-milled FCC powders. (2015). DOI 10.1007/s00339-015-9054-y.
23- Zheng .Yu.Jie., Ying Quek .Su., First Principles Study of Intrinsic and Extrinsic Point Defects in Monolayer WSe2. (2019). arXiv:1901.05238
24- Warren. B. E., X-RAY STUDIES OF DEFORMED METALS.- Review of a research programme sponsored by the U.S. Atomic Energy Oommi~sion. (1959)
25- Feret. F.R, Selected applications of Rietveld analysis in the aluminium industry. International Tables for Crystallography .(2019). Vol. H, ch. 7.6, doi:10 .1107/97809553602060000980
26- Huang. Y., Langdon T.G., "Using atomic force microscopy to evaluate the development of mesoscopic shear planes in materials processed by severe plastic deformation. Materials Science and Engineering, Vol. A 358, (2003).
27- WWW.EDU.nano.ir
28- Jafaril.M, Jamshidian.M, Ziaei-Rad.S, Investigating the Stored Deformation Energy Distribution in a Polycrystalline Metal using a Dislocation Density-based Crystal Viscoplasticity Theory/ Computational Methods in Engineering. Isfahan University of Technology (IUT)/ DOI: 20.1001.1.22287698.1397.37.2.5.1/(2019).
29- Humphreys. M., Hatherly. F., Recrystallization and Related Annealing Phenomena, Second Edition. Elsevier. (2002). ISBN:0080426859.
30- Kazazi. B, Taheri. M. A; Effect of the Consciousness Bond Field on the structure and properties of Aluminum. (2021). www.cosmointel.com

A Study of the Effect of Taheri Consciousness Bond Field on the Mechanical Crushing of Silica Particles

Bahareh Kazazi[1*], Mohammad Ali Taheri[2]

1. Civil Engineering, CEO of Hoobe Construction Company, Tehran, Iran.

2. Sciencefact R&D Department, Cosmointel Inc. Research Center, Ontario, Canada.

* Corresponding author:

Bahareh Kazazi
Civil Engineering, CEO of Hoobe Construction Company, Tehran, Iran.

Email: baharkazazi@gmail.com

ABSTRACT

One of the materials used in various industries is silica. To achieve silica of different dimensions, mainly the method of crushing silica minerals is utilized. Taheri Consciousness Fields (TCFs) were founded and introduced by Mohammad Ali Taheri as new Fields more than four decades ago. These Fields are immaterial and non-energetic, so they have no quantity, but they have direct effects on matter and energy. In other words, although TCFs are not directly measurable, we can indirectly study their effects with various controlled experiments. Therefore, the study of the effect of the Consciousness Bond Field, as one of the Fields, on the process of crushing pure silica is the subject of this study. Initially, relatively pure silica grain (98% purity) was prepared. 10 samples were prepared, 5 of which were put under Consciousness Bond Field. Each sample included 50 grams' of silica in a titanium mechanical mill with 4 bullets of size 20, 20 bullets of size 15, 20 bullets of size 10, and 8 bullets of size 12. They were all under the same thermal and physical conditions and were milled alternately XRD (X-ray diffraction), DLS (Dynamic Light-Scattering), Zeta Potential (Electro-kinetic Potential), once with ultrasonic bath, once without ultrasonic, TEM (Transmission Electron–Microscopy), and SEM (Scanning Electron Microscopy) tests were done on the samples. It was found that in the samples under TCF, the strain of the crystalline lattice decreased, the distribution of the particles was more uniform, and the size of the smallest particles decreased. The electric charge of the particles' surface immediately after milling was dispersed in the samples under the TCF and finally, the resultant charge of the particles' surface neutralized each other after the use of an ultrasonic bath the TCF effect was reduced, and the surface load was measurable.

Keywords: Mechanical milling, crushing, silica, Consciousness Bond Field, Taheri Consciousness Fields

INTRODUCTION

One of the materials used in various industries is silica. Silica is not very usable as a crystal or mineral and for better performance, it needs to be reduced to smaller dimensions and in the best conditions nanometers in different ways. One of the most cost-effective methods is to mill silica rocks. The way of milling can break the material to nanomaterial dimensions. For this purpose, it is necessary for about 50% of the crystal dimensions of the particles to be between 1 and 100 nm [1]. Since the main purpose of this study was not to create nanomaterials but to investigate the effect of the immaterial factor of the Consciousness Field on the mechanical work process, so the test method was chosen to control the adhesion of the material to the wall and only the effect of the Consciousness Field on the mechanical work was studied.

One of the materials used in various industries is silica. Silica is not very usable as a crystal or mineral and for better performance, it needs to be reduced to smaller dimensions and in the best conditions nanometers in different ways. One of the most cost-effective methods is to mill silica rocks. The way of milling can break the material to nanomaterial dimensions. For this purpose, it is necessary for about 50% of the crystal dimensions of the particles to be between 1 and 100 nm [1]. Since the main purpose of this study was not to create nanomaterials but to investigate the effect of the immaterial factor of the Consciousness Field on the mechanical work process, so the test method was chosen to control the adhesion of the material to the wall and only the effect of the Consciousness Field on the mechanical work was studied.

The nature of consciousness and its place in science has received much attention in the current century. Many philosophical and scientific theories have been proposed in this area. In the1980s, Mohammad Ali Taheri introduced novel fields with a non-material/non-energetic nature named Taheri Consciousness Fields (TCFs). In this perspective, T-Consciousness is one of the three existing elements of the universe apart from matter and energy. According to this theory, there are various TCFs with different functions, which are the subcategories of a networked universal internet called the Cosmic Consciousness Network (CCN). The major difference between the theory of TCFs and other theoretical concepts about consciousness is related to the practical application of the TCFs. TCFs can be applied to all living and non-living creatures, including plants, animals, microorganisms, materials, etc.

Mohammad Ali Taheri, the founder of Erfan Keyhani Halqeh, a school of thought, introduced a new science in 2020 as a branch of this school. He coined the term Sciencefact for this new science because it utilizes scientific investigations to prove the existence of T-Consciousness as an irrefutable phenomenon and a fact. Although science focuses solely on the study of matter and energy and Sciencefact, by contrast, explores the effects of the [non-material/non-energetic] TCFs, Sciencefact has provided a common ground between the two by conducting reproducible laboratory experiments in various scientific fields, and it has used the scientific approach in proving TCFs.

The influence of the TCFs begins with the Connection between CCN as the Whole Taheri Consciousness of the universe and the subjects of study as a part. This Connection called "Ettesal" is established by a certified and trained individual who has been entrusted with the TCFs. The human mind has an intermediary role (Announcer) which plays a part by fleeting attention to the subject of study and then the main achievement obtained as a result of the effects of the TCFs. These Fields cannot be directly measured by science, but it is possible to investigate their effects on various subjects through reproducible laboratory experiments.

The research methodology in the study of T-Consciousness has been founded on the process of Assumption, Argument, and Proof, in which the basic Assumption is: The Cosmos was formed by a third element called T-Consciousness that is different from matter and energy.

The Argument: The existence of TCFs can be demonstrated by its effects on matter and energy (e.g., humans, animals, plants, microorganisms, cells, materials, etc.)

The Proof: is the scientific verification of the effects of TCFs on matter and energy (according to the Argument) through various reproducible scientific experiments.

Accordingly, to investigate and verify the existence, effects, and mechanisms of TCFs, the following five research phases (Phases 0 through 4), and the aims of each phase are outlined below.

Phase-0 studies aim to prove the existence of TCFs by observing their effects. The nature of T-Consciousness and what it is will not be addressed in this phase. Phase-1 explores the varied effects of different TCFs. Phase-2 examines the reason behind the varied effects of these fields. Phase-3 investigates the mechanism of TCFs effects on matter and energy. Finally, Phase-4 draws significant conclusions, particularly with regard to the mind and memory of matter and their relation to the T-Consciousness, etc. [2-5]

Method and materials

Materials

Initially, relatively pure silica grain (98% purity) was obtained from a mineral that had previously been subjected to quality control. 10 samples were prepared, 5 of which were put under the Consciousness Field. Each sample included 50 grams of silica in a titanium mill with 4 bullets of size 20, 20 bullets of size 15, 20 bullets of size 10, and 8 bullets of size 12 under the following conditions: Time: 3hr; 15 ‘on; rest: 5’; rate: 400 rpm; ball/(material):10/1

And the same heat and physical conditions were applied to all samples, and they have milled alternately.

Table 1 . Groups synthesized simultaneously and under exactly the same conditions.

Names of the Control Samples	1	2	3	4	5
Names of the Samples under the TCF	H	I	J	K	L

Figure 1 - Schematic drawing of the concrete cracking process by alkali-silica reaction

Application of Taheri Consciousness Fields

One of the introduced TCFs, is called the Consciousness Bond Field and was applied to the samples according to the protocols regulated by the COSMOintel research center (www.COSMOintel.com). A request for Connection to the CCN to utilize TCFs can be placed through the COSMOintel website in the "Assign Announcement" section. This access is available for everyone at no cost. In order to study and experience this Connection, the researchers can register on the website at any time in order to report the experiment to the COSMOintel research center. Certain details of the experiment must be provided to the center; for example, the characteristics or number and name of samples and controls must be specified. This entire experiment was carried out as a double-blind method where lab technicians were completely unaware of the TCFs.

Analysis Method

XRD (X-ray diffraction) according to standard BSIBS En139251-2 and Generator Settings: 40 mA, 40 kV, Anode Material: Cu, Step Size [°2Th.]: 0.0260.

TEM (Transmission electron microscopy) by Zeiss EM900

Zeta Potential (Electro-kinetic Potential) and DLS (Dynamic Light Scattering) Were done by (Malvern-Nano ZS (red badge) ZEN 3600) and Dispersant Name: Water; Dispersant IR:1.336; Viscosity (Cp):0.8872; Dispersant Dielectric Constant:78.5

And zeta-potential re-testing by applying a 50 Hz ultrasonic with Bandelin device for 5 hours. All analyzes were done according to ISO 7-1502-3001 at 25 ℃, 19% RH humidity, and 1atm pressure. And finally, SEM (Scanning electron microscopy) was done on all samples.

Results and discussion

XRD (X-ray diffraction)

To identify the phases of matter Highscore plus X'Pert software was used. The results are presented below.

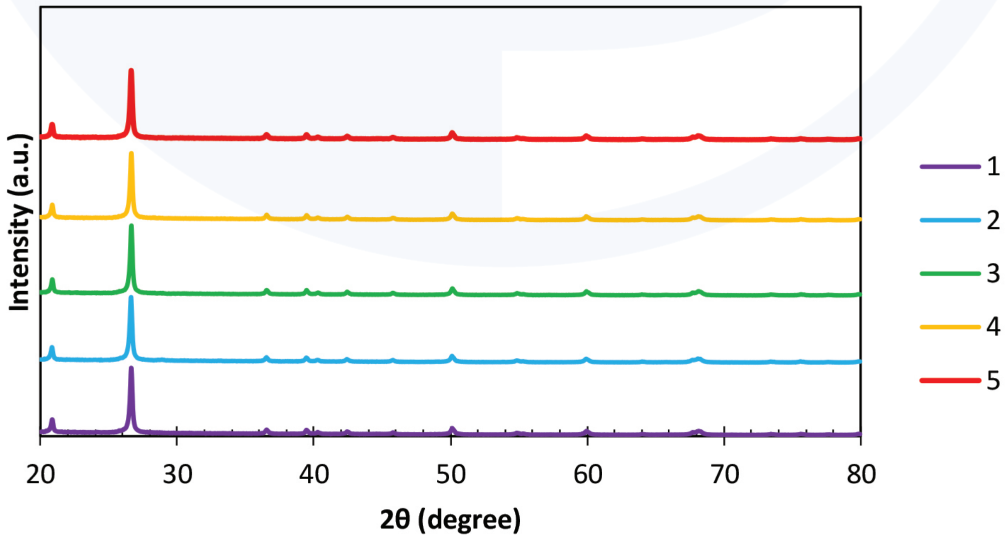

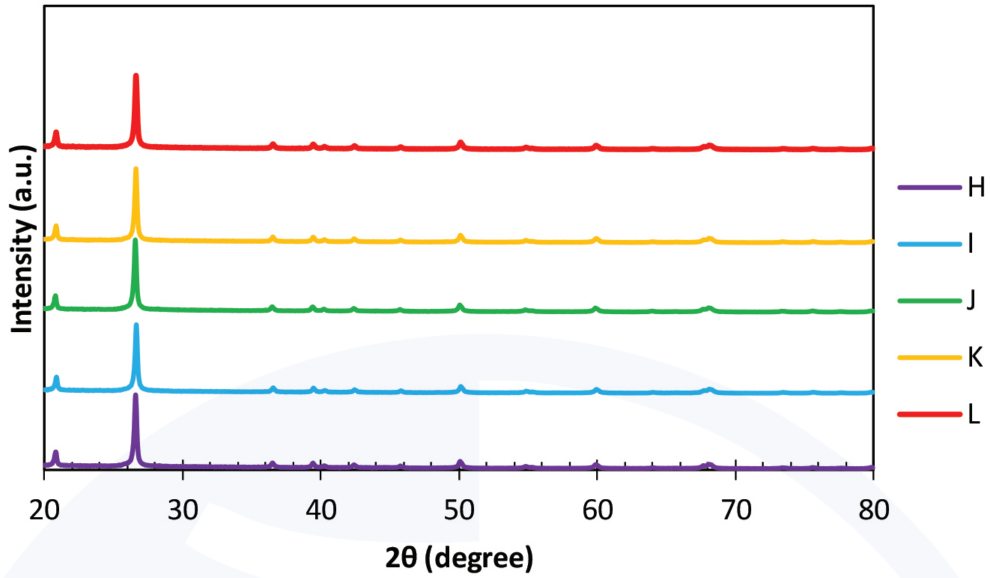

Figure 2 - X-ray diffraction pattern of the sample relating to SiO2 samples

According to Figure 2 and by matching this diffraction pattern with the reference diffraction patterns, it was determined that this diffraction pattern related to the quartz phase (SiO_2) with the reference code JCPDS No. 01-078-1252 had a hexagonal crystal structure and space group P3121. In this structure, diffraction plates (100), (011), (110), (102), (200), (021), (112), (202), (121), (212) and (203) were respectively Observed at angles of 20.8 °, 26.6 °, 36.5 °, 39.4 °, 42.4 °, 45.7 °, 50.1 °, 54.8 °, 59.9 °, 67.6 ° and 68.1 °. These results showed that no phase other than quartz was observed in these samples.

To accurately examine the small values obtained from the XRD test related to these samples, the Rietveld method was used using MAUD software. This method is a technique proposed by Hugo Rietveld for use in the identification of crystalline materials. In this technique, the height, width, and position of each peak in its X-ray diffraction pattern can be used to determine many structural aspects of the material. Rietveld technique uses the least-squares method to better fit the theoretical values on the measured values [6,7]. The results of this method are shown in Table 2.

Table 2 . Quantitative results of Rietveld method XRD test

Samples	a (Angstrom)	c (Angstrom)	Crystallite Size (nm)	Micro strain
1	4.918	5.410	69.639	4.10×10^{-7}
2	4.919	5.410	69.640	3.77×10^{-7}
3	4.919	5.411	69.638	3.99×10^{-7}
4	4.919	5.411	69.640	5.99×10^{-7}
5	4.919	5.410	69.640	4.76×10^{-7}
H	4.918	5.410	69.639	4.10×10^{-7}
I	4.919	5.411	69.640	1.23×10^{-8}
J	4.918	5.410	69.640	1.74×10^{-10}
K	4.918	5.411	69.640	3.37×10^{-10}
L	4.919	5.411	70.916	7.99×10^{-9}

According to the results reported in Table 2, the values of the grid parameter in the hexagonal structure were equal to 4.918 to 4.919 angstroms for the horizontal grid parameter (a) and 5.410 to 5.411 angstroms for the vertical grid parameter (c). These values indicate that the grid parameter values are almost equal in all samples and the variables have no effect on the crystal structure of the material. Also, the size of the crystallite obtained for different samples was very close to each other and only the crystallite size of the sample (L) was slightly larger than the other samples. In addition, the micro-strain in all samples was very small and in the range of less than 10 to the negative power of 6. This indicates that there was no internal stress in the crystal structure of the samples and the grid distortion in the obtained crystal structures was very small. According to these results, the micro-strain and as a result, the distortion of the crystal grid in the samples under the CF was less than in the control samples.

Table 3 . Percentage of changes of mean micro-strain

	Under CF	Control	Percent of changes%
Mean micro-strain	8.616×10^{-8}	4.522×10^{-7}	-80.946

DLS and Zeta potential

Dynamic Light Scattering (DLS) is a physical method used to determine the distribution of particles in solutions and suspensions. This non-destructive and fast method is used to determine the particle size in the range of a few nanometers to microns. In this method, the scattered light by the nanoparticles in the suspension changes with time, which can be related to the particle diameter. What is obtained in this test for the particle size is the hydrodynamic diameter of the particles and, therefore, the values obtained in this test are different from the values obtained from the microscopic test [8].

DLS and zeta potential tests have been used to investigate the hydrodynamic particle size as well as the condition of the particles within the colloid. Figure 3 shows the particle size distribution histograms for the samples.

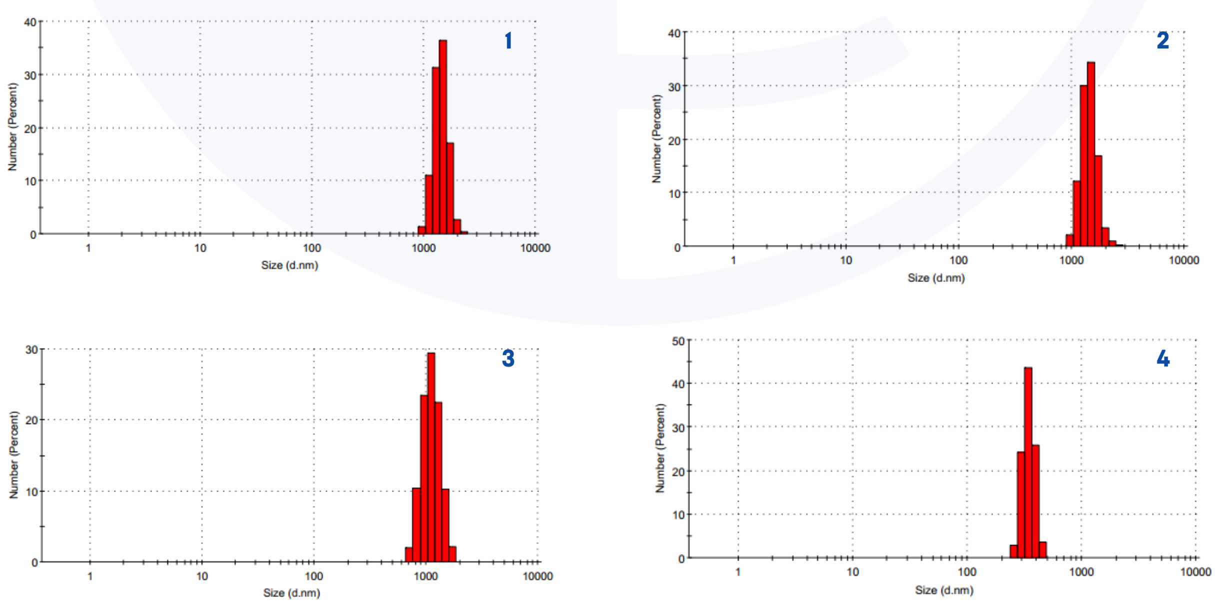

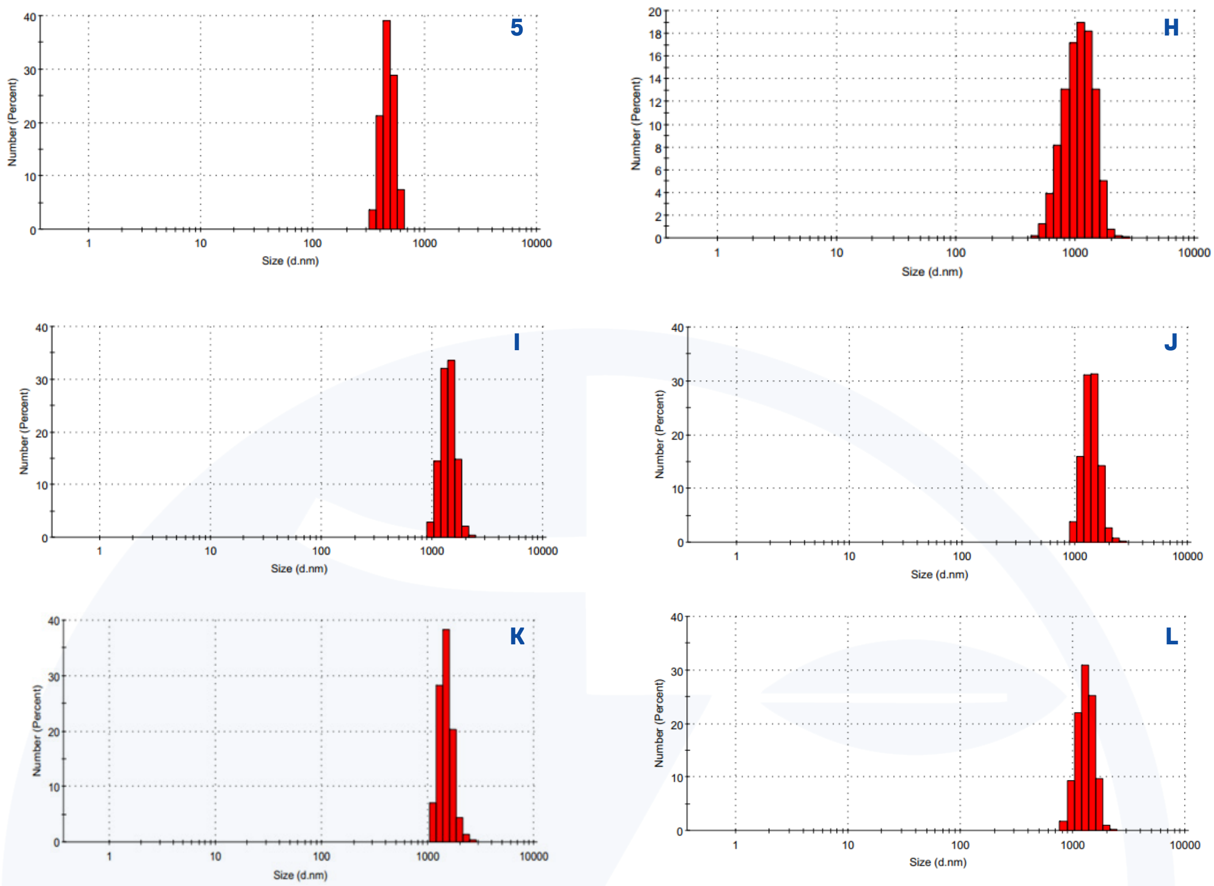

Figure 3 - The particle size distribution histograms from the DLS test for samples 1, 2, 3, 4, and 5 (control) as well as samples H, I, J, K, and L (under the TCF)

According to the results shown in the histograms, it seems that samples (4) and (L) had the lowest and highest particle sizes, respectively. Also, the widest and narrowest particle size distributions were related to samples (H) and (4), respectively. The narrow particle size distribution means that the particle sizes were closer to each other and less different. For a more detailed study of the values obtained in this test, the parameters of mean and standard deviation were obtained and shown in Figure 4.

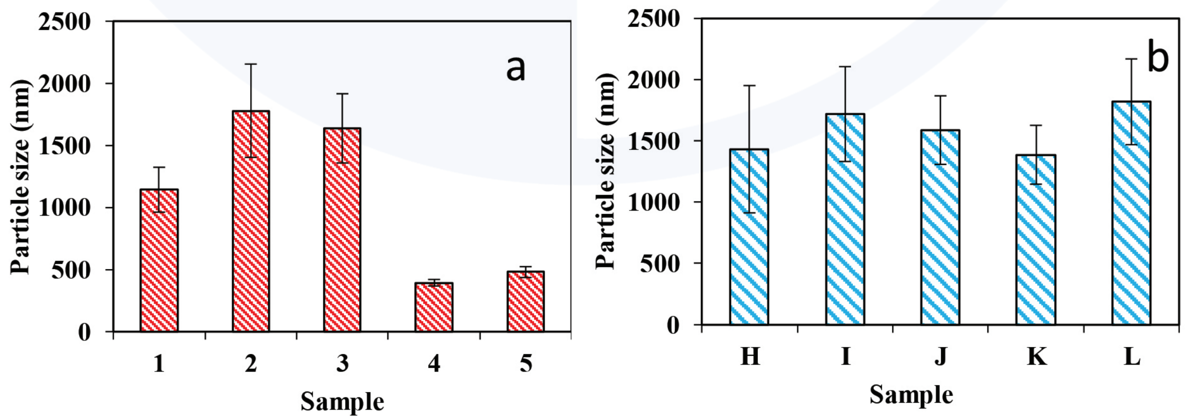

Figure 4- Changes in the mean particle size and standard deviation of the DLS test for samples of the control group (a), and samples under the TCF (b).

According to the results seen in Figure 4, the mean values in the sample (4) in the first group and sample (K) in the second group had the lowest values among the samples of each group. In addition, the largest particle size in the first group belonged to sample (2), and in the second group belonged to sample (L). It is also known that the average particle size in the samples under Consciousness Bond Field is larger than the first group. It is also clear that unlike the control group, where the difference in particle size with each other is relatively large (particle size range of about 400 to 1800 nm), in the group under the Consciousness Bond Field, the particles have almost similar sizes (particle size range of about 1400 to 1800).

Zeta Potential

The surface charge of a particle in a fluid is called zeta potential [10].

Zeta potential test is another method of evaluating the stability of nanoparticles in a suspension, the results of which can be related to the size of the hydrodynamic particles extracted from the DLS test. The results of this test are shown in Figure 5.

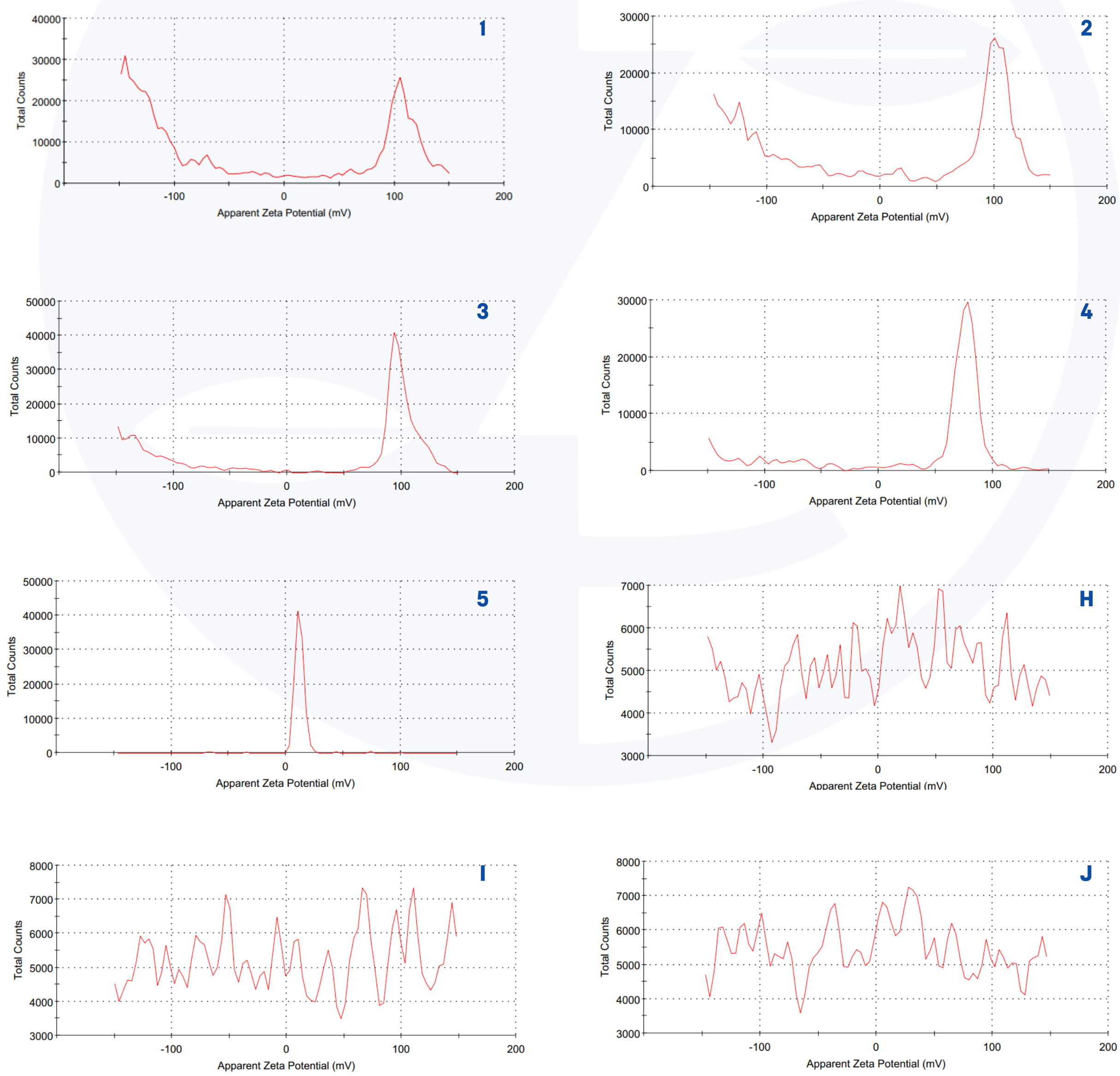

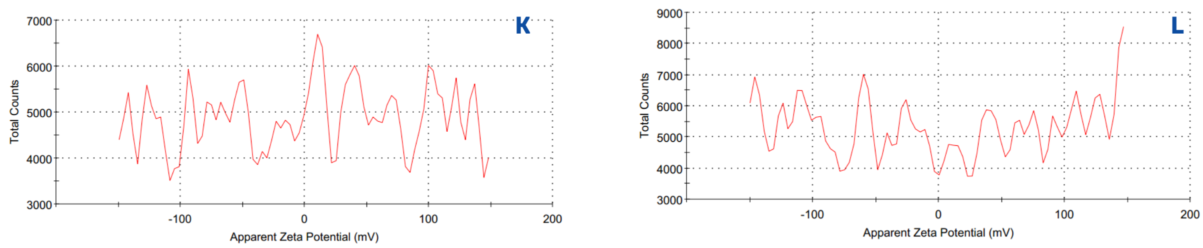

Figure 5- Zeta potential histogram of control samples 1,2,3,4,5 and samples H, I, J, K, L under TCF

According to these histograms, it is clear that all the graphs related to the group under the TCF are noisy, and these noises have caused the area under the curve in the whole histogram to move the mean value compared to the peak sharpness visible in the results. For this purpose, the mean value of the zeta potential is calculated and the bar graphs related to this parameter for different samples are shown in Figure 6.

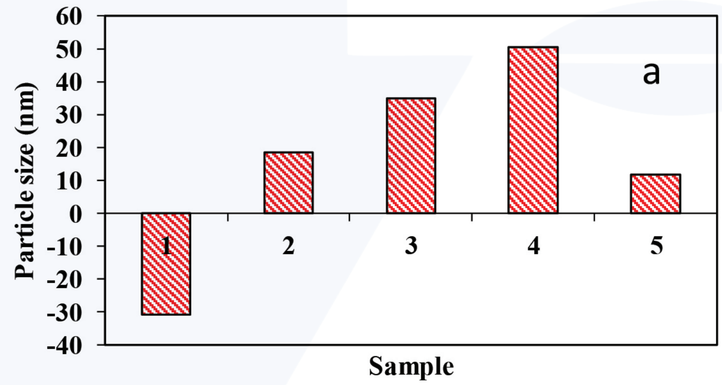

Figure 6- Changes in the mean value of the zeta potential for samples (a), the group as the control

It has been proven that the tendency of particles to repel each other is directly related to the zeta potential and, therefore, the boundary between the stability and instability of the suspension can be determined in terms of zeta potential. It is stated that particles with a zeta potential of more than 30 mV or less than -30 mV are stable in the diffuser bed [8,9]. In fact, the zeta potential of more or less than ± 30 mV causes an electrostatic repulsion force between the particles in the suspension and leads to the stability of these particles. Therefore, according to the results shown in Figure 5 in the control group, samples (1), (3), and (4) can be stable in colloids. In other samples, especially under CF, the cause of excessive noise and probabilities must be considered.

Examining the results of zeta potential, the following can be mentioned:

Sometimes samples contain a variety of chemicals that are not completely homogeneous, and the residual material in solution shows different charges due to the application of an electric field, and scattering or so-called noise appears. Given the complete purity of the material, this assumption is not acceptable. The second assumption is the agglomeration and non-uniformity of the sample, which is not accepted due to the good results of DLS. The third hypothesis is the possibility of the presence of fine particles around larger particles that show their surface charge due to the electric field of each particle [10] and changes in different levels appear as scattering and noise.

To investigate this possibility, in addition to TEM and SEM tests, zeta-potential re-testing was done by applying a 50 Hz ultrasonic bath with a Bandelin device.

Zeta potential with ultrasonic 50 Hz for 5 hours.

The results of the zeta potential test are shown in Figure 7.

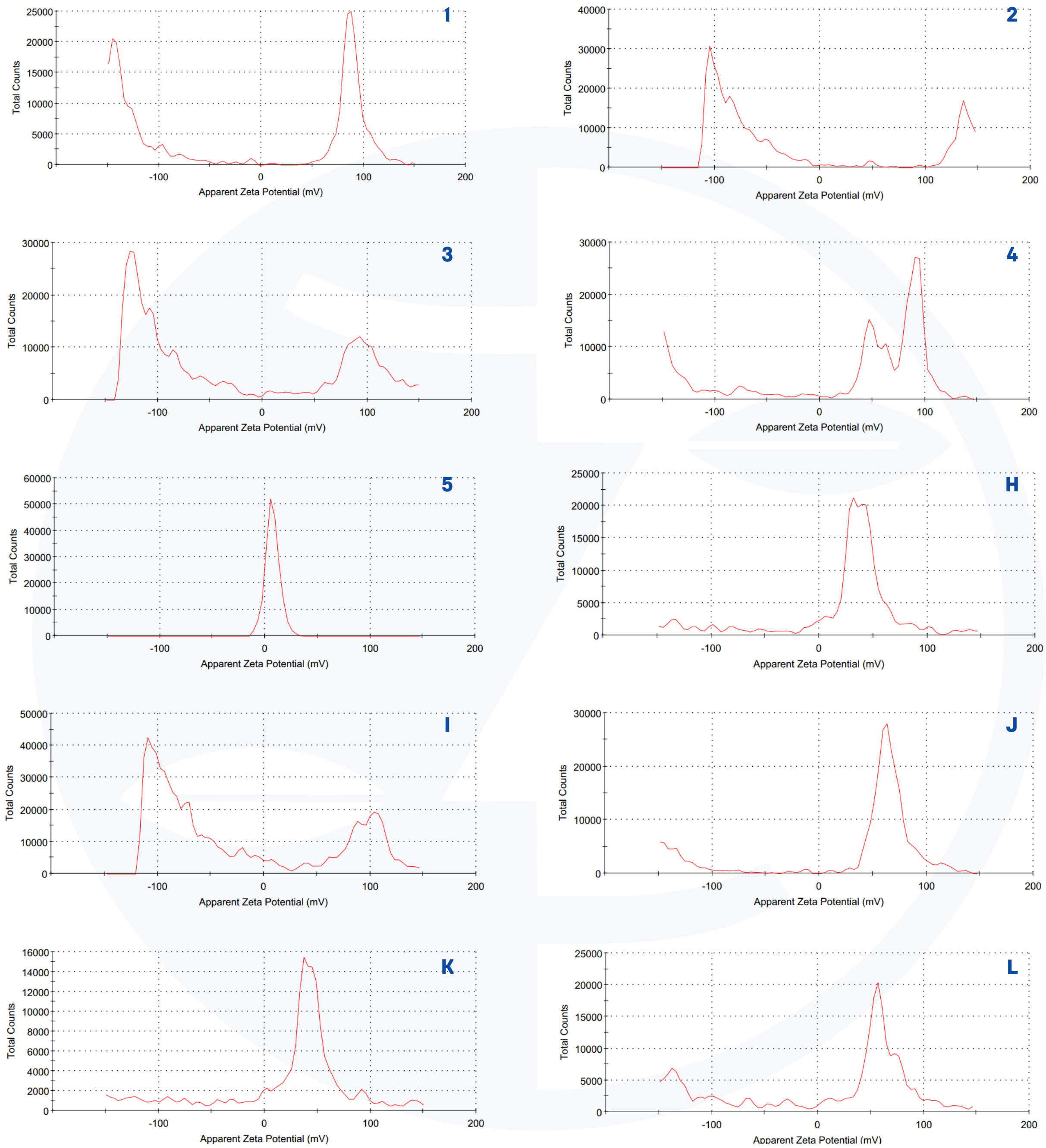

Figure 7- Zeta potential histogram of control samples 1,2,3,4,5 and samples H, I, J, K, L under CF

According to these histograms, it is clear that except for samples (1) and (5) (and to some extent sample 4), the amount of zeta potential of the other samples has changed a lot compared to before. In the second group of samples (under the TCF) in particular, the spectrum of zeta potential changes is completely out of noise and scattering, and certain peaks can be observed in these spectra, which can increase the reliability of the results. The changes in the mean values of the zeta potential are plotted in Figure 8 in the form of bar graphs.

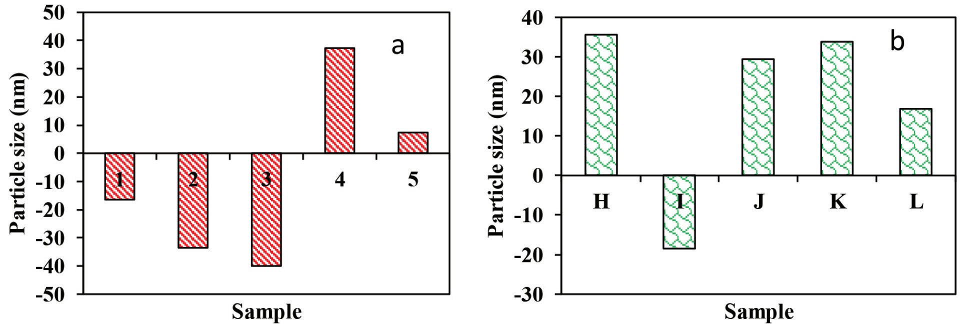

Figure 8- Changes in the mean value of the zeta potential for the control samples (a) and samples under TCF (b)

Therefore, according to the results shown in Figure 8 in the first group, samples (2, 3) and (4) can be stable in colloids. In the second group, samples (J, H) and (K) in the colloid can also be stable.

TEM (Transmission electron microscopy)

The results of the TEM test for the samples are shown in Figure 9.

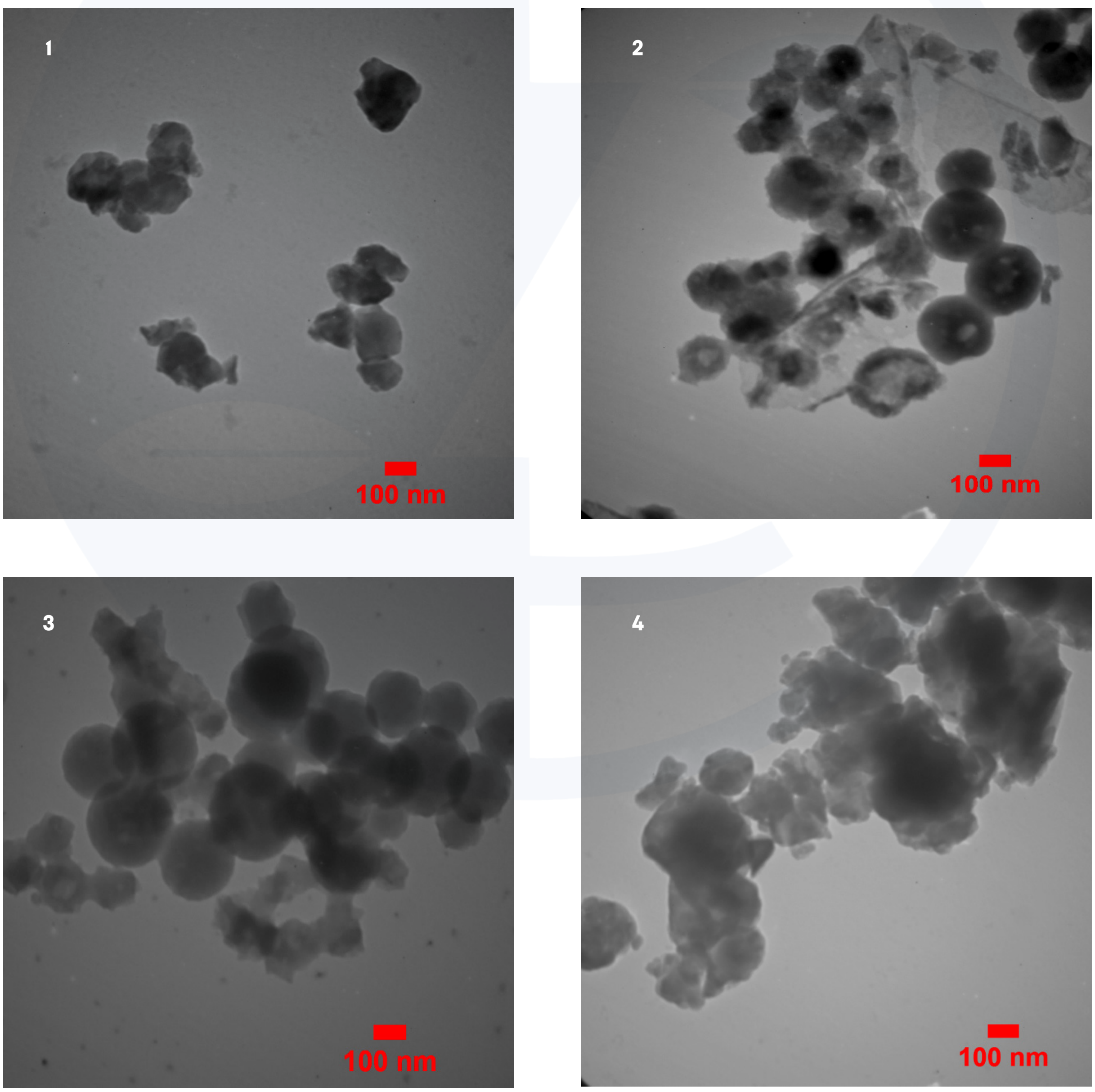

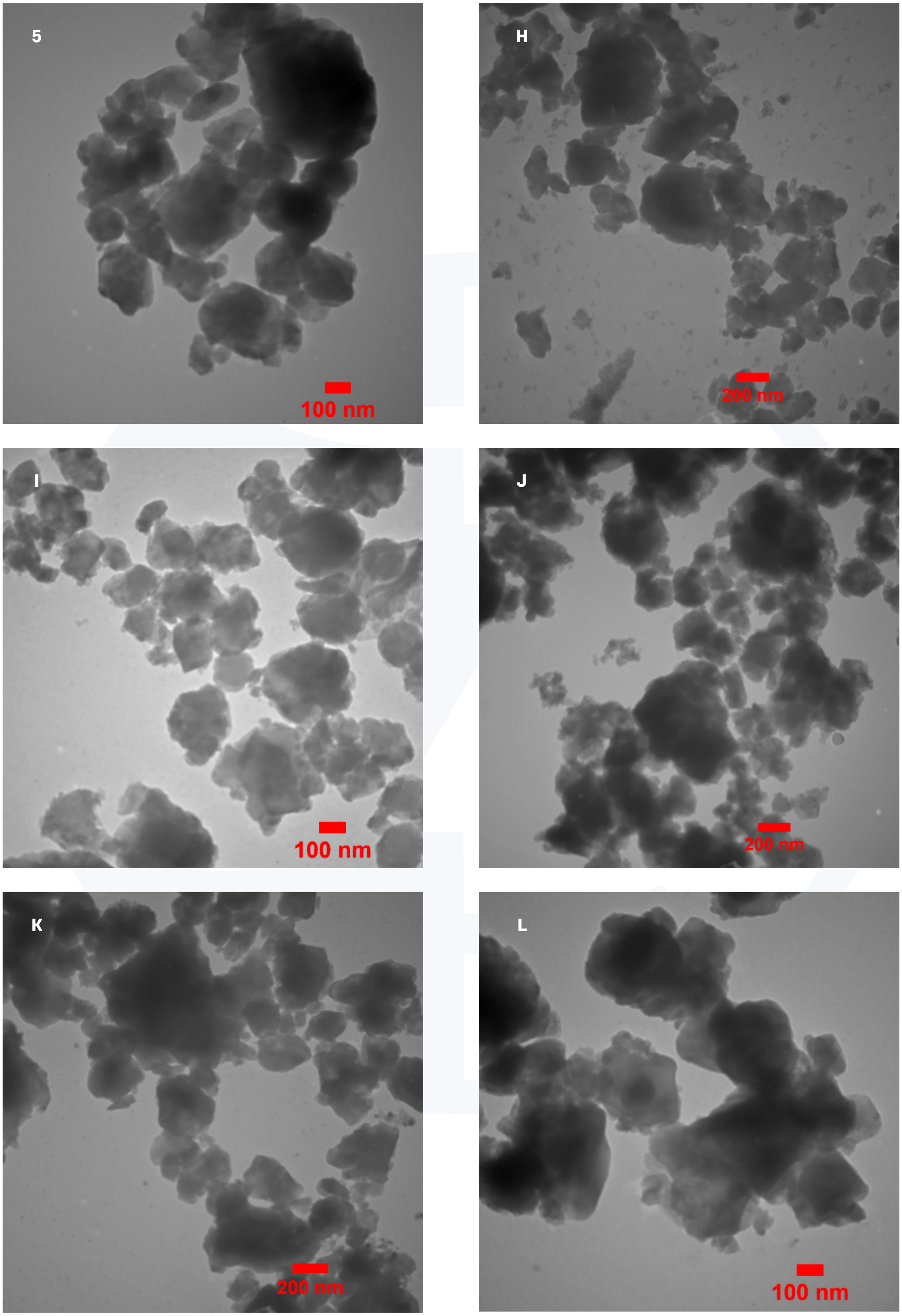

Figure 9- TEM test results for the control samples (1, 2, 3, 4, 5), and samples under TCF (H, I, J, K, L).

To check the particle size of each sample, in each sample, 50 particles of TEM images were measured by J-image processing software, and the histograms obtained from this measurement are shown in Figure 10.

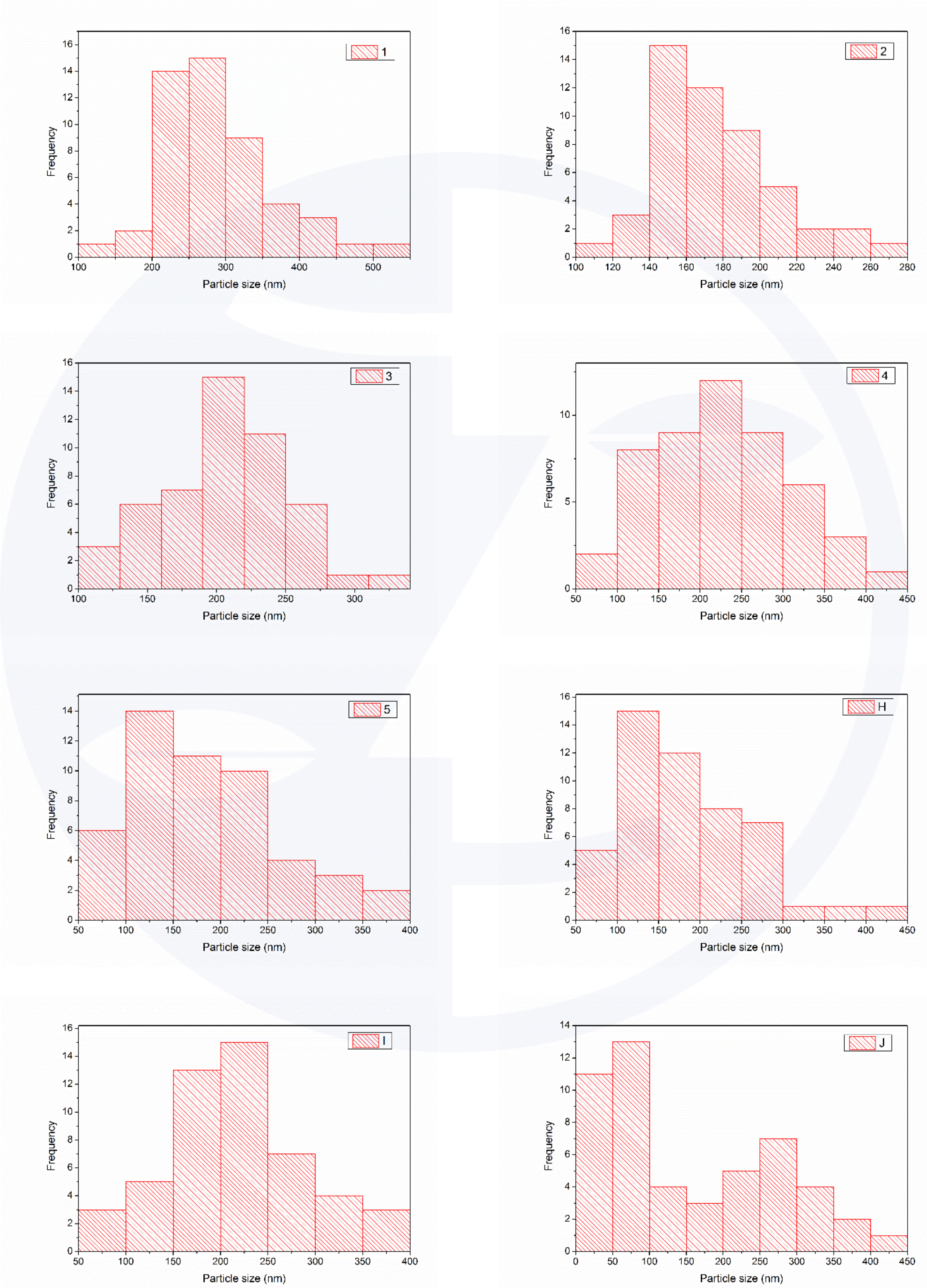

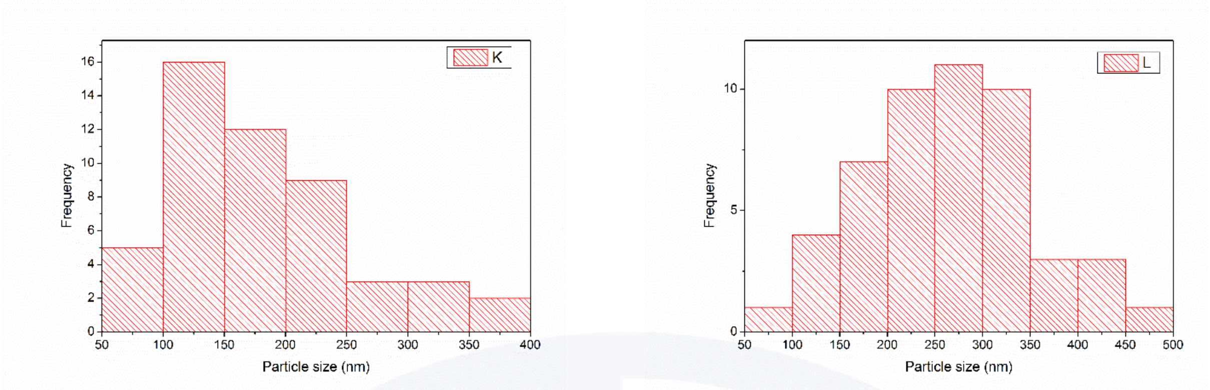

Figure 10. Histograms obtained by measuring 50 particles from TEM images related to the control samples (1, 2, 3, 4, 5) and the samples under TCF (H, I, J, K, L)

In these histograms, the horizontal axis is the particle size visible in the TEM images and the vertical axis is the number of particles in which the size range is measured by the software. According to the histograms shown in Figure 10, samples (2) and (J) have the narrowest and widest particle size distributions among the samples, respectively. The narrower the particle size distribution, the closer the particles are to each other, and the wider the particle size distribution, the greater the dispersion of the particle size. Other statistical data related to these measurements are reported in Table 4.

Table 4 . Statistical results from the histograms shown in Figure 10.(Control:1,2,3,4,5)&(TCF:H,I,J,K,L)

Sample	Total number of measurements	Mean (Nanometer)	Standard Deviation (Nanometer)	The smallest particle measured (Nanometer)	Measured sample of medium size (Nanometer)	The largest particle measured (Nanometer)
1	50	294.275	76.963	124.771	283.157	504.700
2	50	176.490	34.226	119.333	174.736	261.730
3	50	209.651	44.836	111.838	212.380	320.890
4	50	227.927	84.845	72.436	221.069	443.619
5	50	186.313	80.463	60.668	167.222	392.542
H	50	185.204	78.303	51.006	168.416	412.436
I	50	217.043	74.034	73.734	210.109	390.332
J	50	157.702	117.714	21.831	110.381	411.131
K	50	183.782	76.322	76.829	167.566	367.857
L	50	262.849	90.974	89.964	265.292	465.870

For easier examination and comparison of the mean and standard deviation values reported in Table 4, these values are plotted as bar graphs in Figure 11.

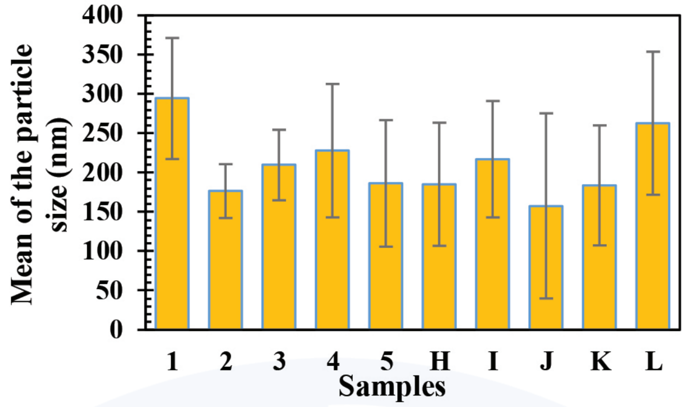

Figure 11- Particle size means and standard deviation of the samples. (Control:1,2,3,4,5) & (TCF:H,I,J, K, L)

According to Figure 11, samples (J) and (2) with particle size mean of 157.7 and 176.5 nm have the lowest particle size mean, followed by samples (K, H) and (5) with sizes of 183.8, 185.2, and 186.3 nm. It is also known that sample (1) with the particle size mean of 294.3 nm had the highest particle size among the samples, followed by sample (L) with the particle size mean of 262.6 nm and sample (4) with the particle size mean of 227.9 nm.

SEM (Scanning Electron Microscopy)

The images related to the samples were presented below (figure 12-21).

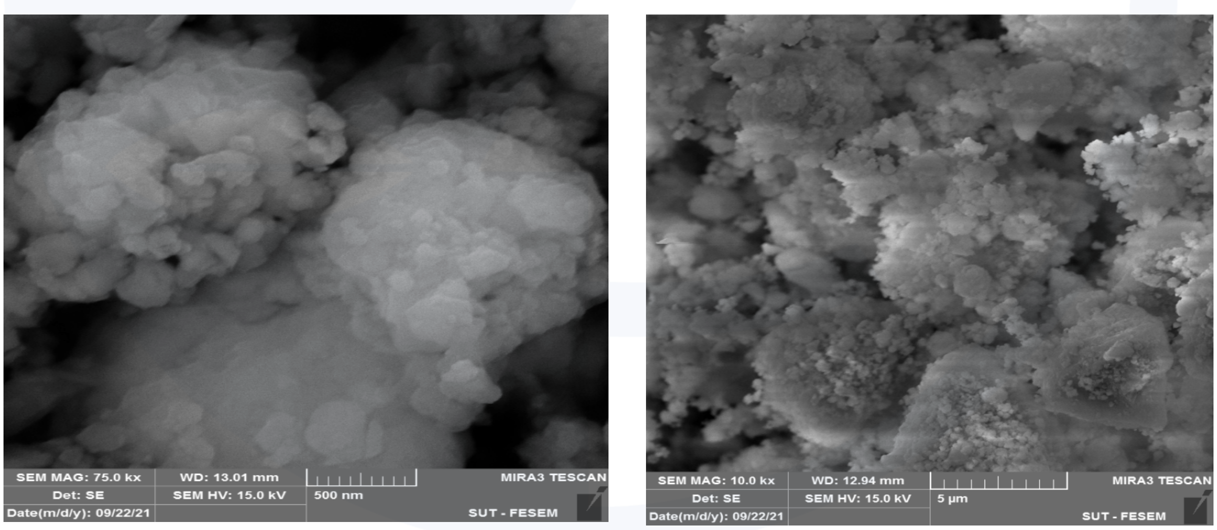

Element	Line Type	Apparent Concentration	k Ratio	Wt%	Wt% Sigma	Atomic %	Standard Label	Factory Standard
O	K series	13.75	0.04627	53.44	0.20	67.00	SiO2	Yes
Si	K series	11.25	0.08911	45.85	0.19	32.74	SiO2	Yes
Fe	K series	0.13	0.00133	0.71	0.12	0.25	Fe	Yes
Total:				100.00		100.00		

Figure 12- Sample 1 (Control)

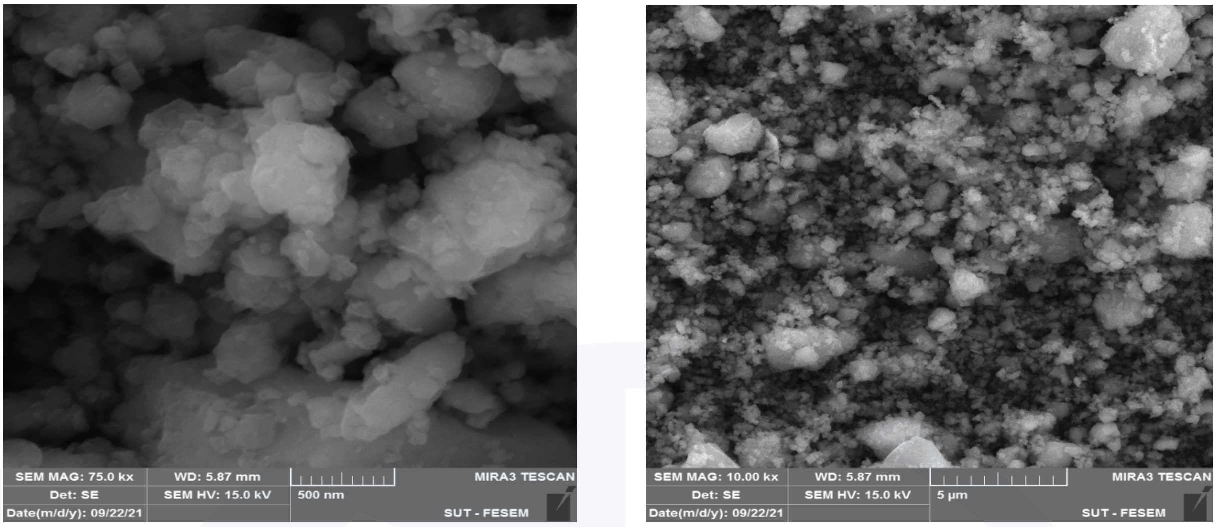

Element	Line Type	Apparent Concentration	k Ratio	Wt%	Wt% Sigma	Atomic %	Standard Label	Factory Standard
O	K series	14.60	0.04914	53.41	0.20	67.02	SiO2	Yes
Si	K series	11.88	0.09414	45.68	0.19	32.65	SiO2	Yes
Fe	K series	0.18	0.00180	0.90	0.12	0.32	Fe	Yes
Total:				100.00		100.00		

Figure 13- Sample 2 (Control)

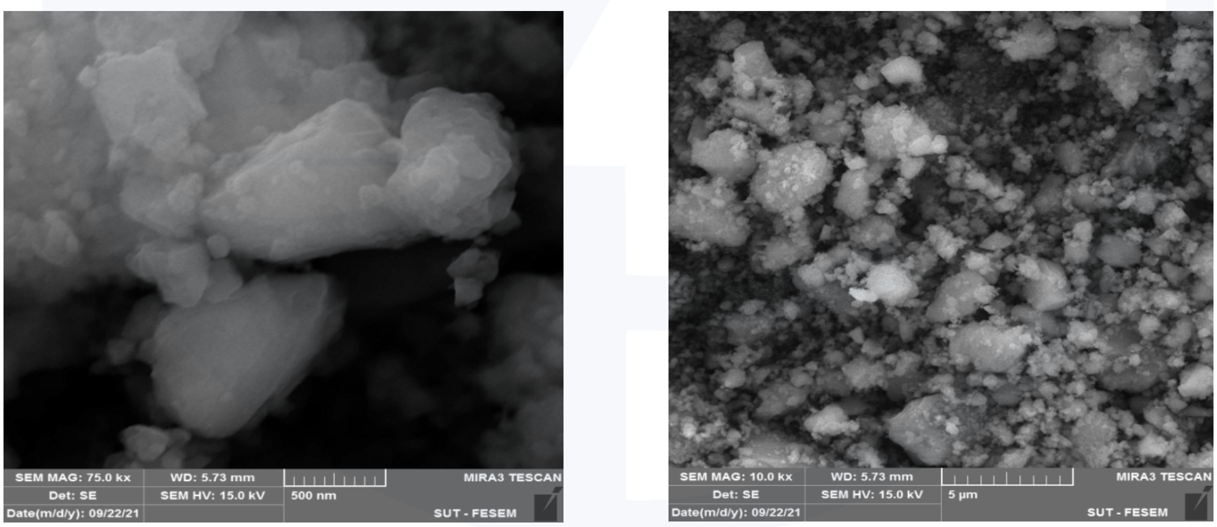

Element	Line Type	Apparent Concentration	k Ratio	Wt%	Wt% Sigma	Atomic %	Standard Label	Factory Standard
O	K series	7.20	0.02423	46.60	0.21	60.92	SiO2	Yes
Si	K series	8.24	0.06527	51.54	0.21	38.38	SiO2	Yes
Fe	K series	0.22	0.00225	1.86	0.16	0.69	Fe	Yes
Total:				100.00		100.00		

Figure 14- Sample 3 (Control)

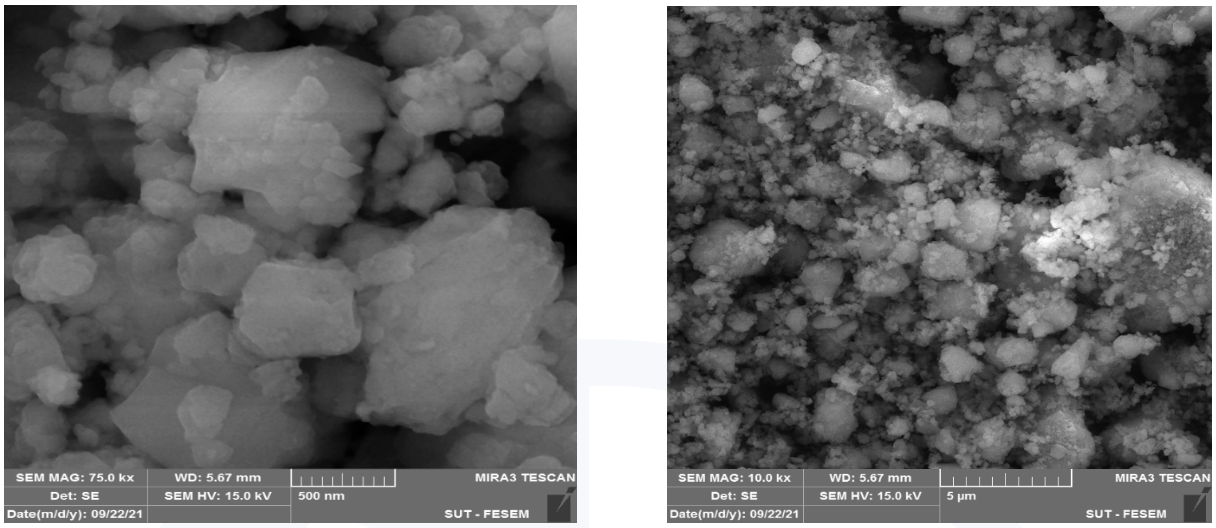

Element	Line Type	Apparent Concentration	k Ratio	Wt%	Wt% Sigma	Atomic %	Standard Label	Factory Standard
O	K series	12.50	0.04206	51.29	0.20	65.15	SiO2	Yes
Si	K series	11.36	0.09002	47.64	0.20	34.47	SiO2	Yes
Fe	K series	0.19	0.00193	1.07	0.13	0.39	Fe	Yes
Total:				100.00		100.00		

Figure 15- Sample 4 (Control)

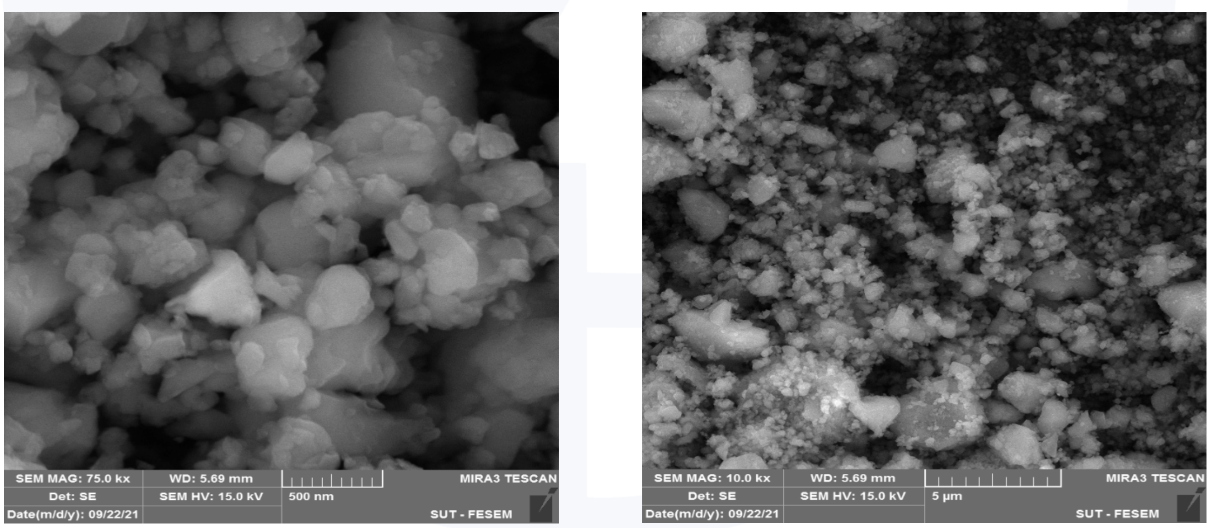

Element	Line Type	Apparent Concentration	k Ratio	Wt%	Wt% Sigma	Atomic %	Standard Label	Factory Standard
O	K series	9.39	0.03159	48.38	0.21	62.39	SiO2	Yes
Si	K series	10.09	0.07993	50.79	0.21	37.31	SiO2	Yes
Fe	K series	0.12	0.00124	0.83	0.14	0.31	Fe	Yes
Total:				100.00		100.00		

Figure 16- Sample 5 (Control)

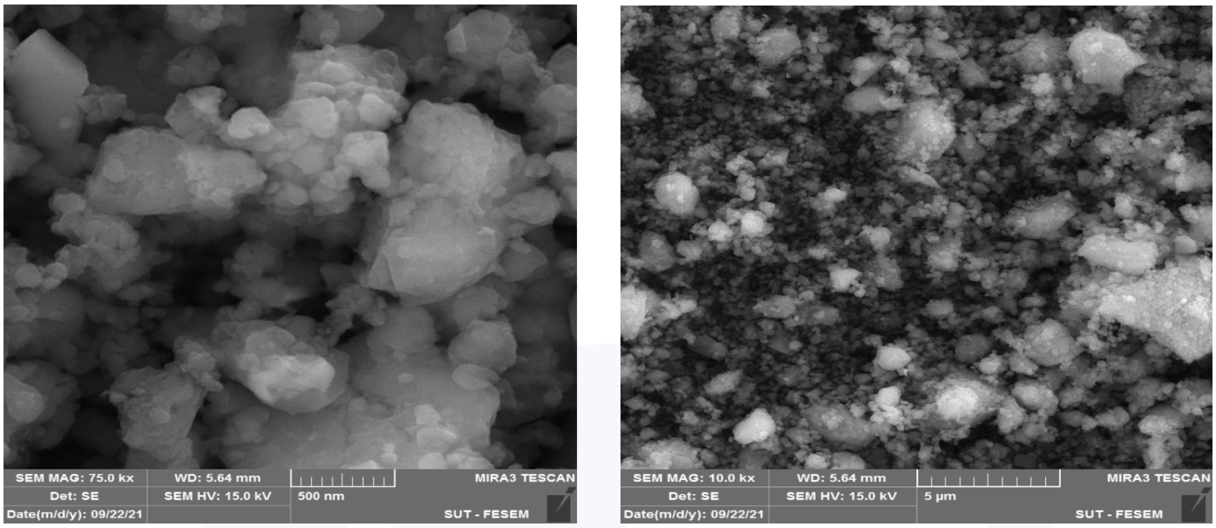

Element	Line Type	Apparent Concentration	k Ratio	Wt%	Wt% Sigma	Atomic %	Standard Label	Factory Standard
O	K series	17.94	0.06038	54.03	0.19	67.57	SiO2	Yes
Si	K series	14.12	0.11187	45.09	0.19	32.12	SiO2	Yes
Fe	K series	0.21	0.00211	0.88	0.12	0.32	Fe	Yes
Total:				100.00		100.00		

Figure 17- Sample H (under TCF)

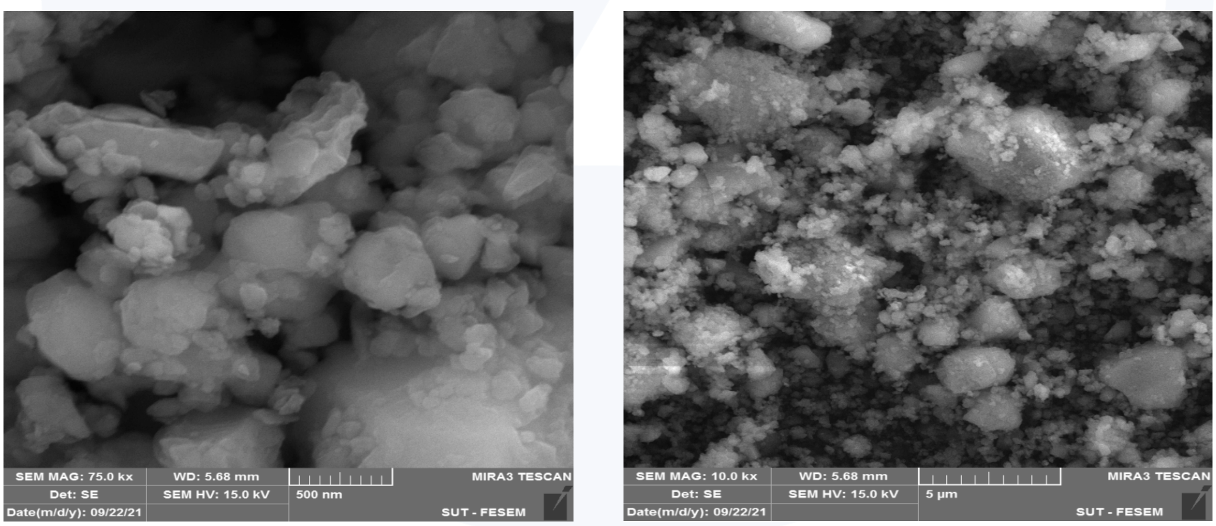

Element	Line Type	Apparent Concentration	k Ratio	Wt%	Wt% Sigma	Atomic %	Standard Label	Factory Standard
O	K series	15.07	0.05071	51.97	0.20	65.80	SiO2	Yes
Si	K series	13.12	0.10395	46.80	0.19	33.75	SiO2	Yes
Fe	K series	0.26	0.00262	1.23	0.13	0.44	Fe	Yes
Total:				100.00		100.00		

Figure 18- Sample I (under TCF)

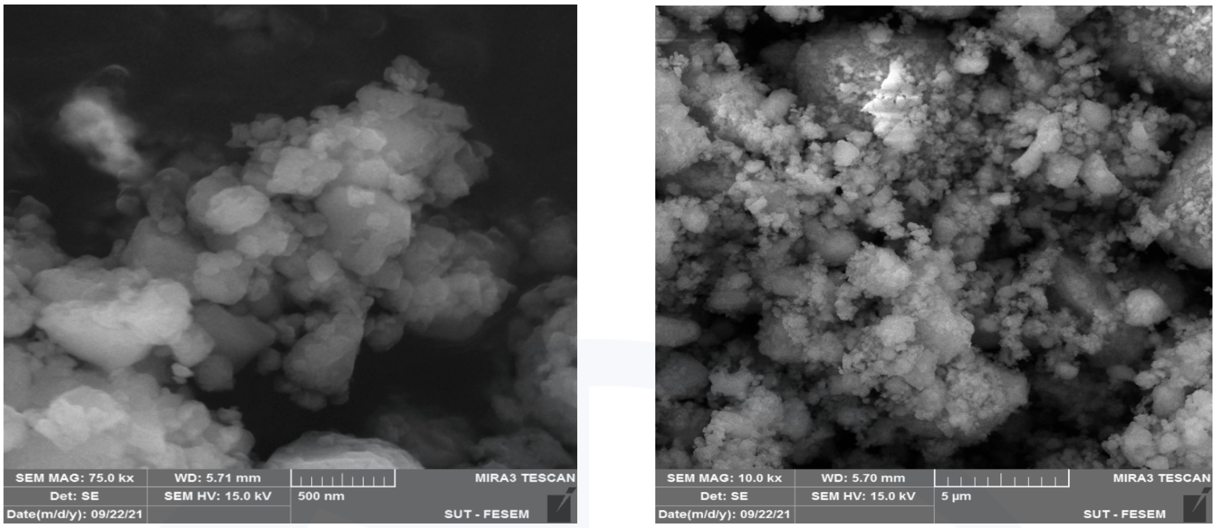

Element	Line Type	Apparent Concentration	k Ratio	Wt%	Wt% Sigma	Atomic %	Standard Label	Factory Standard
O	K series	16.70	0.05620	53.01	0.20	66.70	SiO2	Yes
Si	K series	13.80	0.10937	45.91	0.19	32.91	SiO2	Yes
Fe	K series	0.25	0.00249	1.09	0.12	0.39	Fe	Yes
Total:				100.00		100.00		

Figure 19- Sample J (under TCF)

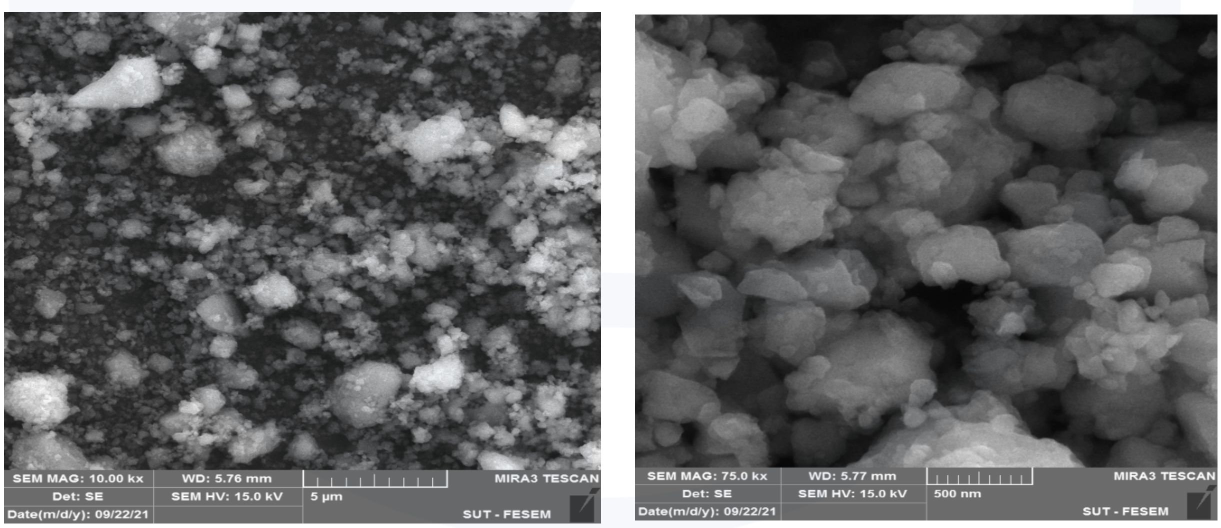

Element	Line Type	Apparent Concentration	k Ratio	Wt%	Wt% Sigma	Atomic %	Standard Label	Factory Standard
O	K series	19.83	0.06672	55.92	0.19	69.15	SiO2	Yes
Si	K series	14.21	0.11259	43.51	0.18	30.65	SiO2	Yes
Fe	K series	0.14	0.00141	0.56	0.11	0.20	Fe	Yes
Total:				100.00		100.00		

Figure 20- Sample K (under TCF)

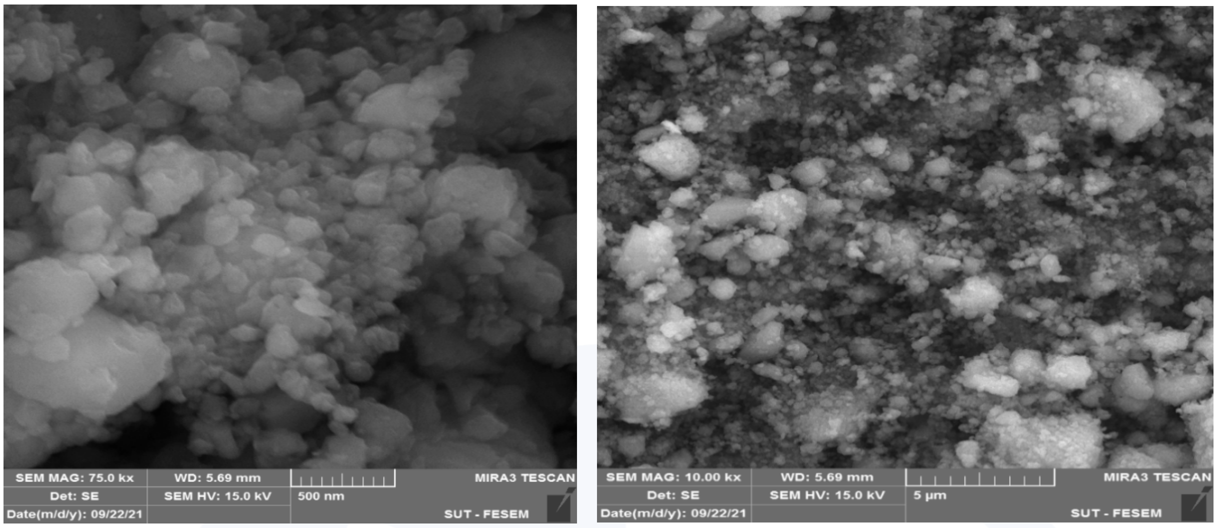

Element	Line Type	Apparent Concentration	k Ratio	Wt%	Wt% Sigma	Atomic %	Standard Label	Factory Standard
O	K series	8.28	0.02787	45.69	0.22	59.87	SiO2	Yes
Si	K series	10.20	0.08081	53.18	0.22	39.70	SiO2	Yes
Fe	K series	0.16	0.00165	1.14	0.15	0.43	Fe	Yes
Total:				100.00		100.00		

Figure 21- Sample L (under TCF)

Conclusion

Milling pure silica under T-Consciousness Bond Field had the following results:

1- Since the material used was silica with 98% purity and pure materials remain pure in the variable T-Consciousness Field, Consciousness Bond Field in this study, so only the silica oxide was still seen in the X-ray diffraction results [11]. The parameters related to the crystal structure remained constant under the TCF and only micro-strain differences were observed. The distortion and stress in the crystal grid structure under the TCF were much less (about 80%).

2- In the particle size distribution and the amount of hydrodynamic particle size, it was found that the dispersion in the samples under T-Consciousness Bond Field was less and the structure was more uniform. Particle size dispersion was obtained at 400 to 1800 nm in control samples and 1400 to 1800 nm in samples under T-Consciousness Bond Field. Particle sizes in the high dimension range were in the majority.

3- TEM analysis and SEM images, show that the size of the smallest particles in the T-Consciousness Bond Field is smaller (~35.9%) and often the dispersion of fine particles is increased in the empty space between the larger particles.

4- One of the occurrences is the high dispersion zeta potential diagrams under the TCF. Finally, it is impossible to study the zeta potential in the TCF, and so-called so much noise is generated that the output of the voltage is eventually estimated to be zero. The causes of this dispersion can be due to several reasons:

Chemical compounds that do not react completely and are still present in the material and cause different ionic rings, which is also not possible with the purity of the material.

Having different particle dimensions and polydispressing of the material, the ionic ring of each particle is different and is seen in the form of noise in interference. This is different from the DLS test because the results show that the maximum statistical population is more uniform.

The ultimate reason is the possibility of creating particles with dispersed dimensions and charge differences, which with a hypothesis of electric charge variation, their surface is high, which ultimately does not create a relative equilibrium and peak sharp, but their number is not large enough to affect the DLS test. To investigate this possibility, the zeta potential test was performed with the previous conditions but by placing the particles in an ultrasonic bath. Ultra-sonication of the particles meant that not all of the particles were completely disintegrated into agglomerates and that whatever was present on the surface of the particles could be received. In the re-test, and especially by examining the results of the control sample, it is clear that the sample particles are completely disintegrated and the variation of the electric charge of the particle surface is in relative equilibrium. Therefore, by examining these results, it is clear that the diversity of particles in the sample under TCF is not necessarily the cause of the diversity of electrical charges. And one of the effects that TCF has on the matter in the short run is the interference with the electric charge of the surfaces of the particles. Although the dimensions and reasons for this still require extensive experiments, in the first impression it can be said that since consciousness has the ability to become matter and energy, it can affect the speed of particle motion and cause apparent dispersion.

References

1- EU (European Union). (2011). 696.EU

2- Taheri, M. A. (2013). *Human from another outlook.* Interuniversal Press. 2nd Edition. ISBN-13: 978-1939507006, ISBN-10: 193950700

3- Taheri, M. A. (2012). *General Connection of particles.* Interuniversal Publishing.Erfan-Hlgheh. ID: 978-1-940491-03-5.

4- Kazazi, B, Taheri. M. A, Meshkin-Far. A. (2020). Influence of the Consciousness Field on the Cement Properties and Behavior. Science of Consciousness, Tucson, Arizona

5- Taheri, M. A. (2020). The main monitoring center for T-Consciousness Fields research and studies based on Sciencefact. www.Cosmointel.com.

6- Hernandez. C.C, Ferreira .F. F, Rosa. D. S. (2018). X-ray powder diffraction and other analyses of cellulose nanocrystals obtained from corn straw by chemical treatments. Carbohydr Polym;193:39–44. https://doi.org/10.1016/j.carbpol.2018.03.08

7. Ju. X, Bowden M, Brown E E, Zhang X.(2015). An improved X-ray diffraction method for cellulose crystallinity measurement. Carbohydr Polym 123:476–81. https://doi.org/10.1016/j.carbpol.2014.12.071

8- Bhattacharjee. S. (2016). DLS and zeta potential – What they are and what they are not? J. Control. Release. 235 .337–351. https://doi.org/10.1016/J.JCONREL.2016.06.017.

9- Honary.S, Zahir.F. (2013). Effect of Zeta Potential on the Properties of Nano-Drug Delivery Systems- A Review (Part 1),Trop. J. Pharm. Res. 12.255–264. https://doi.org/10.4314/tjpr.v12i2.19.

10- Kaszuba .M, Corbett .J, Watson .F.M, Jones .A.(2010). High-concentration zeta potential measurements using light-scattering techniques Philos. *Transact. A Math. Phys. Eng. Sci.* 368 4439–4451.

11- Kazazi. B, Taheri. M. A. (2021). Effect of the Consciousness Bond Field on the structure and properties of Aluminum .www.cosmointel.com

Influence of Taheri Consciousness Bond Field on the Plant Synthesis of Nano-silver

Bahareh Kazazi [1*], Mohammad Ali Taheri [2]

1. Civil Engineering, CEO of Hoobe Construction Company, Tehran, Iran.

2. Sciencefact R&D Department, Cosmointel Inc. Research Center, Ontario, Canada.

* Corresponding author:

Bahareh Kazazi
Civil Engineering, CEO of Hoobe Construction Company, Tehran, Iran.

Email: baharkazazi@gmail.com

ABSTRACT

One of the methods of synthesis of nanomaterials is the use of plant extract in synthesis. The aim of this study was to investigate the effect of the T-Consciousness Bond Field in the synthesis of green silver nanoparticles using plant extract. Taheri Consciousness Fields (TCFs), as new Fields, have been founded and introduced by Mohammad Ali Taheri about four decades ago. These Fields are non-material and non-energetic, so it has no quantity. However, it has a direct influence on both matter and energy. In other words, although TCFs cannot be directly measured, their effects can be indirectly studied by using various controlled experiments. In this experiment, the extract was prepared for 10 samples together. Five samples were considered the control and the names of the other 5 samples were declared to the person in charge of establishing the Consciousness Bond Field. The XRD results showed that the percentage of crystallization was lower in the control samples. The percentage of silver chloride phase formation on average was higher in the samples under the influence of TCF. The silver phase crystallite size on average was smaller on average under TCF. DLS showed that the particles size means in the samples under TCF was higher than in the control samples. Studying Zeta potential showed that the average of the obtained values regardless of the electric charge in the samples under TCF were higher than the control. TEM test showed that the samples under TCF had on average larger particle sizes than the control. The largest particle size in the control was 34.27 nm and, in the samples, under the TCF it was 54.72 nm. In the samples under the TCF, the average, particle size distribution was more uniform. It was found that the mean of particles with medium size in the group under the TCF was 29% larger than the control group. Therefore, Consciousness Bond Field can be used as a method to resize nanoparticles.

Keywords: Consciousness Bond Field, Taheri Consciousness Fields, Nanosilver, Plant Synthesis Silver nanoparticles, Ferula Latisecta

INTRODUCTION

A nanoparticle is a particle that is about 1 to 100 nanometers in size [1]. Nanoparticles are the most common elements in nanoscience and technology, and their remarkable properties have led to a wide variety of applications in the chemical, medical, pharmaceutical, electronic, aerospace, and agricultural industries [2-3]. One of the most widely used nanoparticles is silver nanoparticles, which is used in various areas, including medicine and health (the antimicrobial property of silver is the main reason for attention to it in this area), Chemical industry (production of house cleaners and fabrics), as a catalyst in chemical reactions, making solar cells, petrochemistry, gas, oil and concrete and steel restoration [4-8].

Due to the increasing applications of silver nanoparticles in various areas, there are different methods for the production, each of which has advantages and disadvantages, including vapor-phase synthesis of nanoparticles, photolysis or gamma-ray method, electrochemical method, synthesis of silver nanoparticles through chemical methods, use of microwaves and lasers and production of nanoparticles using biotechnology [9-16].

Since the biosynthesis method is superior to other methods in terms of cost and environmental compatibility, it has received more attention [17-18]. In this research, the extract of Ferula Latisecta has been used in the synthesis of silver nanoparticles and the changes under Consciousness Bond Field have been studied.

The nature of consciousness and its place in science has received much attention in the current century. Many philosophical and scientific theories have been proposed in this area. In the1980s, Mohammad Ali Taheri introduced novel fields with a non-material/non-energetic nature named Taheri Consciousness Fields (TCFs). In this perspective, T-Consciousness is one of the three existing elements of the universe apart from matter and energy. According to this theory, there are various TCFs with different functions, which are the subcategories of a networked universal internet called the Cosmic Consciousness Network (CCN). The major difference between the theory of TCFs and other theoretical concepts about consciousness is related to the practical application of the TCFs. TCFs can be applied to all living and non-living creatures, including plants, animals, microorganisms, materials, etc.

Mohammad Ali Taheri, the founder of Erfan Keyhani Halqeh, a school of thought, introduced a new science in 2020 as a branch of this school. He coined the term Sciencefact for this new science because it utilizes scientific investigations to prove the existence of T-Consciousness as an irrefutable phenomenon and a fact. Although science focuses solely on the study of matter and energy and Sciencefact, by contrast, explores the effects of the [non-material/non-energetic] TCFs, Sciencefact has provided a common ground between the two by conducting reproducible laboratory experiments in various scientific fields, and it has used the scientific approach in proving TCFs.

The influence of the TCFs begins with the Connection between CCN as the Whole Taheri Consciousness of the universe and the subjects of study as a part. This Connection called "Ettesal" is established by a certified and trained individual who has been entrusted with the TCFs. The human mind has an intermediary role (Announcer) which plays a part by fleeting attention to the subject of study and then the main achievement obtained as a result of the effects of the TCFs.

These Fields cannot be directly measured by science, but it is possible to investigate their effects on various subjects through reproducible laboratory experiments.

The research methodology in the study of T-Consciousness has been founded on the process of Assumption, Argument, and Proof, in which the basic Assumption is: The Cosmos was formed by a third element called T-Consciousness that is different from matter and energy.

The Argument: The existence of TCFs can be demonstrated by its effects on matter and energy (e.g., humans, animals, plants, microorganisms, cells, materials, etc.)

The Proof: is the scientific verification of the effects of TCFs on matter and energy (according to the Argument) through various reproducible scientific experiments.

Accordingly, to investigate and verify the existence, effects, and mechanisms of TCFs, the following five research phases (Phases 0 through 4), and the aims of each phase are outlined below.

Phase-0 studies aim to prove the existence of TCFs by observing their effects. The nature of T-Consciousness and what it is will not be addressed in this phase. Phase-1 explores the varied effects of different TCFs. Phase-2 examines the reason behind the varied effects of these fields. Phase-3 investigates the mechanism of TCFs effects on matter and energy. Finally, Phase-4 draws significant conclusions, particularly with regard to the mind and memory of matter and their relation to the T-Consciousness, etc. [19-23]

Materials and Method

10 g of the mixture of dried stems and leaves of Ferula Latisketa prepared from Beheshti nanotechnology lab (Khorasan-Iran), was poured into Erlenmeyer, and boiled with 100 mg of distilled water for 15 minutes. Then the stems and leaves were passed from a filter and the liquid was collected in a Falcon and placed in the refrigerator. After that, the Erlenmeyer was covered with foil and a hole was made in the foil to exchange air. In the next step, we brought the solution of one-tenth of a molar of silver nitrate (0.1M-$AgNO_3$) purchased from Merck company with distilled water to a volume of 500 mL.

Then, to investigate the reaction of the extract and silver nitrate solution, we put them in a ratio of 90 mL of silver nitrate solution to 10 mL of extract for 6 hours on the heater at 45 ℃.

In order to prorate probable experimental errors, such as minor changes in ambient temperature, minor changes in the time spent synthesizing and analyzing, human mistakes, etc. first the extract was prepared for 10 samples. Then 10 Erlenmeyer flasks were named by the head of the laboratory five samples were considered as control and the names of the other five samples were declared to the person in charge of establishing TCF. In each group of synthesis, the sample under T-Consciousness Field and the control sample were placed together on a heater in the same condition for synthesis, and they were named co-grouped. The names of the co-grouped control samples and samples under TCF are described in Table 1. Due to the effect of time on nanomaterials, all tests have been performed in the same way.

Table 1 . Co-grouped samples synthesized simultaneously and under exactly the same conditions.

Control Samples name	1	2	3	4	5
Samples under Consciousness Field name	B2	A2	G2	F2	D2

Application of Taheri Consciousness Fields

One of the introduced TCFs is called the Consciousness Bond Field and was applied to the samples according to the protocols regulated by the COSMOintel research center (www.COSMOintel.com). A request for Connection to the CCN to utilize TCFs can be placed through the COSMOintel website in the “Assign Announcement” section. This access is available for everyone at no cost. In order to study and experience this Connection, the researchers can register on the website at any time in order to report the experiment to the COSMOintel research center. Certain details of the experiment must be provided to the center; for example, the characteristics or number and name of samples and controls must be specified.

Results and Discussion

This entire experiment was carried out as a double-blind method where lab technicians were completely unaware of the TCFs.

Analysis performed

XRD (X-ray diffraction): For the XRD test, the samples were placed at 60 °C for 5 hours. Under BSIBS En139251-2 standard, Gener-ator Settings: 40 mA, 40 kV Anode Material: Cu, Step Size [°2Th.]: 0.0260.
TEM (Transmission electron microscopy): by the device (Zeiss EM900)
DLS (Dynamic Light Scattering) and Zeta Po-tential (Electro-kinetic Potential) were done by the device (Malvern- Nano ZS (red badge) ZEN 3600).
All analyzes were performed under ISO 7-1502-3001 standard, at 19 °C, 19% RH, and 1 atm.

After synthesis	Before synthesis

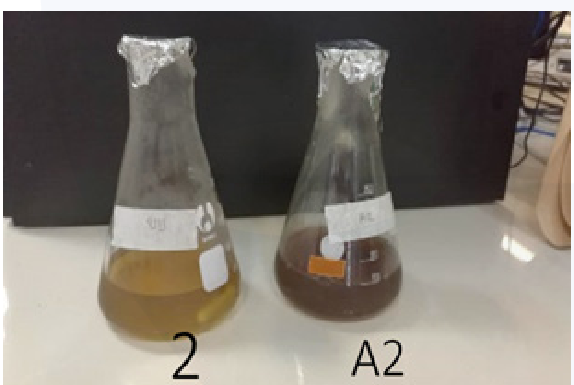

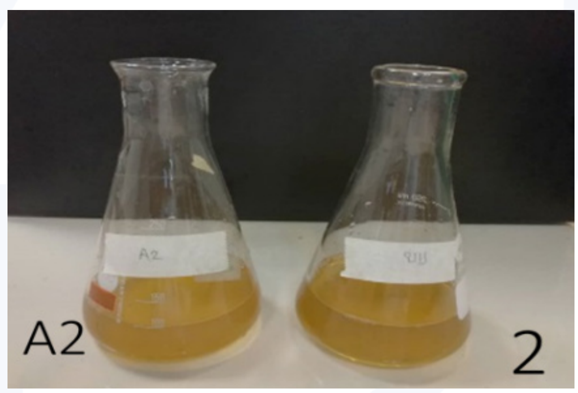

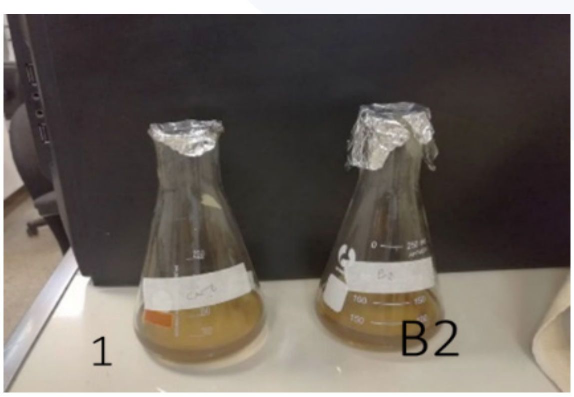

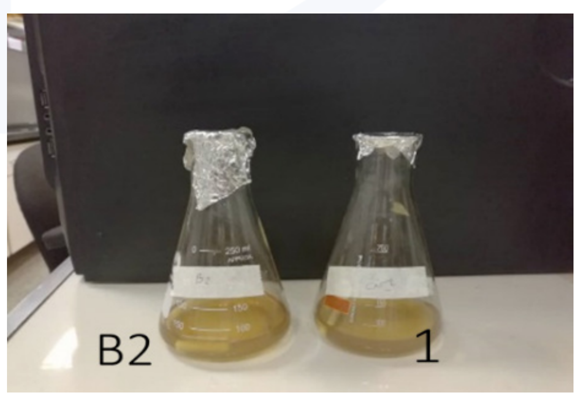

The First Journal in T-Consciousness Research
Vol. 01 No. 08 April 2022

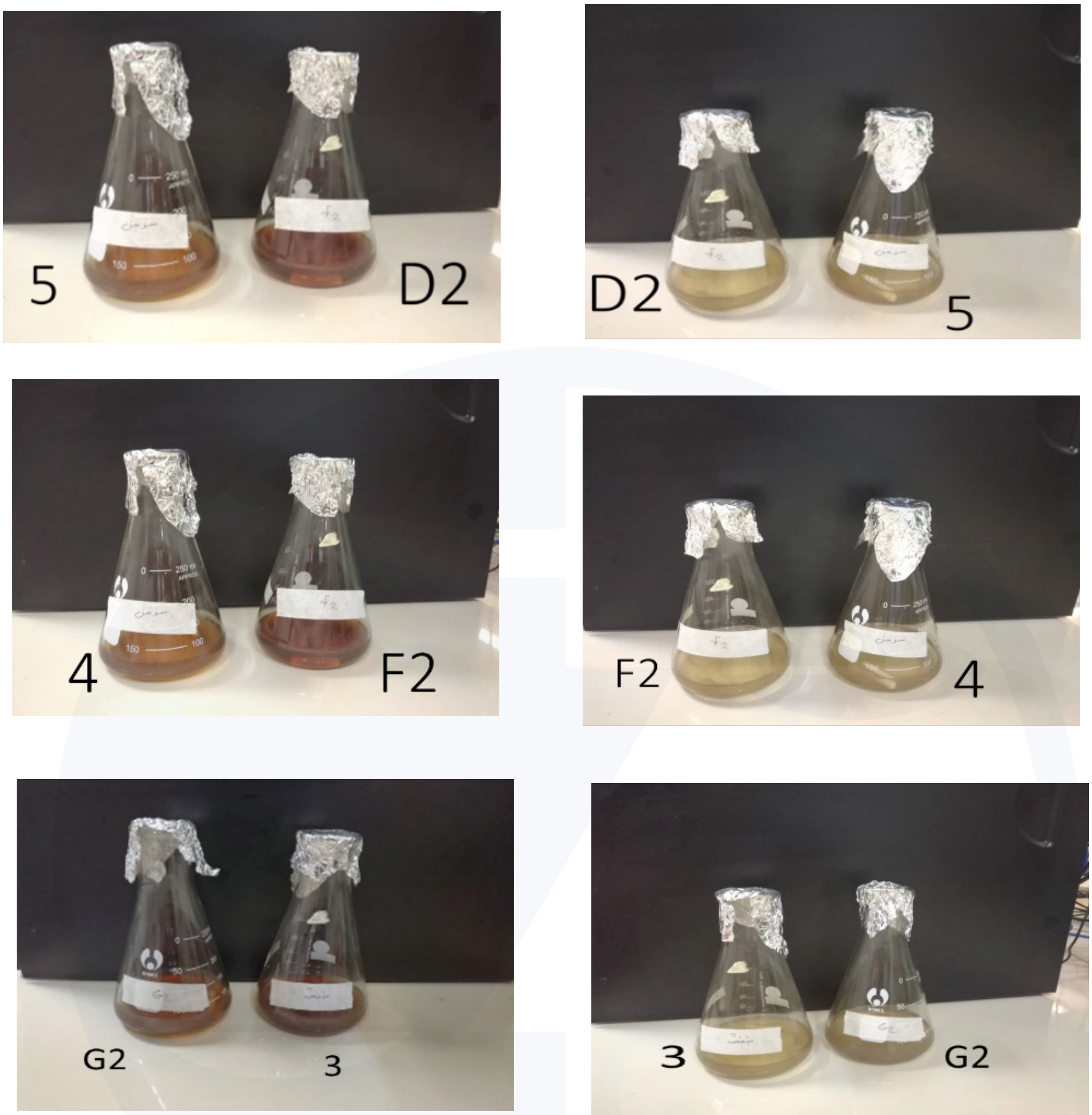

Fig 1. Sample images before and after the synthesis

The XRD results

To study the crystalline structure of nanoparticles, the XRD test was used. The obtained results are shown in Fig. 2.

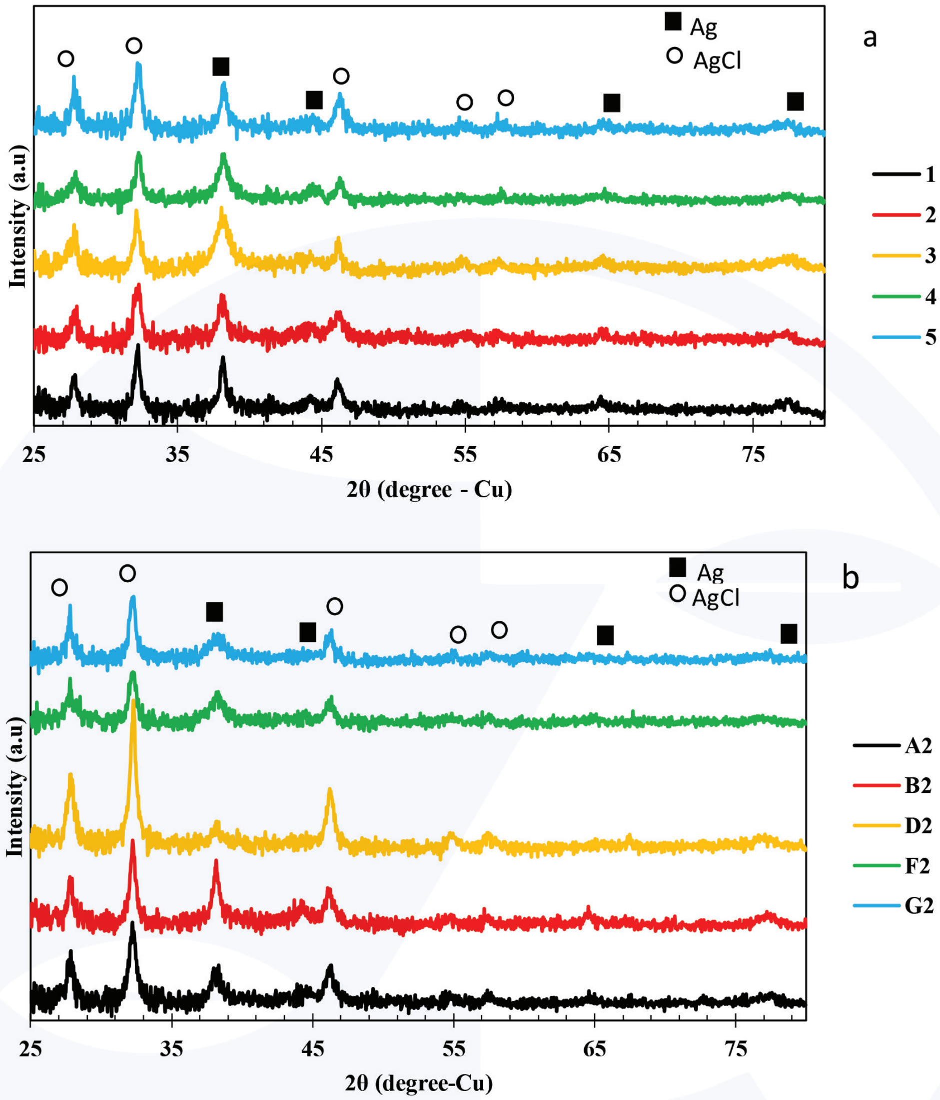

Fig 2. X-ray diffraction patterns of control samples (a), and of the samples under TCF (b)

According to Fig. 2, in almost all samples, two phases of silver (with reference code: JCPDS No: 98-006-2676) and silver chloride (with reference code JCPDS No: 00-006-0480) are observed. In these diffraction patterns, the peaks positioned at the angles of 38.2 °, 44.4 °, 64.4°, and 77.5 ° are related to the diffraction plates (111), (200), (220) and (311) of the silver phase respectively. Also, the peaks positioned at angles of 27.8°, 32.2°, 46.6°, 54.5°, and 56.9° are related to the diffraction plates (111), (200), (220), (311), and (222) of the silver chloride phase, respectively.

For quantitative analysis of the test results, the Rietveld Maud software method was used. The obtained results for lattice parameter, crystallite size, micro-strain, percent crystallinity, and percentage of each phase are reported in Table 2.

Table 2 . Quantitative parameters extracted from Rietveld method XRD test. Samples 1, 2, 3, 4, and 5 are Control and A2, B2, D2, F2, and G2 are under TCF

Silver Chloride Phase				Silver Phase				Percent Crystallinity	Sample Name
Micro-strain	Crystallite Size (Å)	Lattice Parameter (Å)	Phase Percentage (%)	Micro-strain	Crystallite Size (Å)	Lattice Parameter (Å)	Phase Percentage (%)		
0.0052	778.95	5.561	55.08	0.0013	182.31	4.087	44.91	**10.92**	1
0.0023	999.87	5.575	29.04	0.0002	53.59	4.094	70.95	**8.51**	2
0.0044	999.74	5.561	21.17	0.00005	52.31	4.084	78.83	**14.85**	3
0.0052	970.75	5.556	37.03	0.00003	113.85	4.086	62.97	**14.78**	4
0.0052	999.69	5.553	42.30	0.00006	54.31	4.077	57.70	**12.07**	5
0.0070	970.23	5.558	54.67	0.000002	89.32	4.085	45.32	**13.86**	A2
0.0053	999.69	5.559	40.56	0.00002	54.42	4.083	59.44	**13.71**	B2
0.0061	967.42	5.558	63.31	0.000008	36.62	4.073	36.69	**17.64**	D2
0.0061	967.42	5.559	37.44	0.00003	36.72	4.084	62.55	**14.94**	F2
0.0061	967.42	5.552	41.73	0.00006	36.75	4.074	58.27	**13.52**	G2

Table 3 . Percentage of changes in the silver phase crystallite size and the silver chloride phase and silver phase to Control

	TCF	Control	Percentage of changes
Mean of Silver Chloride Phase percentage	47.54	36.92	28.7%
Mean of Silver phase percentage	52.45	63.07	-16.8%
Mean of silver phase crystallite size	50.76	91.27	-44.37%

According to Table 2, the percentage of crystallinity in a sample can indicate the ratio of crystalline phases in that sample to amorphous and non-crystalline phases, which is obtained by dividing the area under the crystalline peaks by the total area under the curve. Also, in Table 2, it is clear that the lowest values of the crystallinity percentage are related to the control samples (1, 2, 3, 4, and 5), among which samples 1 and 2 have the lowest crystallinity percentage. Among the samples under TCF, samples A2 and B2 have less crystallinity percentage than other samples in this category, which are both co-grouped with samples 1 and 2 for synthesis, respectively.

Phase percentage is another parameter that has changed significantly among the studied samples. The average silver chloride phase percentage is higher in the samples under TCF than in the control samples.

The changes in the lattice parameter are not significant in the studied samples, which means the distances of the atoms in the crystalline structure of silver and silver chloride do not change.

Also, due to the lack of annealing of the samples, there is no expectation for a significant change in micro-strain. However, another important parameter is the crystallite size in the samples. To better observe the changes in this parameter, a bar chart related to the crystallite size of the studied samples is shown in Fig. 3.

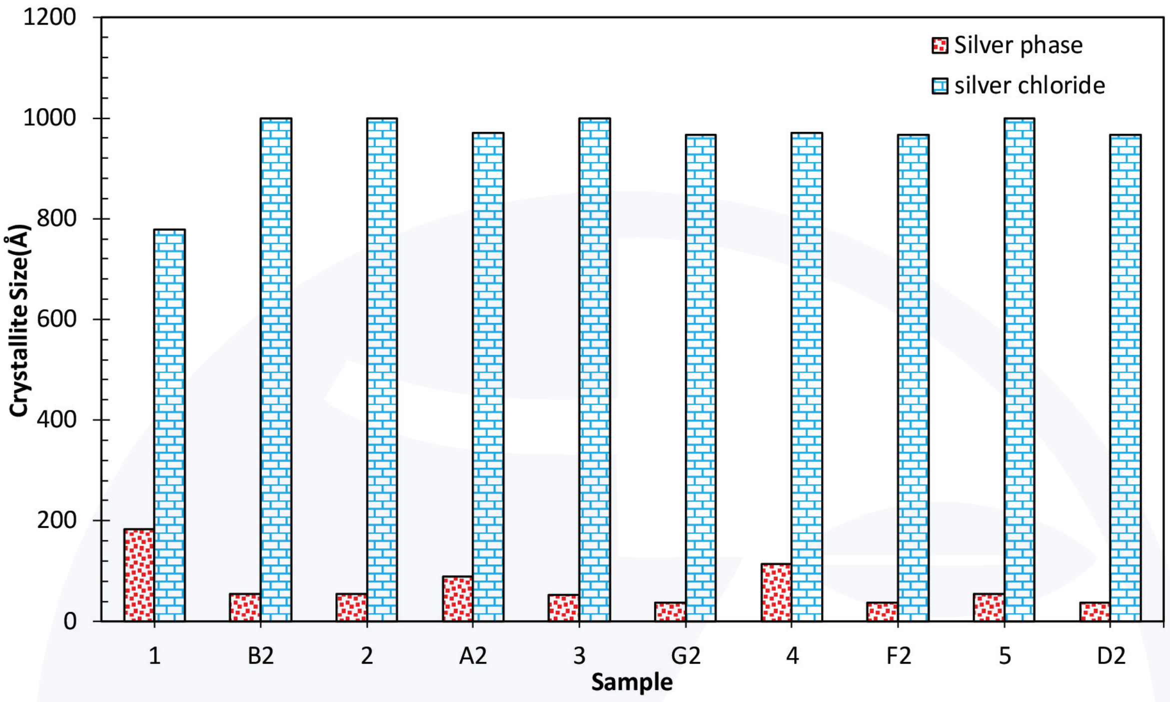

Fig 3. Crystallite size changes in the silver and silver chloride phases in the studied samples. Samples 1, 2, 3, 4, and 5 are the controls, and the samples A2, B2, G2, F2, D2 are under TCF

According to Fig. 3, it is clear that in all samples, the crystallite size of the silver chloride phase is much larger than the silver phase. This Figure also shows that the crystallite size of the silver phase is larger in sample 1, while the crystallite size of the silver chloride phase is smaller in the same sample. After sample 1, sample 4 also has one of the largest crystallite sizes in the silver phase and the smallest crystallite size in the silver chloride phase. In addition, the smallest crystallite sizes of both phases belong to samples D2, F2, and G2.

Examining the synthesized groups, showed that the crystallites size of the silver phase in the samples under TCF was smaller than their co-grouped control samples. Only in sample A2, the crystallite size of the silver phase was increased compared to its co-grouped, i.e., sample 2. But in the silver chloride phase, it still had a smaller crystallite size. On average, the crystallite size of the silver phase was smaller in the samples under TCF.

The DLS results

DLS analysis was used to evaluate the hydrodynamic particle size. The particle size of the samples under study is given in the distribution histograms.

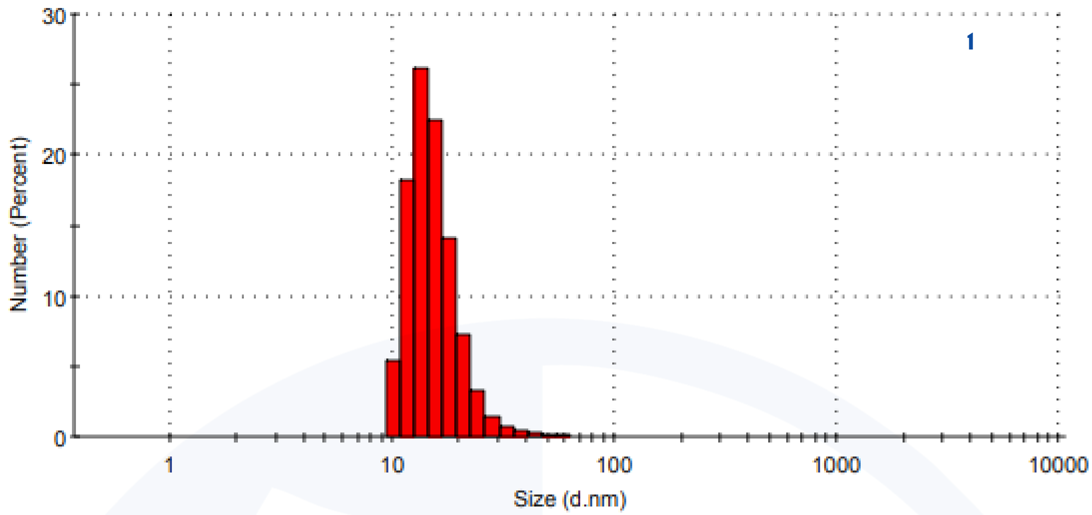
1
Number (Percent)
30
20
10
0
1
10
100
1000
10000
Size (d.nm)

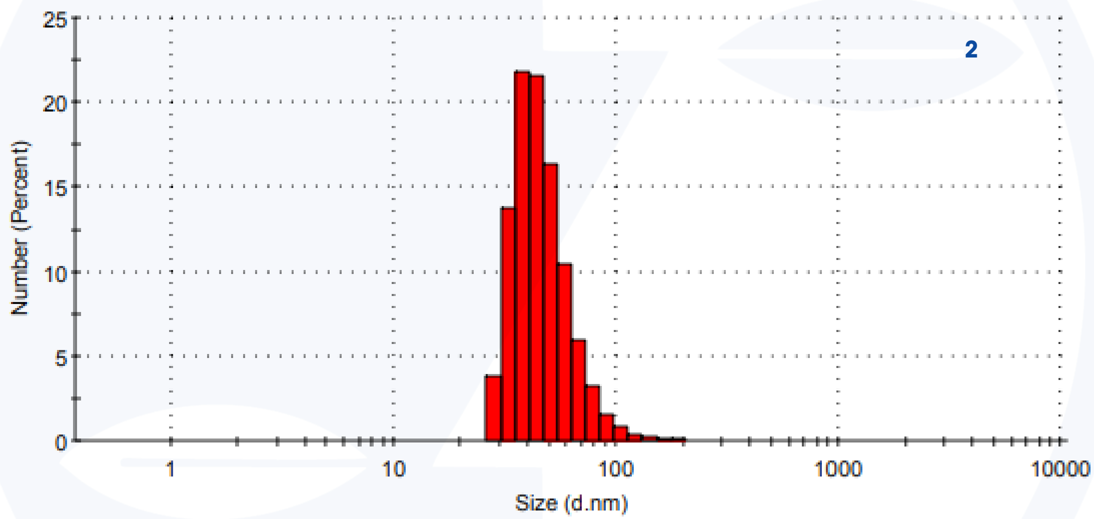
2
Number (Percent)
25
20
15
10
5
0
1
10
100
1000
10000
Size (d.nm)

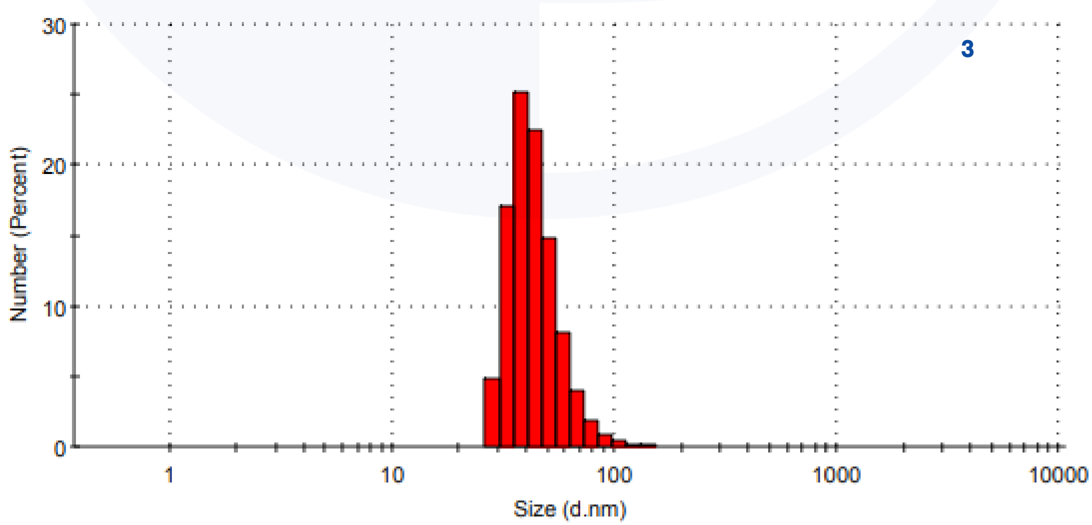
3
Number (Percent)
30
20
10
0
1
10
100
1000
10000
Size (d.nm)

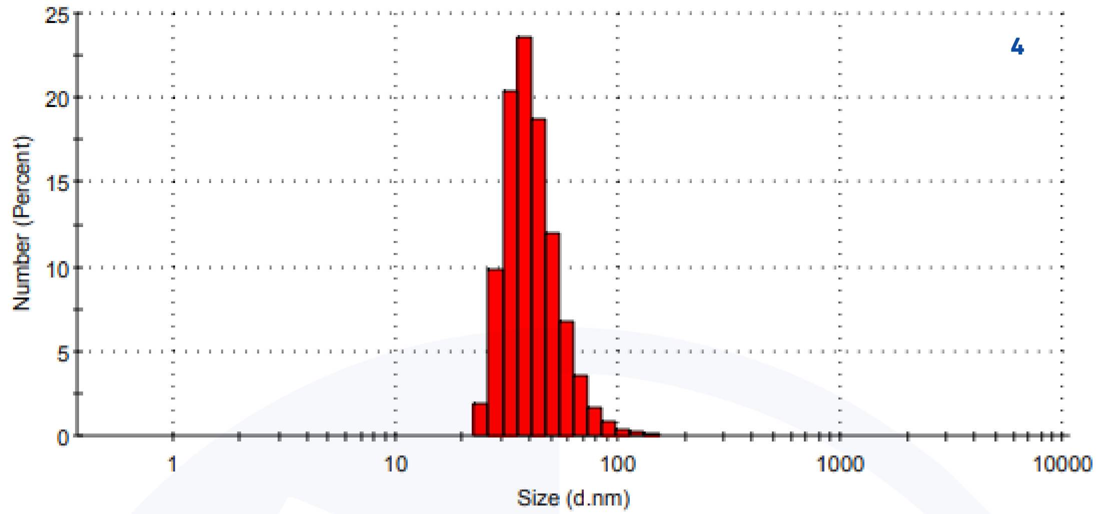
4
Number (Percent)
25
20
15
10
5
0
1
10
100
1000
10000
Size (d.nm)

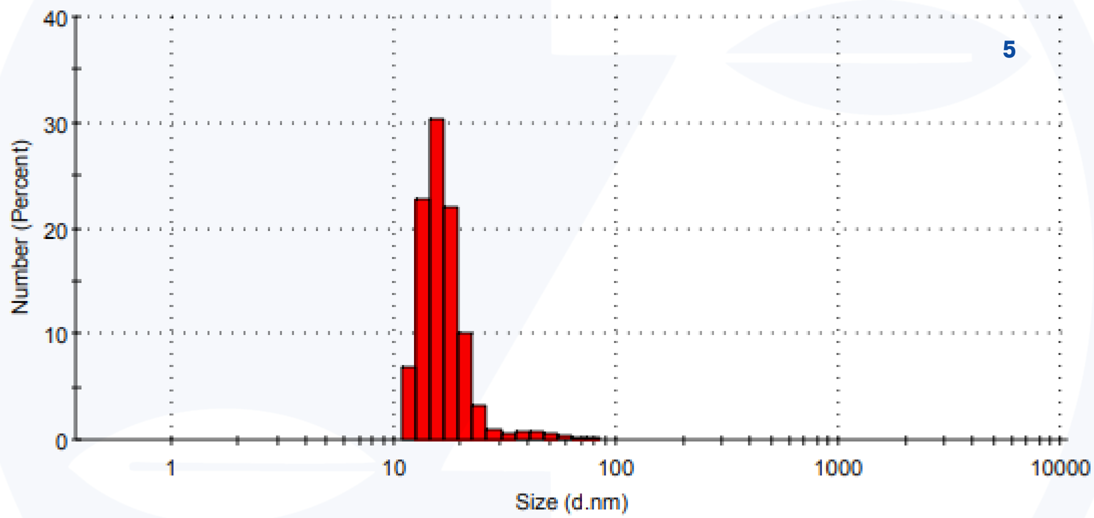
5
Number (Percent)
40
30
20
10
0
1
10
100
1000
10000
Size (d.nm)

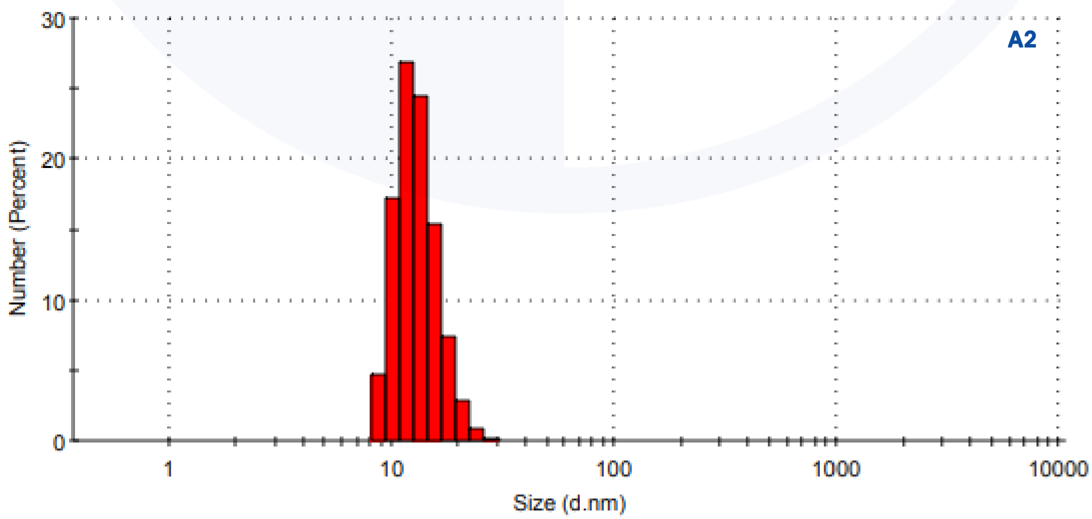
A2
Number (Percent)
30
20
10
0
1
10
100
1000
10000
Size (d.nm)

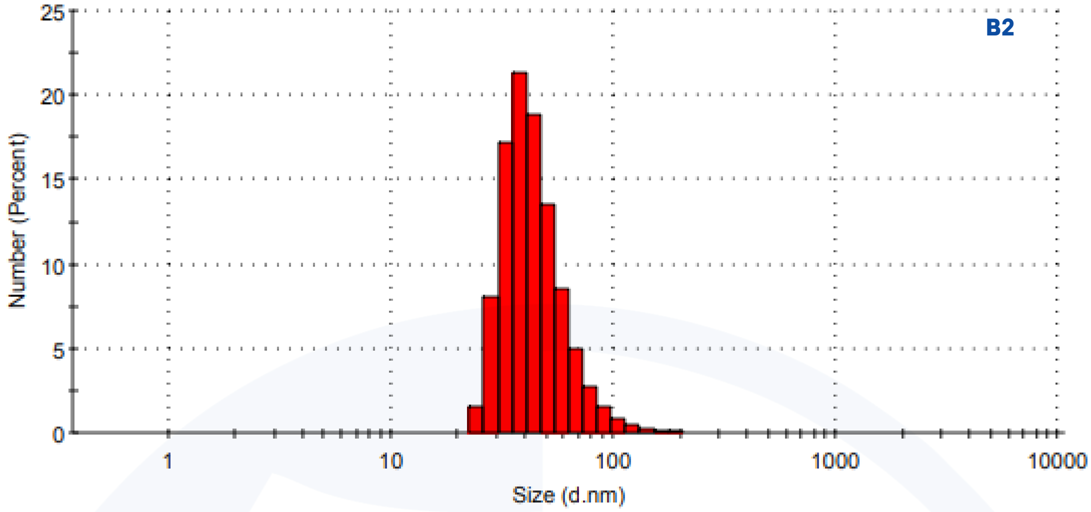
B2
Number (Percent)
0
5
10
15
20
25
1
10
100
1000
10000
Size (d.nm)

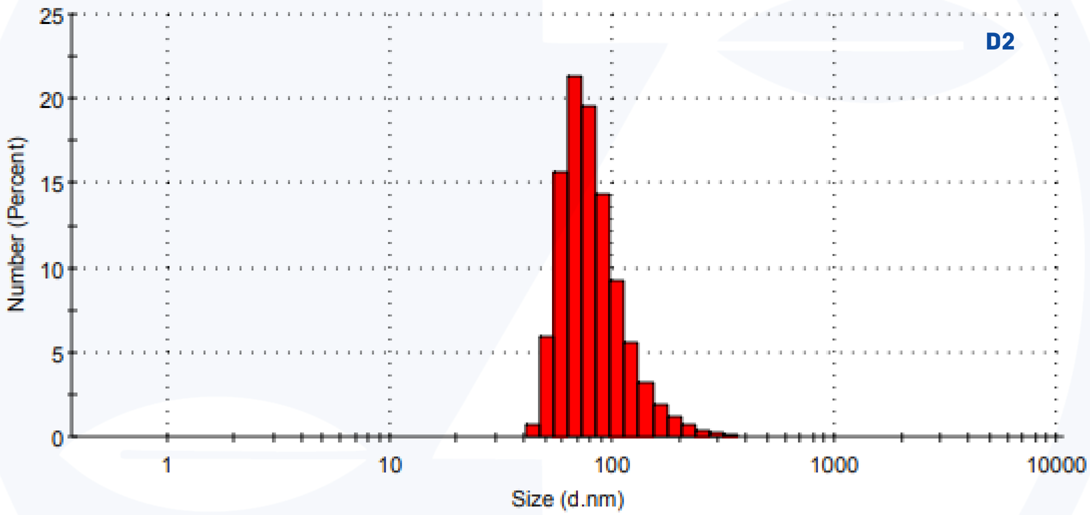
D2
Number (Percent)
0
5
10
15
20
25
1
10
100
1000
10000
Size (d.nm)

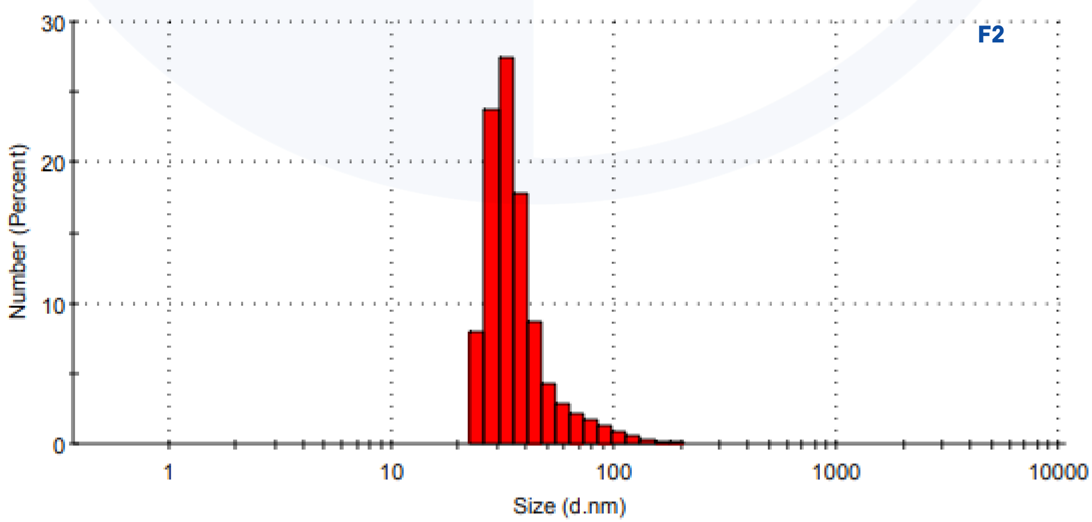
F2
Number (Percent)
0
10
20
30
1
10
100
1000
10000
Size (d.nm)

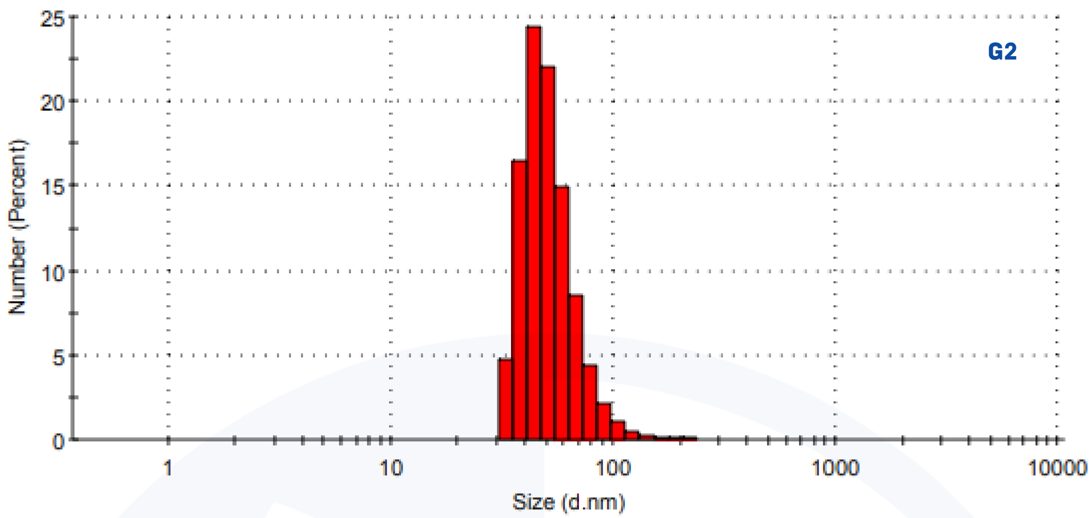

Fig 4. Histogram of particle size distribution from DLS Samples 1, 2, 3, 4, and 5 are the controls, and samples A2, B2, G2, F2, and D2 are under TCF

According to the results shown in the histograms, D2 seems to have had the largest particle size. Also, the widest and narrowest particle size distributions were related to samples 5 and D2, respectively, which were co-grouped in synthesis.

The narrow particle size distribution means that the particle sizes are closer to each other and less different. For a more detailed study of the values obtained in this test, the mean and standard deviation parameters were calculated and shown in Fig. 5.

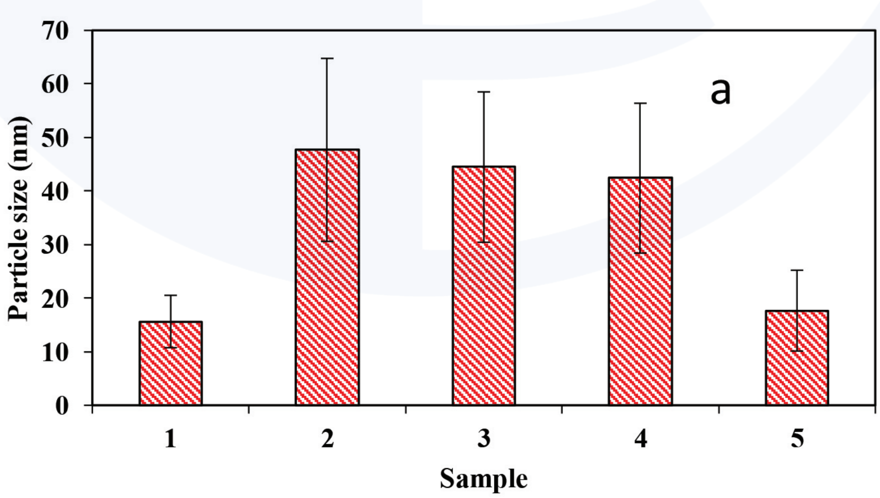

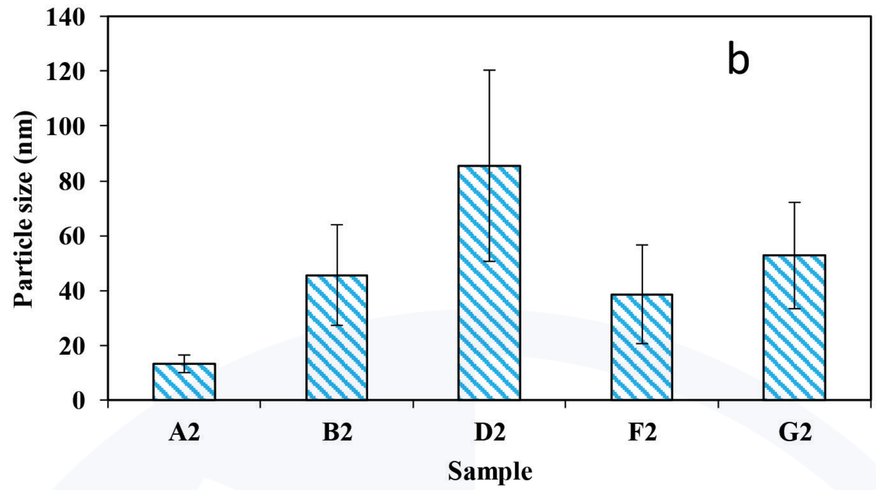

Fig 5. Changes in the mean of the particle size and standard deviation of the DLS test for samples (a) control, and (b) under TCF

The particle size in the samples under TCF was on average larger than the control samples.

In the samples under TCF, the mean of particle size in sample D2 was higher than the other samples under TCF as well as the control samples.

Zeta potential results

Zeta potential analysis was done to investigate the conditions of the particles in the colloid. The surface charge of a particle in a fluid is called the zeta potential [24].

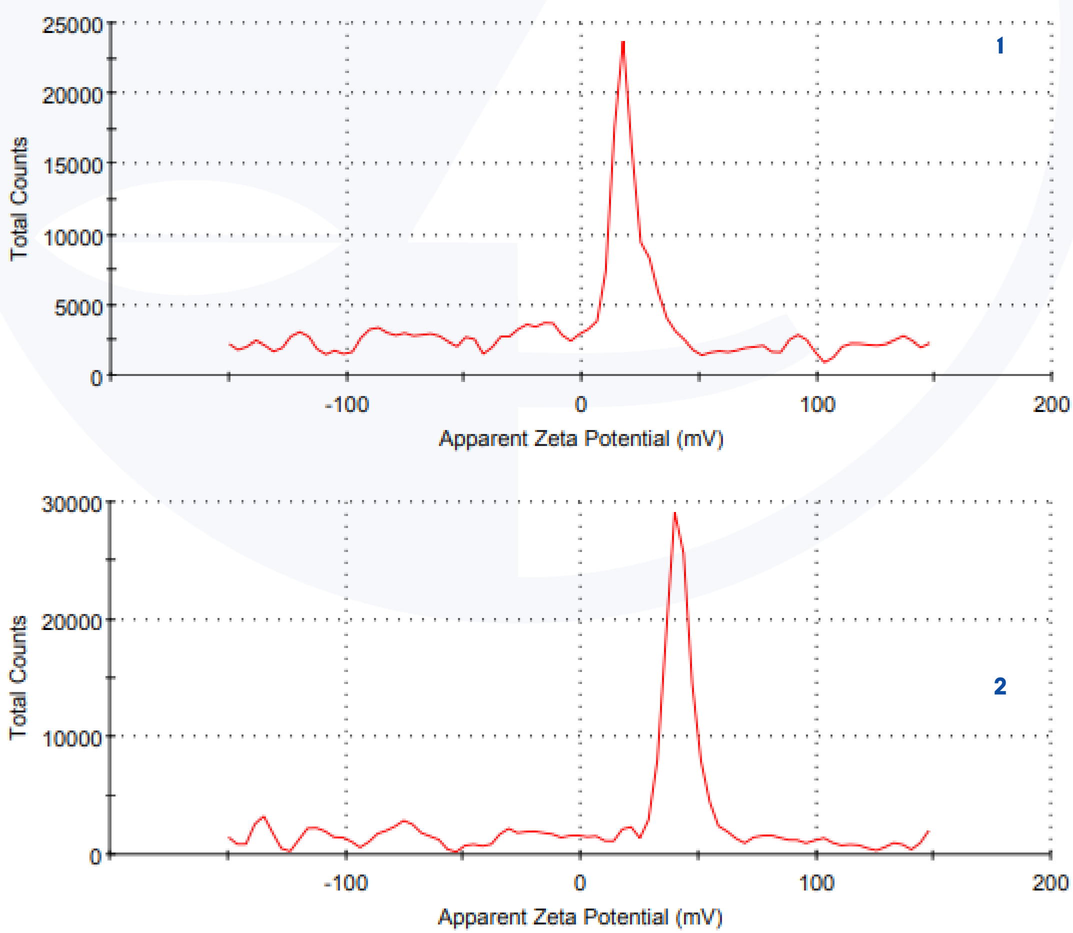

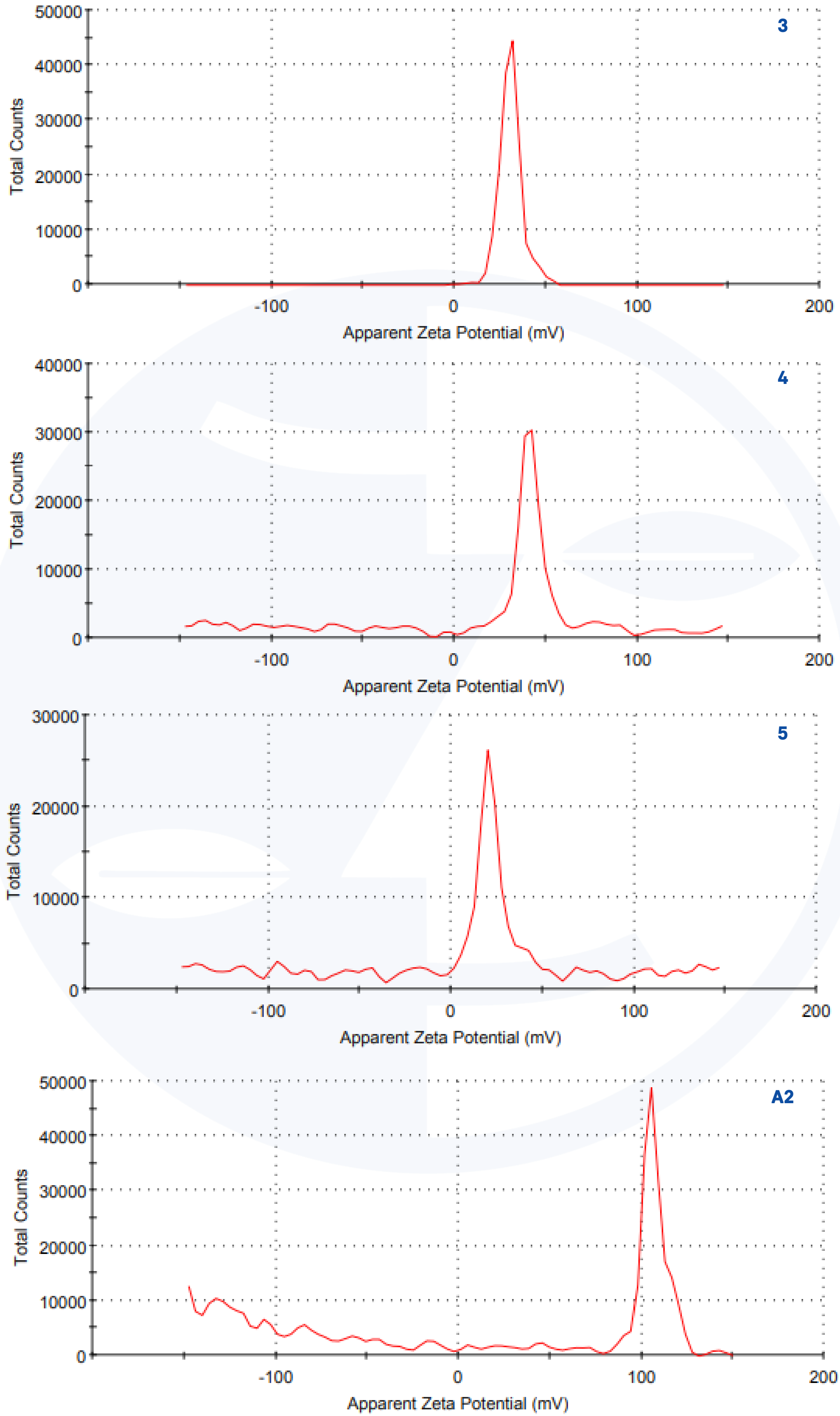
3
50000
40000
30000
20000
10000
0
Total Counts
-100
0
100
200
Apparent Zeta Potential (mV)
4
40000
30000
20000
10000
0
Total Counts
-100
0
100
200
Apparent Zeta Potential (mV)
5
30000
20000
10000
0
Total Counts
-100
0
100
200
Apparent Zeta Potential (mV)
A2
50000
40000
30000
20000
10000
0
Total Counts
-100
0
100
200
Apparent Zeta Potential (mV)

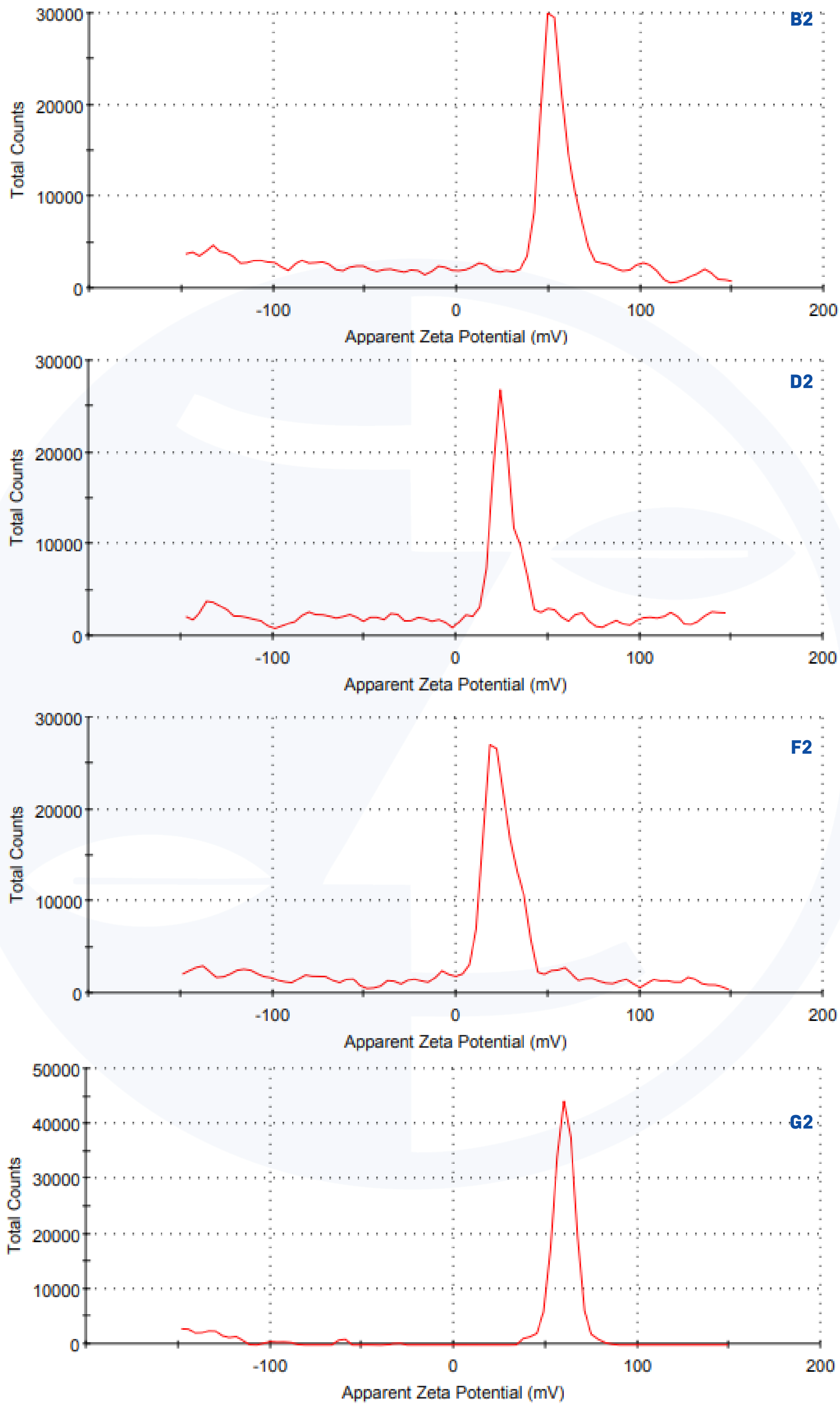

Fig. 6. Zeta potential histograms of the samples 1, 2, 3, 4, and 5 are control and samples A2, B2, G2, F2, and D2 are under TCF.

According to these histograms, except for samples 3 and G2, the rest are noisy. These noises have caused the area under the curve in the whole histogram to change relative to the peak sharpness visible in the results, making the mean shift. For this purpose, the mean value of the zeta potential is calculated and the bar graphs of this parameter for different samples are shown in Fig. 7.

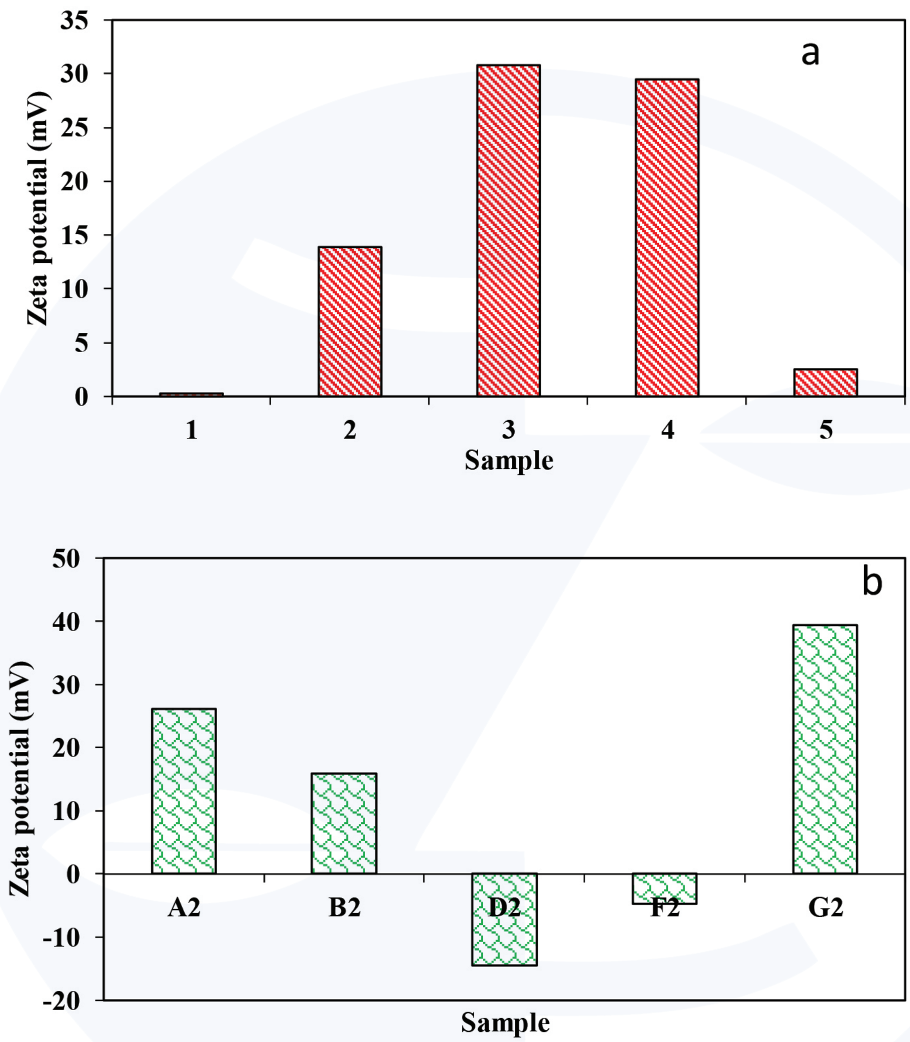

Fig 7. Changes in the mean value of the zeta potential for the control samples (a), and samples under TCF (b)

It has been proven that the tendency of the particles having the same charge to repel each other is directly related to the zeta potential. Therefore, the boundary between the stability and instability of the suspension can be determined based on the zeta potential. It is stated that particles with a zeta potential of more than 30 mV or less than -30 mV are stable in the diffuser bed [25-26]. In fact, a zeta potential of more or less than ±30 mV causes an electrostatic repulsion force between the particles in the suspension and leads to the stability of these particles. Therefore, according to the results shown in Fig. 7, among the control samples, sample 3 and to some extent sample 4 can be stable in the colloid. In the samples under TCF, that's true about sample G2.

If we compare two samples of the same group, we see the zeta potential:

In the group of samples 1 and B2, sample B2 is more

In the group of samples 2 and A2, sample A2 is more

In the group of samples 3 and G2, sample G2 is more

In the group of samples 4 and F2, sample 4 is more (with different charge)

In the group of samples 5 and D2, sample D2 is more (with different charge).

TEM results

The results of the TEM test for the samples are shown in Fig. 8.

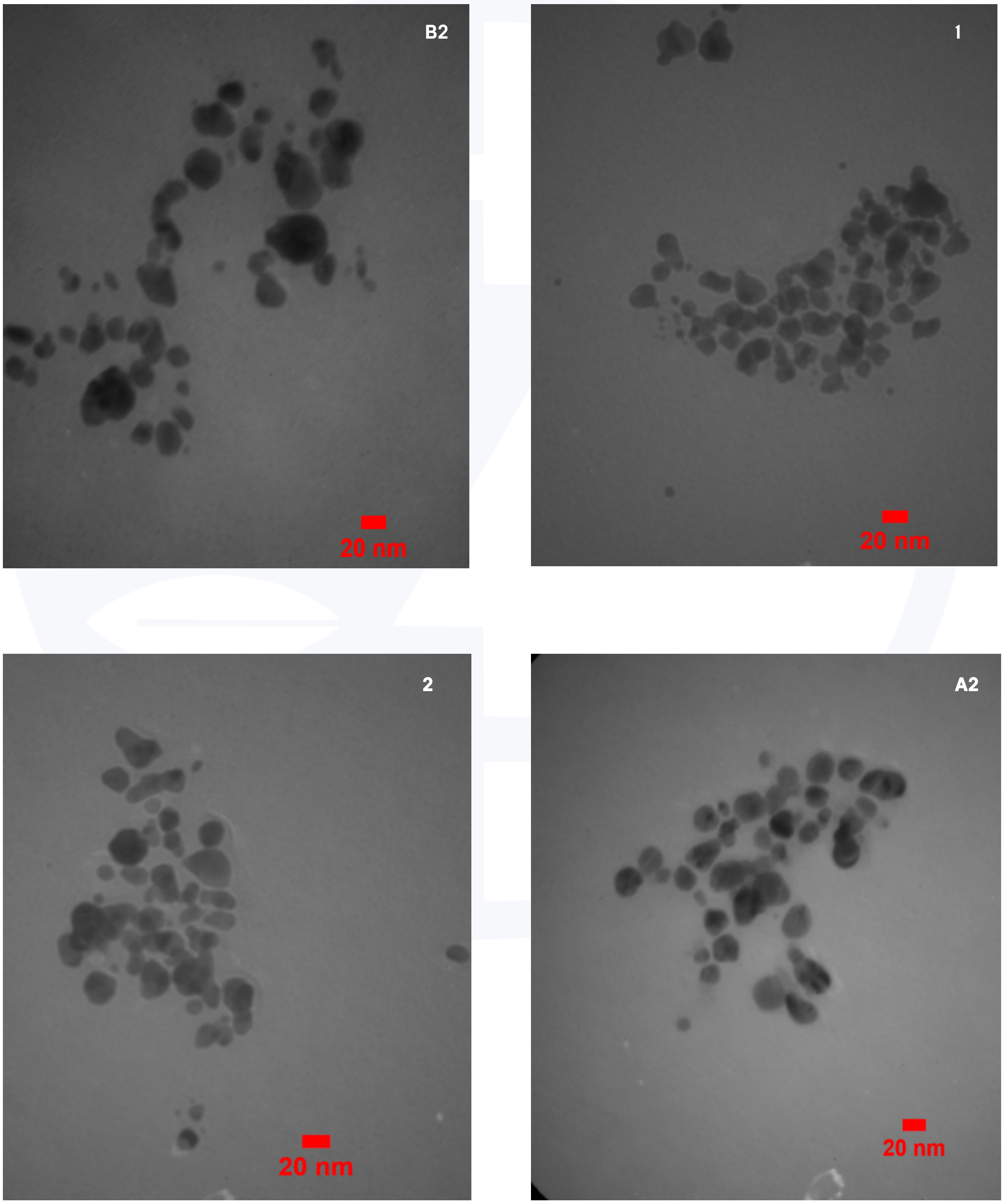

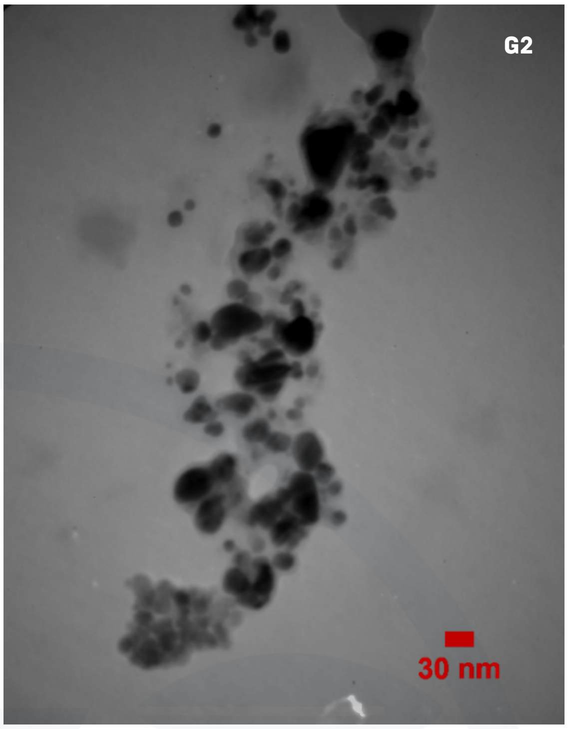

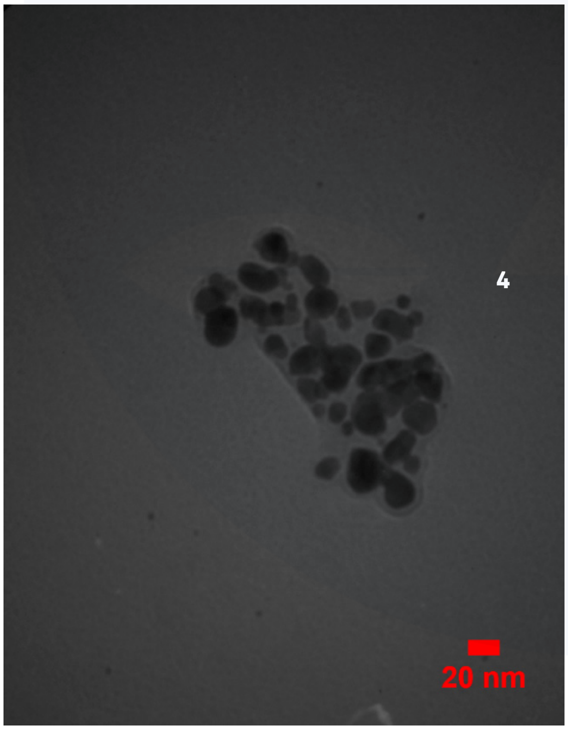

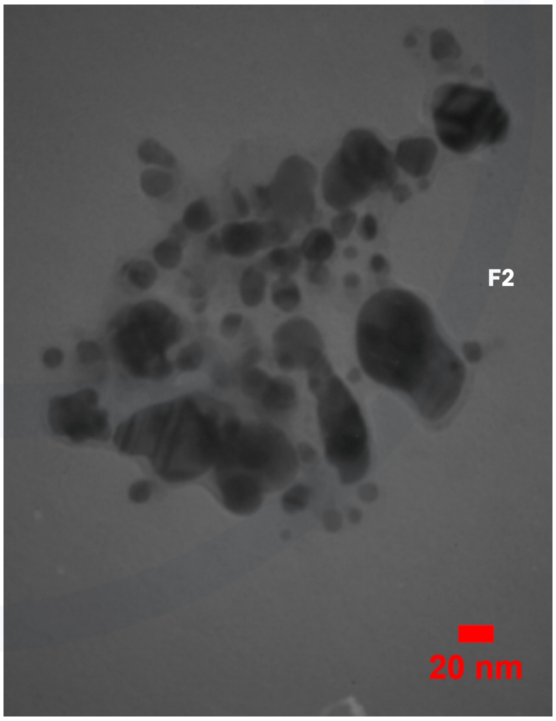

Vol . 01
No . 08
April
2 0 2 2
159
The First Journal in
T-Consciousness Research

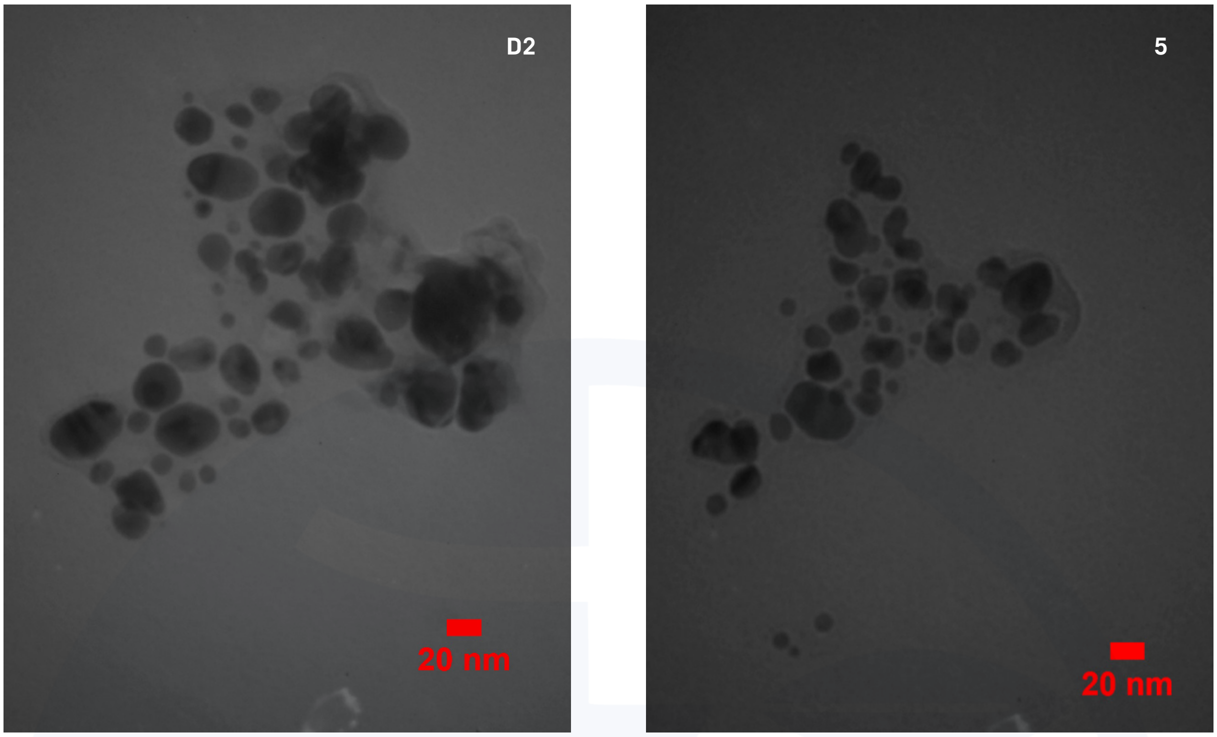

Fig 8. TEM test results. Samples 1, 2, 3, 4, and 5 are control, and samples A2, B2, G2, F2, and D2 are under TCF.

To examine the particles size, in each sample, 50 particles of the TEM images were measured by the image processing software of Image. J. The resulting histograms are shown in Fig. 9.

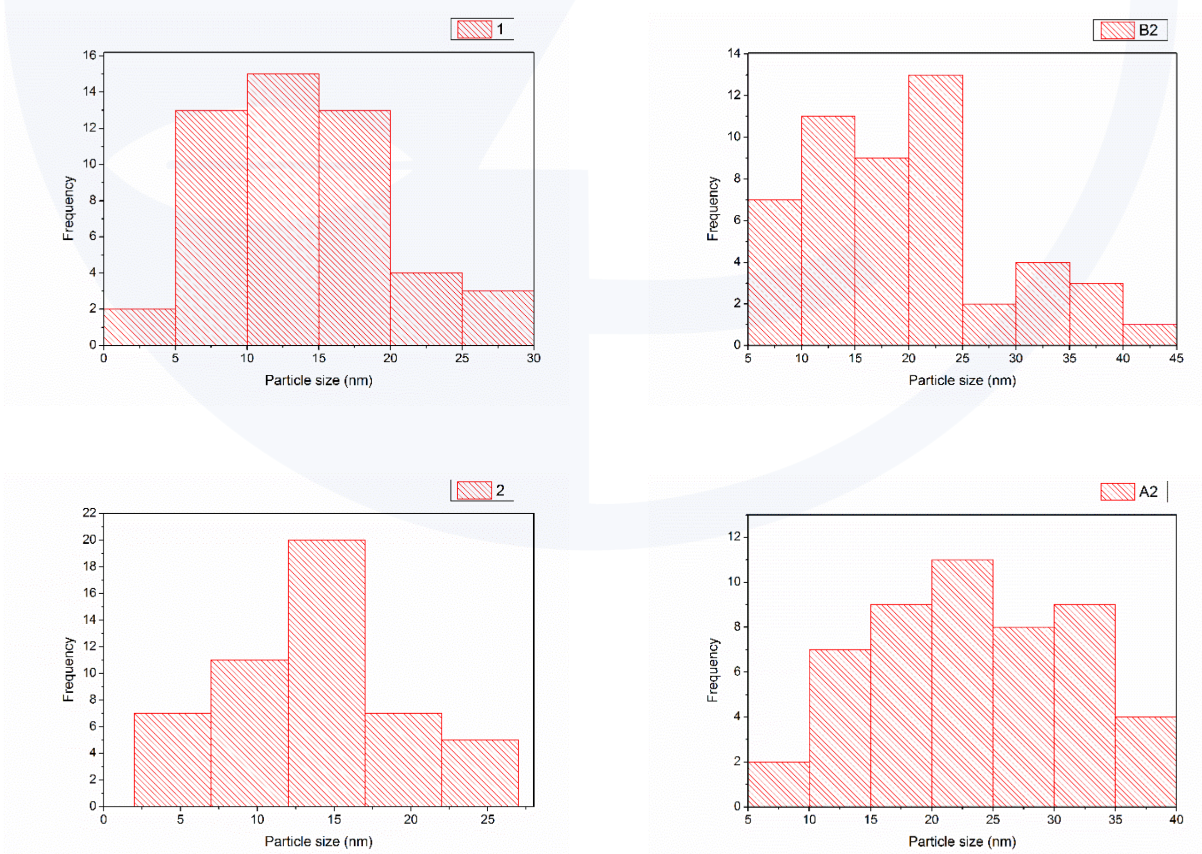

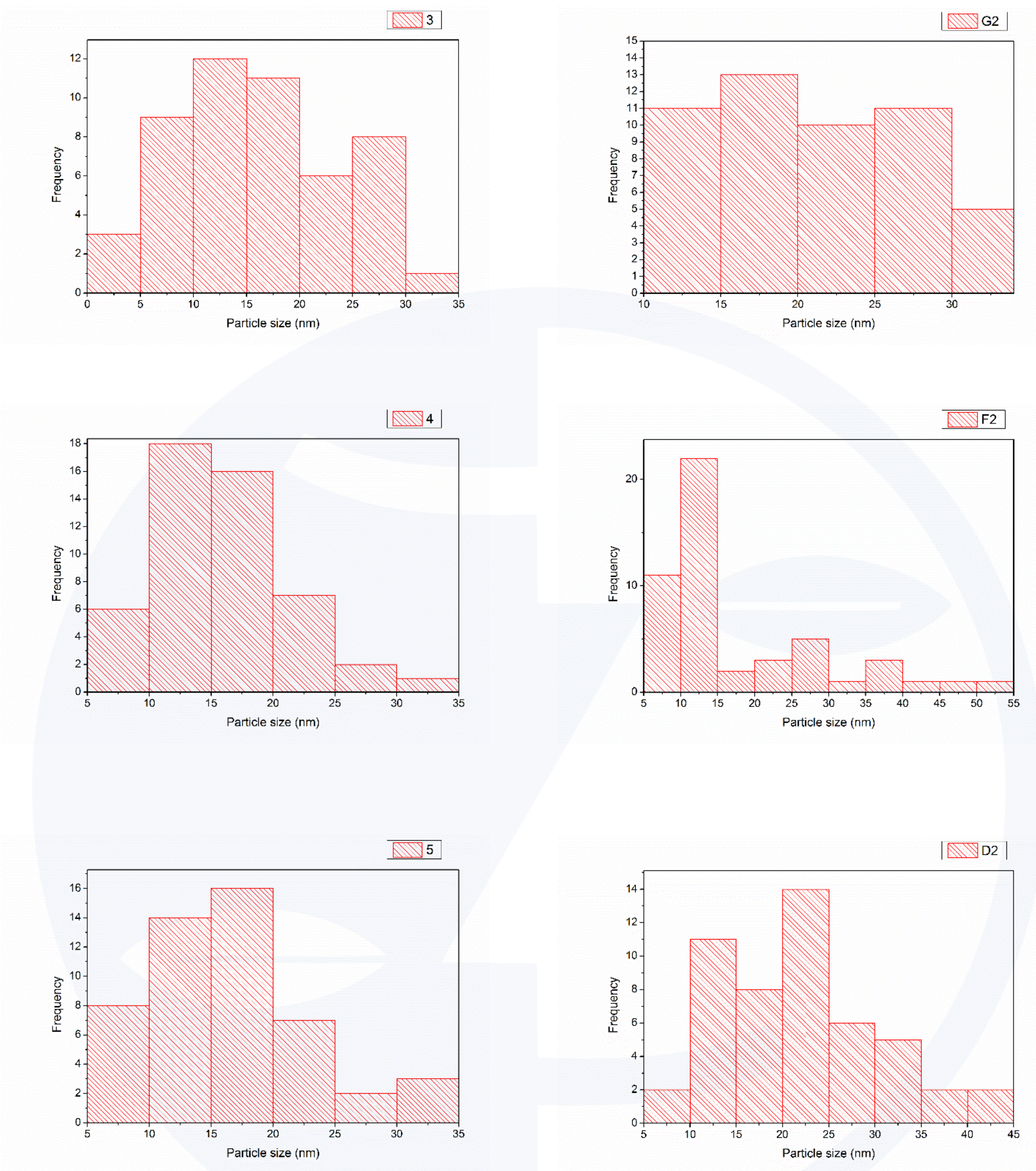

Fig 9. Histograms obtained by measuring 50 particles of TEM images of samples 1, 2, 3, 4, and 5 (control), and samples A2, B2, D2, F2, and G2 (under TCF).

In these histograms, the horizontal axis is the particles size visible in the TEM images and the vertical axis is the number of particles in that size range measured by the software. According to the histograms shown in Fig. 9, F2 and G2 have the narrowest and widest particle size distributions among the samples, respectively. The narrower the particle size distribution, the closer the particles are to each other, and the wider the particle size distribution, the greater the dispersion of the particle size.

Table 4 . Statistical results from the histograms shown in Fig. 9. Samples 1, 2, 3, 4, and 5 (control), and samples A2, B2, D2, F2, and G2 (under TCF)

Sample Name	Total number of measurements	Mean (Nanometer)	Standard Deviation (Nanometer)	The smallest particle measured (Nanometers)	Measured sample of medium size (Nanometers)	The largest measured particle (nanometers)
1	50	13.94	6.15	4.06	12.87	28.55
2	50	13.89	5.32	3.90	14.61	25.80
3	50	16.42	7.83	0.99	15.99	33.31
4	50	16.20	5.52	6.77	15.31	32.11
5	50	16.55	6.90	5.87	15.22	34.27
A2	50	23.38	8.21	9.87	21.81	39.90
B2	50	19.43	9.06	5.76	18.88	41.00
D2	50	21.86	8.48	8.06	21.27	44.50
F2	50	17.56	11.50	5.81	12.92	54.72
G2	50	20.78	6.37	10.89	20.78	32.62

Table 5 . Percentage of changes in the mean of particles with medium size and meaning of the particles size mean of the group under TCF compared to the control

	TCF	Control	percentage of changes
Mean of particles with a medium size (nm)	19.13	14. 8	29%
Mean of particles size mean (nm)	20.6	15.4	33%

For easier examination and comparison of the mean and standard deviation values reported in Table 4, these values were plotted as bar graphs in Fig. 10.

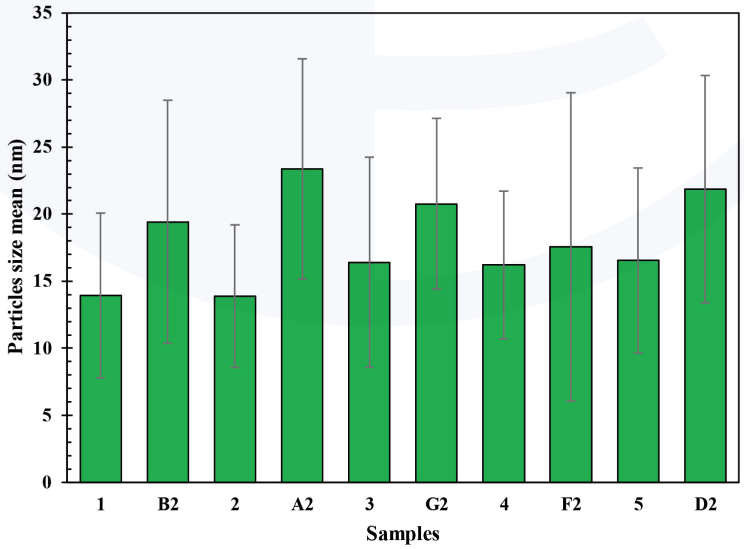

Fig 10. Particles size mean and standard deviation of the samples. Samples 1, 2, 3, 4, and 5 (control), and samples A2, B2, D2, F2, and G2 (under TCF).

According to Fig.10, samples 2 and 1 with particles size mean of 13.89 and 13.94 nm have the lowest particles size mean, followed by samples 4, 3, and 5 with means of 16.20, 16.42, and 16.55 nm. Thus, it is clear that the numbered control samples had the lowest particles size mean. And the samples under TCF had larger particles size. Sample A2 had one of the highest particles sizes means (23.38 nm) among the samples in this category, followed by D2 with the particles size mean (21.86 nm).

Conclusion

1. The results of the XRD test showed that the percentage of crystallization was lower in the control samples. The percentage of silver chloride phase formation (average 28%) was higher in the samples under TCF and so the percentage of silver phase (average 16%) was more in the control samples. The crystallite size of the silver phase decreased on average (44%) under CF. And the minimum crystallite size in both silver and silver chloride phases was for the samples D2, F2, and G2 under TCF.

2. DLS analysis showed that the particles size means of the samples under TCF was higher than that of the control samples.

3. In terms of zeta potential, the mean of the values obtained, regardless of the electric charge, in the samples under TCF were higher than the control samples. In terms of colloidal stability (±30 mV), sample 3 among the control samples and samples G2 among the samples under TCF were relatively stable.

4. TEM analysis showed that the samples under TCF had on average larger particle sizes than the controls and the largest mean particle size belonged to the A2 sample with a mean size of 23.38 nm. The largest particle size was 34.27 nm in the control samples and 54.72 nm in the samples of the TCF. It was found that the mean of particles with a medium size (Nanometers) in the group under the TCF was (~ 29%) larger than the control group.

5. Also, according to Fig. 9. with the exception of G2, the average size distribution of nanoparticles was more uniform in samples under the TCF.

In nanoscale, materials properties, such as color, melting point, chemical properties, strength, resistance, corrosion, etc. change. One gram of nano-silver is equivalent to thousands of square meters of silver. Today, about 320 tons of nano-silver are produced in the world [27-28]. Any change in the structure of nanoparticles nominates them for different functions. Today, we see that under the new method of T-Consciousness Fields, purposeful changes are made in the structure and size of nanoparticles, and this means that their different applications are ahead. In this decade, with the expansion of research in the new science, Sciencefact, T-Consciousness Fields will be one of the special methods of changing dimensions of particles and efficiency of materials.

References

1- Mody. V.V, Siwale. R, Singh, A. and Mody H.R. (2010). Introduction to Metallic Nanoparticles. *Journal of Pharmacy and Bio allied Sciences*, 2, 282-289. http://dx.doi.org/10.4103/0975-7406.72127

2- Sharma. V.K, Yngard, R.A. and Lin, Y. (2009). Silver Nanoparticles: Green Synthesis andTheir Antimicrobial Activities. *Advances in Colloid and Interface Science,* 145, 83-96.
http://dx.doi.org/10.1016/j.cis.2008.09.002

3- Choi. B, Lee. H, Jin. S, Chun. S, Kim. S.(2007). Characterization of the optical properties of silver nanoparticle films. *Nanotechnology.* 18: 1-5.

4- Lu. Y, Spyra. P, Mei. Y, Ballauff. M, Pich. A. (2007). Composite Hydrogels: Robust Carriers for Catalytic Nanoparticles. *Macromol. Chem. Phys.* 208: 254-261.

5- Yamasaki. S, Yamada.T, Kobayashi. H, Kitagawa. H. (2013) .Preparation of Sub-10 nm AgI Nanoparticles and a Study on their PhaseTransition Temperature. *Chem. Asian J.* 8:73–75

6 – Adamson. R. P, Sommerfeld. M. R.(1980). Laboratory comparison of the effectiveness of several algicides in isolated swimming pool algae . Appl. Environ. *Microbiol,* 39 (2), 348–353

7- Chaloupka. K, Malam. Y. and Seifalian. A.M. (2010) Nanosilver as a New Generation of Nanoproduct in Biomedical Applications.*Trends in Bioethanology,* 28, 580-588.

8- Asaad. M.A, Ismail. M, Tahir.M. D, Huseien. G.F, Raja.P.B, Asmara.Y.P (2018), Enhanced corrosion resistance of reinforced concrete: Role of emerging eco-friendly Elaeis- guineensis/silver nanoparticles inhibitor, Construction and Building Materials Pages 555-568 https://doi.org/10.1016/j.conbuild-mat.2018.08.140

9- Khan. Z, Al-Thabaiti. S.A, Obaid. A.Y. and Al-Youbi. A.O. (2011). Preparation and Characterization of Silver Nanoparticles by Chemical Reduction Method. *Colloids and Surfaces B: Biointerfaces*, 82, 513-517.
http://dx.doi.org/10.1016/j.colsurfb.2010.10.008

10- Chen. P, Song. L.Y. and Liu. Y.K. (2007) . Synthesis of Silver Nanoparticles by Gamma-Ray Irradiation in Acetic Water Solution Containing Chitosan. *Radiation Physics and Chemistry*, 76, 1165-1168.
http://dx.doi.org/10.1016/j.radphyschem.2006.11.012

11- Zhang. W.Z, Qiao. X.L. and Chen. J.G. (2006). Synthesis and Characterization of Silver Nanoparticles in AOT Micro-Emulsion System. *Chemical Physics,* 300, 495-500.
http://dx.doi.org/10.1016/j.chemphys.2006.09.029

12- Reicha. F.M, Sarhan. A, Abdel-Hamid. M.I. and El-Sherbiny. I.M. (2012) Preparation of Silver Nanoparticles in the Presence of Chitosan by Electrochemical Method. *Carbohydrate Polymers,* 89, 236-244.
http://dx.doi.org/10.1016/j.carbpol.2012.03.002

13- Abid. J.P, Wark. A.W, Brevetm. P.F. and Girault. H.H. (2002) Preparation of Silver Nanoparticles in Solution from a Silver Salt by Laser Irradiation. *Chemical Communications,* 7, 792-793. http://dx.doi.org/10.1039/b200272h

14- Yang. J. and Pan. J. (2012) Hydrothermal Synthesis of Silver Nanoparticles by Sodium Alginate and Their Applications in Surface-Enhanced Raman Scattering and Catalysis. *Acta Materialia,* 60, 4753-4758. http://dx.doi.org/10.1016/j.actamat.2012.05.037

15- Khan. A, El-Toni. A.M, Alrokayan. S, Alsalhi. M, Alhoshan. M. and Aldwayyan. A.S. (2011) Microwave-Assisted Synthesis of Silver Nanoparticles Using Poly-N Isopropyl Acrylamide/Acrylic Acid Microgel Particles. *Colloids and Surfaces A: Physicochemical and Engineering Aspects,* 377, 356-360.
dx.doi/org/10.1016/j.colsurfa.2011.01.042

16- Alarcon. E.I, Udekwu. K, Skog. M, Pacioni. N.L, Stamplecoskie. K.G, González-Béjar. M, et al. (2012).The Biocompatibility and Antibacterial Properties of Collagen-Stabilized, Photochemically Prepared Silver Nanoparticles.*Biomaterials*, 33, 4947-4956.
http://dx.doi.org/10.1016/j.biomaterials.2012.03.033

17- Srikar. S.S, Giri.D.D, Pal.D.B, Mishra.P.K, Upadhyay.S.N.(2016).Green Synthesis of Silver Nanoparticles: A Green and Sustainable Chemistry.Review- DOI: 10.4236/gsc.2016.61004

18- Abad-Esalam.K.A ,*Nanobiotechnology Applications in Plant Protection* ,ISSN 2523-8027 ,ISBN 978-3=030-13295-8
https://doi.org/10.1007/978-3-030-13296-5

19- Taheri, M., Payervand, F., Ahmadkhanlou, F.,Torabi, S., & Semsarha, F. (2021). Distinction of Consciousness Fields According toTaheri from Other

20- Conventional Physical Fields: Evaluating the Magnetic Properties of Materials.

21- Taheri MA.*Human from another outlook.* Interuniversal Press (2013). 2nd Edition. ISBN-13: 978-1939507006, ISBN-10: 193950700

22- Taheri MA.(2012).*General Connection of particles.* Interuniversal Publishing.Erfan-Halgheh. ID: 978-1-940491-03-5.

23- Kazazi. B, Taheri.M.A, Meshkin-Far. A, .(2020). Influence of the Consciousness Field on the Cement Properties and Behavior. Science of Consciousness, Tucson, Arizona.

24- WWW.Cosmointel.com

25- 24- WWW. I J L K. ir

26- Bhattacharjee.S .(2016).DLS and zeta potential – What they are and what they are not? J. Control. Release. 235 337–351. https://doi.org/10.1016/J. JCONREL.2016.06.017

27- Honary.S, Zahir.F.(2013). Effect of Zeta Potential on the Properties of Nano-Drug Delivery Systems - A Review (Part 1), Trop. J. Pharm. Res. 12 . 255–264. https://doi.org/10.4314/tjpr.v12i2.19.

28- Nowack. B, Krug.H.F, Height.M,.(2011). 120 Years of Nanosilver History: Implications for Policy Makers . http://dx.doi.org/10.1021/es103316q, Environ. Sci. Technol. 45, 1177–1183

Gottschalk. F.Scholz. R. W, Nowack. B. (2010). Probabilistic material flow modeling for assessing the environmental exposure to compounds: Methodology and an application to engineered nano-TiO2 particles. *Environ. Modeling Software* . 25, 320–332.

Vol . 01
No . 08
April
2 0 2 2

The First Journal in
T-Consciousness Research

Influence of Taheri Consciousness Bond Field on the Alkaline Reaction of Concrete

Bahareh Kazazi[1*], Mohammad Ali Taheri[2]

1. Civil Engineering, CEO of Hoobe Construction Company, Tehran, Iran.

2. Sciencefact R&D Department, Cosmointel Inc. Research Center, Ontario, Canada.

*Corresponding author:

Bahareh Kazazi
Civil Engineering, CEO of Hoobe Construction Company, Tehran, Iran.

Email: baharkazazi@gmail.com

ABSTRACT

Some natural aggregates used in concrete contain activated silica and react with the alkalis in the concrete, the product of which is an expansion gel that eventually destroys the concrete. The aim of this study was to investigate the effects of the Consciousness Bond Field on concrete. Consciousness Bond Field is one of many Taheri Consciousness Field (TCFs) that were founded and introduced by Mohammad Ali Taheri as new Fields. These Fields are neither matter nor energy; therefore, do not possess a quantity, but they have direct effects on both matter and energy. In other words, although TCFs cannot be directly measured, we can investigate their effects indirectly through various reproducible experiments. To achieve the goal of this study, alkaline reaction stimulus aggregate was selected, and the aggregate and cement reactivity was tested. Three series of cement mortar were prepared under the ASTM C1260 standard. Tow series were subjected to the TCF, and one series was considered the control. The reactivity of concrete increased (~5%) under the influence of the Consciousness Bond Field.

Keywords: Concrete, Taheri Consciousness Fields, Consciousness Bond Field, Alkaline reaction

INTRODUCTION

Concrete, known as artificial stone consisting of cement, sand, and gravel, is one of the most widely used construction materials. This material is the cornerstone of urbanization and an important component in constructing modern and industrial society today. All residential buildings (one floor to skyscrapers), industrial buildings (bio-energy, power plants, etc.), urban systems, such as water and sewage systems, as well as transportation networks are all dependent on concrete [1].

A large part of concrete is made up of aggregates that are extracted from nature. In many sand mines, there are aggregates that have a high affinity for alkaline silica to react with cement in concrete. The alkaline silica reaction was first identified in 1930 in California, USA [2]. This reaction is a chemical process in which OH- ions in a concrete pores solution are combined with amorphous silica in the aggregates in concrete and then Alkaline gel compounds are produced. The presence of water and continuous swelling due to the increase of this gel leads to increase stress and fracture of concrete. When the internal stress is more than the tensile strength of the concrete, progressive cracks would be formed [3] and eventually leads to the collapse of the structure. In this study, the effect of the Consciousness Bond Filed on this process was investigated.

Taheri Consciousness Fields

The nature of consciousness and its place in science has received much attention in the current century. Many philosophical and scientific theories have been proposed in this area. In the 1980s, Mohammad Ali Taheri introduced novel fields with a non-material/non-energetic nature named Taheri Consciousness Fields (TCFs). In this perspective, T-Consciousness is one of the three existing elements of the universe apart from matter and energy. According to this theory, there are various TCFs with different functions, which are the subcategories of a networked universal internet called the Cosmic Consciousness Network (CCN). The major difference between the theory of TCFs and other theoretical concepts about consciousness is related to the practical application of the TCFs. TCFs can be applied to all living and non-living creatures, including plants, animals, microorganisms, materials, etc.

Mohammad Ali Taheri, the founder of Erfan Keyhani Halqeh, a school of thought, introduced a new science in 2020 as a branch of this school. He coined the term Sciencefact for this new science because it utilizes scientific investigations to prove the existence of T-Consciousness as an irrefutable phenomenon and a fact. Although science focuses solely on the study of matter and energy and Sciencefact, by contrast, explores the effects of the [non-material/non-energetic] TCFs, Sciencefact has provided a common ground between the two by conducting reproducible laboratory experiments in various scientific fields, and it has used the scientific approach in proving TCFs.

The influence of the TCFs begins with the Connection between CCN as the Whole Taheri Consciousness of the universe and the subjects of study as a part. This Connection called "Ettesal" is established by a certified and trained individual who has been entrusted with the TCFs. The human mind has an intermediary role (Announcer) which plays a part by fleeting attention to the subject of study and then the main achievement obtained as a result of the effects of the TCFs. These Fields cannot be directly measured by science, but it is possible to investigate their effects on various subjects through reproducible laboratory experiments.

The research methodology in the study of T-Consciousness has been founded on the process of Assumption, Argument, and Proof, in which the basic Assumption is: The Cosmos was formed by a third element called T-Consciousness that is different from matter and energy.

The Argument: The existence of TCFs can be demonstrated by their effects on matter and energy (e.g., humans, animals, plants, microorganisms, cells, materials, etc.)

The Proof: is the scientific verification of the effects of TCFs on matter and energy (according to the Argument) through various reproducible scientific experiments.

Accordingly, to investigate and verify the existence, effects, and mechanisms of TCFs, the following five research phases (Phases 0 through 4), and the aims of each phase are outlined below.

Phase-0 studies aim to prove the existence of TCFs by observing their effects. The nature of T-Consciousness and what it is will not be addressed in this phase. Phase-1 explores the varied effects of different TCFs. Phase-2 examines the reason behind the varied effects of these fields. Phase-3 investigates the mechanism of TCFs effects on matter and energy. Finally, Phase-4 draws significant conclusions, particularly with regard to the mind and memory of matter and their relation to the T-Consciousness, etc. [4-7]

Methodology

The method of selection in this experiment is to evaluate the alkaline reaction of aggregate under ASTM C 1260 [8].

Consumed aggregates: In order to better study the TCF method, aggregates were selected from the Kish Island rock mine which have high reactivity.

The experiment was performed according to the ASTM C1260 standard by preparing three groups according to this standard, and each series included three prismatic samples. This method is accelerated and strict.

Cement: The Portland cement used for all samples was type II cement from one bag. Since the samples were exposed to NaOH, the number of alkalis in the cement was not an effective parameter in expansion.

All aggregates were graded according to the requirements of Table 1.

Table 1 . Requirements for the grading of the aggregate

Weight Percentage	Sieves Size (mm)	
	Remained	Passed
10	2.36	4.75
25	1.18	2.36
25	0.600	1.18
25	0.300	0.600
15	0.150	0.300

Mortar components ratio: The ratio of dry materials for the mortar test was one part of cement to 2.25 parts of aggregate by weight, and the ratio of water to cement was equal to 0.47.

Mixing: Mixing of mortars was performed in accordance with the requirements of the ASTM C305 standard method.

Molding the samples: Immediately after making the mortar, the samples were molded.

Application of Taheri Consciousness Fields

One of the introduced TCFs is called the Consciousness Bond Field and was applied to the samples according to the protocols regulated by the COSMOintel research center (www.COSMOintel.com). A request for Connection to the CCN to utilize TCFs can be placed through the COSMOintel website in the "Assign Announcement" section. This access is available for everyone at no cost. In order to study and experience this Connection, the researchers can register on the website at any time in order to report the experiment to the COSMOintel research center. Certain details of the experiment must be provided to the center; for example, the characteristics or number and name of samples and controls must be specified. This entire experiment was carried out as a double-blind method where lab technicians were completely unaware of the TCFs.

Storage and reading of samples:

Initial storage and reading: Samples were placed in a wet chamber immediately after molding. They were removed from the mold after 24 hours and the initial reading was performed with an accuracy of 0.002 mm. The samples made with one type of aggregate were placed in a sealed chamber that had enough water to drown the samples, and the chamber was placed in an oven at 80 °C ±2 temperature for 24 hours.

Zero base reading: After 24 hours, each chamber came out of the oven in turn, and after drying their surface, the base reading of each of the prisms was done, then they were returned to the chamber, and all samples made from the aggregates were placed in a chamber with a sufficient amount of normal NaOH at 80 °C ±2 temperature so that the samples were completely drowned and the chamber was sealed and returned to the oven.

Subsequent reading and storage: The change in the length of the samples was read periodically for 14 days after the baseline reading.

Calculation Method:

The difference between base reading (zero) and reading in each time period of the samples was calculated and the expansion of the samples for each period was recorded. The average expansion of four samples for each cement and aggregate composition was reported to be approximately 0.01% of the read periods.

Results and Discussion

The expansion rate of each group with three samples is presented below in two groups under the CF and the control group.

Table 2 . The expansion rate of the samples

Number	Sand Expansion after 14 days		
	A(TCF)	B(TCF)	Control
1	0.569	0. 564	0.532
2	0.549	0.546	0.555
3	-	0.568	0.526
Average	**0.56**	**0.56**	**0. 53**

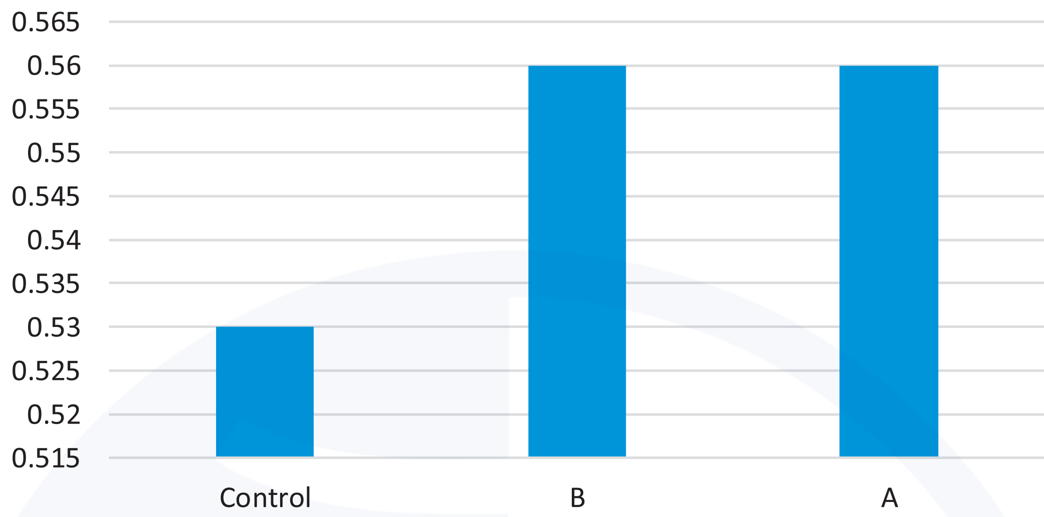

Figure 1. The average increase in expansion of each group under the TCF and the Control.

Conclusion

The effect of TCF on the alkaline reaction was to increase the destructive expansion of concrete (~ 5% -Tables: 2). Also, the results of previous research have shown that the effect of the Consciousness Bond Field on concrete is to increase hydration and thus increase strength, so in the alkaline reaction, an increase in reactivity and consequent faster degradation can be observed [7]. It can also be seen that TCFs can be used independently of each other and with different effects and have their own unique effects. As in previous research, the effect of the TCF(H) on the alkaline reaction was investigated and it was found that this Field slows down the process of concrete degradation [9].

References

1- Department of Civil and Environmental Engineering, Chair of Sustainable Chair of Sustainable Construction, ETH Zürich, Zürich, Switzerland. 2Department of Civil

2- Stanton. T.E. (1940). Expansion of Concrete Through Reaction Between Cement and Aggregate. *Proceedings of the American Society of Civil Engi-neers.* 66: 1781–1811

3- Pan.J,Feng.Y.T,Wang.J,Sun.Q.C.(2012).Modelingofalkali-silicareactioninconcrete:Areview*Frontiers of Structural and Civil Engineering.* 6(1):1–18 DOI 10.1007/s11709-012-0141-2

4-Taheri. M.A. (2013). *Human from another outlook.* Interuniversal Press. 2nd Edition. ISBN-13: 978-1939507006, ISBN-10: 193950700

5-Taheri. M.A. (2012). *General Connection of particles.* Interuniversal Publishing. Erfan-Hlgheh. ID: 978-1-940491-03-5. Taheri MA. *General Connection of* particles. Interuniversal Publishing.Erfan-Halgheh. ID: 978-1-940491-03-5.

6- Taheri, M. A. (2020).The main monitoring center forT-Consciousness Fields research and studies based on Sciencefact. www.Cosmointel.com.

7- Kazazi. B, Taheri. M.A, Meshkin-Far. A.(2020). Influence of the Consciousness Field on the Cement Properties and Behavior. Science of Consciousness, Tucson, Arizona.

8- Astm. ASTM C1260-Standard test method for potential alkali reactivity of aggregates (mortar-bar method). ASTM Int. 2012. 1-5.

9- Kazazi..B,Taheri. M.A.(2021). Effects of the Consciousness Field on Concrete (ASR).

Vol. 01
No. 08
April
2022

The First Journal in
T-Consciousness Research

Mohammad Ali Taheri is a scholar, visionary thinker, and innovationist known for his numerous theoretical concepts, including Cosmic Consciousness Network (CCN) and Taheri Consciousness Fields (TCFs) with over 40 years of history. T-Consciousness is introduced and defined as one of the constituent components of the Cosmos in addition to matter and energy, from which TCFs, as non-material/non-energetic fields, are derived. TCFs are unique qualitative fields that are immaterial in nature but have a direct effect on matter and energy, including humans, animals, plants, microorganisms, molecules, cells, and particles. As far as the practical application of T-Consciousness is concerned, two complementary medicines of **Faradarmani** and **Psymentology** have been introduced and put into practice. In 2020, Mohammad Ali Taheri introduced Sciencefact, that utilizes science as a means to demonstrate and record the effects of TCFs. Although science studies matter and energy alone, Sciencefact and science do share a common ground which is reproducible laboratory experiments that involve matter and energy. What distinguishes Sciencefact from science is the investigation and utilization of CCN through the application of the TCFs.

Established and managed by Mohammad Ali Taheri in 2022, the Journal of Cosmointel is an all-science journal that publishes original research on TCFs. As a scientific journal, all types of scientific research that adhere to ethical guidelines and publishing standards of Cosmointel Journal and T-Consciousness research protocol are eligible for publication. Cosmointel establishes the guidelines for conducting scientific research on TCFs and publishes the results in its journal spanning various disciplines, including biology, T-Consciousness biology, physics, engineering, material science, medicine, neurosciences, psychology, etc.

Interuniversal Press